

Modern Control of Smart Power Grids

A Dissertation

Presented in Partial Fulfillment of the Requirements for the

Degree of Doctor of Philosophy

with a

Major in Electrical Engineering

in the

College of Graduate Studies

University of Idaho

by

Mahmoud Mohammed Abdelfattah Hafez Badreldien

Major Professor: Brian K. Johnson, Ph.D.

Committee Members: Herbert L. Hess, Ph.D.; Abdel Rahman Khatib, Ph.D., P.E.;

Yacine Chakhchoukh, Ph.D.

Department Administrator: Joseph D. Law, Ph.D.

December 2022

Abstract

The desire to reduce the carbon emissions footprint caused by fossil-fueled power plants has increased penetration of renewable energy resources based distributed generating units, in particular photovoltaic plants and wind energy conversion systems, in the power system network. Furthermore, the topology and architecture of the power system have changed from one with large conventional generation to one with a more distributed architecture. This dissertation describes microgrid architectures, their control strategies and the distributed generating units that are used to supply microgrids.

The modeling, design, and control for a wind energy conversion system are described. The work includes a doubly-fed induction generator combined with a battery energy storage system. Photovoltaic power represents most of the microgrid power sources in the literature. Modeling and control of a solar photovoltaic system are also described in the dissertation. An energy storage system is connected in parallel with the photovoltaic system. The battery overcomes the intermittent nature of both wind speed and solar irradiation levels. The proposed system is modeled and simulated in different scenarios to verify the proposed control system and its operation to control the active and reactive power and terminal voltage.

Expansion of renewable energy resources with common control schemes that exhibits low inertia replacing conventional generator tends to reduce the total system inertia. Reduction of the inertia could have a dramatic effect on power system stability. Converter control schemes creating virtual synchronous generators have been adopted in the literature to address the inertia reduction and related stability challenges. The power converters are controlled to emulate and improve the features of the traditional synchronous generator such as inertia and damping, to improve system

stability. A proposed control strategy, mathematical model, and controller design will be described in this dissertation.

Applying a virtual synchronous generator works best with an energy storage system. A hybrid energy storage system composed of superconducting magnetic energy storage and a battery is used to smooth the system's power fluctuations. The superconducting magnetic energy storage system responds to the high rate of change of power fluctuation. Contrarily, the battery system responds to slower long term power fluctuations. This hybrid system reduces the stress on the battery by removing the transient and high rate of change charging and discharging currents to increase its lifetime.

Furthermore, virtual synchronous generator parameters can be set according to the desired and best performance without being limited by the characteristics of a physical synchronous generator. Moreover, these parameters and constants affect the sizing of the converter and of the energy storage system. When the inertia time constant of the virtual synchronous generator increases, the system experiences larger amplitude power oscillations and counteracts the frequency change. Also, the damping constant in the control settings affects the system performance. When the damping constant of the controller increases, the system experience lower amplitude power oscillations, although takes lower time to reach the new steady-state value. The simulation results describe how the values selected for inertia and damping constants affect the system operation and performance. Moreover, they show the power and energy required from the energy storage system to achieve a desired performance of the virtual synchronous generator.

Although the superconducting magnetic energy storage system is more expensive than the battery, it may be more effective and cheaper in some applications requiring fast charge and discharge and deep depth of discharge scenarios. Virtual synchronous generator controllers fed by energy storage systems can play a vital role to facilitate

the penetration of inverter-based renewable energy generators in microgrids and in large interconnected systems. This approach supports fully using the available energy resources, minimize conventional fuel consumption and greenhouse gas emissions.

Acknowledgements

Firstly, I would like to express my sincere and heartfelt gratitude appreciation to my esteemed advisor Prof. Brian Johnson for the continuous help and treasured support of my Ph.D. study and related research, for providing me with the counsel and guidance I need to succeed in the Ph.D. program, for his patience, motivation, and immense knowledge. His guidance helped me in all the time of research and writing of this dissertation. I could not have imagined having a better advisor and mentor for my Ph.D. study.

I also appreciate all the support I received from my family who without this would have not been possible.

My appreciation is extended to the committee: Prof. Herbert L. Hess, Dr. Abdel Rahman Khatib, and Dr. Yacine Chakhchoukh, for their insightful comments and encouragement.

Dedication

To my parents

To my wife and my kids

To my brothers and sister

Table of Contents

Abstract	ii
Acknowledgements	v
Dedication	vi
Table of Contents	vii
List of Tables	xii
List of Figures	xiii
Nomenclature	xix
1 Introduction	1
1.1 Problem Description	4
1.2 Objectives	4
1.3 Literature Review	5
2 Literature Review about Microgrids and Their Control Schemes	12
2.1 Introduction	12
2.2 Distributed Generating Resources.....	14
2.2.1 Solar Photovoltaic Systems	15
2.2.2 Wind Power Plants.....	16
2.2.3 Biomass	17
2.2.4 Hydropower System.....	19
2.2.5 Energy Storage Systems	21
2.3 Types of Microgrid.....	24

2.3.1	AC Microgrid.....	24
2.3.2	DC Microgrid	25
2.3.3	Hybrid AC/DC Microgrids.....	26
2.4	Control Strategies Based on Hierarchical Control Levels.....	26
2.4.1	Primary Control	27
2.4.2	Secondary Control	31
2.4.3	Tertiary Controller	36
2.5	Communication Media	37
2.5.1	Wireless Communication	38
2.5.2	Wired Communication Systems.....	41
2.6	Communication Protocols	43
2.6.1	Modbus.....	43
2.6.2	IEC 61850.....	44
2.6.3	Distributed Network Protocol (DNP3).....	45
2.6.4	IEC 60870-5- 101/103/104.....	46
2.7	Summary.....	47
3	Modeling and Control of Wind Energy Conversion System with Battery Energy Storage System.....	48
3.1	Introduction	48
3.2	Modelling of WECS	50
3.2.1	Modeling of Wind Turbine	50
3.2.2	Modeling of DFIG	50
3.3	Controller Design	52
3.3.1	Rotor Side Controller	52
3.3.2	Grid Side Controller	54
3.3.3	Pitch Angle Control.....	56

3.3.4	Maximum Power Point Tracking Control.....	56
3.3.5	DC-Link Chopper Circuit.....	56
3.4	Battery Energy Storage System.....	57
3.4.1	Battery Bidirectional Buck-Boost Converter (BDBBC).....	58
3.4.2	Modeling of Battery DC-AC Converter.....	58
3.5	Simulation of Wind Energy Conversion System.....	59
3.6	Conclusion.....	66
4	Solar Photovoltaic System Combined with Battery Energy Storage System.....	67
4.1	Modeling and Control of Solar PV System Combined with Battery Energy Storage System (paper 1).....	67
4.1.1	Introduction.....	67
4.1.2	Modeling of the System.....	69
4.1.3	Simulation of Combined PV/BESS.....	74
4.1.4	Conclusion.....	78
4.2	Volt/Var Control of Solar Photovoltaic System (paper 2).....	80
4.2.1	Introduction.....	80
4.2.2	Modeling of the System.....	82
4.2.3	Simulation Results.....	87
4.2.4	Conclusion.....	92
5	Virtual Synchronous Generator Controller.....	93
5.1	Introduction.....	93
5.2	System Layout.....	96
5.3	VSG Controller Structure.....	97
5.3.1	Outer Loops Structure.....	97
5.3.2	Inner Loop Controller.....	100

5.4	Simulation Results	101
5.5	Conclusion.....	106
6	Virtual Synchronous Generator Controller Performance and Evaluation.....	108
6.1	Introduction	108
6.2	System Layout	110
6.3	VSG Controller Structure	111
6.3.1	Inertial Emulation of VSG	111
6.3.2	Voltage Controller	114
6.3.3	Inner Control Loops	115
6.4	Battery Energy Storage System.....	115
6.5	Simulation Results	116
6.6	Conclusion.....	123
7	Virtual Synchronous Generator Controller Based SMES-Battery Energy storage System	125
7.1	Introduction	125
7.2	System layout.....	128
7.3	Energy Storage Systems.....	129
7.3.1	Battery energy Storage System	130
7.3.2	SMES System and Controller	131
7.4	DC-AC Converter Controller	133
7.5	Comparison between Different ESSs	134
7.6	Simulation Results	138
7.7	Phase Compensation Method	157
7.8	Verification of Virtual Synchronous Generator Compared to Conventional Synchronous Generator	160

7.8.1	Introduction.....	160
7.8.2	Conventional Synchronous Generator	161
7.8.3	Simulation Results.....	163
7.9	Conclusion.....	166
8	Summary, Conclusions and Future Work	167
8.1	Summary.....	167
8.2	Conclusions	170
8.3	Future Work.....	172
	Bibliography	175
	Appendix A IEEE Formal Reuse License	210

List of Tables

2.1	Structure of IEC 61850 standard	45
7.1	Comparison between different energy storage systems [249, 250]	134

List of Figures

2.1	Hierarchical control levels in microgrid	28
2.2	Secondary control architectures in microgrid; (a) Centralized scheme, (b) Decentralized scheme, (c) Distributed scheme	35
3.1	Layout of the proposed WECS system	49
3.2	RSC, d-axis current controller	53
3.3	RSC, q-axis current controller	54
3.4	GSC, d-axis current controller	55
3.5	GSC, q-axis current controller	55
3.6	GSC, dc voltage control block diagram	55
3.7	DC-chopper circuit	57
3.8	Equivalent circuit of the battery	58
3.9	Battery bi-directional buck-boost converter	59
3.10	Battery dc-ac converter controller	60
3.11	Wind speed variation profile	61
3.12	Generated active power in response to wind speed variation	61
3.13	Pitch angle profile	62
3.14	Generated reactive power profile	62
3.15	DC-link voltage profile	63
3.16	Reactive power variation profile	63
3.17	Wind system, load and BESS power during wind speed variation	64
3.18	Battery SoC during wind speed variation	65
3.19	Wind system, load and BESS power during load variation	65
3.20	Battery SoC during load variation	66
4.1	Layout of the proposed system	68

4.2	Ideal single diode PV model	70
4.3	MPPT algorithm based on P&O method	71
4.4	Converter control circuit	74
4.5	Generated active power in response to variations in irradiation	75
4.6	Generated reactive power as irradiation is varied	76
4.7	DC-link voltage profile in response to changes in irradiation	76
4.8	Reactive power variation profile	77
4.9	PV system, load and BESS power at different irradiation levels	77
4.10	Battery SoC during irradiation level variation	78
4.11	PV system, load and BESS power during load variation scenario	79
4.12	Battery SoC during load variation	79
4.13	Layout of the proposed PV system with BESS	82
4.14	DC-DC boost converter	84
4.15	Volt/var control function	86
4.16	P-Q priority mode	87
4.17	Voltage variation profile without reactive power support	88
4.18	Reactive power variation profile	89
4.19	Voltage variation profile with reactive power support	89
4.20	Priority signal	90
4.21	Active power profile	91
4.22	Battery state of charge	91
4.23	DC-link voltage profile	91
5.1	General layout of the proposed VSG system	96
5.2	Virtual inertia emulation	97
5.3	Voltage controller	99
5.4	Cascaded voltage and current control loops	101

5.5	VSG active power variation at different inertia time constants	102
5.6	PV array and battery power at different inertia time constants	103
5.7	VSG frequency profile at different inertia time constants	103
5.8	VSG active power variation at different damping constants	104
5.9	PV array and battery power at different damping constants	105
5.10	Terminal voltage variation profile	105
5.11	Reactive power profile	106
6.1	General layout of the proposed system	111
6.2	Virtual inertia emulation	114
6.3	Virtual impedance	115
6.4	Cascaded voltage and current control loops	116
6.5	VSG active power variation at different inertia time constants	117
6.6	Frequency profile at different inertia time constants	118
6.7	Battery power at different inertia time constants	118
6.8	VSG active power variation at different damping constants	119
6.9	Frequency profile at different damping constants	119
6.10	Battery power at different damping constants	120
6.11	Battery power variation with respect to the inertia time constant	120
6.12	Battery power variation with respect to damping constant	120
6.13	VSG frequency change in response to a microgrid frequency change	121
6.14	Output power in response to a microgrid frequency change	122
6.15	VSG frequency change in response to a microgrid frequency change	122
6.16	Output power in response to a microgrid frequency change	122
6.17	Output power in response to a microgrid frequency change	123
6.18	Output power in response to a microgrid frequency change	124
7.1	General layout of the proposed system with a HESS	129

7.2	Schematic diagram of a SMES system	132
7.3	DC-DC chopper of the SMES coil	133
7.4	Cycle life versus DOD curve for a lead-acid battery[251]	136
7.5	Cycle life versus DOD curve for a li-ion battery [252]	136
7.6	Battery capacity versus number of cycles for lead-acid battery [253] . . .	137
7.7	Battery capacity versus number of cycles under different rates for Li-ion battery [251]	137
7.8	Response to a microgrid frequency drop at different damping constants .	139
7.9	Converter output power at different damping constants in response to a microgrid frequency drop	140
7.10	SMES instantaneous power in response to a microgrid frequency drop . .	140
7.11	SMES energy at different damping constant in response to a microgrid frequency drop	141
7.12	Maximum converter output power versus damping constant in response to a microgrid frequency drop	142
7.13	SMES maximum power versus damping constant in response to a micro- grid frequency drop	142
7.14	SMES energy versus damping constant in response to a microgrid fre- quency drop	143
7.15	Converter output power at different inertia constants in response to a microgrid frequency drop	143
7.16	SMES power at different inertia constants in response to a microgrid fre- quency drop	144
7.17	SMES energy at different inertia constants in response to a microgrid frequency drop	144
7.18	Maximum output power versus inertia constants in response to a microgrid frequency drop	145

7.19 SMES maximum power versus inertia constants in response to a microgrid frequency drop	146
7.20 SMES energy versus inertia constants in response to a microgrid frequency drop	146
7.21 Converter power at different damping constants in response to step power setpoint increase	147
7.22 SMES power at different damping constant in response to step power setpoint increase	148
7.23 Frequency change at different damping constants in response to step power setpoint increase	148
7.24 Battery power profile	149
7.25 Converter power at different inertia constants in response to step power setpoint increase	150
7.26 SMES power at different inertia constants in response to step power setpoint increase	150
7.27 Frequency change at different inertia constants in response to step power setpoint increase	151
7.28 Battery power profile	151
7.29 Converter output power at different inertia and damping constants	152
7.30 SMES maximum power at different inertia and damping constants	153
7.31 SMES energy at different inertia and damping constants	153
7.32 VSG frequency response to a microgrid frequency drop with different damping constants applied in the frequency droop function	155
7.33 Converter output power at different damping constants in the frequency droop function in response to microgrid frequency drop	155
7.34 ESS power output at different damping constants in the frequency droop control in response to microgrid frequency drop	156

7.35 Converter output power in response to microgrid different frequency drop values with $T_a=6$ and $K_d=0.2$	156
7.36 ESS power supplied in response to a microgrid different frequency drop with $T_a=6$ and $K_d=0.2$	157
7.37 Lead-lag compensator cascaded with the measured microgrid frequency .	158
7.38 Converter output power at different cases; at case 1 $H(s)=1$, at case 2 $T_{Lead}=0.2$ sec, $T_{Lag}=0.4$ sec and at case 3, $T_{Lead}=0.1$ sec, $T_{Lag}=0.8$ sec .	159
7.39 ESS power at different cases; at case 1 $H(s)=1$, at case 2 $T_{Lead}=0.2$ sec, $T_{Lag}=0.4$ sec and at case 3, $T_{Lead}=0.1$ sec, $T_{Lag}=0.8$ sec	159
7.40 Converter output power at different damping constants for the parameters at case 2, ($T_{Lead}=0.2$ sec, $T_{Lag}=0.4$ sec, and $P_{PV}=0.4$ pu)	160
7.41 ESS power at different different damping constants for the parameters at case 2, ($T_{Lead}=0.2$ sec, $T_{Lag}=0.4$ sec and $P_{PV}=0.4$ pu)	161
7.42 General layout of VSG and conventional SG systems	162
7.43 VSG and SG active power step change at inertia time constant = 1	163
7.44 VSG and SG active power step change at inertia time constant = 5	164
7.45 ESS power at different inertia time constants	164
7.46 Frequency profile at inertia time constant = 2	165
7.47 Frequency profile at inertia time constant = 8	165
A.1 Permission from IEEE to reuse an article as Chapter 3 of this dissertation	211
A.2 Permission from IEEE to reuse an article as Chapter 4 of this dissertation	212
A.3 Permission from IEEE to reuse an article as Chapter 4 of this dissertation	213
A.4 Permission from IEEE to reuse an article as Chapter 5 of this dissertation	214

Nomenclature

AC	Alternating current
DC	Direct current
dq	Direct and quadrature
SG	Synchronous generator
ESS	Energy storage system
REs	Renewable energy resources
RoCoF	Rate of change of frequency
DERs	Distributed energy resources
VI	Virtual inertia
VSG	Virtual synchronous generator
VISMA	Virtual synchronous machine
BESS	Battery energy storage system
HESS	Hybrid energy storage system
SMES	superconducting magnetic energy storage
SoC	State of Charge
PV	Solar photovoltaic
DGRs	Distributed generating resources
MPPT	Maximum power point tracking
PCC	Point of common coupling
DGU	Distributed generating unit
EMS	Energy management system
MGCC	Microgrid central controller
DSO	Distribution network operator
MO	Market operator
WMN	Wireless mesh network

WLAN	Wireless local area network
OFC	Optical fiber cables
CRC	Cyclic redundancy check
RSC	Rotor side converter
WECS	Wind energy conversion system
DFIG	Doubly-fed induction generator
BDBBC	Bi-directional buck-boost converter
GSC	Grid side converter
PID	Proportional, integral, derivative
PCU	Power conditioning unit
LTS	Low-temperature superconducting material
HTS	High-temperature superconducting material
DOD	Depth of discharge
IT	Information technology
EMS	Energy management system
PLCC	Power line carrier communication
POI	Point of inteconnection
MMS	Manufacturer message specification
GOOSE	Generic object-oriented substation events
SMV	Sampled measured value
PLL	Phase locked loop

Symbols

ρ	Air density
A_r	Rotor swept area
v_w	Wind speed
C_p	Wind turbine power coefficient
β	Pitch angle
λ	Tip speed ratio
η	Efficiency
ρ_m	Density of water
g	Acceleration of the water due to gravity
ω_w	Wind turbine rotational speed
ω	Rotational speed of the synchronous machine
ω_g	Grid frequency
J	Rotor inertia
D	Damping coefficient torque associated with the damper winding in SG
K_d	Damping constant associated with the per unit damping power
T_a	Inertia time constant

Chapter 1: Introduction

Carbon dioxide emission is an environmental concern that have motivated governments and regulatory agencies to encourage utilities to embrace renewable energy resources (RERs). Furthermore, the looming shortage of conventional fuel resources has directed research and application of renewable distributed generation resources. This shift in power generation sources allowed microgrids to emerge. This study focuses on distributed generation resources applied in different types of microgrids. The intermittent nature of the renewable energy resources threatened the stability of microgrid operation. Hence, the proper design of the control systems is a vital issue and plays a noticeable role in the operation of microgrids. Control strategies based on hierarchical control levels will be described in this research. Communication systems are one of the main features of operating any power system, and they have a great effect on the operation and control of microgrids. A brief description about the communication media and protocols used for the microgrid control system will also be described in this dissertation.

Wind energy conversion systems are important renewable energy resources that are under continued research. This dissertation describes the design, control and modeling of a wind energy conversion system to implement in a microgrid. This includes the mechanical wind turbine and a doubly-fed induction generator. The wind turbine is combined with a battery energy storage system to overcome the intermittent nature of the wind speed. A doubly-fed induction generator is used in this dissertation due to its ability to operate over wide wind speed ranges and reduced converter power rating. The system is investigated under many operating scenarios to verify the controller operation and benefits of the battery system operation in parallel with the wind energy conversion system to enhance the reliability and dependability of the system.

The sun is the main source of energy in our global system. So continued research

activities are needed to efficiently capture that energy. This dissertation describes modeling, control of a solar photovoltaic system. Because of the intermittent nature of solar irradiation, an energy storage system is connected in parallel with the PV system. The proposed system includes a battery energy storage system with dc-dc and dc-ac controllers. Different scenarios are studied to verify the implemented controller of the proposed system. The control systems are modeled in the direct-quadrature (dq) reference frame for controlling the active and reactive power from the system, and they are simulated in PSCAD/EMTDC to verify the proposed system operation.

The recent changes in the network topologies due to increasing loads and distributed energy resources cause voltage variations. The power variation and reverse power flow phenomena may increase terminal voltage variations at the distributed energy resources. As the performance of the power network depends on the voltage profile, controlling the terminal voltage of the resources in the networks has great importance. A voltage control scheme within the inverter of a photovoltaic system is described. It controls the terminal voltage magnitude to be within acceptable ranges through injecting or absorbing reactive power. Also, the inverter prioritizes the active and reactive power based on the terminal voltage level and its power output and controls both active and reactive power independently. This scheme is regarded as volt/var control.

The conventional power converters for renewable resources work in the power system as grid following controlled current sources. The main function of these converters is to extract the maximum energy from the connected renewable resources. These converters are designed to be connected to a stable-frequency grid with the large rotating inertia of SGs, but these features are not available in a microgrid with high penetration of inverter based renewable energy resources.

The percentage of these inverter based renewable energy resources is expected to continue increasing over the next few decades. However, these resources aren't

dispatchable or stable resources, and their output consists of frequent power fluctuation which may cause grid power oscillation. This non-negligible share of electric power from the power converters with variable resources with respect to conventional synchronous generators could have a dramatic effect on power system stability.

Furthermore, these resources have low inertia and they tend to reduce the total system inertia. Hence, the power system may be vulnerable to stability problems in case of disturbance occurrence and may lose synchronism. To overcome the low inertia and stability problems, inverter-based resources are combined with energy storage to emulate the synchronous generator (SG) characteristics and act as virtual synchronous generators. This approach of control of power converters emulates the effects of the inertia of traditional synchronous generators. In addition, the controller can enhance the damping. Then, the converter controller improves the system stability, reliability, and power quality. Hence, they achieve a satisfactory operation of the power system.

This dissertation describes the general features offered by a virtual synchronous generator control strategy with mathematical models, controller design, and system performance is verified using electromagnetic transients simulation.

Emulating the features of the synchronous generator requires integrating energy storage systems (ESSs) with RERs in microgrid applications. Although ESSs aren't regarded as energy sources, they provide valuable benefits in microgrid operation. Since no energy storage system has all the required features, a hybrid energy storage system composed of superconducting magnetic energy storage and a battery is used to smooth the system's power fluctuations. The superconducting magnetic energy storage system is a high power density system and responds to high rate of change of power fluctuations. On the other hand, the battery provides high energy and responds to low-frequency and steady state power fluctuations. This hybrid system reduces the stress on the battery due to transients with high charging and discharging currents;

increasing its lifetime.

This dissertation describes general features offered by the hybrid energy storage system and derives the mathematical model and controller design. The system performance is verified using an electromagnetic transients simulation program.

1.1 Problem Description

1. Reduction of system inertia and damping results in fast high-frequency variation due to expanding inverter based renewable energy resources such as wind energy conversion system and photovoltaic system in power system.
2. Enhancement of the power system stability on a low inertia system is needed.
3. Creating virtual inertia is an option to increase the inertia of the system.
4. An energy storage system is needed to emulate inertia, provide damping, support grid frequency, or regulate the terminal voltage.
5. Developing an energy storage system that can provide fast power response and high energy capabilities to respond to fast and slow-frequency power fluctuations.

1.2 Objectives

1. Studying the microgrids architectures, control systems, and challenges in the microgrids.
2. Selecting and rating the system components and the distributed energy resources types (wind energy conversion system, solar photovoltaic system, batteries, and superconducting magnetic energy storage system).
3. Developing the mathematical models of the systems and their control systems in PSCAD/EMTDC simulation software.
4. Controlling the frequency and the voltage of the system through emulating vir-

tual inertia and damping using batteries and superconducting magnetic energy storage system.

5. Studying the effect of virtual inertia emulation constants on the energy storage systems sizes and their control algorithm.

1.3 Literature Review

The proliferation of inverter-based RERs such as wind and photovoltaic generation in the power system to replace the large-scale synchronous generators reduces the total system inertia and can destabilize the system. The grid becomes vulnerable to high-frequency fluctuations in case of large disturbances such as varying loads, changing the electric power generated from RERs or the distributed energy resources (DERs). Also, the power system is prone to voltage challenges that affect voltage stability.

Voltage stability is the ability of the system to keep the feeder and bus voltage magnitudes in the normal acceptable range after any contingency events. Voltage problems such as voltage rise, voltage drop, and voltage fluctuation can deteriorate the power quality. Furthermore, they may cause cascading tripping faults and stability issues such as fault-induced delay voltage recovery.

Several techniques are commonly adopted to solve the voltage variation problem. One of the used methods is to change the set point of the on-load tap changers on transformer. However, the frequent use of the tap-changers causes wears of the devices and reduces their capabilities to support voltage stability. Using capacitor banks may mitigate the terminal voltage fluctuations, but they lack flexible control because they provide reactive power in discrete values and use mechanical switches [1, 2].

The authors of [3, 4] used flexible ac transmission system devices (FACTS) such as static synchronous compensator (STATCOM) or static VAR compensator (SVC) to control the voltage stability in the system connected to photovoltaic or wind energy

generation systems. FACTS can control the voltage following disturbances such as load changes, generation changes, or faults through reactive power injection and absorption. On the other hand, FACTS are expensive devices to be used for providing smooth and fast responses to secure power systems during normal and steady-state operations.

The large penetration of RERs and gas turbines replacing the high-inertia conventional coal fired synchronous generators in the power system has negative effects on the system frequency and stability. The system may be prone to high values of rate of change of frequency (RoCoF) and low values for the frequency nadir after any sudden imbalances between generation and demands such as the loss of a large generating unit or large increase in loads.

Several researchers have explored approaches to overcome these problems. The authors of [5, 6] described a constant voltage-constant frequency control methodology that can maintain grid stability in isolated grids. On the other hand, this method has some drawbacks such as requiring communication and exchange of detailed data measurements which may lessen the system flexibility and scalability [7].

Also, the conventional technologies used for power generation such as communication-based [8, 9] and droop-based primary control methods [10, 11, 12] are not always capable of responding quickly enough to prevent unacceptably low frequency in contingency events, especially in large systems.

Since the DERs-based power converters are expanding in the power system, they should have significant roles in maintaining the stability of the system and controlling both the voltage and frequency. RERs as commonly controlled don't have the features of conventional synchronous generators such as inertia and damping constants, so the system stability is degraded. One of the best solutions to solve this challenge is to emulate the features of the synchronous generators in the controllers for power converters, which is known as grid forming inverter virtual inertia (VI),

virtual synchronous generator (VSG), or the other similar terms.

VI requires an energy storage system or operation of the wind or PV below the maximum power point to support the power fluctuation and compensate for the instantaneous difference between the inverter output power and the generated power. Moreover, ESSs can react rapidly to the big disturbances to supply or absorb energy, and so prevent excessive frequency variations. Furthermore, adding large ESSs help to make a RER act as a dispatchable unit that can generate power according to the required demand in the short term.

Converters controlled to provide VI with ESSs can aid frequency regulation and maintain transient voltage stability; thus, reducing the need for load or generation shedding. Moreover, the converters-based VI emulation can emulate synchronous generator characteristics that support the system requirements.

A significant research effort has been devoted to develop control methodologies for power converters to emulate the inertial features of a conventional SG. The inverters provide the grid with the emulation of rotating inertia which is called virtual inertia.

VI emulation control methods underwent several steps over the years. In [13], Beck and Hesse proposed an early control method for VI and it was called a virtual synchronous machine (VISMA). They implemented a current-controlled inverter in the dq reference frame using the Park's transformation.

The authors of [14, 15] implemented a simple model to emulate inertia and damping using the swing equation of a synchronous machine, and called it a virtual synchronous machine (VSM). The control method is based on generating the reference control voltage from the outer loops, getting a real power command from the VI emulation and a reactive power command, and using them in PWM signal formulation. Although this method is simple to model, it is complicated to protect the controller from high currents in case of disturbances or faults.

In [16], the authors overcame the previous disadvantages by applying the generated

reference signals from the outer loops to an inner control structure which consists of cascaded voltage and current controllers. In these inner loops, the controllers' current and voltage references can be limited and protected against disturbances such as fault currents. This methodology is called a synchroverter, which can be summarized as a voltage-controlled voltage source inverter emulating conventional SG.

The authors of [17, 18, 19] proposed control methods called virtual synchronous generator which can emulate the inertial performance of SGs. Some of them were implemented as a current-controlled inverter such as VISMA, others work as a voltage-controlled inverter like the synchroverter. VSG emulates and enhances the conventional generator inertia and damping characteristics and also enables the inverter to operate in both grid-connected and isolated modes. Moreover, VSG parameters can be adjusted to emulate any arbitrary SG without any constraints to match a specified SG and can be easily adjusted without affecting the Park's equations that represent system modeling [18].

Each topology of VSG has its advantages and disadvantages. The most common topologies that are introduced worldwide in the VSG field are the VSYNC project under the 6th European Research Framework Program, the Institute of Electrical Power Engineering (IEPE) at the Clausthal University of Technology in Germany, the VSG research team at Kawasaki Heavy Industries (KHIs), and the ISE Laboratory in Osaka University in Japan. The main features of these topologies are described briefly in [20, 21, 22].

Energy storage systems are the main part of VI emulation topology. Many different types of ESSs are viable to be added to VI emulation systems. One of the most commonly used types in ESSs is the battery energy storage system (BESS). Batteries have many advantages such as high energy density, high efficiency, long lifetime, and low self-discharge. BESSs can be used in power system applications to enhance power quality and management, and smooth the long-term power fluctuations in microgrids

[23].

On the other hand, batteries have some disadvantages that make them unable to achieve all the system requirements. They have a slow response time, limited voltage and current ratings, and low power capacity. Hence, BESSs can't respond rapidly to the fast disturbances in power systems. Furthermore, many battery chemistries have a poor cycle life so the number of both charging and discharging is limited. Moreover, the deep frequent charging and discharging processes can shorten the battery lifetime. In addition, some environmental hazards may be caused in the disposal of their hazardous materials.

To address the limitations of the batteries and improve the operational performance of the power system, a hybrid energy storage system (HESS) has been proposed. The authors of [24, 25] described the different types of ESSs, their contributions in HESS, and their effect in improving power system operation. HESS can be implemented to provide high energy and power capabilities and rapid response times. Hence, they can address different transient disturbances, smooth the power flow, and improve system stability and operation. Plus the HESS reduces battery cycling and the stresses due to large charging and discharging currents over transient periods, improving battery lifetime.

Various types of ESSs can be integrated with RESs in microgrids or large grids in a HESS. The most common energy storage types are batteries, pumped storage hydroelectric systems, flywheels, supercapacitors, and superconducting magnetic energy storage (SMES). The authors of [25] summarized these ESSs and their usage in microgrids in detail.

Supercapacitors and SMES are competing with each other because they have comparable advantages such as a high power density, long lifetime, high speed response, high efficiency, and good cycle life. However, supercapacitors have many disadvantages. A supercapacitor is a series of capacitor cells with a voltage range limited to

2.5-3 volts. This series connection is inevitable to obtain the required voltage, but it reduces the total capacitance. Moreover, a protection circuit should be integrated with the system to protect the cells from overvoltage and non-uniform cells problems. Furthermore, step-up and step-down converters are required to match supercapacitor voltage with the power system voltage. The converters have a complicated design, since the stored energy varies with square of the stored voltage, complicating the converter control of the charging and discharging processes.

The authors of [26] stated that SMES is one of the best ESS among the different ESS options. It can address short-term transient power fluctuations and it can overcome the supercapacitor disadvantages.

In this dissertation, SMES will be used in conjunction with a battery system to form a HESS for providing the inertial features emulating a conventional synchronous generator. In case of disturbances or a transient difference between the generated power and the load, the power converter combined with HESS handles this disturbance emulating the conventional SG. This dissertation focuses on emulating the inertial features of a conventional SG. In addition, this dissertation will compare the effects of inertia constant selection and damping coefficient selection as rating power and energy for the HESS subsystems. This dissertation also, describes how these constants can affect the system's performance.

Questions remain about the coordination between the two ESSs, as well as what the state of charge (SoC) limit be for each ESS where the controller should disconnect this ESS.

The proposed controller in this dissertation can emulate the inertial features of conventional synchronous generator, control each ESS in the HESS, monitor their SoC, and operate them within their normal and safe regions. Simulation of the proposed control methodologies to demonstrate the system performance is carried out using PSCAD/EMTDC simulation software.

The dissertation is organized as follows. Chapter 2 presents a literature review about microgrids and their control schemes. Chapter 3 describes the wind energy conversion system, the modeling of the different subsystems, the design of the proposed controller, and the simulation of different scenarios using an electromagnetic transients simulation. Chapter 4 describes the PV system, modelling of the different subsystems, and the controller design. Also, a proposed control strategy is described. The system performance at different scenarios is verified using electromagnetic transients simulation. Chapter 5 describes the VI emulation method and the proposed controller design. The performance of the VI emulation system is described in Chapter 6. Also the effect of different values for the damping and inertia time constants on the system performance is studied. A HESS composed of a battery system and SMES system is described in Chapter 7. The performance of the different subsystems and control design options are also demonstrated. Furthermore, the proposed controller is verified by comparing its operation with a conventional synchronous generator. Finally, summary, conclusions and future work are presented in Chapter 8.

Chapter 2: Literature Review about Microgrids and Their Control Schemes

2.1 Introduction

Increasing population and increased economic development have increased electrical power demand; furthermore, concerns about climate change has led to government policies to encourage utilities to adopt clean and renewable energy resources for supplying the power demand. The percentage of penetration of renewable energy resources in the grid is expected to increase by 2050 to 20% - 50% in Europe and to 42% in USA. Moreover, government policies have motivated a lot of investors and players in the power market to build small-scale energy resources.

The outstanding types of renewable energy resources are solar photovoltaic (PV), wind, fuel cells, hydro, and biomass. The increasing number of affordable small generating units of diverse generation types made microgrid concepts feasible. However, the shift from a central conventional power plants to distributed ones with power converter interfaces creates many challenges which can be solved by applying microgrid concepts.

The conventional central power plants are implemented with large capacity synchronous generators and the electric power is transmitted through the transmission lines to the load centers. Hence, the conventional power plant schemes have transmission power losses and lesser efficiency. On the other hand, in microgrids, the energy resources are implemented nearby the loads, so the transmission power losses are eliminated, which increases the efficiency of the system if the DERs are as efficient as large generators.

However, microgrids have some challenges that should be overcome such as maintain power balance and maintaining stability. In many cases, an energy storage system is desired for keeping both voltage and frequency fluctuations within an acceptable

range.

Selecting the microgrid type is affected by many factors such as geographical location, load types, and connection to the main grid. Most utilities support implementing an ac microgrid. This is done to exploit the implemented infrastructures which are predominantly ac. Also, most vendors and market players usually provide ac products. Moreover, most of the loads on the power systems are ac. Furthermore, connecting synchronous generators in wind and hydropower to an ac microgrid is more economical and practical [27]. However, controlling the frequency, phase shift issues using power converters are challenging in an ac microgrid. These drawbacks directed some researchers to explore dc microgrids. As PV power plants are becoming more dominant in microgrids along with the use of hydrogen fuel cells encourages prioritizing dc microgrids [28].

The intermittent nature of renewable energy resources causes voltage fluctuation and stability issues, which needs to be solved by adding ESS in an ac or dc microgrids, even if it is at the expense of the cost.

The key elements in the microgrid are voltage, frequency, and power. RERs such as wind and PV are dependent on weather conditions, and their intermittent nature creates threats for load balance and hence voltage and frequency. This fluctuation has directed the researchers in this field to pay more attention to developing and designing control systems. A solid controller is mandatory to counter the non-synchronous nature of many RERs, and so consistency and stability of the power system can be maintained. Also, sharing the power among the distributed generating resources (DGR) is an important function of the controller in a microgrid. The controllers should guarantee proper performance of the microgrid in isolated and grid-connected operating modes and handle any abnormal circumstances. With the growing number of generators, utilities advocate exploiting distributed control strategy rather than a centralized controller. The distributed controller offers some advantages for the

system such as reducing the local energy management problems and the challenges of housing data storage in one place which enhances privacy and security. Furthermore, a single point of failure problem is eliminated [29].

Communication media between controllers and resources are essential in microgrids. The distributed nature of elements in microgrids requires more communication and a more complex network for data acquisition and control of the microgrid elements. Also, microgrid communication and information exchange systems are fundamental for improving the reliability and efficiency of the microgrid.

This chapter is organized as follows. In Section 2.2, distributed generating resources are described. Types of microgrids are discussed in Section 2.3. Section 2.4 describes the control strategies based on hierarchical control levels and different control schemes. Communication media and protocols used in microgrids are described in Sections 2.5 and 2.6 respectively. Finally, in Section 2.7, a summary is presented.

2.2 Distributed Generating Resources

It is expected that there will be about 16% of the people in the world without electricity by 2030 [30, 31], and their needs for microgrids should be met. So microgrid with small cost effective local generation sources has attracted great interest and is increasing rapidly. Determining the best generating resources type for DER relies on many factors such as geographical location and environmental conditions. Generation available for microgrids includes solar, wind, biomass, and hydropower combined with natural gas and diesel generator sets [32]. These generating resources can be categorized as synchronous and nonsynchronous sources. The synchronous sources such as conventional diesel generator sets and hydro-generators can be used for controlling the microgrid against power fluctuations and stabilizing the microgrid under disturbances [33]. On the other hand, the nonsynchronous sources such as solar and

wind, due to their intermittent nature, have unpredictable generation output and lead to a reduction of the system inertia. Because of the irregular nature of solar and wind power, energy storage systems can be combined with the generating sources in microgrids or a large national grids.

2.2.1 Solar Photovoltaic Systems

The sun can be regarded as the best source of energy, it is clean and ubiquitous. Also, the advancement of power electronics allowed solar energy to gain greater interest. Using modern power electronics enables the output voltage to be increased using boost converters, converted from dc to ac using inverters, and reduced undesired harmonics.

Application of PV in microgrids has increased in the literature, because of its advantages such as its sustainability, carbon free emission, potential long lifetime, silent operation, and low maintenance cost. Though PV is mostly used in conventional transmission and distribution systems, it has some disadvantages such as high installation cost, low efficiency, intermittence, environmental conditions dependent. These challenges increase in microgrids. Like any generation, PV needs a lot of site studies before installation [34]. The variable nature of solar insolation during the day requires maximum power point tracking (MPPT) techniques for obtaining the maximum power during different times of the day and weather conditions. The authors of [35, 36, 37] described different techniques for MPPT that can be exploited for PV systems. Also, due to the intermittent nature of solar energy, many papers suggest energy storage be combined with the PV system. Although still limited in practice, use of energy storage is growing rapidly.

PV arrays consist of several parallel and series combinations of cells to produce the required voltage and current. The cost of the PV system is size-dependent. PV

systems have many applications that depend on the size, ranging from the rooftop to utility-scale PV power plants. One of the cumbersome issues in the PV industry is the sizing of the plant; design a plant producing acceptable energy with a good power reliability at minimum cost. In [38, 39], the authors described some artificial intelligence techniques for sizing PV systems.

2.2.2 Wind Power Plants

Wind energy has long been considered a promising energy sources to use. Improvement in material and power electronic controls has led to explosive growth all over the world. Research and development in the USA, China, and Europe are increasing the size of onshore and offshore wind turbines at a reduced price; consequently, 9.5 MW wind turbines have become commercially viable in many countries [40]. Wind energy has some advantages that make it preferred such as being pollution-free, and having no fuel cost. Though they spread over a large area, the footprint of individual wind turbines covers a small portion of the total land, and the rest of the land is still viable for farming and animal husbandry applications.

Wind energy conversion systems (WECS) transfer the kinetic energy in the wind to electrical energy. This is done in two steps; the kinetic energy is converted to rotating mechanical energy through the wind turbine blades and then the mechanical energy is converted to electrical at the generator. The output mechanical power from the wind turbine can be derived from the following equation [41].

$$P_m = 0.5 \rho A_r v_w^3 C_p(\beta, \lambda) \quad (2.1)$$

where ρ is the air density in kg/m^3 , A_r is the rotor swept area in m^2 , v_w is the wind speed in m/sec and C_p is the power coefficient of the turbine. The power coefficient depends on the pitch angle β and the tip speed ratio λ . It is shown in (2.1) that,

the output power depends on the cube of wind speed, so a slight variation in wind speed may result in a dramatic change in the output power. Hence, selecting the placement of the wind plant and individual turbines in that plant is an important matter for exploiting wind energy potential. The preferred locations for the wind turbines are offshore and high latitude, where the wind speed is higher and generally has a constant value.

Wind turbines may be classified as vertical or horizontal axis wind turbines. A comparison and details between them is provided in [42, 43]. Wind turbines can be designed to be a single standalone power turbine or a combined in a wind farm that has an output power that varies from a few MWs to hundreds of MW. The layout of the wind turbines in the wind farm is a important application matter. In [44, 45, 46], the authors presented optimal solutions for the placement of wind turbines in wind farms.

WECS can be classified as a fixed speed generator system such as a squirrel cage induction generator or a variable speed such as a doubly-fed induction generator or permanent magnet synchronous generator. In [47, 48], the authors described the performance of each type and provide comparisons between them.

Although wind energy has a lot of advantages that make it a promising energy source, it has some disadvantages such as noise creation and the intermittent nature of wind. Due to the variable nature of the wind speed, MPPT techniques are used to capture the maximum output power from the system at agiven wind speed. In [49, 50], the authors described the most used MPPT techniques in WECSs.

2.2.3 Biomass

Biomass is one of the broadest energy sources. It uses a biological material that is produced from living organisms such as animals and plants. Sugar canes and cotton

crops example plants that are used for making the biomass. Also, the remains of wheat and rice can be used. After harvesting processes, the leftover leaves, straws, stalks, and roots can be used for making biomass. In some areas, farmers were removing these remains by burning them, which loses massive energy resources and pollutes the environment by releasing a huge amount of carbon dioxide, carbon monoxide, sulfur dioxide, and nitrogen oxide [51].

Biomass is an encouraging source of renewable energy because it is potentially carbon pollution-neutral resource. Also, it helps to get rid of some garbage, animals wastes, and agriculture leftovers, but it requires a large portion of land and water. Growing crops exclusively for biomass energy generation requires energy, often in form of fossil fuel. More research and development is required to reduce its cost and increase its efficiency [52]. Biomass is burnt for steaming water to drive prime mover for generating electricity, or it can be used for heating homes and buildings. The authors of [53, 54] presented technical and economical investigations of the potential for using biomass for electrical power generation in microgrids.

In addition to biomass, biofuel and biogas have attracted a interest in transportation systems and some interest for power systems. Biofuel can be generated from the plants in the form of used or new vegetable oil. Vegetable oil fuel can be used as a source of energy for diesel engines. The exhausts of the engines fueled by biofuel are less harmful to the environment compared with the use of conventional diesel fuel.

Biogas can be made from biomass or biofuel such as agriculture waste, manure, sewage, plant material, green waste, or food waste. The material go through anaerobic digestion and fermentation processes. Biogas comprises mainly of methane and carbon dioxide. Biogas can be exploited in heat and power generation, extracting energy from processes that will release green house gases in any case and avoiding production of more gases. Due to its controllability, biogas may be used in generating electric power in a microgrid, and also the development of the main grid. The authors

of [33, 55] presented the usage of biofuel and biogas in microgrid applications.

One of the important matters in biomass is making it economically competitive without subsidies. The authors of [56, 57] proposed linear programming models to determine the optimal biomass production and supplies allocation which results in the lowest cost to meet electricity demand.

2.2.4 Hydropower System

Hydropower systems extract the energy in water from oceans and rivers and converts it to mechanical or electrical energy. There are several forms for generating electric power from water. The most common forms are through flowing water and falling water using dams as described in [34, 58]. As the water has a high density, a slow-flowing stream of water can generate an ample amount of energy. It can be a reliable source for energy production because it has many advantages such as being pollution-free and having a low operating cost. Moreover, the water doesn't change on a time scale of minutes to tens of minutes like the sun or the wind and it may have a high efficiency if it is designed and implemented precisely. In [58, 59], the authors described methodologies for the design and implementation of hydropower systems. On the other hand, this system suffers from some drawbacks. It is geographically dependent and the variation in water due to inconstant rainfall during the year seasons. This affects the output power in some areas and energy especially in dry seasons [60].

In some cases, a portion of the water goes through channels to drive turbines or water wheels to provide mechanical power, which is used for driving electrical generators. The output mechanical power from the water can be derived as [61]:

$$P_{mech} = \rho_w g H Q \eta \quad (2.2)$$

where ρ_w is the density of water, g is the acceleration of the water due to gravity, H

is the head height of the water, Q is the volume flow rate that passes through the turbine and η is the efficiency of the turbine. The extracted mechanical power can be controlled by regulating the turbine flow rate to meet the variation in load, and a detailed description of the output generated power from the hydropower system is described in [62].

Some microgrids use micro-hydropower systems, especially in standalone systems. A small hydro system, less than 100 kW, doesn't use governor control-based turbine prime mover and this reduces the cost and makes the system economically competitive. Many generator types may be used in this system. The most commonly used type is a self-excited induction generator as presented by the authors of [63]. Details about the variant types of generators are described in [64, 65, 66]. The authors of [67, 68] proposed models for the hydro system in the microgrid. One of the important matters in the hydro system is its sizing. The authors of [69, 70] presented the optimal sizing for the hydro systems in microgrids.

The non-hydro renewable energy resources listed above suffer from intermittent nature which affects the stability and inertia of the grid. Hence, in many cases, they are combined with a diesel or natural gas generator set or other energy storage devices in remote applications [71, 72]. The diesel provides a controlled power output for the system where it compensates for the difference between the load and the generated power from the renewable energy resources. The load following ability and high inertia of the diesel generator set allows it to respond well to transient load changes and softness the intermittent nature effects of the renewable resources. The authors of [73, 74, 75] propose using wind or PV with diesel for improving the stability and performance of the system. Many other studies propose using ESSs in conjunction with renewable energy resources in microgrids [76, 77].

2.2.5 Energy Storage Systems

Although ESSs increase the cost of the system, they are important in microgrids, especially if the microgrid has sources that have a large time constants for changing output to achieve system load balance in case of system disturbance or load change. When the loads change, the system frequency varies depending on the size of change in load. So ESSs are required to balance the difference between the load demand and the generated power in case of load change. Hence, they stabilize the microgrid frequency fluctuation due to load variation [78].

In the case of islanded operation of a microgrid, an ESS is recommended for balancing both active and reactive power due to irregular behavior of wind and PV based renewable sources, especially those operate at unity power factor where the storage control the voltage and frequency. On the other hand, in the case of grid-connected operating mode, the frequency is controlled by the hosting grid, and ESS is only needed for improving power quality and regulating local reactive power or voltage magnitude [79].

The wind and the sun's power can't be stored, and it is desirable that the maximum amount available should be extracted at all times. ESS can be used to store power during off-peak hours to be exploited later to supply the demand loads [78].

There are several types of energy storage systems; electrochemical such as batteries, mechanical such as flywheels and compressed air ESS. Other types ESS are capacitors, superconducting magnetic energy storage, or thermal ESS. The most used types are batteries and capacitors [33, 80, 81]. SMES has long been considered a promising ESS device, so a brief discussion is presented in the following subsections. The authors of [82] described the best choice of ESSs for the different applications. Others propose to use hybrid ESS in microgrids [25, 83]. The authors of [78, 84, 85] presented a detailed review about the different types of ESS. Challenges and trends

of energy storage systems are described in [83, 86, 87].

2.2.5.1 Battery Energy Storage System

Batteries are the most used ESS in power system applications. Batteries store the energy as a charge in electrochemical cells during charging and this energy is converted to electric energy during the discharge process. These processes are performed through a chemical reaction. Batteries can be used to store the energy at low demand periods and deliver this power at the high demand times. The required voltage and current of the battery system are achieved by parallel and series connections of the different cells [88].

Although batteries increase the cost of the system, they have some advantages that make them viable in microgrids such as low maintenance requirements, environment-friendly, and flexibility in modularity. Furthermore, they can be dispersed geographically at the load centers [89], and can provide distributed assistance in load leveling and frequency control.

The most commonly used batteries are lead-acid, nickel-cadmium (Ni-Cd), sodium-sulfur (NaS), and lithium-ion (Li-ion) batteries [89]. A comparison between all types of batteries and their application is detailed in [90, 91]. Battery sizing plays a significant role in the operation and performance of microgrids. The authors of [92, 93] presented the sizing, design, and operation management of battery ESS in microgrids.

2.2.5.2 Supercapacitors

Supercapacitors are also referred as ultracapacitors. Supercapacitors charge and discharge fast. Also, the frequency of charging and discharging maybe hundreds or thousands of times [94].

Supercapacitors are constructed from two-conductor electrodes, an electrolyte and

porous membrane that allow ion transfer between the two electrodes. Its arrangement forms two electrodes; electrolyte-positive electrode and electrolyte-negative electrode, so they are also called double layer capacitors [81, 85].

The capacity of the capacitors depends on the electrode surface area and the distance between the two conductor electrodes. The energy stored in capacitors depends on the capacity and the voltage. The desired total voltage and capacity are attained by parallel and series combinations of cells. The authors of [95, 96] described the design and sizing of a supercapacitor as ESS for microgrids.

Supercapacitors have some disadvantages such as relatively high cost and the need for protection circuits for voltage balancing to protect the cells from overvoltage. Also, dc-dc converters are used to match the supercapacitor's output voltage with the system voltage magnitude prior to inversion. On the other hand, supercapacitors have many advantages such as high-power density and fast charging and discharging rates possibly within seconds. In addition, supercapacitors have a long lifetime, low-temperature performance, have a wide operating temperature range, and are considered environment-friendly devices [97, 98]. Supercapacitors can be used to relieve the load or RERs variation in the grid and can respond to transient disturbance conditions. Also, supercapacitors storage system can compensate for the difference between the load demand and the available power with a quick response. Hence, supercapacitors are superior ESS in microgrid different applications that require fast, high power response and low energy transfer [99].

2.2.5.3 Superconducting Magnetic Energy Storage

SMES has many advantages giving them the potential to be ideal ESSs in power system applications. SMES has many advantages such as a low-self discharge rate, high power density, and an unlimited number of charge and discharge cycles. More-

over, it is easy to control and has high round trip efficiency. SMES can address high peak currents needed to damp power oscillations and improve the system's stability and operation. SMES is used for controlling both the active and reactive power, and as a result the voltage and the frequency of the system. The authors of [83, 86, 100] described that the SMES system can be used for load leveling, power quality improvement, frequency regulation, automatic generation control, and power system stability improvements. Also, they presented a complete description of the different subsystems in the SMES system.

Although the SMES system is proposed in power system application to improve stability, it has some drawbacks such as high cost and coil sensitivity to temperature variations. But, the continuous research and developments in the SMES systems have reduced cost and improved reliability.

2.3 Types of Microgrid

Microgrid design is affected by many factors such as its geographical location, the available generating resources, and load types. The type of microgrid defines its operation and strategies for management and control systems. Microgrids can be classified as ac, dc, and hybrid ac-dc microgrid. The selected type of implementation would depend on many factors such as economic, technical, and environmental [101, 102, 103].

2.3.1 AC Microgrid

The most predominant type of microgrids is ac because it offers solutions for some problems of the conventional grid and connects the resources directly to the utility grid using some of the existing implemented infrastructures. As a result most research and development work has focused on the ac system. Also, the players in the electric

market have been providing ac products that can be connected directly to the ac grid [27, 102]. In an ac microgrid, the main bus is ac and the microgrid is connected to the utility grid at the point of common coupling (PCC). All the resources and the loads are connected to the ac bus through power electronic converters. AC microgrids have many merits such as the easy connection of ac generators in wind and PV set to the ac bus system. In [104], the authors described the advantages of ac microgrids in detail. Also, the voltage level can be stepped up or down easily using conventional transformers. Moreover, the protection devices in ac system are more established and viable than those for dc systems. In addition, the maintenance cost of the ac microgrid more economical than for the dc microgrid [105]. Conversely, ac microgrids have some challenges such as controlling the grid voltage and frequency and synchronizing the different resources with each other and with the utility grid. These challenges are presented in detail in [27, 104, 105].

2.3.2 DC Microgrid

The development in power electronics and increasing use of enduse dc loads such as in information technology (IT) applications and LED lighting, has gained dc distribution system and microgrids more interest and research. Hence, the manufacturers started developing dc systems to supply such loads and connect renewable energy resources-based dc generation [28, 104].

In dc microgrids, the main bus is dc and both the sources and loads are connected to the dc bus through power electronic converters. A dc microgrid is connected to the utility grid through a power electronic interface. The different voltage levels can be attained using dc/dc converters. Use of dc microgrids has some challenges such as voltage support, good power-sharing performance, fault detection location and clearing. These challenges' details and their solution are discussed in [10, 106, 107].

On the other hand, the dc microgrid has many advantages which make it competitive. A dc microgrid doesn't need synchronization or frequency control, making control simpler. Renewable energy resources such as PV, fuel cells, and battery energy storage systems supply dc power, which makes the connection to a dc microgrid simpler. This reduces complexity of power electronic converters, and so saves cost and increases the system efficiency. Furthermore, dc microgrid power quality problems relating to frequency deviation and reactive power balance are eliminated [108].

2.3.3 Hybrid AC/DC Microgrids

There are two buses in the hybrid microgrid. An ac bus is connected to both ac loads and sources and a dc bus is connected to dc side devices. In this configuration, the ac and dc devices are connected to the grid with a minimum number of power electronic devices [109]. Although management strategies and power flow among all the resources that are distributed in the two types of sub-grids are challenging, this combination provides the advantages of both ac and dc microgrids such as reduction in the total cost and energy losses, which increases the efficiency of the system. The authors of [110, 111, 112] reviewed some strategies for power management and control in hybrid microgrids.

2.4 Control Strategies Based on Hierarchical Control Levels

The intermittent nature of the renewable energy resources connected to microgrids has a dramatic effect on the power quality. Hence, a decent control system should be accomplished to enhance the power quality, and so ensure reliable, secured, and stable operation of microgrids.

The controller objective depends on the microgrid mode of operation. In a grid-connected mode, the voltage and frequency are forced by the host grid, and the key

function of the controller is to regulate the output power of the DGRs. On the other hand, in isolated mode, the controller has to control the voltage and frequency as well as manage power-sharing. Because of the small inertia of the microgrid, a small change in the system may cause a considerable change in frequency and voltage [113]. Hence, the control system should provide the following functions [113, 114]:

- Handling the uncertainties in the output of generating units and load variations.
- Active and reactive power balancing.
- Independent control of both active and reactive power.
- Detecting isolated and grid-connected operating modes.
- Regulating both the voltage and frequency within safe operating margins.
- Allowing scalability of the power system through adding new resources, protection, or measurement devices.
- Autonomous operation of microgrid and handling the voltage sags in case of disturbances.

The control system in microgrids can be categorized into three levels; primary control, secondary control, and tertiary control [115, 116]. Fig. 2.1 describes the difference between the three types of control.

2.4.1 Primary Control

Primary control can be considered as the base control in the microgrid. It is named as the field or local control. It is the fastest controller among other levels of control, its response may be a few milliseconds [117]. It is local to each DGR in the microgrid. The function of the primary control can be briefly listed as the following [113, 11]:

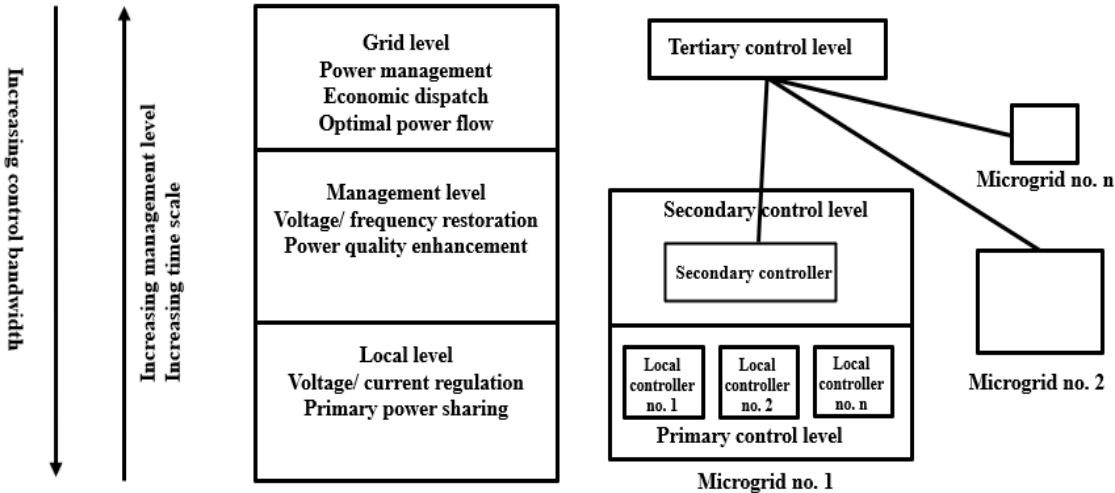


Figure 2.1: Hierarchical control levels in microgrid

- Detect the islanding of the microgrid and control the output of the converters.
- Provide a stable operation for the DGRs.
- Regulate the voltage and frequency of the DGRs which helps in limiting the circulating currents between them.
- Contribute descent sharing of active and reactive power among the different generating units which helps to improve the stability of the system.

The primary control has a very limited communication system which results in a simple implementation and lower cost. In general, the generating resources are connected to the microgrid through power electronic interfaces, which commonly is a voltage source converter (VSC). VSC in microgrids have two common control schemes in the literature; inverter output control and power-sharing control. They will be summarized in the following subsections [118].

2.4.1.1 Inverter Output Control

Inverter output control is usually responsible for regulating the inverter output voltage and frequency. In many papers, the inverter operates as an uninterruptible power supply (UPS). Control usually consists of two main loops; the inner current loop and the outer voltage loop. Controllers such as proportional-integral (PI), proportion-integral-derivative (PID), or proportional resonant (PR) provide acceptable results in controlling both the voltage and the current [11]. There are different reference frames used to implement these control systems such as a synchronous direct and quadrature (dq) frame and a stationary α - β frame. The commonly used frame is the rotating dq reference frame, the comparison between different types and advantages of the dq frame is presented in detail in [119, 120, 121].

It is common for the designer to embed the inverter output control in the inverter itself, which means it is not accessible by the customers or the utilities that use the generating units. The controller can only receive set points to produce the desired output. Other authors of [122] proposed a different method at which the inverter is based on a synchronverter, such that the inverter is controlled so that its response resembles a synchronous generator (SG). This model is derived from the synchronous generator, and this enables the inverter to be compatible with the conventional SGs in the microgrid. This helps to increase the system inertia and control the system frequency and so maintain system stability. This concept is known as the virtual synchronous generator control.

2.4.1.2 Power Sharing Control

Power-sharing control is responsible for controlling the output active and reactive power of the generating units while maintaining both the voltage and frequency in safe operating regions [123]. It uses the droop technique at which the controller mimics the

droop characteristics of the conventional SG, and the voltage and frequency regulation is done according to active and reactive power curves (P-f and Q-V) [11]. This permits parallel acceptable operation of many operating units, such that the frequency reduces when active power demand increases [124, 125].

Power-sharing control techniques implementation depends on the generating unit. When the generators are a synchronous type like diesel-generator set or gas turbine prime mover, then the droop methods are viable to them. On the other hand, if they are a non-synchronous type such as PV or wind type, then adaptive control techniques are an alternative control techniques [125].

Droop methods have many advantages such as flexibility, reliability and lower engineering cost. On the other hand, they have some drawbacks such as having challenges in distribution systems that have a high resistance to reactive ratio, since droop methods are more efficient in highly inductive systems. Also, droop methods have poor power-sharing between inverters based DGRs and affect both the frequency and voltage while adjusting the active and reactive power. In addition, they are not efficient with non-linear loads [11].

Due to these drawbacks, modified droop methods were developed such as the virtual impedance method, adaptive droop method, angle droop method, virtual inertia-based method, virtual frame transformation, and signal injection method. The authors of [11, 113] provide a comparison between these different types and list the advantages and disadvantages of each type. The state of charge-based adaptive droop techniques can be used for controlling the energy storage systems [84, 125]. Furthermore, non-droop-based techniques can be used to control DER units to maintain the system voltage within a permissible range [11].

The primary control schemes have some problems with producing the best global to a voltage or frequency deviations that may be caused by variation in the loads or the intermittent output power of the RERs. Unfortunately, the battery energy

storage system can't completely compensate for this frequency deviation nor provide the required load frequency control if they have limited storage capacity or rating ability [11]. A secondary control system is required to counter the drawbacks of the primary control to provide secure, economical, and reliable operation of the microgrid.

2.4.2 Secondary Control

Secondary control should be capable of operating in either a grid-connected or isolated mode of operation. It can be regarded as the energy management system (EMS) for the microgrid that sends the setting points to all the local controllers of dispatchable DGRs and restores the frequency and voltage magnitude to their normal operating values. The secondary controller is slower than the primary controller to avoid conflict with the primary control and allow more complex calculation to be done at the hierarchical level and curtail the bandwidth needs for the communication system [126]. The secondary control can be developed in centralized, decentralized, or distributed control [8, 127]. These options will be described in the following subsections. Whatever controller architecture is chosen, it should achieve the following functions [11, 33]:

- Voltage and frequency restoration: When a disturbance occurs, the voltage and frequency may vary from their reference values. The secondary controller compensates for the voltage and frequency variation to restore voltage and frequency to their set values. The authors of [128] used the secondary control scheme for both voltage and frequency restoration in autonomous microgrids.
- Synchronization with the utility grid: The secondary control synchronizes the microgrid with the utility grid; voltage, frequency, and phase shift. The synchronization algorithms depend on the control scheme of the microgrid. In [129], the authors proposed synchronization methods for microgrids.

- Load shedding in case of emergencies: In case of emergency events such as loss of generation or increasing incredible loads, the control system should be able to stabilize the system by generating extra power to the grid. Sometimes, the available generation in the microgrid may be insufficient for supplying the loads especially upon transition to islanded mode, so load shedding should be initiated for avoiding blackout. The load shedding algorithm should be robust, fast to prevent the occurrence of undervoltage, under frequency, and avoid shedding extra unnecessary loads [130]. The authors of [131, 132] proposed algorithms for load shedding by the secondary control to guarantee a reliable operation of the microgrid.
- Black start restoration: Blackout restoration is the ability of the grid to return to its normal operating condition after the event of a blackout. Microgrids should be able to withstand blackout events. But if this occurs, they should be able to restore to their normal operating condition independently without relying on other grids. In [133, 134, 135], different methodologies and energy management systems for microgrid restoration after blackout are described.
- Forecasting of generation and loads: The secondary controller sends the reference set points of active and reactive power for the local controllers, especially if the generating resources operate in P-Q mode. Hence, it is crucial to forecast the generation in the microgrid. RERs are the main resources in the microgrids, and their output depends on the environmental conditions [136], so forecasting techniques exploit atmospheric and historical databases and computational models for estimating the generating power. Load forecasting depends on environmental conditions, load types, times of day, and times of year [137]. Load forecasting is essential for balancing the generation with the loads, and accurate forecasting techniques guarantee a decent balance between the generation and

loads [130].

The architecture of the secondary controller can be categorized into centralized, decentralized, and distributed control. Distributed control can be considered as a combination of the first two types, and a complete description of these types is presented in [8, 127]. Fig. 2.2 shows the key differences between the three types.

2.4.2.1 Centralized Controller

Variations on centralized control schemes have been used for many years in the utility grid. The centralized secondary controller depends on the microgrid central controller (MGCC), which uses a bidirectional communication system between the different devices in the microgrid including generating units and loads. The controller collects all the information such as measurements, and states of the microgrid. Using these values, the secondary controller generates the reference set points for the local controllers.

A centralized controller is applicable for both grid-connected and isolated modes of operation. In the grid-connected mode, the controller operates in power control mode. It uses the grid voltage and frequency as a reference for the microgrid and compares the actual values of active and reactive power with the reference values, and so regulates the output of the distributed generating units (DGU). On the contrary, in isolated mode, the controller can't receive any reference values from the grid [125].

One of the main disadvantages of the central controller is that it forms single point of failure, such that a failure in the central controller may affect the operation of the whole microgrid so a redundant controller is needed. Moreover, changing the microgrid architecture may require redesign for the controller system. In addition, a high bandwidth communication system is required. In addition, unless properly designed, it may not handle nonlinear loads properly [138].

Different centralized approaches may be used in microgrids such as the optimal dispatch approach, non-model-based approach, bidding, and model predictive approach. The authors of [11, 139] presented a description of these approaches and the differences between them.

2.4.2.2 Decentralized Controller

Some of the drawbacks of the centralized controller can be overcome by using the decentralized control system, where each unit in the microgrid is controlled by the local controller [29]. The decentralized controller has the highest level of independent operation of DERs and loads in microgrid, especially where in isolated mode of operation. The decentralized controller generates the reference set points for the different generating units based on the local measurements. The communication system here is simpler than the centralized controller since there is no central controller [140].

2.4.2.3 Distributed Controller

The distributed secondary controller is a compromise approach of the previous two types. The reference setpoints are generated locally, and the local controllers can communicate with each other. The distributed controller approach is shown at the bottom in Fig. 2.2. This controller type uses a small amount of exchanged data between the devices in the microgrid [141]. The distributed controller offers the system many advantages such as a simpler communication system. Also, it requires a lower computational time. This reduces the system cost [142]. Also, the distributed controller lacks a single point of failure problem, which then enhances the system's resilience and robustness.

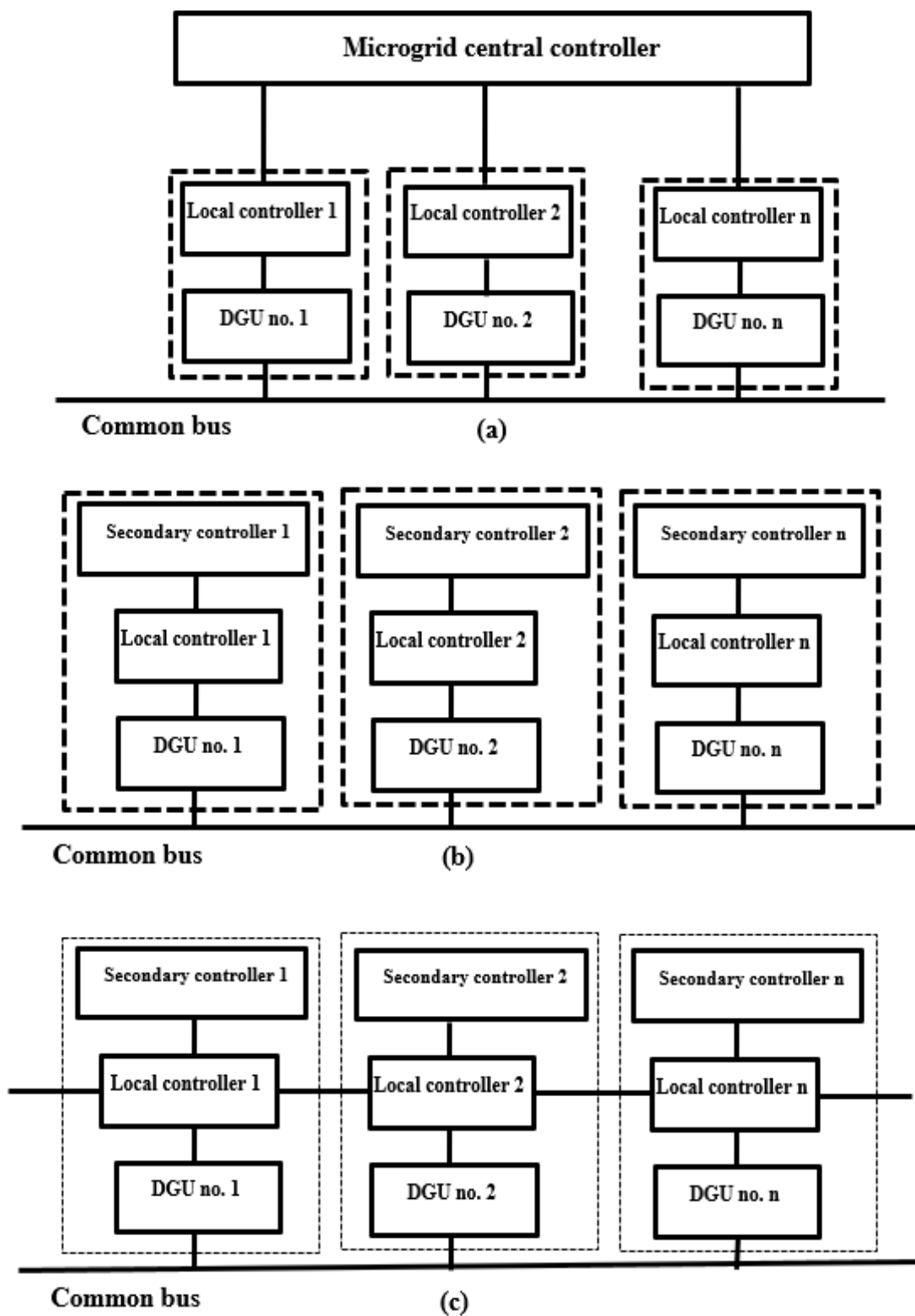


Figure 2.2: Secondary control architectures in microgrid; (a) Centralized scheme, (b) Decentralized scheme, (c) Distributed scheme

2.4.3 Tertiary Controller

As the electric power demand and the reliance of electricity in daily life increase, the desire to apply microgrids may also increase. The coordination between a large number microgrids with each other became essential to maintain stability of the utility grid as well. Synchronizing the connected microgrids and regulating the power flow among them is potentially a cumbersome issues. As a result tertiary control was adapted to microgrids. Tertiary control is the highest level of control in microgrids and is usually part of the utility grid control, not the microgrid. It can be referred to as microgrid supervisory control. The distribution network operator (DSO) and market operator (MO) exist at this level. DSO handles the distribution of electric power to loads, while the market operator engages the microgrid in the power market.

Tertiary control provides technical and economical operation of the microgrids. From the technical aspect, it coordinates the operation and synchronization of multiple microgrids on the power system with the host grid. Also, the control adjusts the power flow between the microgrids and the host grid. Tertiary control accepts the requirements of the host grid such as active and reactive power, then manages this power among the connected microgrids. At the tertiary level, the values of active and reactive power are measured, then compared to the reference values, and based on the difference between these values, it sends the reference set points for the secondary control system [138]. Consequently, the power distribution losses and cost of the power generated from each DGU are reduced, while keeping the power balance and voltage regulation within acceptable margins. From the economical point of view, tertiary control provides economic dispatch. Economic dispatch is the allocation of the electric demand to the available DGUs in a way to reduce the cost of energy generated and microgrid system operation, while satisfying the power balance of the network and both generation and load constraints. In [143, 144], the authors present

algorithms for achieving the economic operation of a microgrid.

Tertiary control is the slowest among other hierarchical levels, its timescale may be in several minutes or hours. Similar to the secondary control, the tertiary control can be categorized into centralized or distributed control. The centralized control technique is commonly used in tertiary control. It depends on a communication system, and the controller is located at microgrid central controller. Many papers support using the central tertiary control algorithm such as [12, 145, 146]. The control system measures the active and reactive power at the point of common coupling and compares them with the reference values to generate the frequency and voltage reference signals for the secondary control. The algorithms represent energy management systems for multiple microgrids, and they consider many factors that affect the operation of microgrids such as power flow and load forecasting, electricity price, and load profiles.

On the other hand, the authors of [147, 148, 149] supported a distributed control system. In [148], a consensus-based tertiary control strategy is implemented. The authors of [149] developed a gossip-based tertiary control algorithm. The distributed tertiary control enhances the flexibility of microgrid, but it is not commonly used in the microgrid literature because the factors on which it depends such as forecasting of generation and demands and energy flow in the microgrid are difficult to integrate on each device [150].

2.5 Communication Media

The control systems depends on data exchange for monitoring and control of microgrids. Hence, the communication media are essential for reliable and secure operation of microgrids. The deficiencies of communication such as the latency and delays may cause improper operation for faster control scheme resulting in voltage and frequency

oscillations which worsen the power quality. Consequently, the communication system for local and primary control should satisfy some requirements such as low latency, high speed of data transfer rate, reliability, security, affordability, and scalability [151]. Moreover, the communication system should have the ability to support a bi-directional flow of information. The communication media can be classified as wireless and wired communication media [152, 153].

2.5.1 Wireless Communication

Wireless communication media transmit the data without any physical links between the controller and different devices in microgrids [154]. They possess some advantages such as low installation cost, mobility, fast deployment, scalability, and ease of repair and replenishment [151]. The commonly applied wireless communication systems can be categorized as the following.

2.5.1.1 Wireless Mesh Network (WMN)

WMN is a group of radio nodes that are systematized in a mesh system. Each node serves as an independent router [155]. WMNs have some beneficial properties such as self-configuring and self-healing. These properties ensure information signals communicate through active nodes in case of failure of any node or any communication path [156]. Moreover, these properties enhance the reliability, performance of the communication system, and load balancing on the network. Furthermore, WMNs have some advantages such as low implementation cost, ease of configuration, and good scalability features [154]. On the other hand, WMNs have some drawbacks such as fading, network capacity limits, and susceptibility to interference. Furthermore, sizing the network and determining the numbers and placement of nodes are cumbersome issues [157]. Also, data packages traveling around many neighbors and loop

problems may arise, creating reduction in bandwidth [158].

2.5.1.2 Cellular Communication Network

A cellular communication network is a radio network that is dispersed over geographical land areas called cells, with each cell served by at least one base station. A cellular network may be the convenient solution for communication between utilities, distributed generation sources, faraway nodes, and smart meters. Today, the viable cellular communication for the utilities are 3G, 4G, 5G, GSM, LTE, WiMAX. The 3G, 4G and 5G regarded as fast and cost-effective systems to cover large areas [159]. Hence, utilities can save a lot of money by exploiting the present communication infrastructure that covers a large geographical area instead of building a new communication system. This encourages the utilities to spread their devices over large geographical areas.

Cellular network systems have many advantages that potentially make them important communication systems for microgrids, such as their availability in many areas, low cost, good coverage, less maintenance, and fast implementation [160]. However, cellular networks have some disadvantages such as impact of environmental conditions such as rain, wind, dust storms and lightning storms, so they may be not a fixed quality network. Moreover, many customers exploit these networks, so some problems may arise such as congestion and performance deterioration in some situations.

2.5.1.3 Satellite Communication

Satellites cover most of the globe, so they can be considered a convenient solution for monitoring and controlling devices in remote locations. Some communication satellites are in geostationary orbits above the earth, and so provide good coverage for

specified places on the earth's surface. The satellites have receivers and transmitters to receive and transmit signals to ground stations that have antennas to receive signals from the satellites [161].

Utilities also use the global position system (GPS) for accurate location updates and time synchronization between different locations in the grid.

Satellite communication can be used as a backup system in case of emergencies or failure of the terrestrial communication system [162]. The main advantages of satellite communication are the fact that it covers a large area which makes monitoring remote locations not accessible through wired networks or cellular networks or microwave system viable. Satellite communication can be cost-effective for monitoring and controlling the rural substations and distributed generators, where there is no communication infrastructure [163]. However, satellite communication has some disadvantages such as dependency on the weather environment, solar storms and fading, which can degrade the performance and quality of the communication system. Also, the high cost of leasing a satellite communication channel is an issue for satellite communication systems [164].

2.5.1.4 Microwave Communication

Microwaves are electromagnetic waves with a frequency range from 1 to 300 GHz. Microwave is a point-to-point communication technique. It can be considered a unidirectional communication technique, where the antennas send out the signals in one direction, and both the sending and receiving antennas are aligned with each other [161]. It can be exploited for sending information and data from rural and remote areas. Microwave communication has some advantages such as portability, high transmission ability. Moreover, the broad microwave frequency range permits a high data rate to be viable and hinders interference probabilities [165, 166]. There

are limitations for using microwave communication in some frequency bands without permission from the authorities. Also, microwave is a line of sight, which means it is affected by the obstacles, and repeaters may be required. Moreover, its quality depends on environmental conditions [160].

2.5.1.5 Wi-Fi Communication

Wi-Fi is used for wireless local area network (WLAN) based on IEEE 802.11 standard that adopted spread spectrum technology. This standard is important for microgrid applications, robust, high-speed point-to-point, and point-to-multipoint communication [166, 167]. Wi-Fi can be used inside many areas, buildings, and factories. Some utilities prefer to use Wi-Fi in substations so as not to dig the ground for implementing or upgrading communication infrastructure. One of the main challenges of Wi-Fi communication is improving its reliability, where it interferes with the electromagnetic wave which affects the rate of data transfer. Moreover, Wi-Fi communication requires cyber-security protection for implementing a secured system [159].

2.5.2 Wired Communication Systems

2.5.2.1 Power Line Carrier Communication

Power line carrier communication (PLCC) is a method for transmitting data and information over the existing power lines. PLCC has been used by utilities to implement communication infrastructure. Utilities prefer using power line communication to transmit data and metering information, as the lines are already connected to the meters. Power line communication was used 20 years ago in low voltage distribution networks [168]. Essentially, power line communication is normally used for low data rates, but high-speed communication for long distances still needs some scientific research effort.

Many papers describe power line communication as a convenient communication technique in microgrids because power lines may be used for coverage in large areas especially in urban areas or in remote places that don't have communication infrastructure. Furthermore, power line communication is cost-effective, since all the power lines are already implemented [163], and can be exploited to connect all the microgrid devices to the data concentrator. On the other hand, the power line communication technique has low bandwidth characteristics, which prohibits its use in high bandwidth-based applications. In addition, power conductors are a noisy environment for data communication which may result in degrading the quality of service and high error rate during data transferring [169]. Furthermore, the load fluctuation and imbalance may attenuate and distort the signals. Also, one of the main problems in power line carrier communication is the open circuit which causes a communication loss [170].

2.5.2.2 Optical Fiber Communication

Optical fiber cables (OFCs) are manufactured from glass mixed with other materials to make them flexible. OFCs can transmit signals in the form of light. They are available supporting single or multiple modes [171]. OFCs possess a high bandwidth and high data rate. In addition, they are immune to interference, so in an environment with electromagnetic or radio frequency interference, OFCs can be regarded as the optimum communication techniques [165]. OFCs can be exploited for transmitting data for a long distance, hundreds of kilometers, with fewer repeaters [171]. An optical fiber communication system has some advantages such as low operating cost, no licensing requirement, no energy radiation, and lightweight. Due to the aforementioned advantages, OFCs are considered high performance and reliable communication techniques [170]. However, OFCs possess some disadvantages such as

the high cost of the fiber and the other devices used to implement the system such as transmitters, receivers, repeaters, splicing, and test equipment. Also, this technology needs skillful and expert persons to manipulate this sort of technique [161].

2.6 Communication Protocols

There are a lot of vendors in the power market producing devices and components. The various devices from the different manufacturers should be interoperable, so the presence of standardized protocols is important. Communication protocols are a set of rules that govern sharing of data and information among different devices in a network. The most used protocols in microgrids are Modbus, DNP3, and IEC 60870-5-101/104, IEC 61850. Because of their extensive applications in power systems, these types are listed in the following subsections. The authors of [172, 173, 174] presented the different protocols and their usage in power systems.

2.6.1 Modbus

Modbus was introduced by Modicon in 1970 as a proprietary protocol that later became an open protocol. It was developed as a communication protocol for programmable logic controller applications, and it became popular and used for transmitting information over serial lines between industrial electronic devices. Modbus was developed to support serial communication, but it has been upgraded for supporting other schemes. It can support RS-232, RS-485, and TCP/IP [172]. Modbus is a master-slave protocol that is used for connecting the master controller with other devices in the microgrid to enable communication between them [175]. Polling is initiated from the master, and the master may message a defined slave or simultaneously all the slaves. There are a variety of Modbus implementations; Modbus RTU, Modbus ASCII, Modbus Plus, SunSpec Modbus, and Modbus TCP/IP. The authors of [176,

177] presented a detailed explanation comparison between these different modes.

Modbus has many advantages such as its simplicity to read, plus data integrity checking has been built in using cyclic redundancy check (CRC). Furthermore, it is an open standard, and many vendors support Modbus which makes it simple to troubleshoot and manipulate [161]. However, Modbus has drawbacks such as a requirement for a local clock for providing time reference, since it is a time-based protocol. Also, cybersecurity need to be added and extended to Modbus to obtain a secured communication system.

2.6.2 IEC 61850

IEC 61850 is a family of standards developed by the IEC Substation control and protection interfaces working group of IEC Technical Committee 57 (Power systems management and associated information exchange). They are designed to be used as a single communication protocol for the whole system [161], enabling complete substation automation and communication between the substation controller and both upstream and downstream devices. IEC 61850 protocols provide interoperability between the devices from diverse manufacturers and designates a methodology for data format and data transfer between different devices [178]. At first, IEC was designed as a standard for substations, then vendors for non-substation applications applied these standards because of the advantages of following a single international standard for electric systems [179].

The data model that is described in IEC 61850 standard configuration language (SCL) can be mapped to other protocols such as manufacturer message specification (MMS), generic object-oriented substation events (GOOSE), and sampled measured values (SMV) [180]. IEC 61850 is an Ethernet network-based protocol that positively affects the cost and operation of power system devices [181]. IEC 61850 is divided

into 10 parts, and Table 2.1 describes the structures of these standards [173].

Table 2.1: Structure of IEC 61850 standard

Part number	Title
1	Introduction and overview
2	Glossary
3	General requirements
4	System and project management
5	Communication requirements for functions and device models
6	Configuration language in electrical substations related to IEDs
7	Basic communication structure for substation and feeder equipment
8	Communication service mapping (MMS)
9	Specific communication service mapping (SCSM)
10	Conformance Testing of compliant devices

2.6.3 Distributed Network Protocol (DNP3)

DNP3 is a communication protocol first produced by Westronics in Calgary, Canada. Because DNP3 is now an open and public protocol, it is a widely used protocol by electric utilities and can also be found in other applications such as oil, gas, and wastewater. DNP3 is based on the international electrotechnical commission (IEC) technical standard committee 57, working group 03. The structure of DNP3 uses three layers of the enhanced performance architecture (EPA) model [182], but some extra functionalities are included by vendors [161].

DNP3 is object-oriented where data are arranged into a large library which is separated into separate groups. Each group characterizes a definite object. DNP3 supports a large data frame that may hold larger messages between clients and hosts. Multiple data objects may be added to the message and the header of each data object describe its relationship. Furthermore, different data types such as boolean and floating point may be used in a single message to diminish data traffic [183].

DNP3 can be exploited with different network topologies such as peer-to-peer,

multiple masters, multiple slaves, and master-slave communication [184]. Also, the slaves can send unsolicited messages to the master without waiting to be polled by the master. DNP3 supports multiplexing, data fragmentation, linking control, and local time synchronization with different devices such as RTUs and IEDs. DNP3 uses a CRC to detect errors and data quality checking is built into the message [185].

DNP3 is supported by many vendors which means any manufacturer can produce DNP3 equipment that would be inoperable with other DNP3 equipment. Due to the advantages of DNP3, it can be regarded as a robust, interoperable, and efficient protocol.

2.6.4 IEC 60870-5- 101/103/104

IEC 60870 is an open protocol it consists of a series of communication standards, and was designed for SCADA telemetry by IEC technical committee 57 in 1995. This protocol is designed for application in the electrical industries, inside and outside the substation. IEC has extended this standard for data modeling in wind power plants, hydropower plants, and DERs. Furthermore, it is suitable for general SCADA applications in any industry such as water, oil, gas, and transportation. IEC 60870-5 protocol is mainly used in the electrical industries of European countries [186].

IEC 61870 standard describes message related automated control for substation management, operating the substation control devices, and communicating between a master controller and slave devices. It can be used over the Ethernet and other TCP/IP-based networks [187]. IEC 60870 depends on three layers of the EPA; physical, data link, and application. A user layer is added to support interoperability between devices in the telecontrol system. IEC 60870-5 consists of six sections. They are found under the general title (Telecontrol equipment and systems) [188] and each one includes multiple sections [189].

IEC 60870 has 4 companion standards; T101, T102, T103, and T104 [161]. T101 is exploited for power system monitoring, control, and associated functions. It uses master-slave communication. The application functions involve station initiation, data acquisition, cyclic data transmission, and clock synchronization [190]. T102 is the companion standard for transmission of integrated totals in electrical power systems, and this standard is not commonly used. T103 supports protection communication functions. T104 is a network version to be exploited in TCP/IP networks. T104 data units are application service data units (ASDUs) that are combined with control frames called application protocol control information (APCI) [191]. A combination of APCI and ASDU creates the application protocol data unit (APDU). APDU has a minimum size of 6 bytes, whereas the maximum size is 255 bytes including control and header frames [191]. Hence, transfer of a large amount of small-sized data units in each time cycle is bounded.

2.7 Summary

Microgrid operation, power management, and control systems are important in microgrids. This chapter presented the different types of microgrids, the distributed energy resources, and the different energy storage systems mostly used in microgrids. Also, this chapter reviewed the different control strategies based on hierarchical control levels. Decentralized control systems have many advantages such as reliability, scalability, and resilience. The control system strongly depends on communication systems, which are vital for monitoring and controlling the overall system. This chapter presented the most used communication media and protocols in the microgrid.

Chapter 3: Modeling and Control of Wind Energy

Conversion System with Battery Energy Storage System

This chapter consists of material from a paper that is published in the proceedings of the IEEE 53rd North American Power Symposium (NAPS 2021) that was held in Texas A&M University, College Station, Texas, on November 14 through November 16, 2021.

3.1 Introduction

The environmental pollution issues and the expected shortage of conventional fuel resources have motivated governments and regulatory agencies to push utilities to embrace renewable energy resources for securing electric power supplies. Wind energy conversion systems (WECS) are one of the common and reliable renewable energy resources. Also, the most used generators type in WECS is the doubly fed induction generator (DFIG) due to its advantages such as the ability to operate over wide ranges of wind speed and reduced converter power rating leading to a reduction in losses and cost [192]. So the DFIG is exploited in this research. One of the main disadvantages in WECS is the variable nature of the wind speed, so a control system should be implemented to ensure reliable system operation and extracting the maximum available power from the system at different wind speeds.

Moreover, there is increased interest in combining battery energy storage systems with WECS to overcome the challenges created by the intermittent nature of wind generation output to enhance its reliability [78]. At high wind speeds, the battery stores the excess power and when the wind speed is insufficient to supply the load, the battery can supply the remaining required load power [193]. Hence, the combined WECS/BESS system can appear dispatchable to a grid or microgrid controller.

The layout of the implemented system is described in Fig. 3.1. The power con-

verters in the system are modeled and controlled based on a vector control scheme in the stator-voltage-oriented synchronous reference frame. The vector control achieves a decoupled control of both active and reactive power output of the wound rotor induction machine through dq components in the rotor currents. Since the reactive power can be controlled independently, the WECS can be used for reactive power control in a microgrid, and so voltage support.

The dc-link should be protected against overvoltage in case of ac system disturbances, so dc-chopper circuit is used for protecting the dc-link voltage. This system is implemented and simulated in an electromagnetic transients simulation.

The rest of this chapter is arranged as follows. Modeling of the system is described in Section 3.2. In Section 3.3, the design of the proposed controller is reviewed. Section 3.4 describes the battery energy storage system and its power converters. Simulation of the proposed system is demonstrated in Section 3.5. Finally, in Section 3.6 some relevant conclusions are drawn.

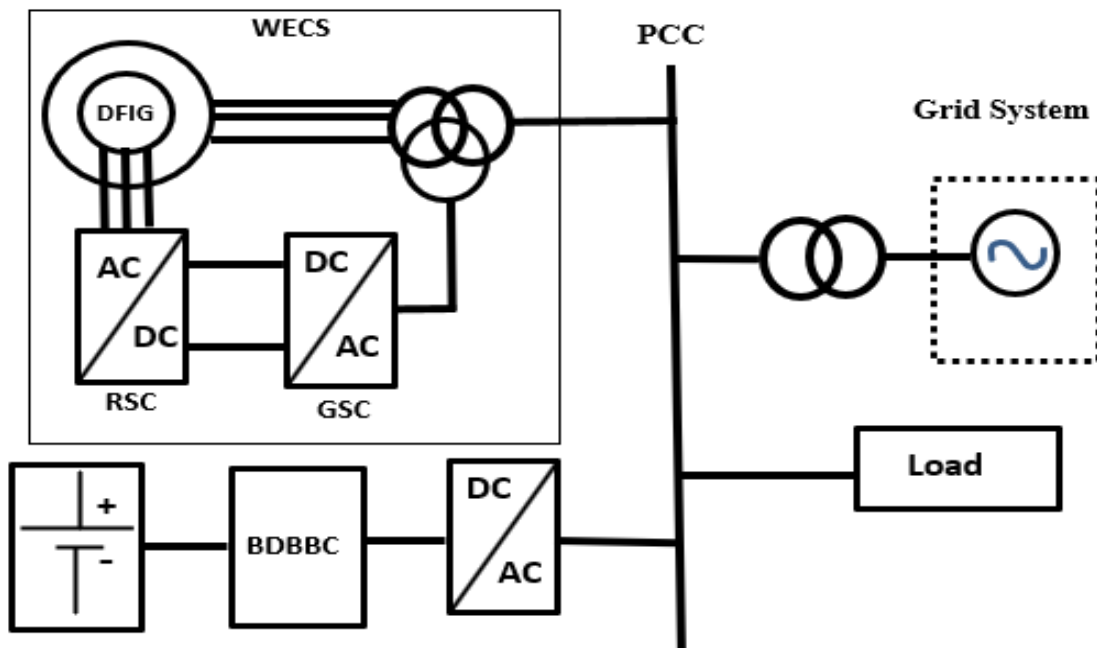


Figure 3.1: Layout of the proposed WECS system

3.2 Modelling of WECS

3.2.1 Modeling of Wind Turbine

The wind turbine extracts the power from the wind and transfers it to rotational mechanical energy. The mechanical extracted power of the wind turbine can be expressed as [41, 194]:

$$P_m = 0.5 \rho A_r v_w^3 C_p(\beta, \lambda) \quad (3.1)$$

where ρ is the air density, A_r is the rotor swept area, v_w is the wind speed and C_p is the power coefficient of the turbine. Power coefficient depends on the pitch angle β and the tip speed ratio λ . The tip speed ratio can be written as:

$$\lambda = \frac{r\omega_w}{v_w} \quad (3.2)$$

where r is the wind turbine radius and ω_w is the wind turbine rotational speed. The power coefficient can be written as:

$$C_p = 0.5176 \left(\frac{116}{\lambda_i} - 0.4\beta - 5 \right) e^{\frac{-21}{\lambda_i}} + 0.0068 \lambda \quad (3.3)$$

where

$$\lambda_i = \left(\frac{1}{\lambda + 0.08 * \beta} - \frac{0.035}{\beta^3 + 1} \right) - 1 \quad (3.4)$$

3.2.2 Modeling of DFIG

Representing DFIG model in ABC frame is complicated since it is rotor position and time-dependent resulting in cross-coupled differential equations with time-varying parameters in addition to time-varying voltages, currents and fluxes. Hence, the

Park's transformation is used for modeling the system. Then, all the time-varying variables can be regarded as constants in steady-state operation. The full order model for DFIG can be expressed as [195]:

$$V_{ds} = R_s I_{ds} - \omega_s \phi_{ds} + \frac{d\phi_{qs}}{dt} \quad (3.5)$$

$$V_{qs} = R_s I_{qs} - \omega_s \phi_{qs} + \frac{d\phi_{ds}}{dt} \quad (3.6)$$

$$V_{dr} = R_r I_{dr} - S\omega_s \phi_{qr} + \frac{d\phi_{dr}}{dt} \quad (3.7)$$

$$V_{qr} = R_r I_{qr} - S\omega_s \phi_{dr} + \frac{d\phi_{qr}}{dt} \quad (3.8)$$

Power and torque equations can be expressed as:

$$T_e = (\phi_{ds} I_{qs} - \phi_{qs} I_{ds}) = L_m (I_{qs} I_{dr} - I_{ds} I_{qr}) \quad (3.9)$$

$$P_s = (3/2)(V_{ds} I_{ds} + V_{qs} I_{qs}) \quad (3.10)$$

$$Q_s = (3/2)(V_{qs} I_{ds} - V_{ds} I_{qs}) \quad (3.11)$$

$$P_r = (3/2)(V_{dr} I_{dr} + V_{qr} I_{qr}) \quad (3.12)$$

$$Q_r = (3/2)(V_{qr} I_{dr} - V_{dr} I_{qr}) \quad (3.13)$$

where P , Q , T_e , S , ω_s and ϕ refer to active power, reactive power, electromagnetic

torque, slip, synchronous rotational speed and flux respectively. The components ds, qs, dr and qr refer to the direct and quadrature in stator and rotor axes respectively.

3.3 Controller Design

The controller for the WECS consists of two controllers; a rotor side converter controller (RSC) and a grid side converter controller (GSC). Each controller consists of two main loops; an outer loop and a fast inner current control loop.

3.3.1 Rotor Side Controller

The outer loops of the RSC control both the active and reactive power exchanged between the generator's stator and the grid. Also, they generate the reference currents for the inner loops. The inner loops control the current values to follow their references. The controller is designed in a stator-voltage oriented reference frame where the d-axis of the reference frame is aligned with the stator-voltage space vector. Then the stator voltage and power equations can be written as [196]:

$$V_s = V_{ds} = -\omega_s \phi_{qs}, \quad V_{qs} = 0 \quad (3.14)$$

$$P_s = -(3/2) \frac{L_m}{L_s} V_{ds} I_{dr} \quad (3.15)$$

$$Q_s = -(3/2) \frac{L_m}{L_s} V_{ds} (I_m - I_{qr}) \quad (3.16)$$

From equations (3.15) and (3.16), the active and reactive power can be controlled independently through the rotor currents. The reference voltage signals (V_{dr-ref} , V_{qr-ref}) generated by the rotor side controller can be defined as:

$$V_{dr-ref} = V_{dr}^1 - S \omega_s (L_r I_{qr} + L_m I_{qs}) \quad (3.17)$$

$$V_{qr-ref} = V_{qr}^1 + S \omega_s (L_r I_{dr} + L_m I_{ds}) \quad (3.18)$$

where

$$V_{dr}^1 = (R_r + \sigma \frac{d}{dt}) I_{dr} = (K_{pr} + \frac{K_{ir}}{s})(I_{dr-ref} - I_{dr}) \quad (3.19)$$

$$V_{qr}^1 = (R_r + \sigma \frac{d}{dt}) I_{qr} = (K_{pr} + \frac{K_{ir}}{s})(I_{qr-ref} - I_{qr}) \quad (3.20)$$

where $\sigma = L_r - L_m^2/L_s$, I_m represents the magnetizing current, L_r is the rotor inductance, L_s is the stator inductance, L_m is the magnetizing inductance, K_{pr} is the proportional constant in the PI controller, and K_{ir} is the integral constant in the PI controller. Fig. 3.2 and Fig. 3.3 show the block diagrams for controlling the direct and quadrature axis currents in the inner control loops. The reference values of I_{dr-ref} and I_{qr-ref} are produced from the outer control loops and used for achieving the decoupled control of both active and reactive power. The two signals V_{dr-ref} and V_{qr-ref} represent the direct and quadrature reference voltage control signals which are generated by the rotor side controller.

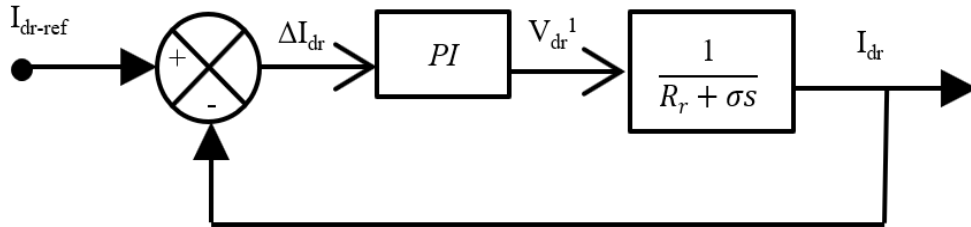


Figure 3.2: RSC, d-axis current controller

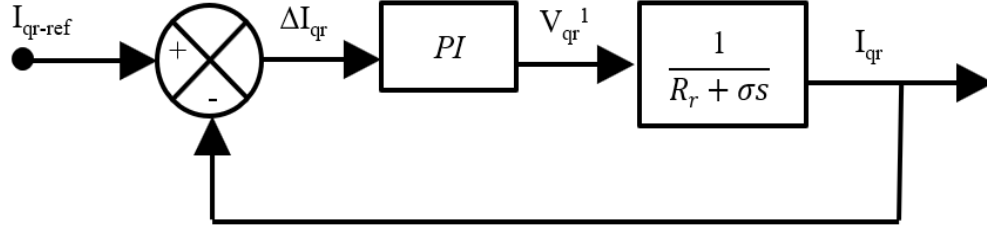


Figure 3.3: RSC, q-axis current controller

3.3.2 Grid Side Controller

GSC also consists of two cascaded loops; outer and inner. It controls both the reactive power exchanged with the grid and as well as the real power transfer between the grid and the rotor by controlling the dc-link voltage through its outer loops. The inner loop controls the rotor direct and quadrature currents. The relations between the voltage, current on the grid side converter can be stated as the following [197].

$$V_{dg-ref} = V_{ds} - V_{dg}^1 + \omega_s L_c I_{qg} \quad (3.21)$$

$$V_{qg-ref} = V_{qs} - V_{qg}^1 - \omega_s L_c I_{dg} \quad (3.22)$$

$$V_{dg}^1 = (R_c + L_c \frac{d}{dt}) I_{dg} = (K_{pg} + \frac{K_{ig}}{s})(I_{dg-ref} - I_{dg}) \quad (3.23)$$

$$V_{qg}^1 = (R_c + L_c \frac{d}{dt}) I_{qg} = (K_{pg} + \frac{K_{ig}}{s})(I_{qg-ref} - I_{qg}) \quad (3.24)$$

where L_c and R_c represent the total inductance and resistance of the used impedance between the converter terminals and the point of interconnect with the grid. The constants K_{pg} and K_{ig} are the proportional and integral constants in the PI controller. The two signals V_{dg-ref} and V_{qg-ref} represent the d and q reference voltage control signals which go to the switching pulse generation. The d and q current regulation

parts of the grid side converter are described in Fig. 3.4 and Fig. 3.5.

The reactive power is controlled through quadrature axis current reference, with a current reference of zero for unity power factor operation. The dc-link voltage is used as an indicator of the power demand of the RSC. An increase in dc-link voltage indicates the converter needs to increase the real power reference for the GSC. The reference value of the d-axis current can be produced from the outer loop of the dc-link voltage [196]. The dc voltage regulator block diagram is shown in Fig. 3.6.

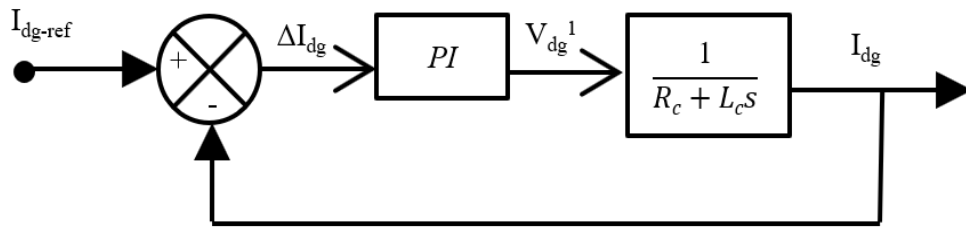


Figure 3.4: GSC, d-axis current controller

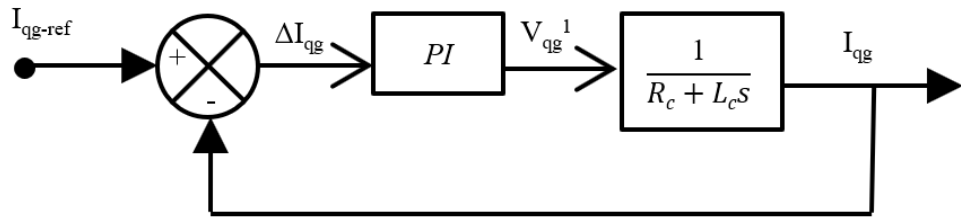


Figure 3.5: GSC, q-axis current controller

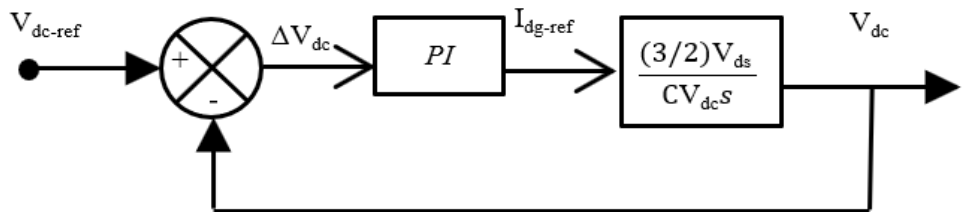


Figure 3.6: GSC, dc voltage control block diagram

3.3.3 Pitch Angle Control

The power coefficient is dependent on the pitch angle value, so the output power can be controlled through the pitch angle controller. Beyond the rated wind speed, the rotor speed and output mechanical power would be increased over the rated values; then, the pitch angle controller should be activated to increase the pitch angle. Thus, the rotor speed and the wind turbine output power are reduced to be within the safe operating regions [198, 199].

3.3.4 Maximum Power Point Tracking Control

One of the simplest and common methods for MPPT methods is to determine the reference power based on the wind speed [200, 201]. This method is based on the power curve that determines the maximum power that can be generated at each wind speed, and this curve should be provided by the manufacturer. The authors of [201] provide a survey about the MPPT techniques that are applicable to wind energy systems. Based on the wind speed, the power reference is generated and sent to the generator control system. The controller should always track the reference power so as to maximize the power generation from the wind system.

3.3.5 DC-Link Chopper Circuit

When a disturbance such as ac fault that trips ac lines occurs, the power that can be delivered to the grid decreases, so the dc-link voltage may increase beyond the acceptable level when the DFIG rotor is exporting power. So a dc-chopper circuit is connected in parallel with the dc-link to protect it from overvoltage [202]. The operation of the circuit depends on the dc-link voltage such that, when the dc-link voltage lies within the normal operating region, the switch is opened. On the contrary,

when the voltage is too high, the switch is closed to dissipate the power in the chopper resistance to reduce the voltage. The dc-chopper circuit is shown in Fig. 3.7

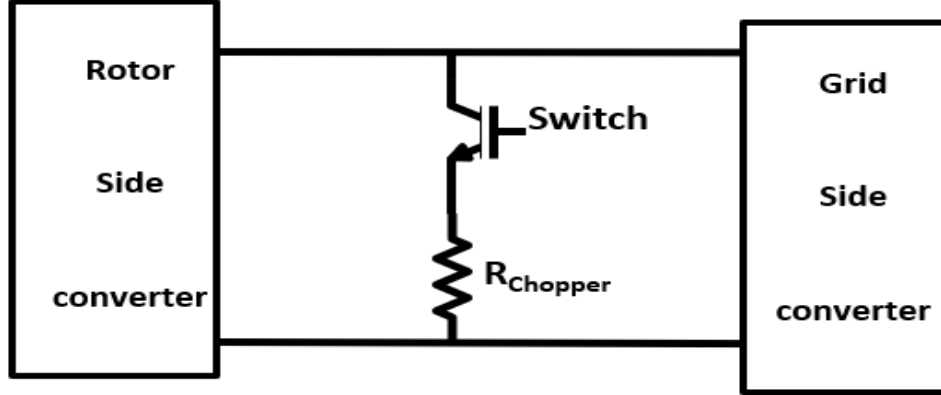


Figure 3.7: DC-chopper circuit

3.4 Battery Energy Storage System

The battery equivalent circuit model can be described by a non-linear equation and the battery is modeled using a controlled voltage source that is connected to a series resistance as shown in Fig. 3.8. The open voltage source E is calculated by using a non-linear equation based on the actual battery state of charge. The generic battery model equation can be written as [203]:

$$E = E_0 - K \left(\frac{Q}{(Q - it)} \right) + A \cdot e^{(-B \cdot \int i_{bat} dt)} \quad (3.25)$$

$$V_{bat} = E - R_{bat} * i_{bat} \quad (3.26)$$

where E is no load voltage source controller (V), E_0 is a battery constant voltage (V), Q is the battery's capacity (Ah), K is polarization voltage constant (V), the integral $\int i dt$ represents the actual battery charge (Ah), B is exponential constant inverse capacity (Ah)⁻¹, A is exponential voltage zone amplitude (V), R_{bat} is the

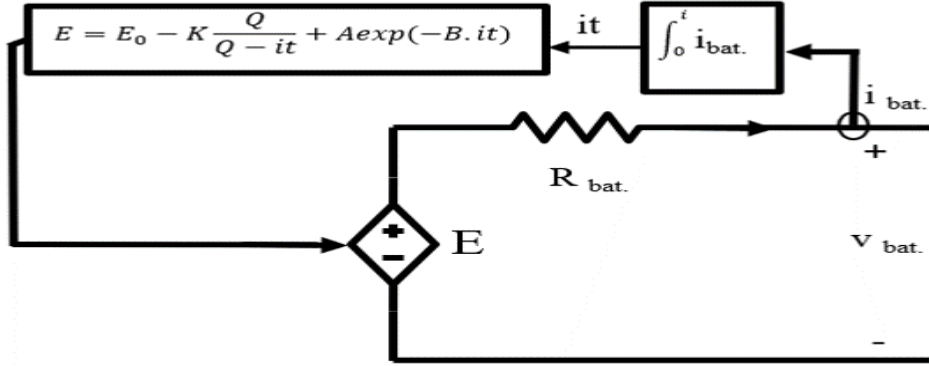


Figure 3.8: Equivalent circuit of the battery

internal resistance (Ω), V_{bat} is the battery terminal voltage (V) and i_{bat} is the battery current (A). A detailed explanation of the battery model is described in [204].

3.4.1 Battery Bidirectional Buck-Boost Converter (BDBBC)

The operation of the battery is controlled by a bidirectional dc-dc buck-boost converter. The converter operates in buck mode when the battery is charging. On the contrary, the converter works on the boost mode to discharge the battery to meet the load demands in case of insufficient wind energy generation. Fig. 3.9 shows the schematic diagram of the converter which consists of two main switches S_1 and S_2 that enable the battery to charge or discharge. A complete explanation of the BDBBC and its controller is described in [204, 205].

3.4.2 Modeling of Battery DC-AC Converter

The battery is connected to the ac system point of common coupling (PCC) through the dc-ac converter. The converter and its controller work with the strategy of the grid following vector current control as described in [206, 207]. The adopted strategy enables the converter to control both the active and reactive power independently. The reference active power is set based on the difference between the generated wind

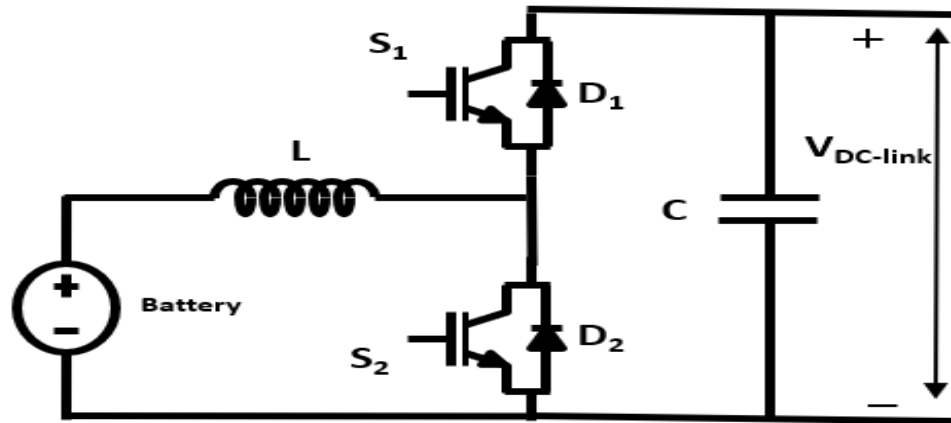


Figure 3.9: Battery bi-directional buck-boost converter

power and the load power. As described in Fig. 3.10, the converter controller consists of two main loops; the outer and the inner loops. The outer loops control the active and reactive power and produce the current references for the inner loops. The reactive power is set to zero for unity power factor operation. The inner loops control the direct and quadrature axes currents and then produce the voltage control signals that are used for generating the pulse width modulation signals that drive the converter switches. The authors of [205, 206] provide a complete description of the inverter schematic diagram and its controller.

3.5 Simulation of Wind Energy Conversion System

To examine the operation of the combined system in Fig. 3.1, a 2 MW WECS is modeled and simulated with an electromagnetic transients simulation. The simulation has been carried out at different cases for different conditions. The first case describes the system performance without the BESS. Fig. 3.11 describes the variation in wind speed from 7 m/sec to 16 m/sec. The active power generated by the WECS changes in response to the wind speed variation as shown in Fig. 3.12. When the wind speed equals to 9 m/sec, the generator produces 1.3 MW. When the wind speed

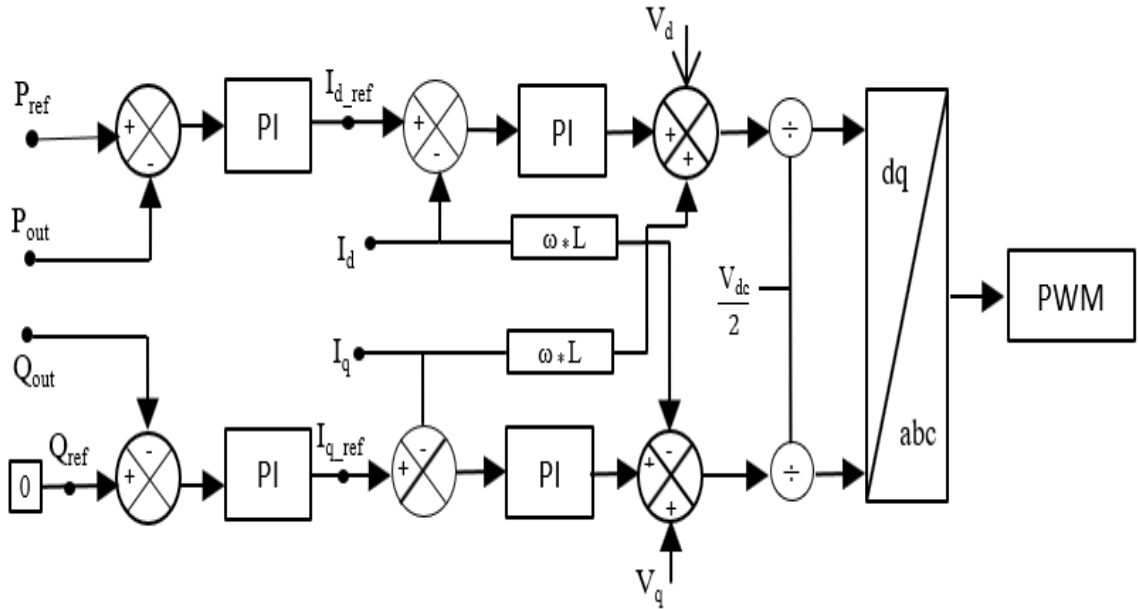


Figure 3.10: Battery dc-ac converter controller

increased to 16 m/sec which exceeds the rated value that equals to 11 m/sec, the active power is increased to 2 MW. Moreover, the pitch angle controller is activated to protect the system from overspeed or overgeneration. As shown in Fig. 3.13, the pitch angle decreased to zero when wind speed decreased below the rated value. Furthermore, when the wind speed decreased to 7 m/sec, the output power of the generator decreased to 0.65 MW. Finally, when wind speed equals to the rated speed, the output power increased to 2 MW; the rated output power.

In this simulation case, the reactive power from the WECS is set to be at zero value for unity power factor operation. Fig. 3.14 demonstrates that the reactive power stays at zero value as the wind speed varies for the case shown in Fig. 3.11. Also, the dc-link profile is shown in Fig. 3.15. The dc voltage value is constant and doesn't show significant changes as the wind speed varied.

This system can be used for regulating the reactive power delivered to the grid. Fig. 3.16 shows that the GSC controls the reactive power to vary from + 0.5 MVAR to -0.5 MVAR as the wind speed varies for the case shown in Fig. 3.11. These reactive

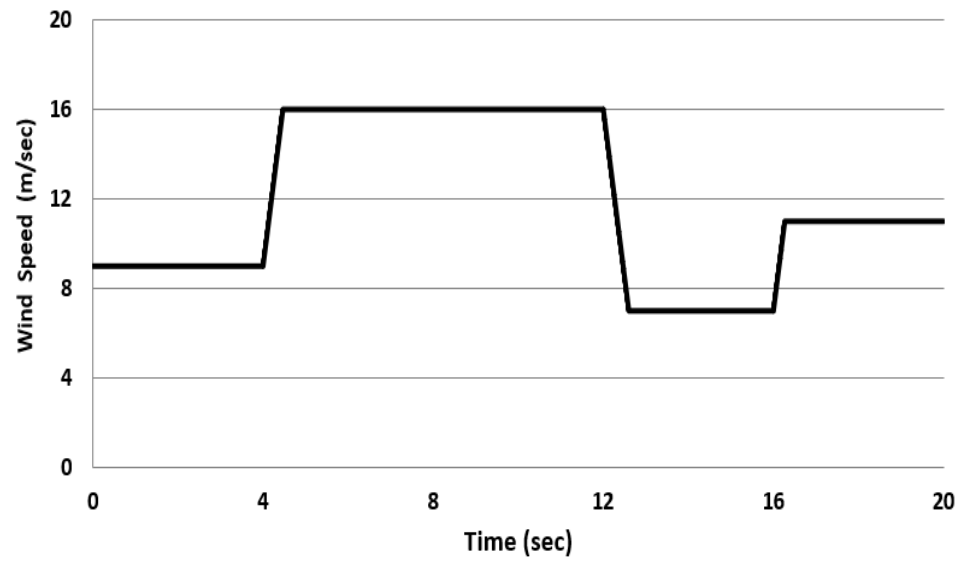


Figure 3.11: Wind speed variation profile

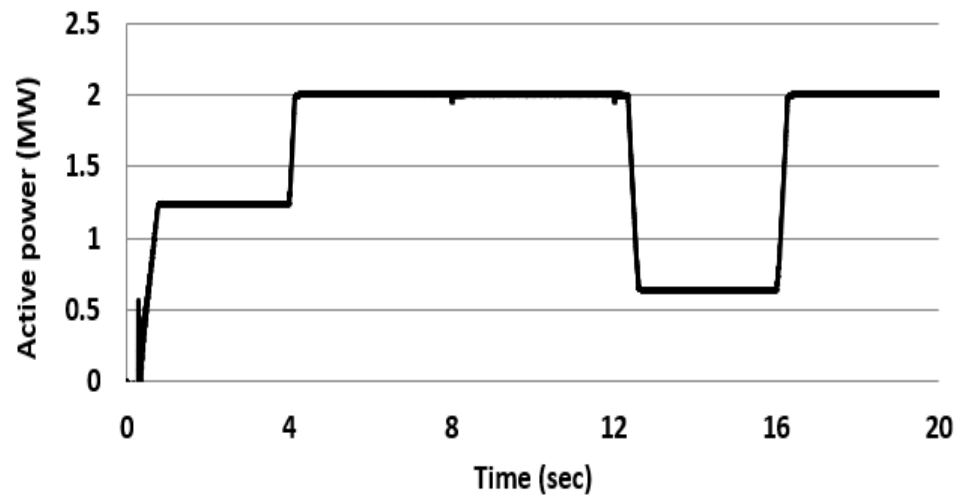


Figure 3.12: Generated active power in response to wind speed variation

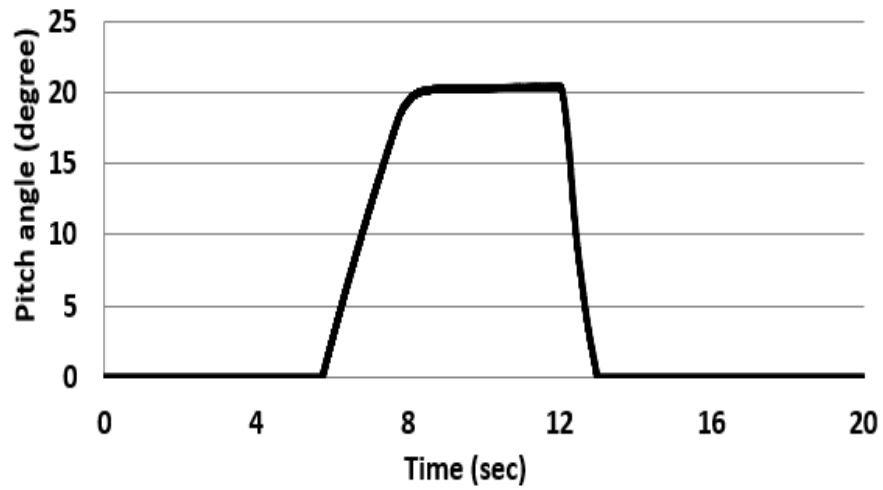


Figure 3.13: Pitch angle profile

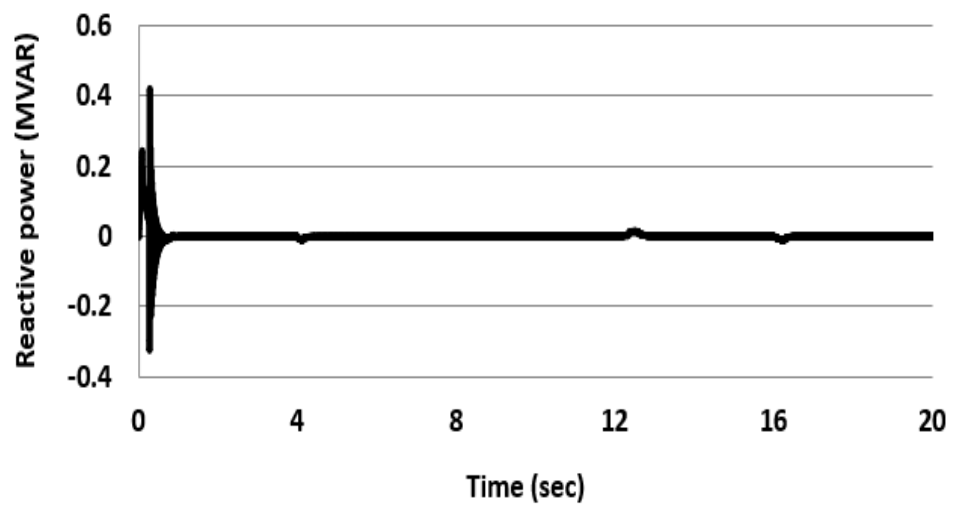


Figure 3.14: Generated reactive power profile

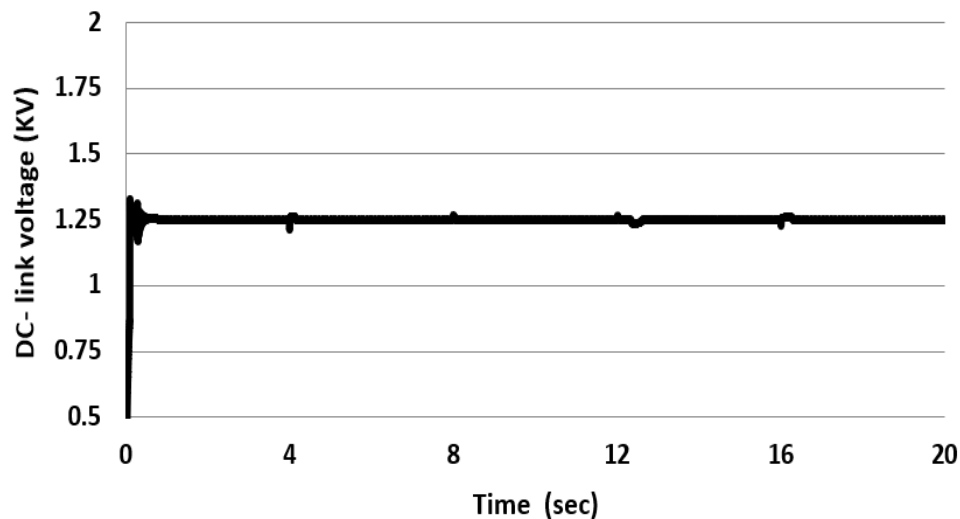


Figure 3.15: DC-link voltage profile

power command values may be activated by the local controller or from hierarchical control system in response to a voltage variation.

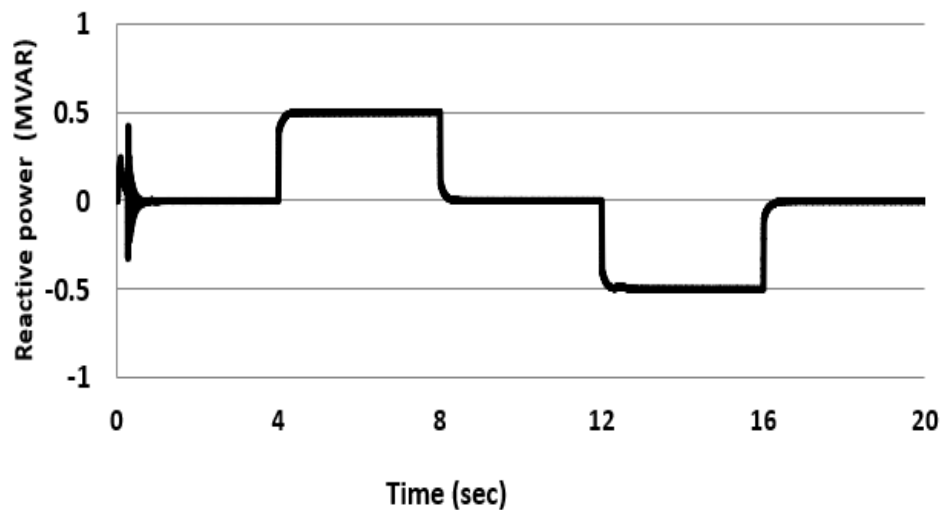


Figure 3.16: Reactive power variation profile

The next simulation examines the performance of the system when the BESS is connected to the system. In this case, the system is simulated under different wind speeds and with a constant load equal to 1.3 MW. Fig. 3.17 shows how the battery compensates for the difference between the WECS power generation and the load power. When the wind speed equals to 10 m/sec, the wind system generates 1.6 MW

and 0.3 MW is used for charging the battery. When the wind speed drops to 9 m/sec, the output power is 1.3 MW which is equal to the load and the battery is just floating. Once the wind speed drops to 8 m/sec, the wind system generates 1 MW and the battery system supports the load by 0.3 MW. Fig. 3.18 shows the state of charge (SoC) of the battery. When the battery is charging, SoC is increasing. On the other hand, battery SoC is decreased when the battery started to supply the load. When the wind speed is almost sufficient for generating power equals to the load power, the battery power is zero and the SoC is kept constant.

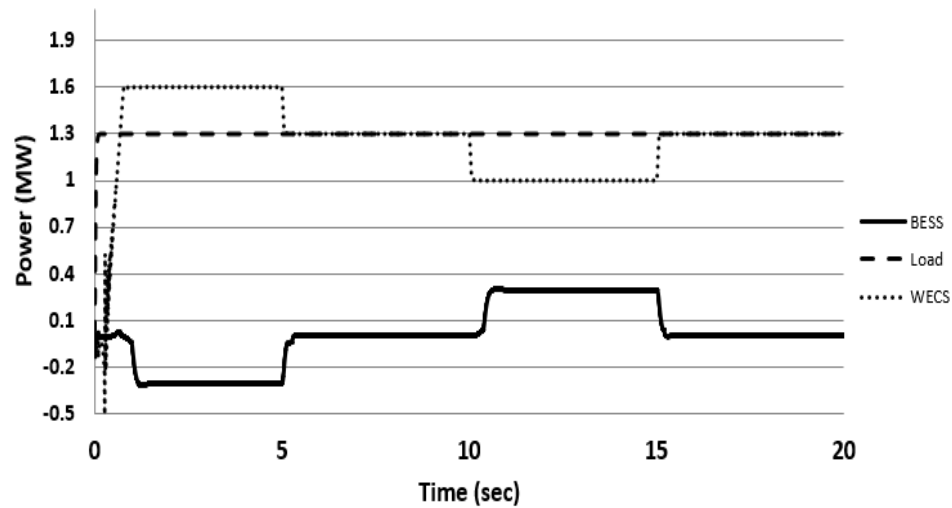


Figure 3.17: Wind system, load and BESS power during wind speed variation

The next set of simulations examines the performance of the system when the wind speed is kept constant at 9 m/sec, the WECS generates 1.3 MW and the load is changing from 1 MW to 1.6 MW. As shown in Fig. 3.19, when the load exceeds the WECS generated power, the battery discharges to supply the load. On the other hand, when the load is less than the WECS output power, the battery is charging. Battery SoC variation is shown in Fig. 3.20 and SoC varies in response to the battery charging and discharging mode. Battery SoC is increased when the battery is charging and reduced when the battery is discharging.

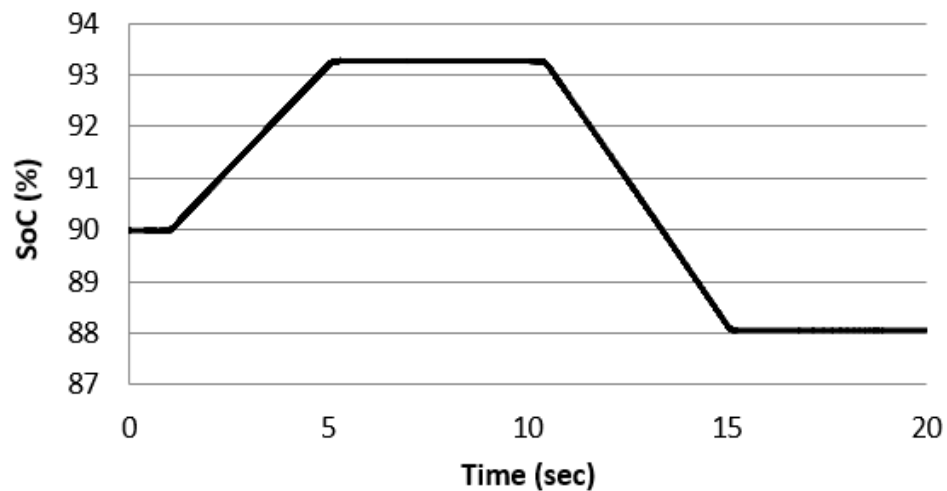


Figure 3.18: Battery SoC during wind speed variation

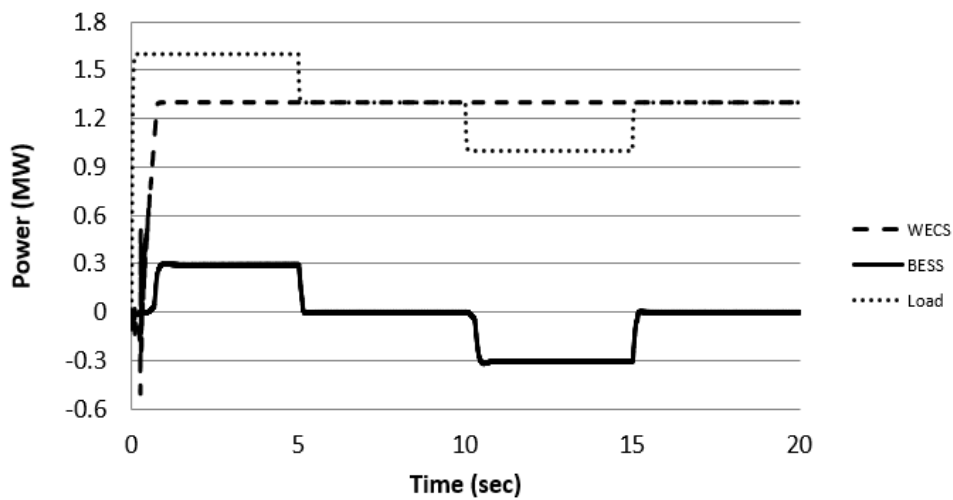


Figure 3.19: Wind system, load and BESS power during load variation

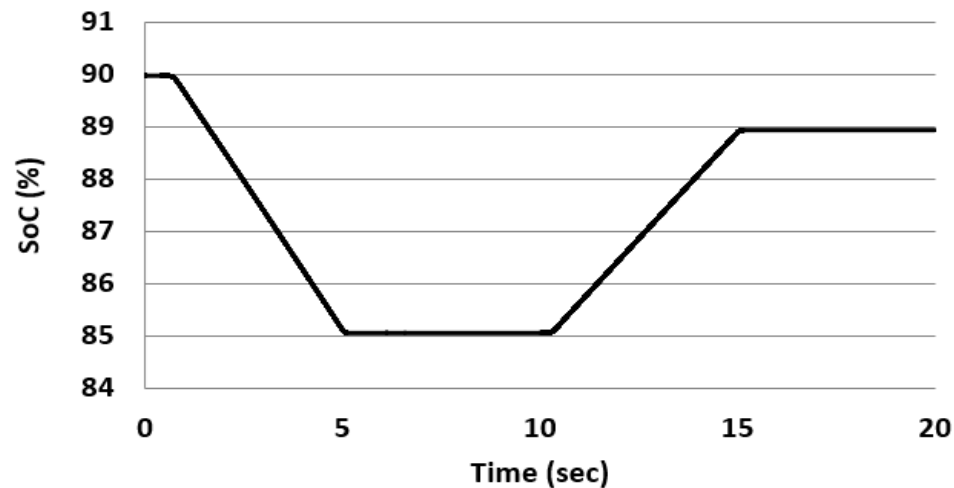


Figure 3.20: Battery SoC during load variation

3.6 Conclusion

WECS is an important resource among renewable energy resources and is seeing significant adoption. The majority of WECS installations used DFIGs. In this chapter, modeling for the system was proposed.

The work involved the modeling of the wind turbine, includes the RSC, the GSC, maximum power point tracking, pitch angle controller, dc-link chopper protection circuit, and a separate battery energy storage system. Simulation for the system at different wind speeds was described. The results demonstrate that both active and reactive power can be controlled independently through the rotor current components. Also, wind energy systems can be used for supporting the grid voltage through controlling the reactive power generation. The battery energy storage system is a reliable solution for supporting the reliability of the system. It can match the difference between the generated power and the load, and hence improve the system reliability and undependability on the grid power.

Chapter 4: Solar Photovoltaic System Combined with Battery Energy Storage System

This chapter consists of material from two papers, the first paper is published in the annual IEEE Canada Electrical Power and Energy Conference (EPEC 2021) that was held virtually on October 22-24 and Oct. 30-31, 2021. And the second paper is published in the proceedings of the IEEE 53rd North American Power Symposium (NAPS 2021) that was held in Texas A&M University, College Station, Texas, on November 14 through November 16, 2021.

4.1 Modeling and Control of Solar PV System Combined with Battery Energy Storage System (paper 1)

4.1.1 Introduction

Renewable energy sources such as photovoltaic generation are becoming more attractive since they are an environmentally friendly energy source and free of pollution that is coming down in cost. Power generation from the solar energy is mostly dependent on climatic conditions. For example, photovoltaic array can't produce power during the nighttime or cloudy periods. To overcome these issues, PV systems should be combining with other energy storage systems such as battery banks, flywheels, or ultracapacitor banks [208].

Battery energy storage systems are one of the most commonly used types of energy storage systems. Their functions are to enhance the reliability of the system and reduce the dependency on the main grid power to temporarily supply loads. BESS is used to store the extra power at high irradiation levels, where the generated power surpasses the loads. At low irradiation values, when the generated power is less than the load power, the BESS supplies the loads. This enhances the system's reliability

and reduces the power consumed from the main grid. The battery system uses a bi-directional buck-boost converter for both charging and discharging operations and delivers power to the grid through an inverter [206, 209]. The layout of the proposed system is shown in Fig. 4.1.

In this chapter, a complete PV system description will be presented. Also, the model of the PV array system will be described. As the PV output power depends on the variable solar irradiation level, a maximum power point tracking algorithm is implemented to extract the maximum available power from the PV system. Furthermore, a control system and dc-dc converter are implemented for controlling the output voltage of the PV system [210, 211].

In this chapter different operational scenarios on the proposed system will be simulated using an electromagnetic transients simulation.

The rest of the first part of this chapter is arranged as follows. Subsection 4.1.2 describes the modeling of the system, including modeling of the PV array, MPPT, BESS and power converters. In Section 4.1.3, simulation results for the proposed system are described. Finally, some conclusions are drawn in Section 4.1.4.

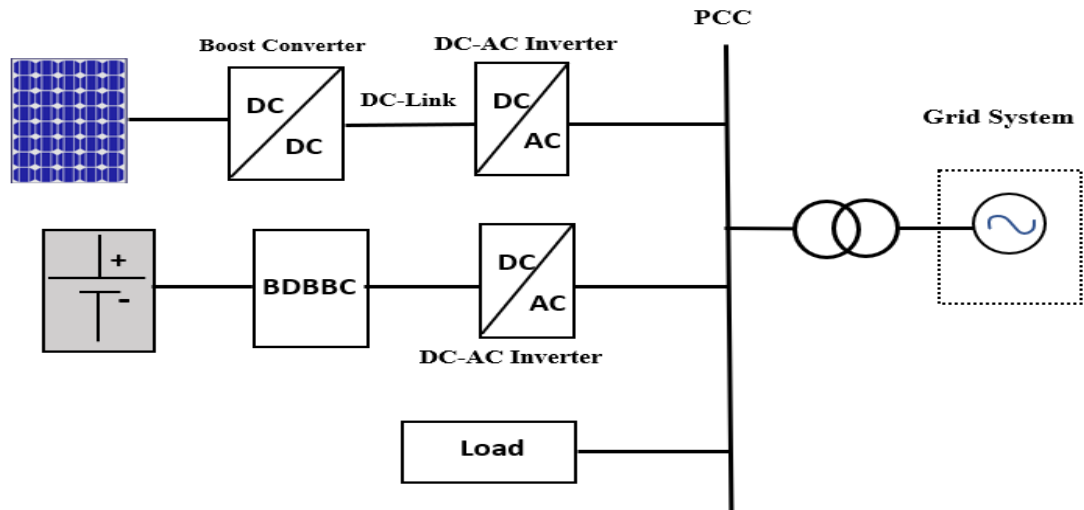


Figure 4.1: Layout of the proposed system

4.1.2 Modeling of the System

4.1.2.1 Modeling of PV Array

PV arrays consist of parallel and series combinations of cells to produce the required voltage and current. The voltage and current behavior of the PV array can be expressed using nonlinear mathematical equations described in [212, 213].

Fig. 4.2 shows the equivalent circuit model of the PV cell which consists of a diode connected in parallel with resistance (R_p), current source and series resistor (R_s).

The output current I_{pv} of a PV array which consists of a group of modules that are connected with N_s cells in series and N_p strings in parallel is represented by the following equations.

$$I_{pv} = I_{ph} - I_d - I_{sh} \quad (4.1)$$

$$I_{ph} = I_{SCR} * \frac{G}{G_{nom}} [1 + \alpha (T - T_{nom})] \quad (4.2)$$

$$I_d = I_0 \{ \exp(q(V_{pv} + I_{pv}R_s)/nN_sKT) - 1 \} \quad (4.3)$$

$$I_{sh} = \frac{V_{pv} + I_{pv}R_s}{R_p} \quad (4.4)$$

where I_{SCR} is the short circuit current at normal radiation conditions (A), G is the radiation level (W/m^2), G_{nom} is the radiation level at standard test conditions that equals to 1000 (W/m^2), α is the light generated current co-efficient temperature that is chosen to equal to 0.001 A/K, T is the measured cell temperature, T_{nom} is the normal standard test conditions cell temperature that equals to 25°, V_{PV} is the

solar PV cell outputs voltage (V), I_{PV} is the solar PV cell outputs current (A), n is the emission constant of the diode that is chosen to equal to 1.5. The series and parallel resistances (R_s and R_p) are chosen to equal to equal to 0.02Ω and 1000Ω respectively.

More details about the PV array modelling and operation can be found in [205, 214, 215].

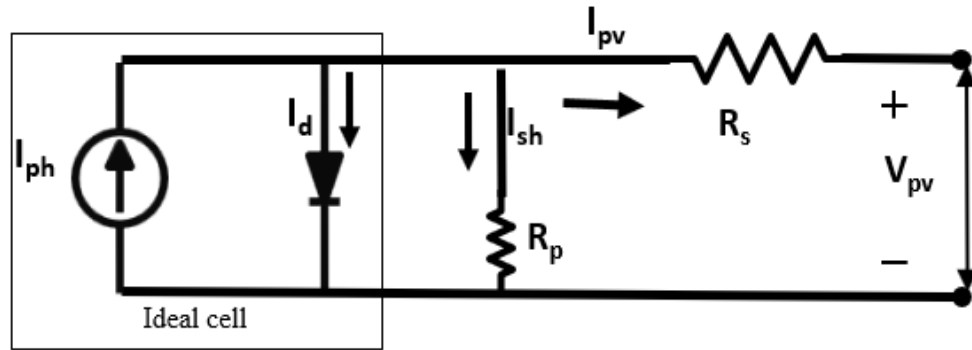


Figure 4.2: Ideal single diode PV model

4.1.2.2 MPPT Algorithm

The solar irradiation is always variable, so a MPPT technique should be utilized to get the maximum power from the PV system. There are different algorithms and controls used to extract the maximum power. The perturb and observe method ($P\&O$) is one of the techniques that is commonly used for its simplicity and low cost [210]. This method is based on perturbation of the cell bias voltage and observation to compare the change in the measured power after applying a disturbance [206]. The disturbance would decrease or increase the duty cycle of the boost converter and then observe the direction of change of PV output power. The sequence of this method is described in Fig. 4.3. The relationship between the power variation with respect to the voltage variation should be zero at the MPP and the duty cycle remains constant.

If the duty cycle is increased, it means that the instant power is more than the

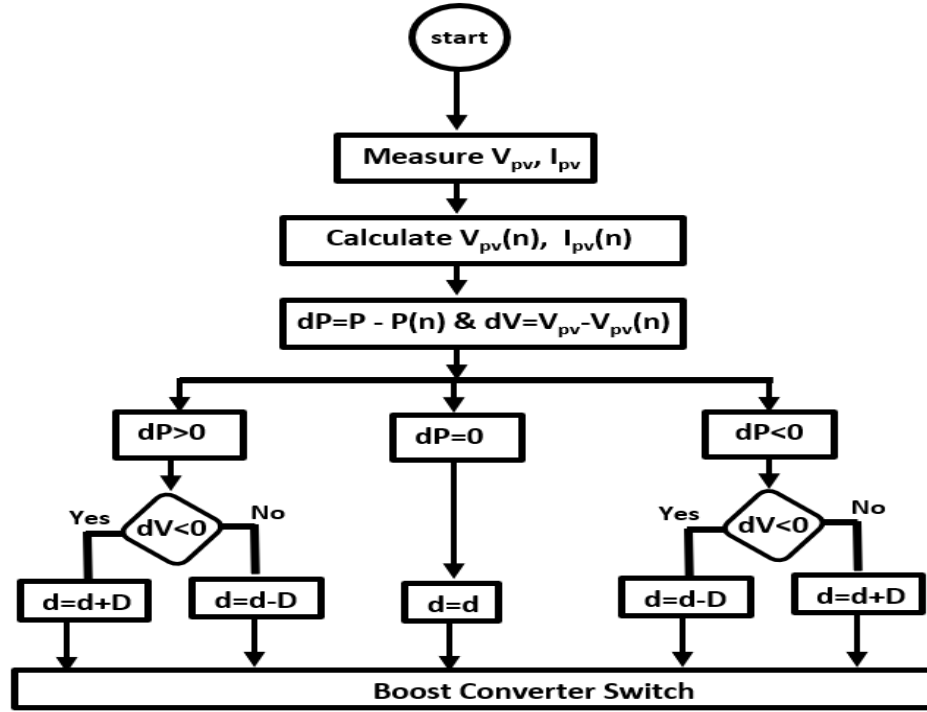


Figure 4.3: MPPT algorithm based on P&O method

previous power and the slope is positive ($\frac{dp}{dv} > 0$), so the duty cycle will operate with a higher value. On the other hand, if the instant power is less than the previous power, the slope will be negative, and then the duty cycle should be decreased by a small perturbation amount until MPP is reached. Depending on the sign of $\frac{dp}{dv}$, the algorithm in Fig. 4.3 decides on whether the duty cycle should be increased or decreased. Once the steady state power is achieved, the MPPT technique will oscillate around the MPP [210, 216].

Most of the time, PV arrays are connected to a large grid and the output PV voltage is not the same as the grid voltage. Therefore, a dc-dc boost converter is added between the PV array and the dc-ac inverter. DC-DC boost converter steps up the PV voltage and matches the voltage level at the dc-link [205]. The boost converter uses the duty cycle from the MPPT technique to control the output of PV and steps the voltage up according to equation (4.5).

$$\frac{V_{dc}}{V_{pv}} = \frac{1}{1 - D} \quad (4.5)$$

Where V_{pv} is the photovoltaic voltage, V_{dc} is the voltage at the dc-link, D is the duty cycle of the boost converter.

4.1.2.3 Modeling of the Battery

The equivalent circuit for the battery is based on a non-linear equation and the battery is modeled using a controlled voltage source connected with a series resistance as described in Fig. 3.8. The battery system and its bidirectional buck-boost converter were explained in Section 3.4.

4.1.2.4 Modelling of DC-AC Converter

The PV array and the BESS are connected to the grid through dc-ac converters. The converter average model is used in this part. The voltage source converter works with the specified strategy of the grid following vector current control as described in [207, 206]. The basic concept of the vector current controlled VSC is to independently control the instantaneous active and reactive power injected into the ac system. The converter can also transfer power in both directions. The average model of dc-ac converter is described in [206].

The equations of average model positive (I_{Pabc}) and negative (I_{Nabc}) currents can be given by (4.6) and (4.7) [207]:

$$I_{Pabc} = \left(\frac{1 + m_{abc}}{2}\right) \cdot i_{abc} \quad (4.6)$$

$$I_{Nabc} = \left(\frac{1 - m_{abc}}{2}\right) \cdot i_{abc} \quad (4.7)$$

while the equations of the average model for the three phase voltages (V_{tabc}) can be described as (4.8):

$$V_{tabc} = m_{abc} \cdot \frac{V_{dc}}{2} \quad (4.8)$$

The control strategy of VSC consists of two cascaded loops; the outer and inner loops [217].

Converter Outer Loop Controller

One part of the outer loop controller controls the voltage at dc-link and so, the active power transfer from the voltage source converter tracks the PV output and the battery charging or discharging power. The second outer control loop regulates the reactive power output from the dc-ac converter. The outer control generates the reference values for the inner loops. Fig. 4.4 shows the i_q^* and i_d^* set points which are the output from the outer controller and the input to the inner current loop controller. The active current component, i_d , is responsible for the regulation of the voltage at the dc-link (V_{dc}) or control of the active power flowing to the grid. The reactive current component, i_q , is responsible for the regulation of the voltage at the ac grid side or control of the reactive power flowing through the grid to follow its reference value (Q^*) [206, 207].

Inner Loop Control

The function of the inner current loop is to control the direct and quadrature current components of the current such that the converter's injected current tracks the reference closely. Fig. 4.4 shows the inner current loop which consists of PI controller, feed-forward voltage gain, and decoupling terms which is scaled to ac voltage to compute the modulation function quantities of the direct and quadrature m_d and

with the irradiation level. At an irradiation level equals to 1100 W/m^2 , the output power is 0.9 MW . When the irradiation decreases to 800 W/m^2 , the PV output power declines to 0.6 MW . At time 10 sec , the output power decreases to 0.3 MW when the irradiation level is 450 W/m^2 .

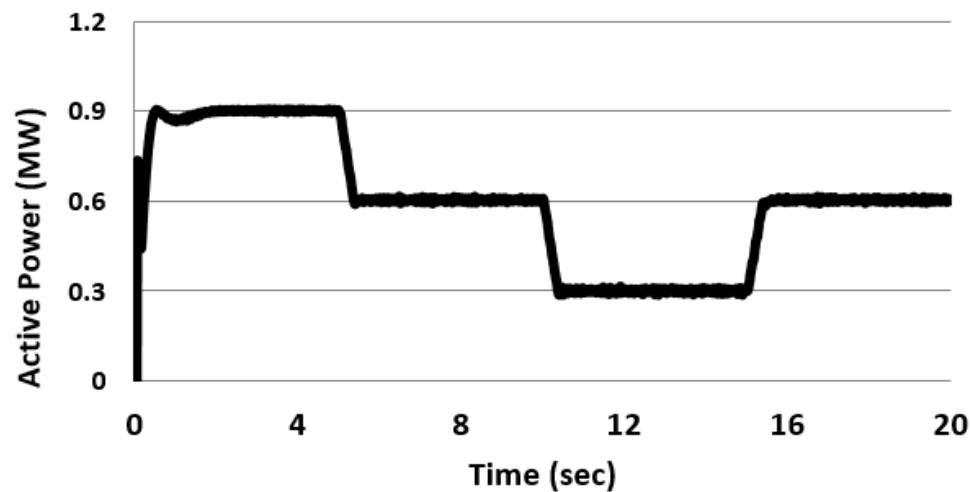


Figure 4.5: Generated active power in response to variations in irradiation

The reactive power is set to be at zero for unity power factor operation. Fig. 4.6 shows that the reactive power stays at zero as the irradiation varies for the case shown in Fig. 4.5. Also, the dc-link voltage curve is shown in Fig. 4.7. The dc voltage does not show significant changes as the real power is varied.

The PV system can be used for controlling the reactive power to support the grid voltage. Fig. 4.8 shows the reactive power profile that changes from $+0.4 \text{ MVAR}$ to -0.4 MVAR while the real power is also varying in response to irradiation changes. It can be shown from Fig. 4.5 that the active output power is dependent on the irradiation level and so it is better to connect the PV system to a battery energy storage system to supply the load in the low-level irradiation periods and to reduce independence on the grid power.

The system is simulated at different irradiation levels and constant load at 0.6 MW . When the irradiation level is 1100 W/m^2 , the output PV system is 0.9 MW

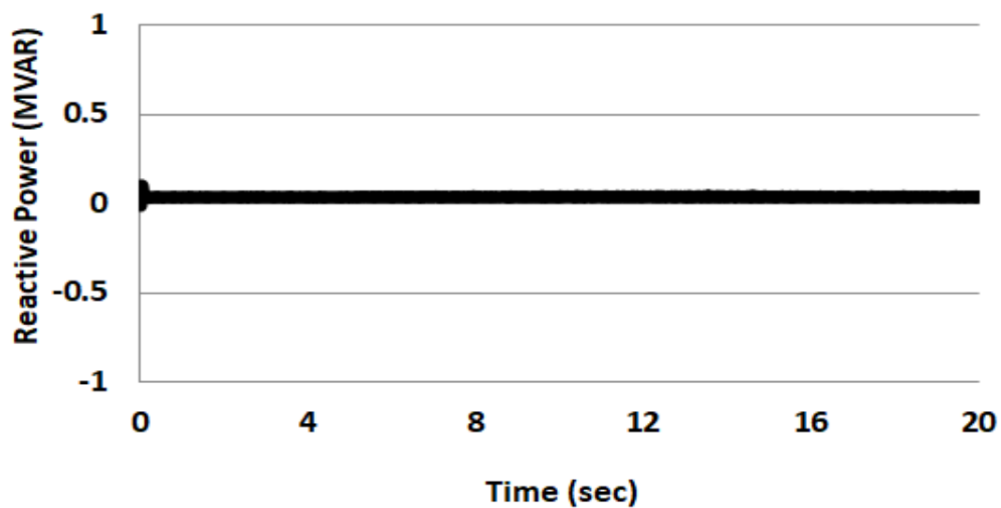


Figure 4.6: Generated reactive power as irradiation is varied

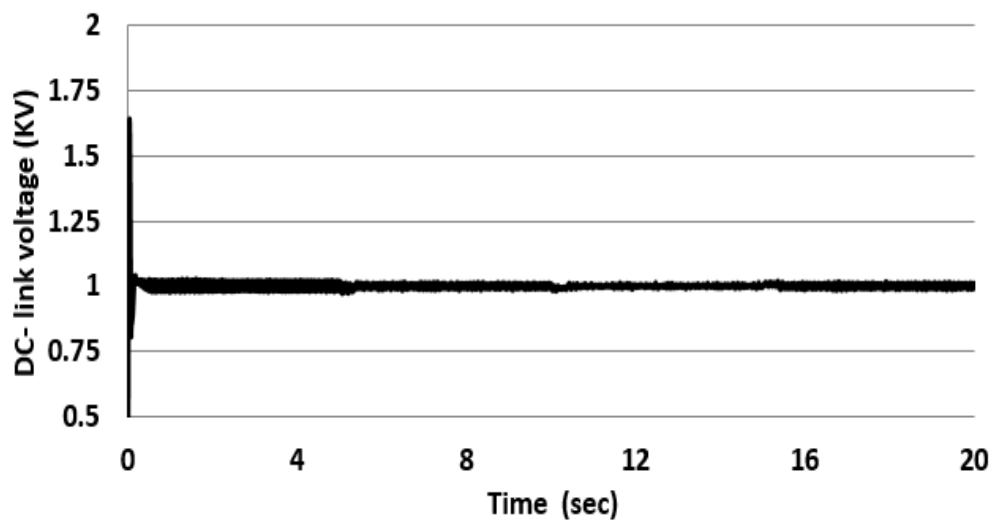


Figure 4.7: DC-link voltage profile in response to changes in irradiation

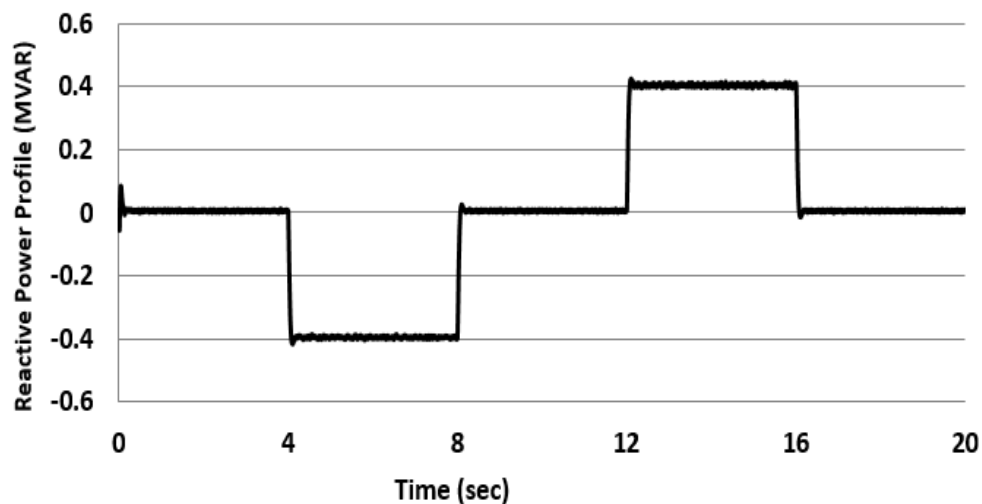


Figure 4.8: Reactive power variation profile

and the battery system is charging. When the irradiation level equals 800 W/m^2 the output power equals the load power and so the battery is just floating. Once the irradiation level drops to 450 W/m^2 , the PV output power is decreased to 0.3 MW and the battery discharges to support the load with the difference between the generated PV power and the load; 0.3 MW. Fig. 4.9 shows this sequence.

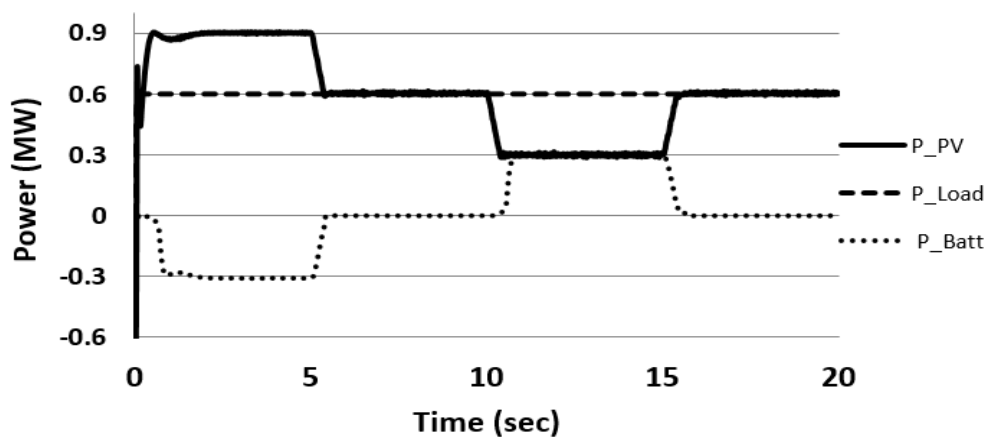


Figure 4.9: PV system, load and BESS power at different irradiation levels

Fig. 4.10 shows the state of charge (SoC) of the battery. When the battery is charging, the battery SoC is increasing. When the irradiation level decreases and

the output PV output power equals the load power, the battery system is floating and SoC is almost constant. When the battery supplies the load, the SoC starts to decrease.

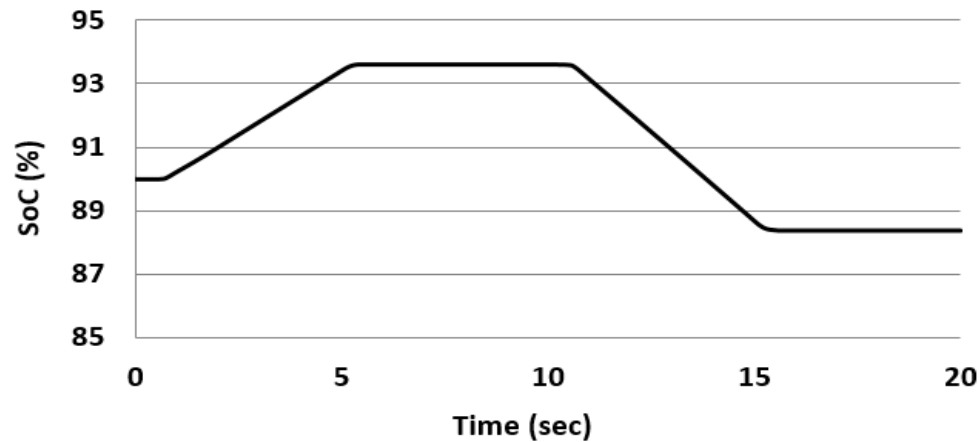


Figure 4.10: Battery SoC during irradiation level variation

The system is simulated for another simulation scenario, where the irradiation level is kept constant at 800 W/m^2 and the load is changed from 0.3 MW to 0.9 MW . Fig. 4.11 shows that when the load surpasses the generated power, the battery energy storage system discharges to supply the load. When the load power is less than the PV system output power, the battery is charging. SoC variation is shown in Fig. 4.12 and SoC vary according to battery charging and discharging mode.

4.1.4 Conclusion

Both active and reactive power can be controlled independently, so PV systems can be used to support the grid voltage by controlling the reactive power generation. Also, the resilience of the system can be enhanced by using a battery energy storage system for supporting the loads in case of large variations in the PV irradiation. The developed scheme can supplement the difference between the generated power and the load.

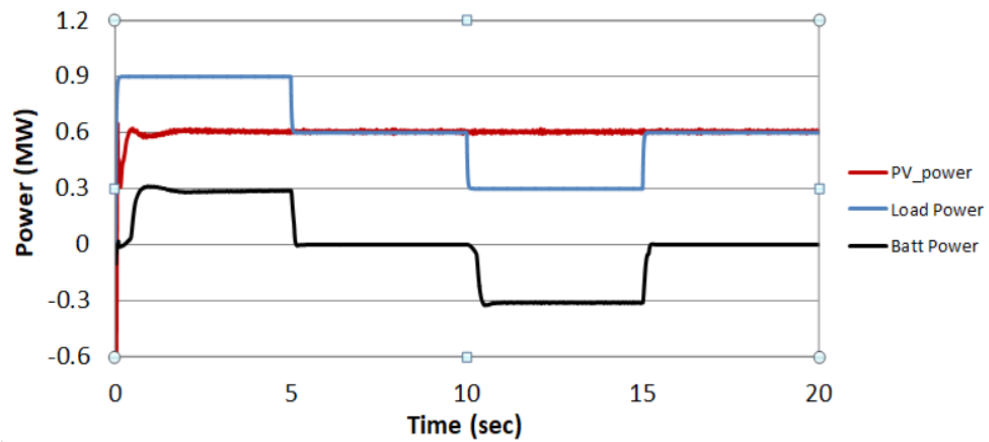


Figure 4.11: PV system, load and BESS power during load variation scenario

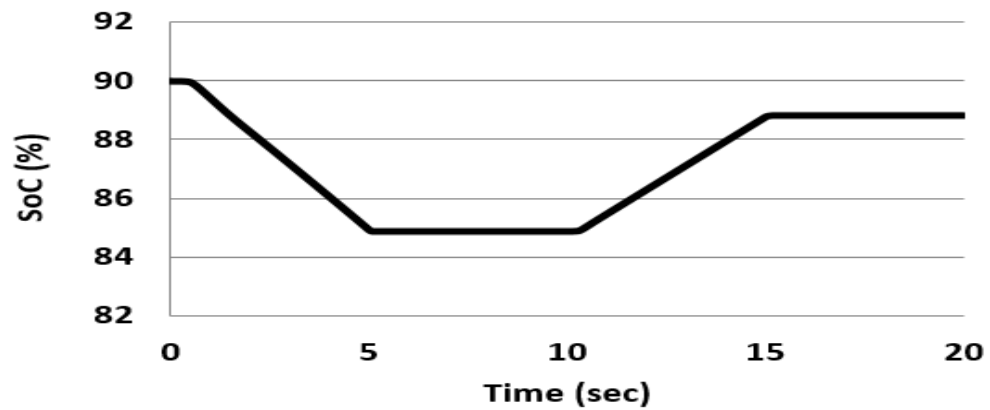


Figure 4.12: Battery SoC during load variation

4.2 Volt/Var Control of Solar Photovoltaic System (paper 2)

4.2.1 Introduction

The continuous growth in population is accompanied by increasing electric power demand. The greenhouse gas problems caused by conventional power resources and the eventual shortage of conventional fuel resources have led governments to encourage utilities to adopt renewable energy resources. Photovoltaic solar systems are popular among the RESs because of their advantages such as low running cost and pollution-free capabilities. Increasing the use of PV systems may add some challenges to the power system such as harmonic generation, but this can be corrected by adding power electronic devices and filters. Furthermore, PV integration causes voltage rise or drop due to the current variation and the reverse power flow among the power networks. Some standards such as ANSI C84.1 recommend that, at normal operating conditions, the terminal voltage magnitude should be within 5% of the normal voltage [218]. There are several traditional techniques that were adopted to solve the voltage variation problem. One of the used methods is to change the set point of the on-load tap changer in the high voltage side of the transformer. On the other hand, this method has some drawbacks such as arc production in the contacts and frequent maintenance requirements [219]. Using capacitor banks may mitigate the terminal voltage fluctuations, but they lack flexible control because they provide reactive power in discrete values [1, 2].

The authors of [218, 220] suggested curtailing the output PV power in case of voltage increase at the point of common connection. Needless to say, this solution was not popular with PV system owners. Other publications describe different techniques such as voltage regulators, capacitor banks, but the converter-based PV system can do the same function with many advantages.

In this research, the solar PV system can participate in voltage regulation through injecting and absorbing the reactive power. Reactive power control is used for controlling the terminal voltage level. Moreover, the controller sets the priority for the active or reactive power based on the voltage magnitude. The converter controller can control both active and reactive power independently. Also, it may curtail the active power to inject extra reactive power if the converter capacity is insufficient to generate both the required reactive power and the available active power from the sun. The dc-dc controller is used to direct the curtailed power to be stored in a battery energy storage system (BESS). This methodology is a form of volt/var droop control that enables the reactive power to regulate the voltage at the PV system terminals or at a location remote from the substation at which the voltage may drop below the normal operating value. The voltage control can be accomplished through linear droop characteristics which set the reference reactive power as a function of the terminal voltage of the PV system.

A description of the PV system is described, and the layout of the proposed system is shown in Fig. 4.13. Also, the model of the PV array is described. The output of the PV array depends on the variable irradiation level, so there should be maximum power point tracking technique is used for operating the PV array at the maximum power point. The used MPPT technique is presented in this chapter. Furthermore, the power electronic devices such as dc-dc boost converter and dc-ac converter are described. The volt/var control method is then presented followed by a description of the approach for varying reactive power in response to voltage variations. Also, synchronous rotating dq reference frame is used for modeling and design the active and reactive power controllers. Then, simulation using electromagnetic transients simulation is done to provide evidence that this control strategy is convenient for eliminating the voltage variation.

The rest of this chapter is arranged as follows. Section 4.2.2 describes the mod-

eling of the system, includes modeling of the PV array, MPPT technique, BESS and power electronic converters. In Section 4.2.3, a simulation of the proposed system is presented. Finally, in Section 4.2.4, some relevant conclusions are drawn.

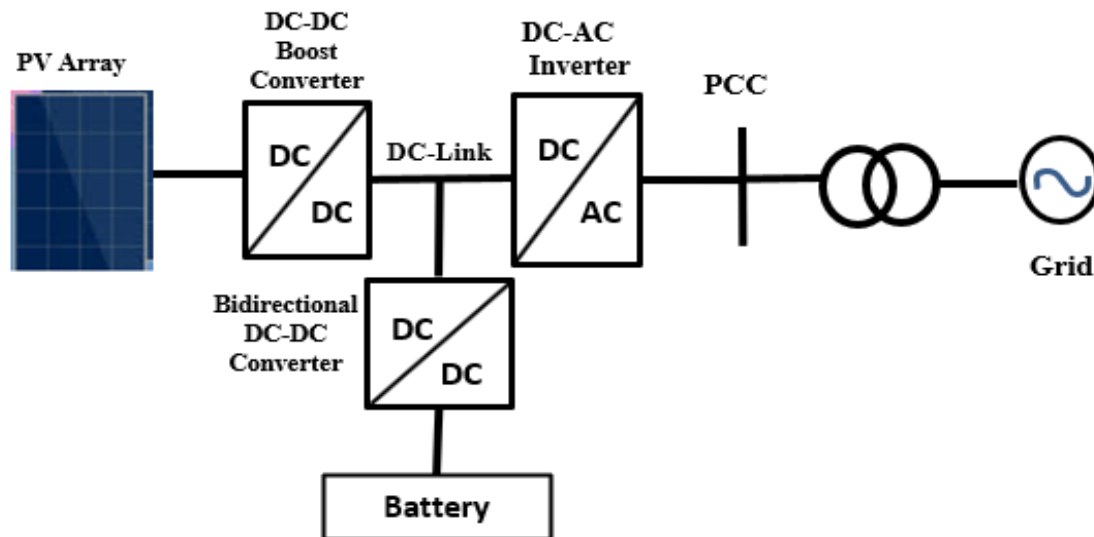


Figure 4.13: Layout of the proposed PV system with BESS

4.2.2 Modeling of the System

4.2.2.1 Solar PV Power Generation

A solar PV array is used to transfer the energy from the sun to electrical energy, it works similarly to a P-N junction diode. The electrical equivalent circuit and the equations relating the voltage and current were described in Section 4.1.2. The output of the PV array is greatly affected by the temperature and irradiation levels. Since the radiation level is continuously variable, MPPT technique should be used for generating the maximum power from the PV array.

There are several MPPT algorithms that can be used with PV systems, and they are detailed in [221, 222]. One of the preferred methods is the incremental conductance method (IC). It has some advantages such as its smaller response time and

limited oscillation around the MPP. Furthermore, the IC method can track the MPP accurately in case of variable climate conditions. At a certain operating conditions, the PV array generates current (I_{pv}), voltage (V_{pv}) and power (P_{pv}). If this operating point is the MPP, then the derivative of power with respect to the voltage should equal to zero ($\frac{dP_{pv}}{dV_{pv}} = 0$). When this ratio doesn't equal zero, the algorithm tries to reach to the MPP, where it compares the conductance ($\frac{I_{pv}}{V_{pv}}$) with the conductance variation ($-\frac{dI_{pv}}{dV_{pv}}$), and the result will be used to force the PV to work at the MPP according to equations (4.11) - (4.13).

$$\frac{dP_{pv}}{dV_{pv}} > 0 \quad \text{if} \quad \frac{I_{pv}}{V_{pv}} > -\frac{dI_{pv}}{dV_{pv}}, \quad \text{left to MPP} \quad (4.11)$$

$$\frac{dP_{pv}}{dV_{pv}} = 0 \quad \text{if} \quad \frac{I_{pv}}{V_{pv}} = -\frac{dI_{pv}}{dV_{pv}}, \quad \text{at MPP} \quad (4.12)$$

$$\frac{dP_{pv}}{dV_{pv}} < 0 \quad \text{if} \quad \frac{I_{pv}}{V_{pv}} < -\frac{dI_{pv}}{dV_{pv}}, \quad \text{right to MPP} \quad (4.13)$$

The speed of the MPP tracking depends on the size of the incremental step. A fast-tracking algorithm can be accomplished by increasing the incremental step, although this may cause the system to oscillate around the MPP. Decreasing the incremental step reduces the oscillation around the MPP; however, it requires a lot of processing and computations. Then determination the right size of the incremental step is important in the MPP algorithm [221]. The authors of [223] provided a description for determining the optimal incremental step.

The MPPT technique regulates the duty cycle that is required for the dc-dc boost converter. This converter is used to increase the voltage from the PV array that is presented to the converter, and it will be introduced in the next subsection.

4.2.2.2 DC-DC Boost Converter

The PV array generates a low and variable ac voltage that depends on the climate conditions. This voltage should be increased to be connected to the grid converter. A unidirectional dc-dc boost converter is used to step up the PV array output voltage. The voltage increase depends on the duty cycle generated from the MPPT technique according to (4.14).

$$\frac{V_{dc}}{V_{pv}} = \frac{1}{1 - D} \quad (4.14)$$

Where V_{pv} is the PV array output voltage, V_{dc} is the voltage at the dc-link and D is the duty cycle. Fig. 4.14 shows the layout of the dc-dc boost converter and its PWM control system. The theory of operation of the dc-dc boost converter is described in detail in [224]. According to the control strategy, the dc-ac converter transfers active power from the dc-link to the grid and controls reactive power exchange independently.

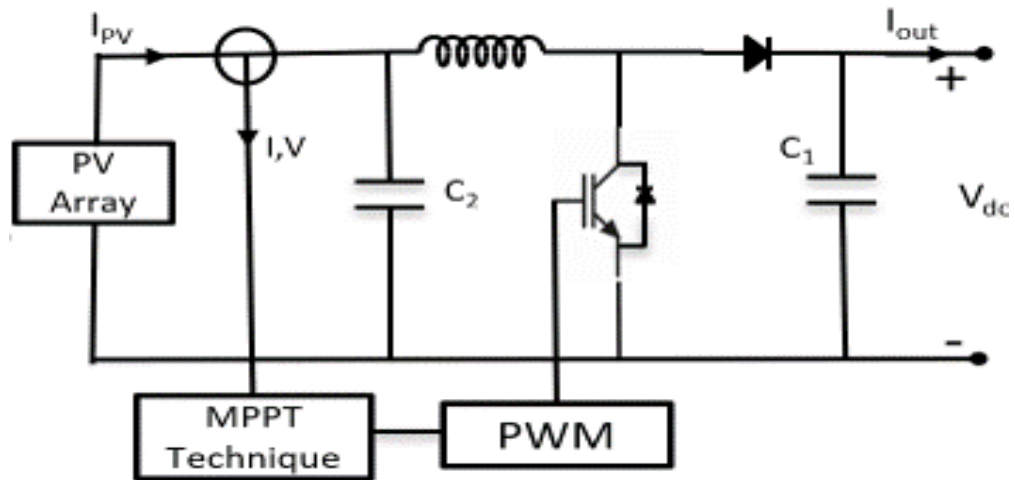


Figure 4.14: DC-DC boost converter

4.2.2.3 Volt/Var Control Strategy

This section describes the control method which controls the reactive power injection of the converter based on the ac voltage magnitude. The reference reactive power value is set by the controller using a linear droop characteristic that sets the reactive power value based on the measured voltage value as shown in Fig. 4.15. The controller considers the generated active power, converter current limits and priority of active and reactive power modes of the converter. As shown in Fig. 4.15, the droop characteristics can be defined by six points. The first point is v_a , when the voltage magnitude is at this point or lower the converter supplies the maximum possible reactive power. At this operating point, the converter doesn't supply rated active power since it prioritizes the reactive power and curtails the active power so as not to overload the converter. The second point is v_b , and it is the largest reactive power value at which the converter can generate at the rated active power generation while supplying reactive power. From v_c to v_d is a deadband where the voltage terminal level lies within the acceptable operating range and no reactive power injection is needed. The last two points v_e and v_f are similar to the first two points but in the opposite direction where the converter consumes reactive power to try to lower the voltage.

According to the measured voltage value, the converter sets the reference reactive power. When the voltage level is less than v_c , the converter starts to inject reactive power. On the contrary, if the voltage increased beyond v_d , the converter absorbs reactive power from the system. Within the deadband, the voltage level within the acceptable operating region, and the reference reactive power value is set to zero.

Selecting the volt/var curve is influential in the reactive power control. It depends on the network characteristics, network performance metrics, and load conditions. Then it is very important to use the suitable curve in the converter control system

[225]. The curve profile determines the limits for both the supplied and absorbed reactive power. Also, it sets the rate at which the reactive power will change with respect to the voltage variation. The authors of [219] described that the network losses can be minimized through the accurate optimization of volt/var profile. Furthermore, determination of the voltage points in Fig. 4.15 are set at the design and implementation of the system according to the recommendation of the utility that will be responsible for operating the system and to its following codes. In the future grids, these values should be able to be modified by the network operators to enhance the system performance optimization when the load pattern or the network topology are modified.

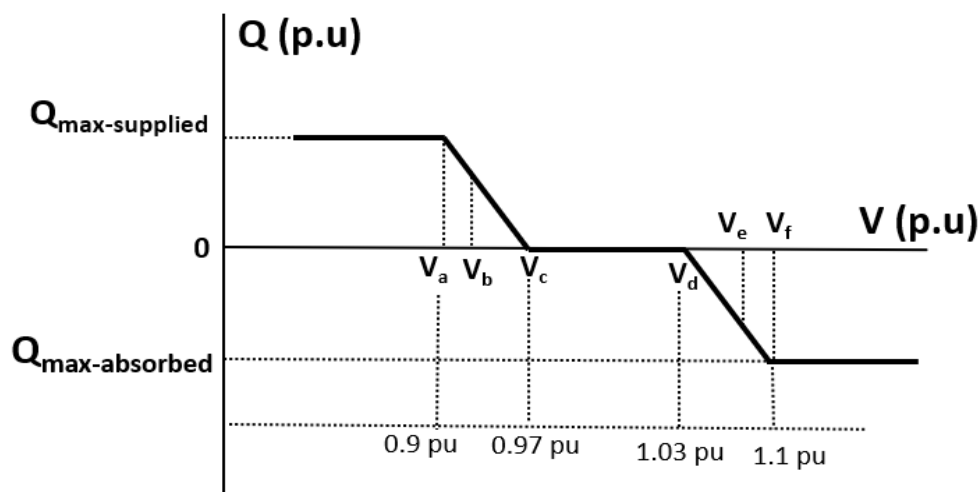


Figure 4.15: Volt/var control function

The controller should be able to prioritize either the active or reactive power and control both independently. Fig. 4.16 describes the determination of the maximum and minimum values of direct and quadrature axis current components based on the control signal. The control system is built using synchronous rotating dq reference frame at which d-axis controls the active power and the reactive power is regulated by q-axis. The default priority is set to d-component (control signal is set to 1), which prioritizes the active power and the maximum value for the converter current is set

to be the maximum value of the d-axis current component. On the other hand, if the control signal (CS) is set to zero, the reactive power and q-axis current component will be prioritized. Then the maximum value of the q current component will equal to the maximum value of converter current.

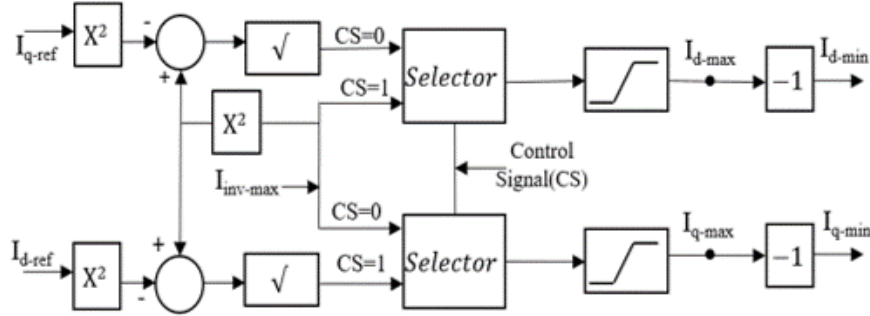


Figure 4.16: P-Q priority mode

4.2.2.4 Battery Energy Storage System

The battery energy storage system is mainly used for supporting the dc-link voltage to keep its value constant. Both the charging and discharging processes depend on the value of the dc-link voltage. When the converter output power increases beyond the PV generated power, the dc-link voltage decreases, and the battery is discharged to maintain the dc-link voltage constant. If the output power is decreased, the battery will be charged to prevent the dc-link voltage from increasing. The battery system and its converters were described in Section 3.4, and 4.1.2.

4.2.3 Simulation Results

The proposed control system is verified through modeling and simulation of a PV system in a simple microgrid using an electromagnetic transients simulation program. The simulation is carried out with the irradiation level equal to 1000 W/m^2 to operate the system at its rated output power and the load is changing during the simulation

period.

Fig. 4.17 shows that the variation in the terminal voltage due to load changes without the contribution of converter reactive power to support the terminal voltage magnitude. The terminal voltage varies beyond the acceptable range; where it ranges from 0.9 to 1.1 pu due to load variation. The acceptable margin for the voltage values is set to be between 0.97 and 1.03 pu. Then the reactive power generation should be controlled to support the voltage profile such that it doesn't go out of the acceptable margin.

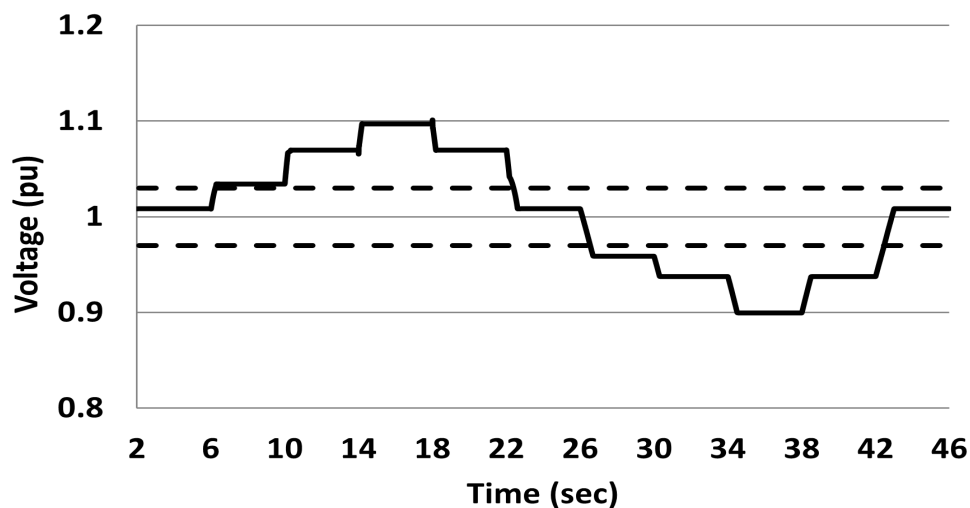


Figure 4.17: Voltage variation profile without reactive power support

Fig. 4.18 shows the variation in the reactive power from the converter in response to the terminal voltage variations. When the voltage level falls within the acceptable margin, the reactive power generated equals to zero. When the voltage level increased above 1.03 pu, the converter absorbs reactive power to reduce the voltage. When the voltage is decreased below 0.97 pu, the converter supplies reactive power to increase the voltage to be within the normal range.

The generation of reactive power has improved the voltage profile as shown in Fig. 4.19. The voltage levels are bounded within the normal acceptable range. This describes that the control system is responding to the voltage variation.

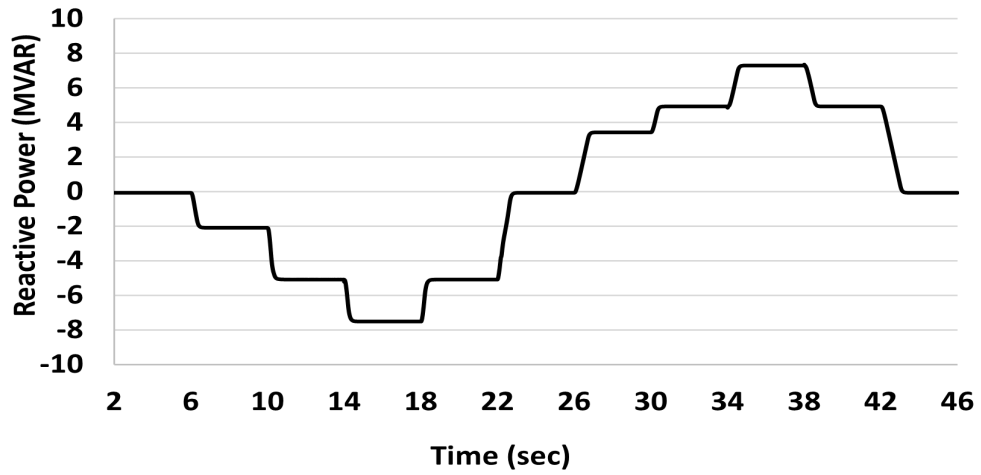


Figure 4.18: Reactive power variation profile

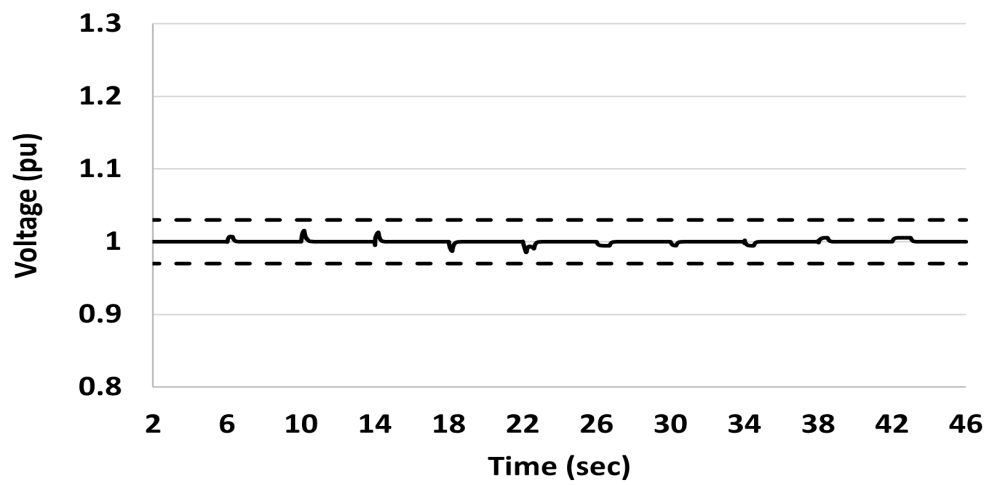


Figure 4.19: Voltage variation profile with reactive power support

At the extreme voltage change, where the voltage value reaches to 0.9 or 1.1 pu, the converter is unable to produce both the rated active and required reactive power so as not to be overloaded. The converter prioritizes the reactive power at these intervals and curtails the active power generated to provide the required reactive power to support the voltage level. The priority signal changing is shown in Fig. 4.20, where it changes from (1); to prioritize the active power to (0); to prioritize the reactive power.

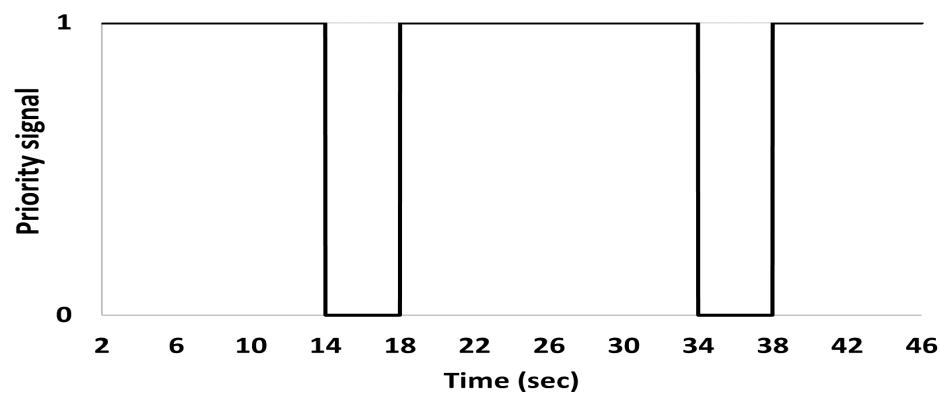


Figure 4.20: Priority signal

Fig. 4.21 shows the active power profile. When the priority signal is (1), the converter generates the rated power. On the other hand; when the priority signal is (0), the active power is curtailed so as not to overload the converter.

When the converter curtails the active output power, this power is stored in the battery energy storage system so as to make the best use of the available PV power and to keep the dc-link voltage at its rated value. Fig. 4.22 shows the state of charge of (SoC) the battery system, when the active output power is curtailed and the battery is charged, SoC is increasing. On the other hand, battery SoC is kept constant at the other intervals. Fig. 4.23 shows the dc-link voltage, its value doesn't change with the load and power variation.

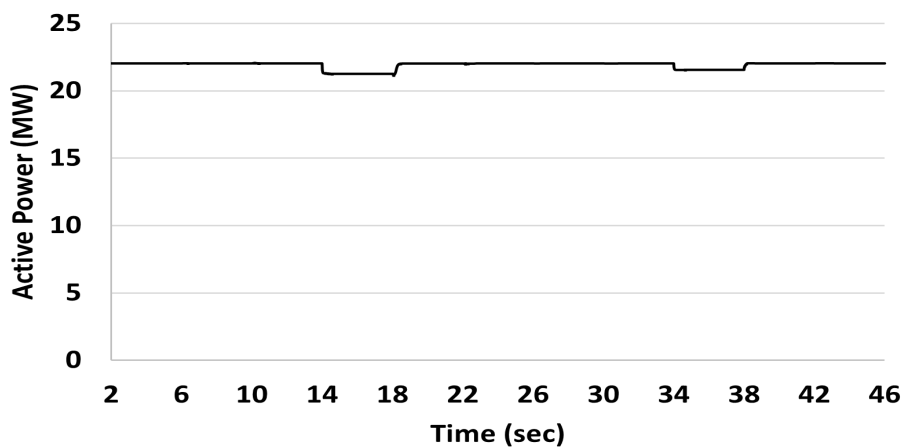


Figure 4.21: Active power profile

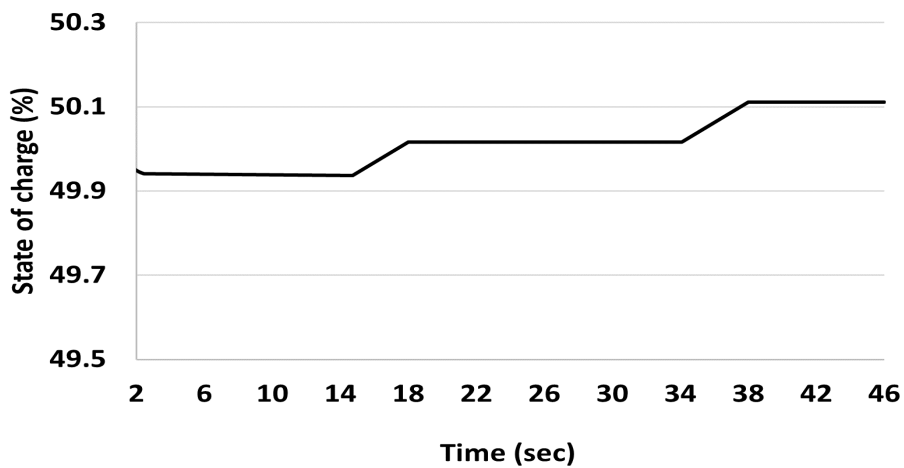


Figure 4.22: Battery state of charge

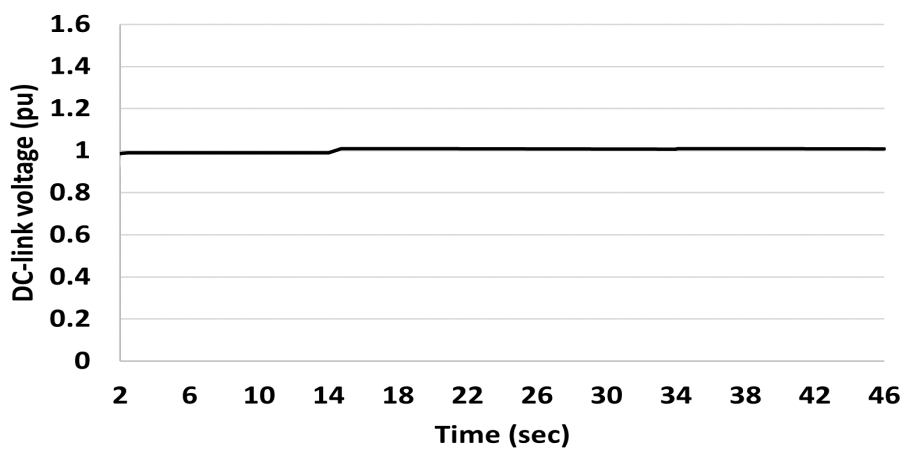


Figure 4.23: DC-link voltage profile

4.2.4 Conclusion

Mitigating the voltage variation in the power system is vital for achieving a decent power system performance and operation. In this chapter, the voltage variation was mitigated by absorbing or supplying the reactive power from the PV converter. Consequently, the voltage level was controlled to be within acceptable limits. In this chapter, modeling of the PV system was described. The converter prioritizes the active and reactive power based on the voltage level and controls both independently. Furthermore, the maximum power point tracking technique implemented for this system was described. Simulation of the system was carried out using an electromagnetic transients simulation program, and the simulation was conducted at different load values that changed the voltage levels. From the simulation results, it can be concluded that the voltage can be successfully controlled through the volt/var strategy to be within the safe operating margin. Furthermore, the battery energy storage system is vital in PV systems to increase its reliability such that, it absorbs the excess power or supplies the load if the PV available power is not sufficient to meet the load demand. Also, it enables the inverter to control its active output power based on the voltage level and priority control signals.

Chapter 5: Virtual Synchronous Generator Controller

This chapter consists of material from a paper that is published in the annual IEEE Canadian Electrical Power and Energy Conference (EPEC 2021) that was held virtually on October 22-24 and Oct. 30-31, 2021.

5.1 Introduction

The number of converter-based renewable energy resources in the power system is increasing due to their decreased cost, improved efficiency, and government policies encouraging their development. The increasing penetration of RERs is happening at the same time older coal and nuclear plants are being decommissioned. Synchronous generators have inertia and damping characteristics that help to support the system's stability. They can be controlled to provide frequency regulation. These common features for the SGs are not available in most power converters that are used for integrating RERs to microgrids or to the large grid.

The conventional power converters work in the power system as a grid following controlled current sources [226]. They try to maximize the energy extraction from the connected distributing resources, based on operation with a stable-frequency grid. This stable frequency is fixed through the large rotating inertia of SGs, but these features are not available in the future smart grid or isolated grids with high penetration of inverter-based RERs.

Thus, in the future, power converter control methodologies should play a noticeable role in the operation and control of smart grid. The proliferation of converter-based RERs to replace the traditional large-scale SG diminishes the total system inertia and could destabilize the system for smaller disturbances than are the case now. The grid becomes vulnerable to high-frequency fluctuation in case of disturbances such as varying loads or variations of electric power generated from RERs

such as PV power plants. Several researchers have explored approaches to overcome these problems. The authors of [5, 6] described a constant voltage-constant frequency control methodology that is able to maintain grid stability in isolated grids. On the other hand, this method has some drawbacks such as communication system requirements and detailed data measurements which may lessen the system flexibility and scalability [7].

Additional significant research effort was devoted to develop several control methodologies for power converters to emulate the desirable features of conventional SG. The inverters provide the grid with the emulation of rotating inertia which is called virtual inertia (VI). Then, VI control can contribute to system frequency stabilization.

VI emulation control methods underwent several steps over the years. In [13], Beck and Hesse proposed the first control method for VI and it was called a virtual synchronous machine (VISMA). They implemented a current-controlled inverter in the dq-reference frame using the Park's transformation. Later, a lot of research work was done to apply the VI concept in the power converters to emulate the SG, and with a variety of different names for the algorithms.

The authors of [14, 15] implemented a simple model to emulate inertia and damping using the swing equation of a synchronous machine, and called it a virtual synchronous machine (VSM). The control method is based on generating the reference control voltage from the outer loops; getting a real power command from the VI emulation and a reactive power command, and using them in PWM signal formulation. Although this method is simple to model, it is complicated to protect the controller from high currents in case of disturbances or faults.

In [16], the authors overcame the previous disadvantages by applying the generated reference signals from the outer loops to an inner control structure which consists of cascaded voltage and current controllers. In these inner loops, the controllers' currents and voltages can be limited and protected against disturbances such as fault

currents. This methodology is called a synchroverter, which can be summarized as a voltage-controlled voltage source inverter emulating conventional SG.

The authors of [17, 18, 19] proposed control methods called virtual synchronous generator (VSG) which can emulate the performance of SGs. Some of them were implemented as a current-controlled inverter such as VISMA, other works as a voltage-controlled inverter like the synchroverter. VSG emulates the conventional generator inertia and damping characteristics and also enables the inverter to operate in both grid-connected and isolated modes. Moreover, VSG parameters can be adjusted to emulate any arbitrary SG without any constraints to match a certain SG and can be easily adjusted without affecting the Park's equations [18, 227].

In this chapter, the dynamic characteristics of SG are emulated by VSG such as the damping and inertia constants. VI emulation technique should replicate the conventional SG inertial features, and it can offer frequency support based on local measurements without the need for extra communication media. Moreover, the inverter is able also to work in a hierarchical control system where the inverter can receive the reference set points from the central controller.

The VSG controller consists of outer and inner loops. The outer loops represent the VI emulation and terminal voltage control. They produce the reference signals to the inner cascaded voltage and current loops. The current reference signals can be calculated from algebraic equations. The current and voltage signals are controlled and limited in the inner loops. Hereafter, the mathematical model is described in the synchronous dq reference frame, and the simulation of the proposed control methodology is carried out using an electromagnetic transients program.

The rest of this chapter is arranged as follows. Section 5.2 describes the layout of the system. In Section 5.3, the VSG controller structure is presented including both the outer and the inner loops. The simulation of the proposed system is presented in Section 5.4. Finally, in Section 5.5, some relevant conclusions are drawn.

5.2 System Layout

The proposed system layout where a VSG-based controller is used to control the PV system with a storage system is shown in Fig. 5.1. The PV array is the main source of electrical energy. It produces electrical power at a low voltage, so a dc-dc boost converter is used to step up this voltage and try to maximize the energy extracted from the PV array using a maximum power point tracking scheme.

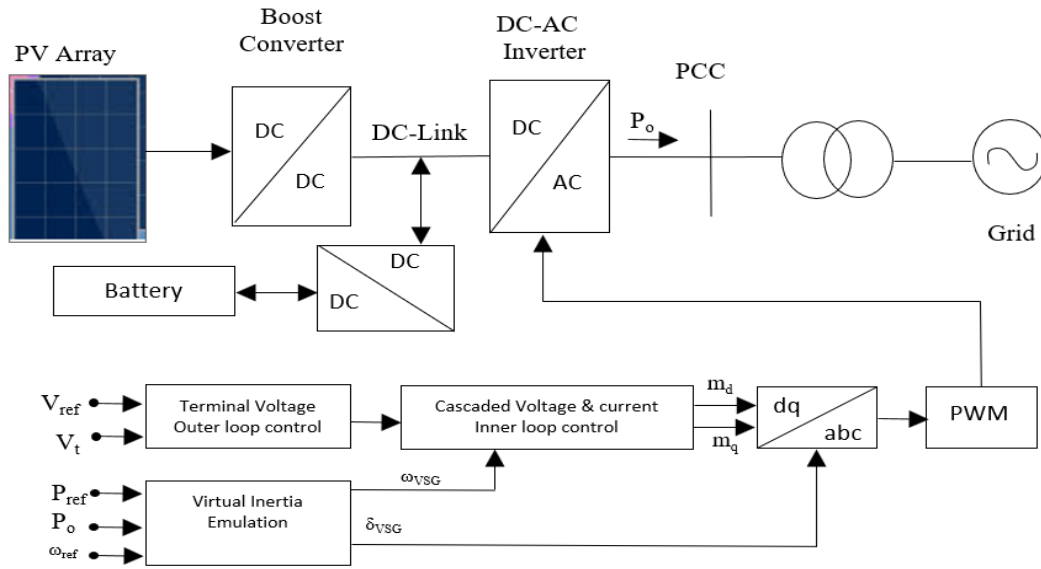


Figure 5.1: General layout of the proposed VSG system

Emulating the rotating inertia requires an energy storage system, and VSG performance relies on the dc-link configuration such that the power fluctuation is supplied or absorbed from the dc-link and so, from the storage system. Thus a battery energy storage system is used as well as a bidirectional buck-boost converter to charge or discharge the battery. The inverter transfers power from the dc-link to the electric power grid which is simulated by a voltage source. The model and the control system were implemented in a dq reference frame. A detailed explanation of the system can be found in [214, 228, 229].

The control structure consists of two main loops, the outer loops are representing

the inertia emulation and ac terminal voltage magnitude control. VI emulation produces the virtual rotor angular position of the VSG and this represents the load angle of VSG. Furthermore, the voltage controller produces the VSG voltage magnitude and this will be applied to the inner loop.

From the reference voltage signals, the controller calculates and produces the reference currents to the inner control loops. Thus, the inverter is able to operate in both the grid-connected and isolated operating modes. Furthermore, it can provide a smooth transition between these two operating modes. In the following subsections, an explanation and the mathematical model of the parts of the system will be described.

5.3 VSG Controller Structure

5.3.1 Outer Loops Structure

The active power is associated with the VSG emulated torque and angular speed of the rotor (ω). As shown in Fig. 5.2, the variation in the rotor speed can be determined by applying the difference between the reference and output active power to a proportional gain constant K_p and first-order lag element which has a time constant T_p . These two constants represent the damping effect and the rotating rotor inertia of the SG.

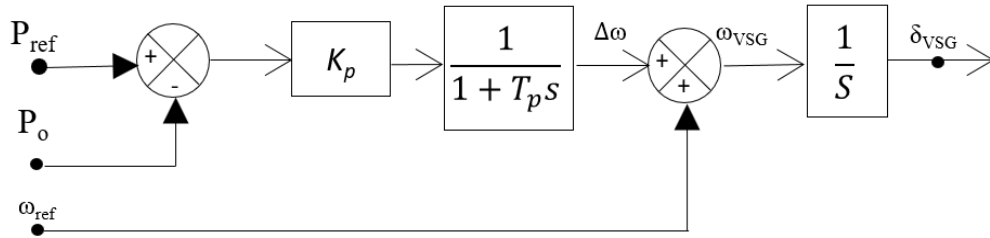


Figure 5.2: Virtual inertia emulation

The virtual rotor angular speed is then calculated by adding this difference to the

rated angular speed. Integration of this angular speed produces the virtual generator load angle. This angle is used in the inner loops and for the Park's transformation in the inverter control. Then, frequency variations due to abrupt changes in the load or generating power can be suppressed by the rotating rotor inertia created by the proposed control system. Furthermore, the VSG can improve system stability and replicate the desirable inertial attributes of conventional SG performance.

The proportional control and first-order lag element which are used in calculating the angular velocity, represent the combination of the damping and rotor inertia. The mathematical expression can be derived as follows. The swing equation of the conventional SG which can be derived from Newton's Law of Motion for rotating objects can be written as [230, 231]:

$$T_m - T_e - D\Delta\omega = 2H\Delta\dot{\omega} \quad (5.1)$$

where T_m is the mechanical torque driving the generator (N.m), T_e is the electromagnetic torque due to electric load on the generator (N.m), D is the damping torque coefficient associated with the damper windings (N.m.sec), H is the per unit inertia constant for the stored kinetic energy in the rotor at rated speed divided by the chosen MVA base, and $\Delta\omega$ is the deviation from synchronous speed.

It is more common to write the swing equation expressed in (5.1) in terms of power instead of torque. In case of a little oscillation around the synchronous speed, the equation representing the power balance which is approximately represented in s domain is expressed as [14]:

$$T_a.s.(\Delta\omega) = P_m - P_e - k_d(\Delta\omega) \quad (5.2)$$

where P_m is the emulated mechanical input power, P_e represents the electrical power, T_a denotes the time constant which is related to the inertia, and K_d represents the

damping constant.

From the previous relations, the following equation can be derived.

$$\frac{\Delta\omega}{\Delta P} = \frac{1}{T_a s + K_d} = \frac{K_p}{1 + sT_p} \quad (5.3)$$

So, the damping and the rotating rotor inertia can be represented in a first-order lag element with a proportional gain ($K_P = \frac{1}{K_d}$) which represents the inverse of the damping. Also, it has an inertia constant ($T_P = \frac{T_a}{K_d}$), which represents the time taken by the rotor of the machine to reach its rated speed, when accelerated by the rated torque from rest.

The voltage amplitude of VSG output can be obtained by separate voltage or reactive power outer control loop which is decoupled from the inertia emulation loop. The terminal voltage should be controlled to enable the inverter to work in both grid-connected and isolated modes of operation. As shown in Fig. 5.3, the difference between the terminal voltage and the reference value is passed through PI controller to generate the VSG voltage magnitude. This component is used as an input to the inner loop cascaded voltage and current controller.

In this control strategy, the reference terminal voltage is aligned to coincide with the direct axis of the inverter voltage reference frame, and so the reference quadrature axis voltage is set to zero.

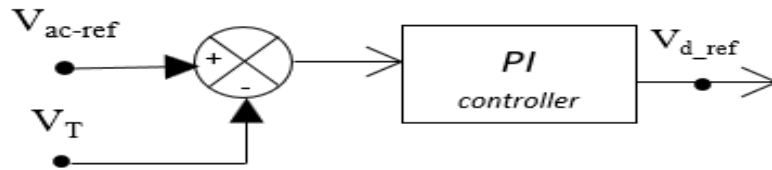


Figure 5.3: Voltage controller

5.3.2 Inner Loop Controller

To enhance the controllability of the system, the inner loop controller consists of two cascaded voltage and current parts as shown in Fig. 5.4. It is also modeled in synchronously rotating dq reference frame, so it can be controlled by PI controllers. The first part is for controlling the output voltage and is responsible for generating the references for the current controller part using PI controller gains K_{pv} and K_{iv} . The reference current generation can be expressed as:

$$I_{ref} = K_{pv}(V_{ref} - V_o) + \int K_{iv}(V_{ref} - V_o) + jCV_o\omega_{VSG} \quad (5.4)$$

where I_{ref} denotes to the components (I_{d-ref} and I_{q-ref}), V_o denotes to the output voltage components (V_d and V_q), and C is the capacitance of the filter between VSC and the grid. The current reference values (I_{d-ref} , I_{q-ref}) which are generated from the voltage controllers can be limited against over-currents due to faults or other abnormal conditions. This provides flexibility and can provide an embedded protection strategy.

The second inner loop current controller is a conventional PI controller with gains K_{pc} and K_{ic} and decoupling terms that generating voltage reference signals; V_d^* and V_q^* . The output voltage reference from the controller can be described as:

$$V^* = K_{pc}(I_{ref} - I_o) + \int K_{ic}(I_{ref} - I_o) + jI_o\omega_{VSG}L + V_o \quad (5.5)$$

where I_o denotes the output direct and quadrature current components (I_d and I_q) and L is the filter inductance.

The voltage reference signals resulting from the current controller are divided by the half of dc-link voltage to generate the modulation indices M_d and M_q as shown in Fig. 5.4. The reference signals are transformed to abc frame by an inverse of the

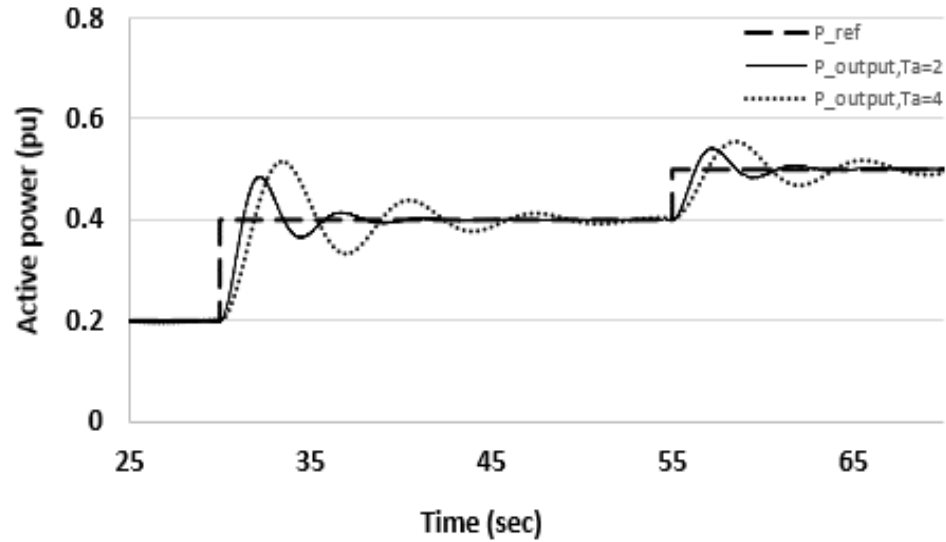


Figure 5.5: VSG active power variation at different inertia time constants

and $T_a = 2$) and the damping constant is kept constant ($K_d=0.7$). The difference between the generated PV and inverter output power is compensated by the battery. The power profile depends on the inertia time constant such that, at a larger inertia time constant (or per unit inertia constant), the system has larger amplitude power oscillations. On the other hand, when the inertia time constant or per unit inertia constant is reduced, the peak overshoot in power supplied from the battery is reduced. Fig. 5.6 shows the power generated from PV array and the power that is compensated by the battery.

The change in the output power affects the frequency of the VSG. This effect is described in Fig. 5.7. It is clear that at lower inertia time constant value, the frequency variation is more pronounced and it has a higher rate of change of frequency. On the other hand, when inertia time constant increases, it helps the system to counteract the frequency change and it has a lower rate of change of frequency.

The next set of simulations examines the impacts of the settings for the damping constant in the VSG design. Fig. 5.8 shows the inverter active power variation at different damping constant values when the inertia time constant is constant ($T_a=2$).

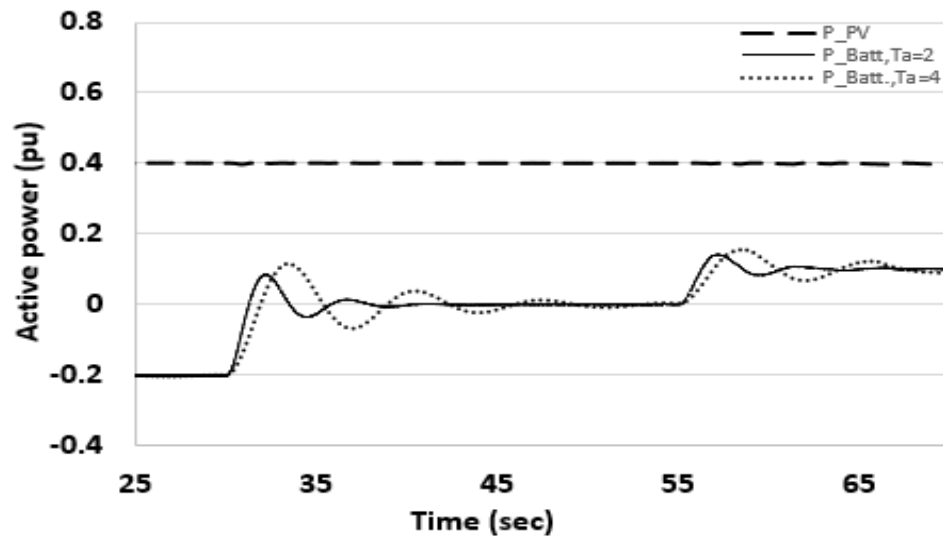


Figure 5.6: PV array and battery power at different inertia time constants

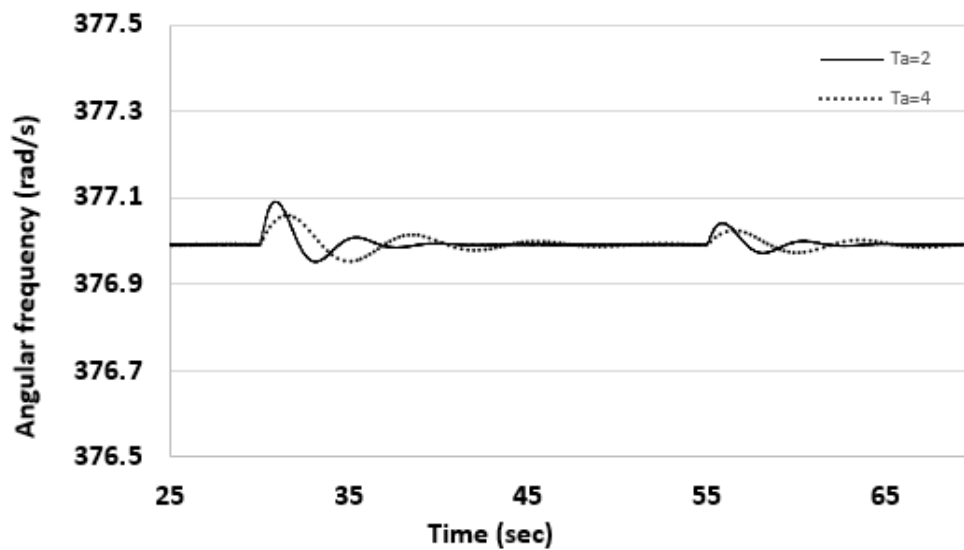


Figure 5.7: VSG frequency profile at different inertia time constants

Fig. 5.9 shows the power is supplied by the battery. It can be seen that increasing the damping constant helps the system to reach its steady state value sooner and reduces the peak power supplied by the battery energy storage system. On the other hand, when the VSG controller has a smaller value of damping constant, larger peak power is required from the battery energy storage system and the system takes a larger time to reach its steady state value. It is worth to be mentioned that, inertia time constant and damping constant affect the maximum power supplied by the battery and the time it takes to settle down, and so the energy that should be stored at the battery. Then these parameters affect the sizing of the battery energy storage system.

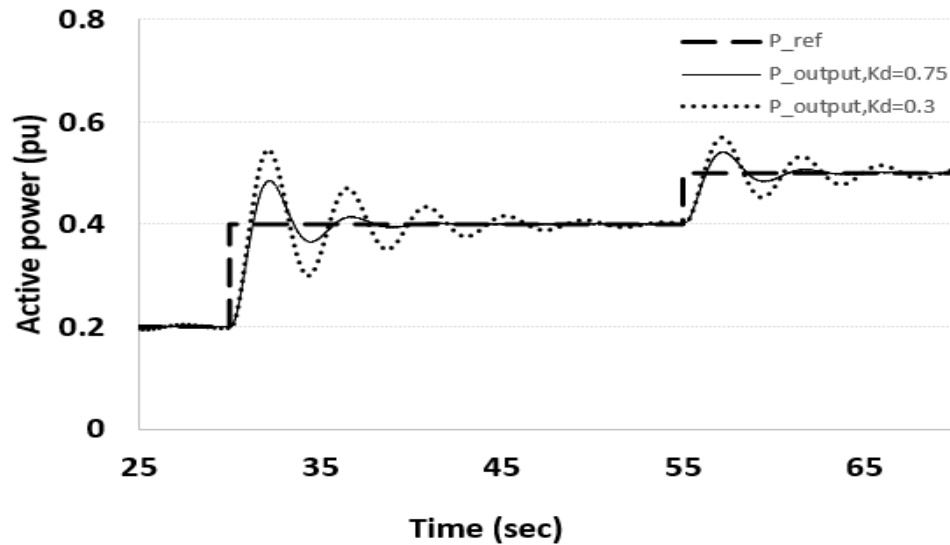


Figure 5.8: VSG active power variation at different damping constants

In this design, the VSG is controlled to regulate ac voltage magnitude at the point of common coupling. The reactive power changes in response to system conditions to maintain the voltage magnitude at the set point. This enables the system to work at constant voltage during isolated mode of operation. Fig. 5.10 shows a case where the grid voltage changed from 0.95 to 1.05 pu, but the voltage at the PCC is controlled to be constant at 1 pu. Fig. 5.11 shows the variation of the reactive power output from the converter in response to the disturbance. In this case, the apparent power

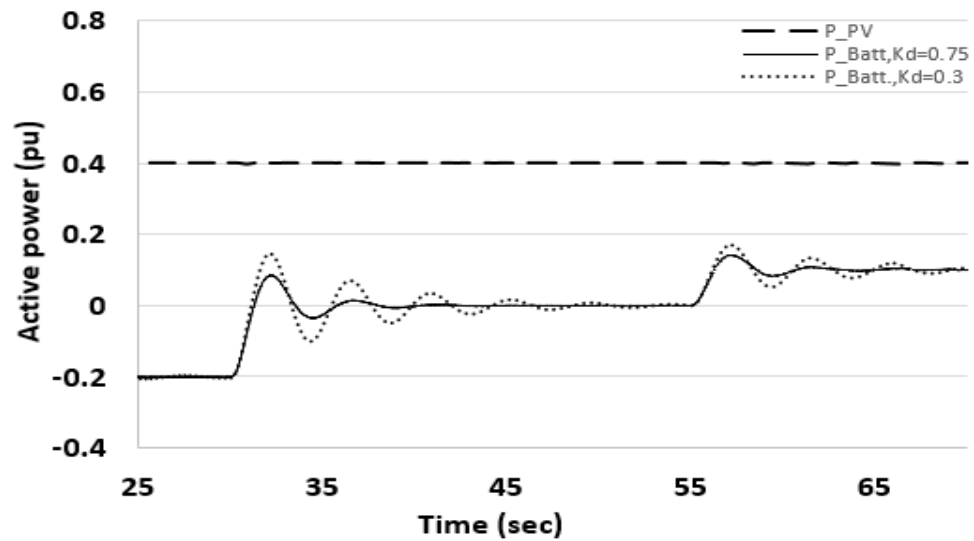


Figure 5.9: PV array and battery power at different damping constants

stays within the converter limits. The VSG is able to achieve the dynamic voltage regulation for the system and help reduce the impact of disturbances on the voltage.

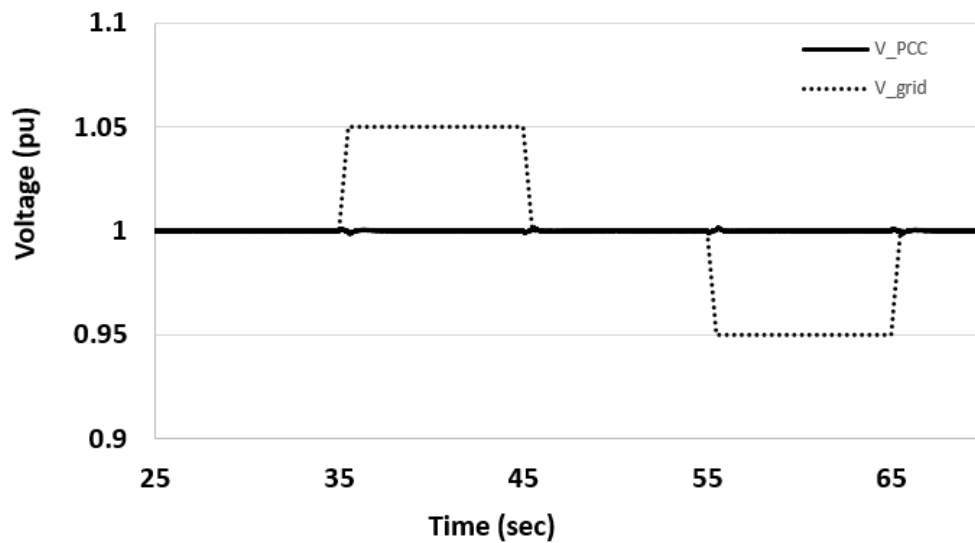


Figure 5.10: Terminal voltage variation profile

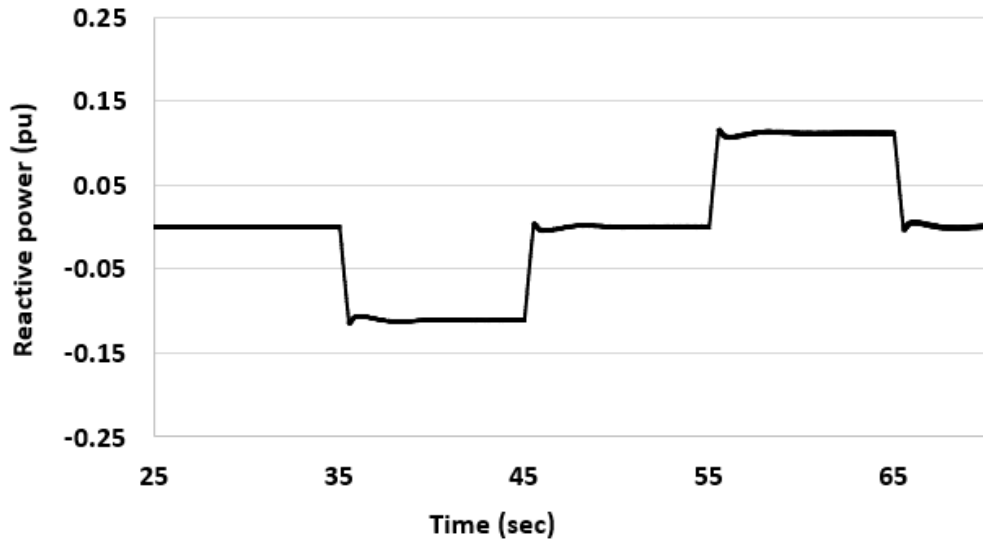


Figure 5.11: Reactive power profile

5.5 Conclusion

Large changes in load or the generated power from RERs cause the frequency of the system to fluctuate. The amplitude, frequency, and damping of this fluctuation depend on the rotor inertia and damping coefficient of synchronous machines in the system. In this chapter, a brief explanation of VSG was presented with the aim of emulating inertial features of conventional SG. Then modeling of VSG control structure was discussed in synchronously rotating dq reference frame. All the system including PV array, power electronic converters, and BESS was integrated and implemented using an electromagnetic transients program.

From the simulation results, it can be concluded that rotor inertia and damping constants can be emulated by the converter. Also, a VSG-based controlled inverter combined with BESS can emulate the inertial behavior of conventional SG to regulate and support the frequency of the power system following a disturbance and improve system performance. Furthermore, VSG parameters can be set according to the best performance without being limited by the characteristics of a physical SG. Moreover,

it can support the system voltage even in the case of grid voltage fluctuations. As a result, VSG controllers can promote exploiting and expanding RERs in microgrids.

Chapter 6: Virtual Synchronous Generator Controller

Performance and Evaluation

This chapter consists of material from a paper that is accepted for the Grid of the Future Symposium / CIGRE to be held on November 7 through November 10, 2022 in Chicago, IL, USA.

6.1 Introduction

Renewable energy resources such as wind, solar photovoltaic, and fuel cells usually supply electric power to the utility grids through power electronic converter interfaces. Compared with the conventional synchronous generators, RERs don't have rotor intrinsic kinetic energy (mechanical inertia). The applications of these RERs are expanding in the electric power system and it is expected to be increased more and more in the future. Connecting the RERs with the low or zero inertia in the power system drastically reduces the overall system inertia, especially if they offset conventional synchronous generation. Hence, the power system stability and its dynamic performance are negatively affected. To obtain a decent power system performance, the converters have to be well designed and controlled. The power system operation and its dynamics performance depend on the converter controllers and their operation methodologies. Traditional droop methods were used to control the converters and share their output power by controlling the output voltage magnitude and frequency according to their output active and reactive power. Also, the controllers try to mimic the droop characteristics of the SGs [232].

Additional research work has been developed to mimic the steady-state droop characteristics and the dynamic characteristics of the SGs to enhance the inertia of the system. Virtual synchronous generator and virtual inertia emulation approaches were proposed as solutions to integrate the RERs into the power system and enhance

the system inertia. With energy storage systems, the converters will be able to supply or absorb abrupt power fluctuations and mimic the kinetic energy in SG to provide inertia. Moreover, VSG converters will move from just grid following to grid supporting and grid forming converters. Hence, VSG methodologies enhance the stability and dynamic performance of renewable energy generators. Moreover, the power electronic converters can provide ancillary services such as voltage regulation and help to improve the stability of the power system.

VSG development underwent several research steps over the last years. The first control method was introduced by Beck and Hess in [13]. It was called a virtual synchronous machine. The authors tried to emulate SG features and provide virtual inertia to increase the system inertia and support its stability.

This concept was embraced by many authors later with different characteristics and operation methodologies. The authors of [14, 233] adopted current source-controlled VSG converters. This category is applicable for grid-connected systems with a low renewable energy resources penetration. The authors proposed virtual synchronous machines to enhance the system inertia and support its stability.

The second category is the voltage source-controlled VSG converter. This type of VSG is applicable for both grid-connected and isolated modes of operations. The authors of [16, 234, 235] proposed synchroverters that work as voltage-source VSG converter controllers to emulate the SG inertia. In this chapter, the inertial features and damping constants of the SG are emulated in VSG. This can enhance the system's performance and support its frequency against different disturbances. Furthermore, the converter can work with the hierarchical control levels and may receive its reference set values from the different controllers. The converter is connected to a battery energy storage system to supply the required power. The models for different subsystems are described including the converter controllers' outer and inner loops that mimic the inertial features of the SG, and the system is modeled using an

electromagnetic transients simulation program to verify the proposed controller.

The rest of this chapter is arranged as follows. Section 6.2 describes layout of the system. In Section 6.3, the VSG controller structure is presented. Section 6.4 describes the energy storage system and its controller. The simulation of the proposed system is presented in Section 6.5. Finally, in Section 6.6, some relevant conclusions are drawn.

6.2 System Layout

Fig. 6.1 describes the proposed system in which the PV is the primary source of electric power. The dc-dc boost converter is used to step up the PV output voltage and maximize the energy extracted from the PV array. Modeling of the PV array and its converter is well described in [236, 228, 237]. The dc-ac converter is used to connect the power from the dc-link to the grid that is simulated by a voltage source. An energy storage system is required to emulate the SG features, so a battery energy storage system is used to supply the required power and energy to the system through a bidirectional buck-boost converter. DC-AC converter controller consists of two main loops, outer and inner loops. The outer loops consist of two main parts. The first part is the virtual inertia emulation part, it generates the virtual load angle. The second part is the terminal voltage control part, it generates the reference signals to the inner control loops. The inner control loops consist of two cascaded voltage and current control loops to generate the signals that drive the switches. In the following subsections, an explanation and the mathematical model of the parts of the system will be described.

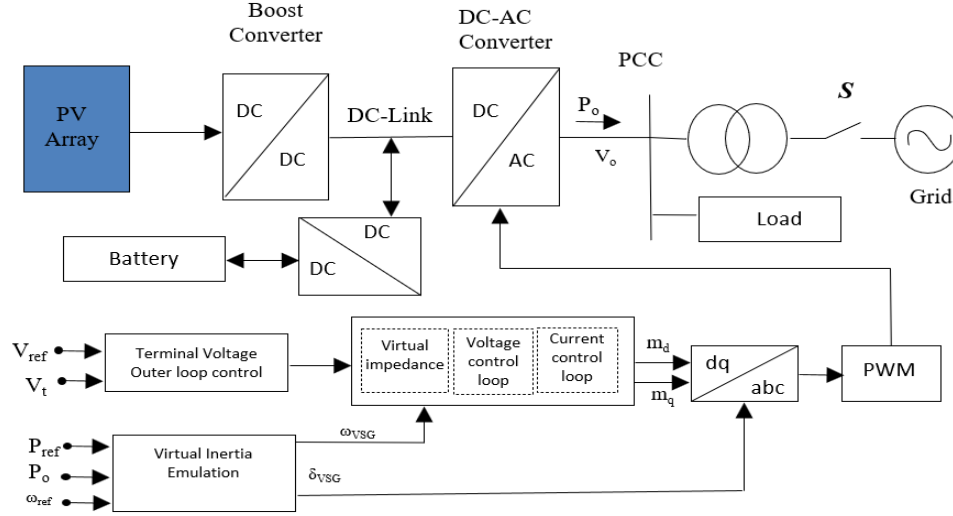


Figure 6.1: General layout of the proposed system

6.3 VSG Controller Structure

6.3.1 Inertial Emulation of VSG

The main objective of VSG is to emulate the inertial feature of conventional synchronous generators by controlling the power converter. Moreover, the model of VSG is an arbitrary design choice to determine what is modeled from the SG. If the purpose of the VSG is to accurately replicate the SG, then the fifth-order electrical model and the second-order mechanical model have to be modeled in VSG [14]. Although the full order model matches the behavior of SG, it adds unnecessary complexity if the purpose of VSG is to emulate the inertial and damping properties of SG since the inertial response and damping are the essential features in the VSG. Furthermore, the transient and sub-transient dynamics are included or excluded based on the required degree of complexity and accuracy.

In this chapter, the inertia and damping constants that are emulated can be described by the swing equation of the conventional SG. Also, the frequency droop in the governor model is added here to the model. The swing equation can be written as [14, 230]:

$$T_m - T_e - D(\omega - \omega_g) = J \frac{d\omega}{dt} \quad (6.1)$$

where T_m is the mechanical torque driving the generator (N.m), T_e is the electromagnetic torque due to electric load on the generator (N.m), D is the coefficient accounting for the damping torque associated with the damper winding (N.m.sec), ω is the rotational speed of the machine (r/sec), ω_g is the grid frequency (r/sec), J is the rotor moment of inertia (km.m²).

It has to be mentioned that the coefficient D in the SG is not constant for all operating points, and it depends on the operating point. So a fixed value of D in the simplified model for representing the main features of SG will not be able to match the SG behavior in all operating ranges [14].

The swing equation can be written in terms of power instead of torque by multiplying the equation (6.1) by frequency ω . The power equation can be written as:

$$P_m - P_e - D\omega(\omega - \omega_g) = J\omega \frac{d\omega}{dt} \quad (6.2)$$

where P_m is the emulated mechanical input power (W) and P_e is the electrical output power (W). The coefficient $J\omega$ is the angular momentum of the rotor at synchronous speed and is denoted by M . The angular momentum M is not strictly constant and depends on the angular velocity that varies somewhat during the swings which follow a disturbance. However, in practice, the synchronous generator runs at synchronous speed when the machine is stable. So the speed will be considered the synchronous speed. Equation (6.2) can be written as:

$$P_m - P_e - D\omega(\omega - \omega_g) = M \frac{d\omega}{dt} \quad (6.3)$$

In stability studies, another constant related to inertia of the machine is the H

constant that is defined by:

$$H = \frac{\text{Stored kinetic energy in MJ at synchronous speed}}{\text{Machine rating in MVA}} \quad (6.4)$$

$$H = \frac{\frac{1}{2}J\omega_s^2}{S_{rated}} = \frac{\frac{1}{2}M\omega_s}{S_{rated}} \quad (sec) \quad (6.5)$$

where ω_s is the synchronous angular speed of the SG, it is considered the base angular speed and S_{rated} is the three-phase rating of the synchronous machine in VA. Then M can be written as:

$$M = \frac{2H}{\omega_s} S_{rated} \quad (6.6)$$

Substituting M in equation (6.3) and dividing the equation by S_{rated} , then the swing equation can be written as:

$$P_{ref} - P_o - k_d(\omega - \omega_g) = \frac{T_a}{\omega_s} \frac{d\omega}{dt} \quad (6.7)$$

where P_{ref} is the per unit emulated reference mechanical input power, P_o is the per unit electrical output power, the time constant $T_a = 2H$, is the inertia time constant, and K_d is the damping constant associated with the per unit damping power.

For a small oscillation around the synchronous speed, the power balance may be described in the Laplace domain by the approximation given by:

$$P_{ref} - P_o - k_d(\omega - \omega_g) \cong T_a s \omega_{pu} \quad (6.8)$$

where s is the Laplace operator.

The block diagram describing the swing equation is shown in the right block in Fig. 6.2. The active power is associated with the VSG emulated torque and angular

speed of the rotor. The virtual rotor angle δ_{VSG} generated from Fig. 6.2 emulates the phase angle of the voltage induced by VSG and it is used in the Park's transformation and the inner loops on the converter controllers.

The active power control part that is shown in the left part in Fig. 6.2 represents a droop control. It describes the equivalent frequency speed governor steady-state characteristics to control the output power of the VSG. The active power control (speed governor) produces the virtual mechanical reference power P_{ref} by multiplying the difference between the reference frequency ω_{VSG_ref} and the actual frequency ω_{VSG} with the frequency droop constant gain Kw and adding the external active power reference P_{set} .

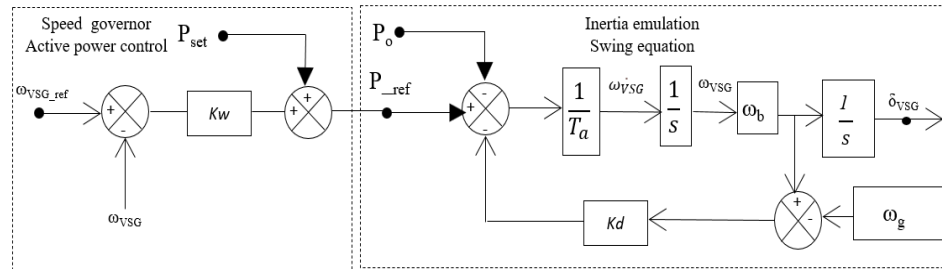


Figure 6.2: Virtual inertia emulation

6.3.2 Voltage Controller

The voltage magnitude of VSG can be controlled by a decoupled voltage or reactive power control loop. Controlling the terminal voltage enables the converter to operate in both grid-connected and isolated modes of operation. Fig. 5.3 describes the voltage control outer loop that generates the voltage control signals. The reference voltage is aligned to coincide with the direct axis of the converter voltage reference frame and the quadrature axis voltage is set to zero.

The reference signals are passed through a virtual impedance. The virtual parameters (R_v and L_v) are used to emulate the stationary impedance in the synchronous

generator. It can stabilize the VSG against small disturbances in the system. The virtual impedance block diagram is shown in Fig. 6.3. The control signals (V_{d_set} and V_{q_set}) generated from Fig. 6.3 are used as the input reference signals to the cascaded inner voltage and current control loops.

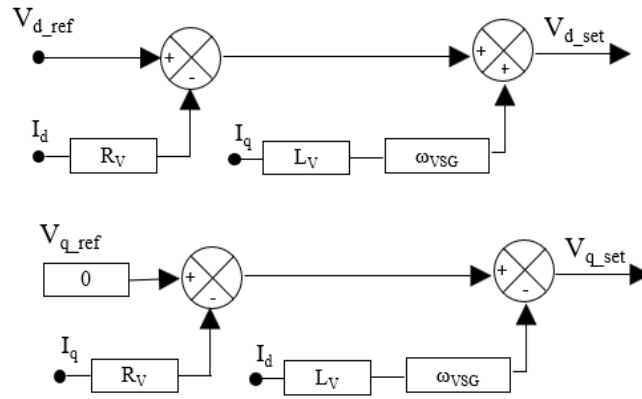


Figure 6.3: Virtual impedance

6.3.3 Inner Control Loops

The inner control loops consist of two cascaded voltage and current control loops. The first voltage control loop generates the reference current signals to the second current loop. These current signals are controlled against over current due to abnormal conditions. The second current control loop controls the current to follow its reference values. The inner cascaded loops are shown in Fig. 6.4. The system is modeled in a synchronously rotating dq reference frame.

6.4 Battery Energy Storage System

The battery energy storage system is mainly used for supporting the dc-link voltage to keep its value constant. Both the charging and discharging processes depend on the value of the dc-link voltage. When the converter output power increases beyond the

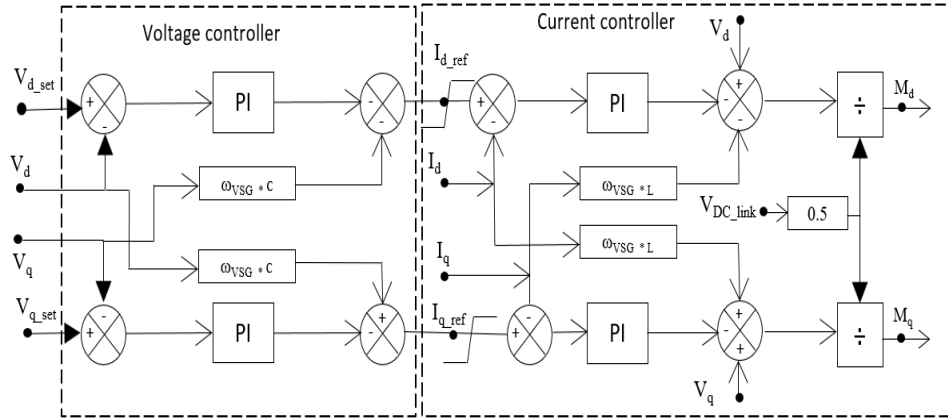


Figure 6.4: Cascaded voltage and current control loops

PV generated power, the dc-link voltage decreases, and the battery is discharged to maintain the dc-link voltage constant. If the output power is decreased, the battery will be charged to prevent the dc-link voltage from increasing. A bidirectional dc-dc buck-boost converter is used to control the operation of the battery. The converter operates in both buck and boost modes based on the dc-link voltage magnitude. It tries to keep the value of the dc-link constant. The battery system and its converters are described in Section 3.4, and Section 4.1.2.

6.5 Simulation Results

The system shown in Fig. 6.1 is implemented and modeled with an electromagnetic transients program to verify the proposed control structure. Different cases are carried out to describe the features and capabilities of the VSG.

Fig. 6.5 describes the first case with a change in the reference power to the converter at different inertia time constants and a constant damping constant ($K_d=0.16$). This change may be set by the local or hierarchical level controllers in response to a sudden change in the load or generated power from the PV array or on the local power subsystem. It can be shown that the converter's output power follows its refer-

ence, and the output power profile depends on the value of the inertial time constant. When the inertial time constant increases, the system has a larger amplitude power oscillation. This change affects the mechanical virtual frequency of the VSG. The frequency profile is shown in Fig. 6.6, it can be shown that when the inertia time constant decreases, the frequency change is more profound. Also, it has a higher rate of change of frequency.

The difference between the converter output power and the PV generated power is compensated by the battery system. Fig. 6.7 describes the battery power, it can be shown that when the inertia time constant increases, the battery power increases. So the energy storage system power design and rating should be based on the emulated inertia constants.

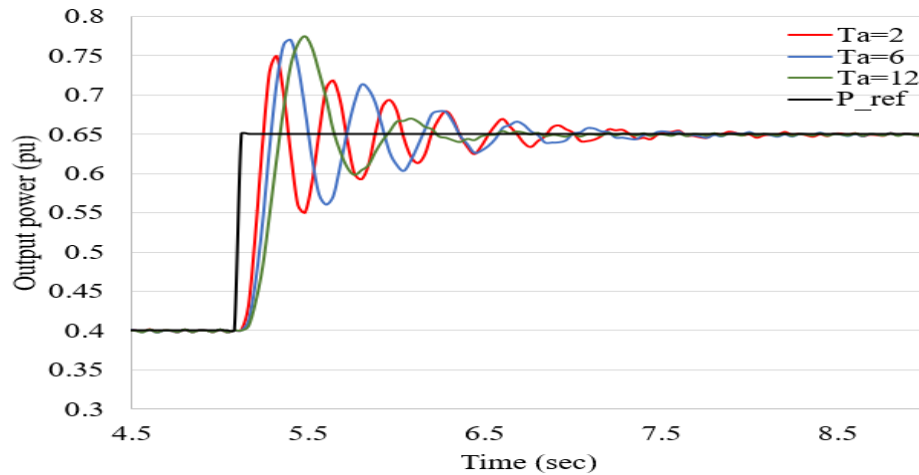


Figure 6.5: VSG active power variation at different inertia time constants

The next set of simulations describes the effect of damping constant change on the VSG operation. The inertia time constant is fixed at this simulation case ($T_a=6$). Fig. 6.8 describes the output power profile at different damping constants. It is shown that increasing the damping constant reduces the amplitude of power oscillations, and the system reaches its steady state sooner. Moreover, the frequency is improved as shown in Fig. 6.9 such that the frequency nadir is increased when the damping constant

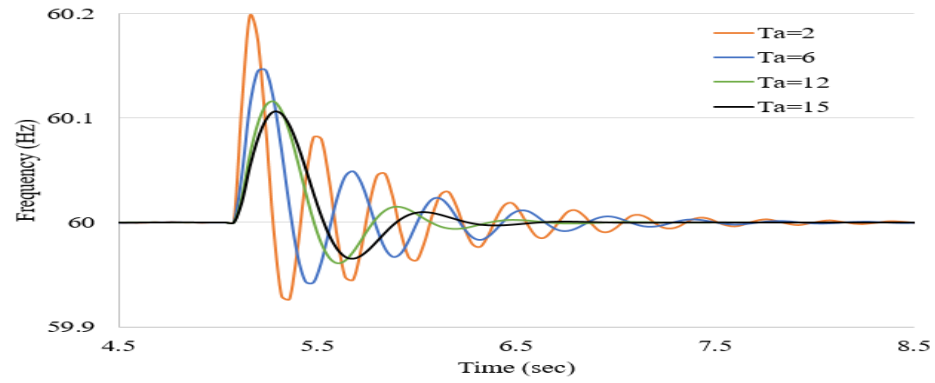


Figure 6.6: Frequency profile at different inertia time constants

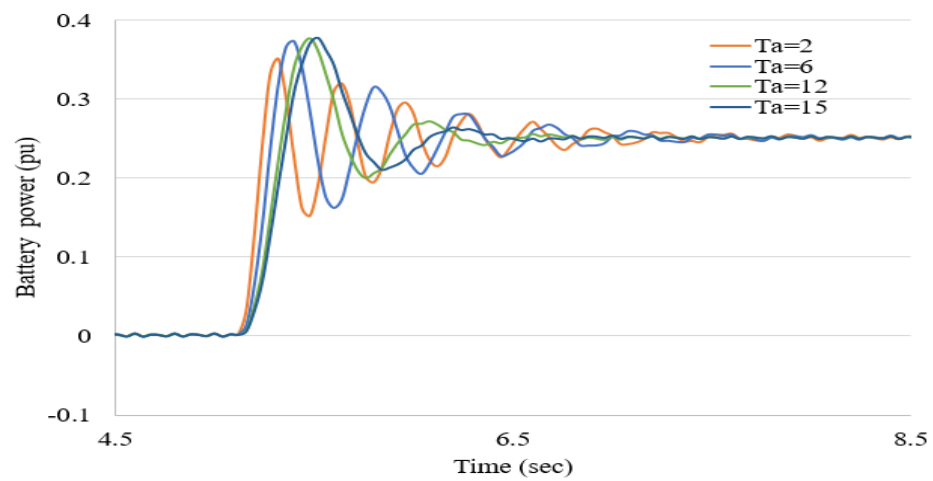


Figure 6.7: Battery power at different inertia time constants

increases.

Fig. 6.10 describes the battery power, it can be shown that the battery power is decreased when the damping constant increases. So the size of the battery system connected with the VSG is affected by the emulated inertia and damping constants. Fig. 6.11 and Fig. 6.12 describes how the battery energy storage power changes with the emulated inertia and damping constants. At small inertial or large damping constant values, the battery supplies small power values and they increases when the inertia time constant increases or the damping constant decreases.

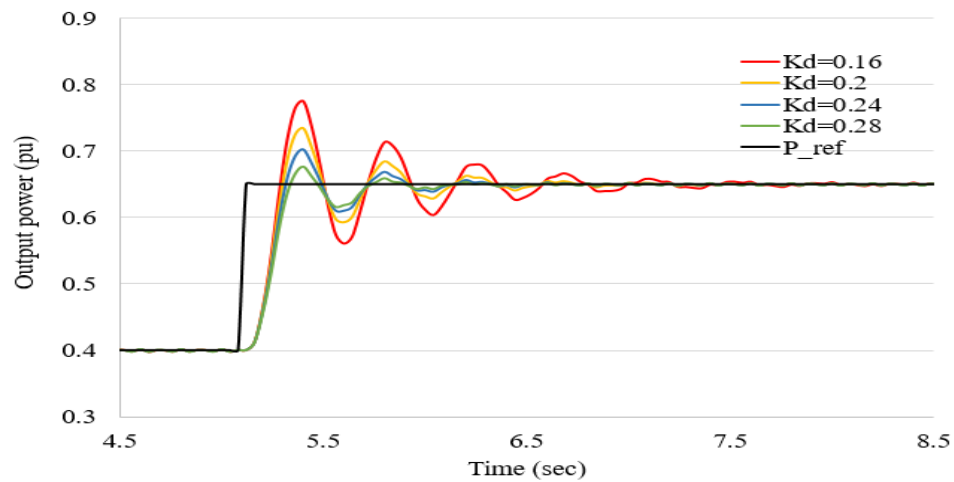


Figure 6.8: VSG active power variation at different damping constants

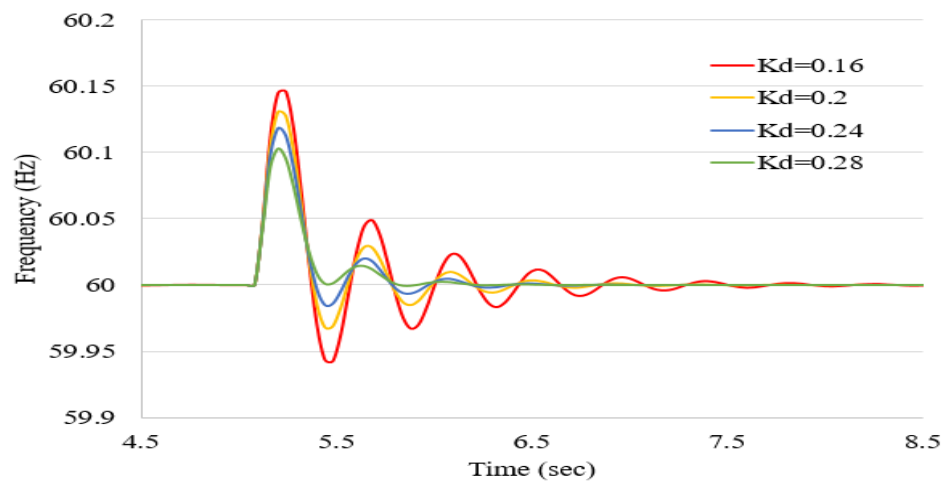


Figure 6.9: Frequency profile at different damping constants

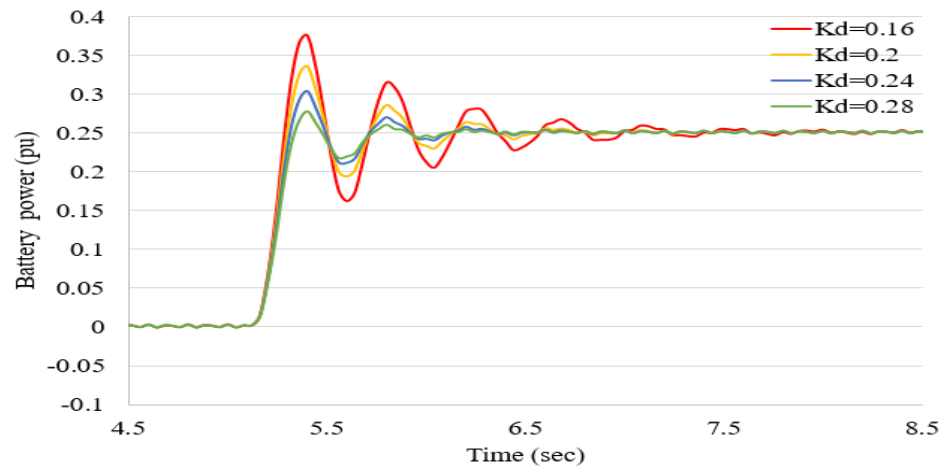


Figure 6.10: Battery power at different damping constants

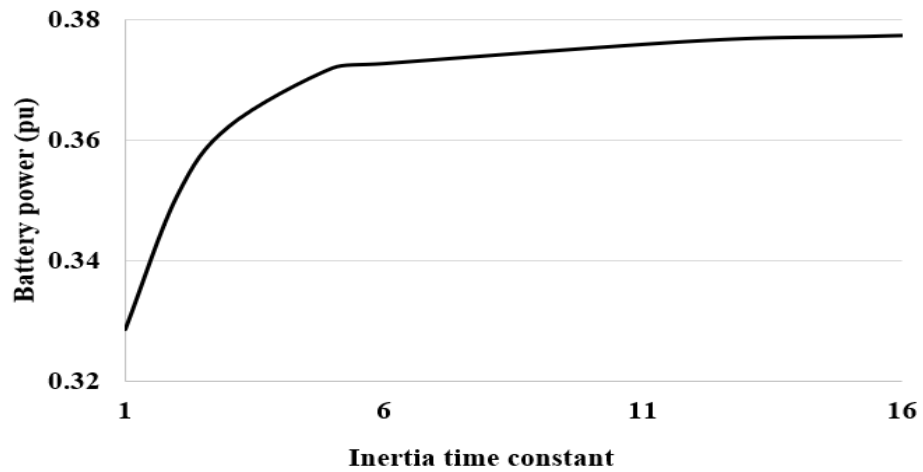


Figure 6.11: Battery power variation with respect to the inertia time constant

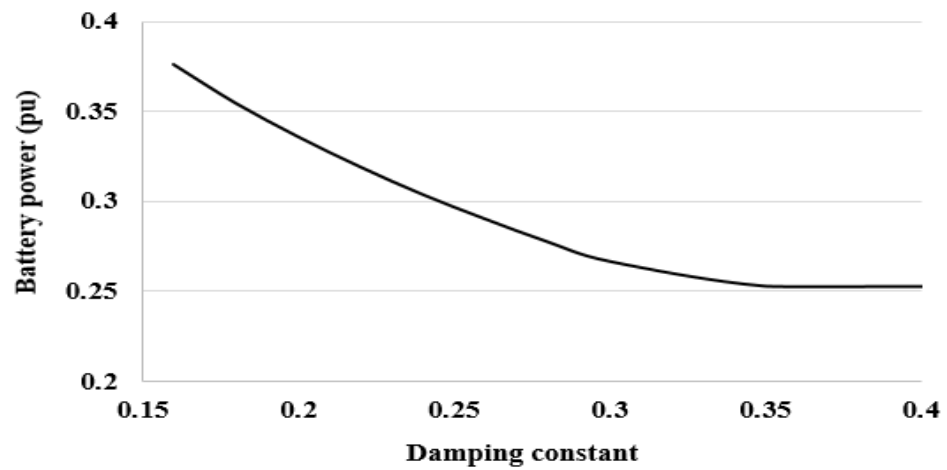


Figure 6.12: Battery power variation with respect to damping constant

The next simulation set describes how the VSG responds to the change in the system frequency. The system frequency decreased at a time equal to 5 sec from 60 Hz to 59.6 Hz due to an external event elsewhere in the microgrid as shown in Fig. 6.13. The system is simulated at different inertia time constants, while the damping constant is fixed to a constant value ($K_d=0.2$). The VSG supplies active power in response to the frequency change such that the higher the inertia time constant is, the more power is supplied by the converter as shown in Fig. 6.14. The output power reaches a higher steady state output power due to the droop effect of the virtual emulated governor.

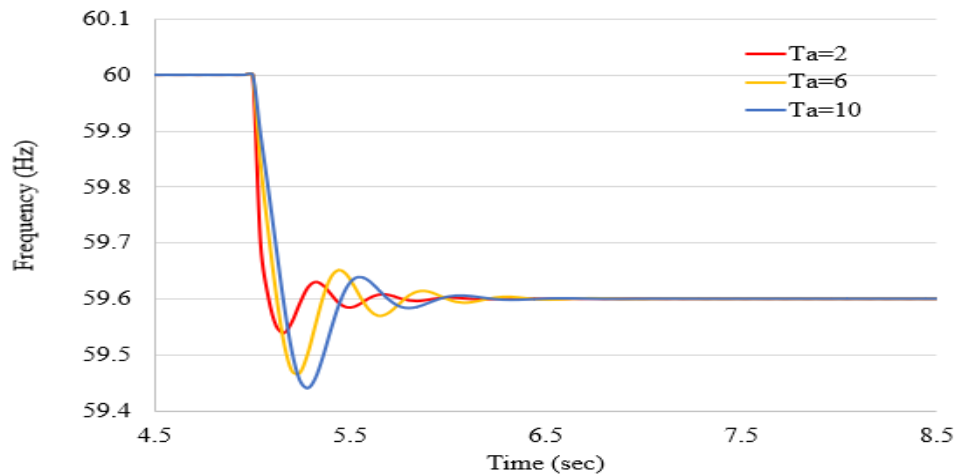


Figure 6.13: VSG frequency change in response to a microgrid frequency change

The previous simulation case is repeated at different damping constants; however, the inertia time constant is fixed to a constant value ($T_a=6$). Fig. 6.15 describes the frequency drops from 60 Hz to 59.6 Hz and Fig. 6.16 describes the converter output power. It can be seen that increasing the damping constant reduces the maximum amplitude of the output power oscillations and helps the system to reach a steady state sooner.

The change in the steady state output power in Fig. 6.14 and Fig. 6.16 is due to the frequency droop gain effect in the governor model. To describe only the effect of

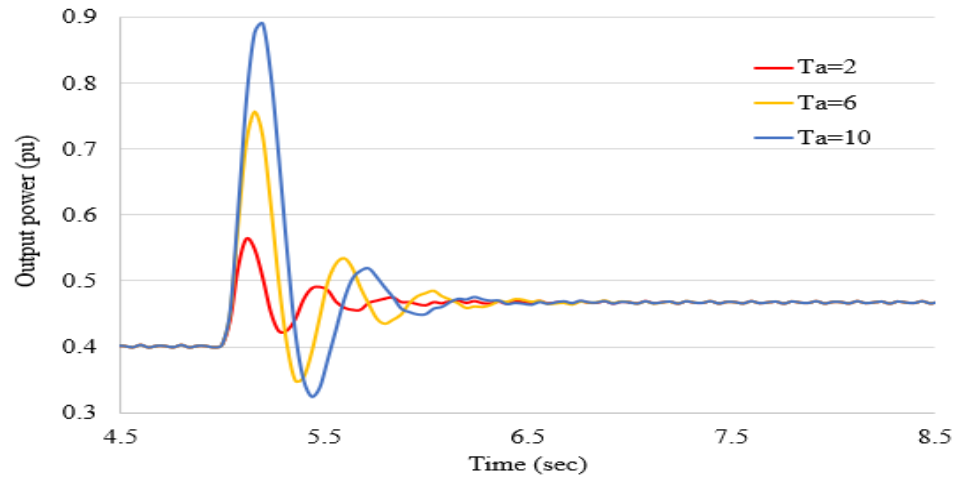


Figure 6.14: Output power in response to a microgrid frequency change

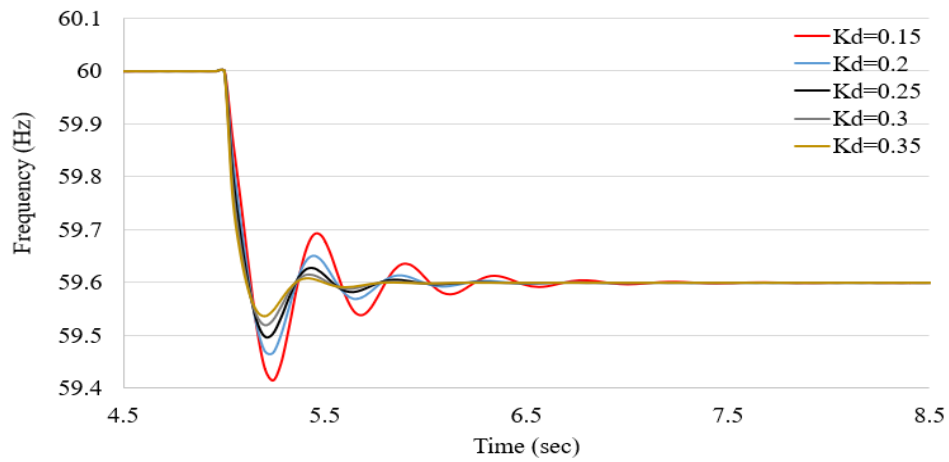


Figure 6.15: VSG frequency change in response to a microgrid frequency change

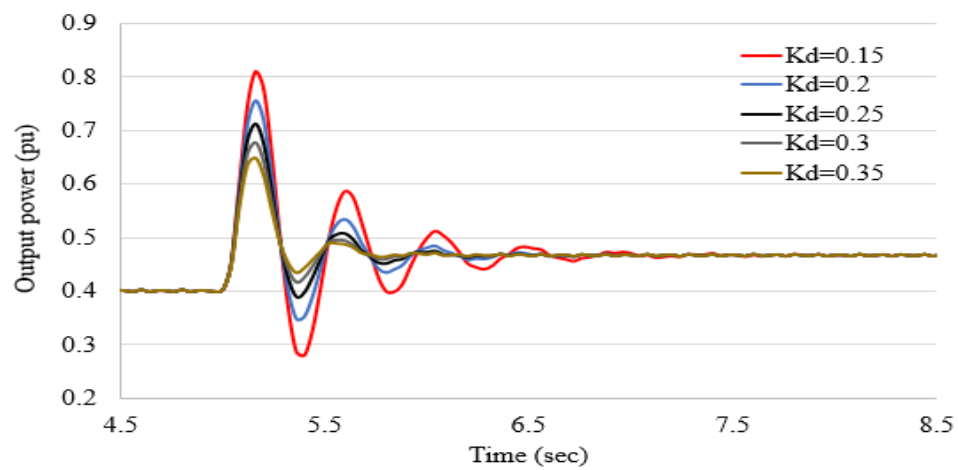


Figure 6.16: Output power in response to a microgrid frequency change

the inertia time constant on the system performance at this case study, the frequency droop constant is set to equal to zero and the test is repeated. Fig. 6.17 describes the output power profile at different inertia time constants. It can be seen that the high inertia system can supply more power when the system frequency changes and thus needs a battery and associated converters with higher power ratings.

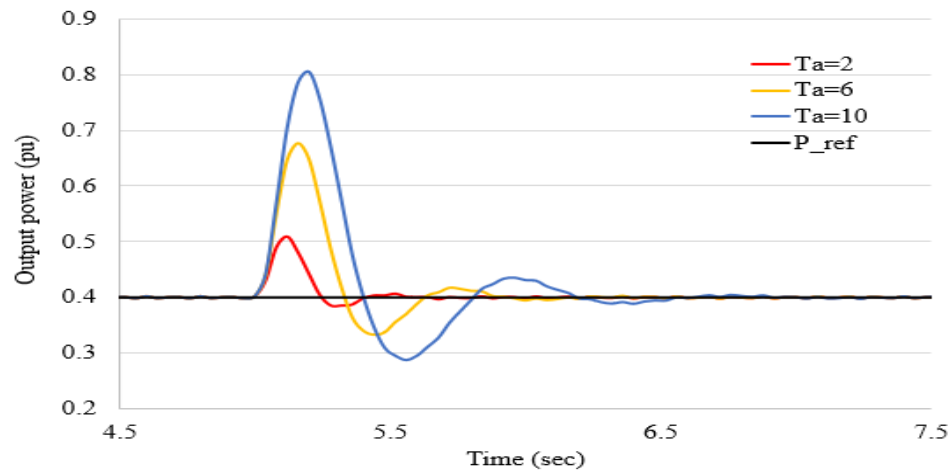


Figure 6.17: Output power in response to a microgrid frequency change

The simulation case is repeated at different damping constant, Fig. 6.18 describes the output power profile when the grid frequency changes from 60 Hz to 59.6 Hz at a time equal to 5 sec. It is shown that increasing the damping constant reduces the converter output power and the system can reach its steady state sooner.

6.6 Conclusion

The stability of the system is impacted by the total system inertia which is affected by the number of conventional synchronous generators and renewable energy resources connected to the grid. The concept of VSG as a technique to control the power converter to mimic the inertial features of SG was described in this chapter. The implementation of VSG in the chapter is based on the swing equation to generate the reference control signals to the converter's inner control loops. Also, the model

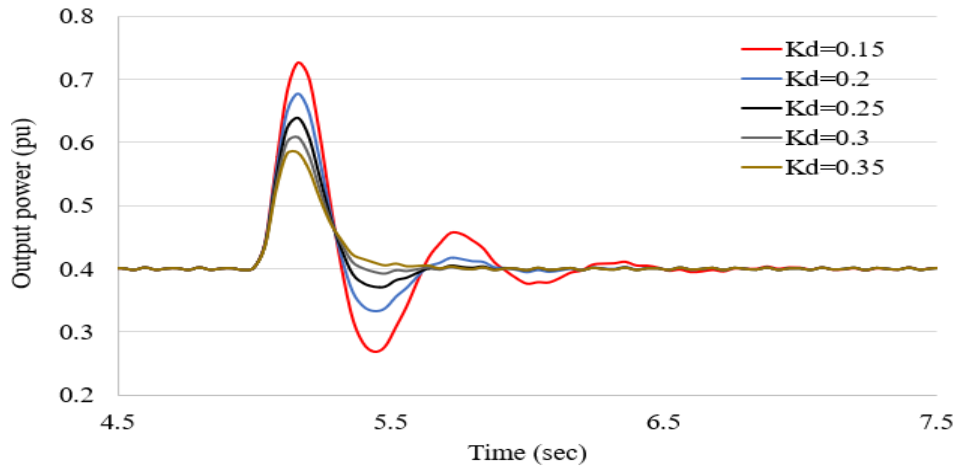


Figure 6.18: Output power in response to a microgrid frequency change

for VSG was described in a synchronously rotating reference frame. The whole system including the PV array, ESS, and power converters is implemented using an electromagnetic transients program.

From the simulation results, it can be concluded that the power converter combined with ESS can emulate the inertial features of SG. Moreover, the parameters of VSG can be changed to mimic the inertial features of many synchronous generators. Furthermore, the ESS depends on the emulated inertia and damping constants, such that when the inertia constant increases or the damping constant decreases, the ESS power capability has to be increased, and vice versa. Moreover, when the inertia and damping constants increase, the frequency oscillation is reduced which helps to stabilize the system against different disturbances. Finally, the power converter based on VSG techniques helps to increase the dependency on RERs and spread them in the power grids.

Chapter 7: Virtual Synchronous Generator Controller Based SMES-Battery Energy storage System

This chapter consists of material from a paper that is accepted for the Grid of the Future Symposium / CIGRE to be held on November 7 through November 10, 2022 in Chicago, IL USA.

7.1 Introduction

The desire to reduce the carbon footprint caused by fossil-fuelled power plants has increased the adoption of renewable energy resources and distributed generating units in particular photovoltaic plants in the power system network. Furthermore, the topology and architecture of the power system have changed from a system with large conventional, centralized, and dispatchable power generators to one with non-conventional distributed generating resources.

The power output from these RERs and DGUs depends on uncontrolled environmental factors. Their power output fluctuates according to the availability of the resources which are intermittent and uncontrollable, and sometimes they may fail to meet the load demand. So the reliability of generating resources to supply the available loads continuously is reduced. Also, increasing their penetration in the power system may cause stability problems. Such issues have become major hurdles to the widespread of RERs in power systems especially small systems such as microgrids.

The most common problem is the reduction of the intrinsic kinetic energy (rotor inertia) and damping property that results from the mechanical friction and electrical losses in stator, field, and damper windings of the conventional synchronous generators. Hence, there is a reduction in the total system inertia. RERs such as wind power plants have a low inertia and PV systems don't have any rotating kinetic energy. This system inertia reduction makes the system vulnerable to stability

problems. The system may lose synchronism in case of disturbances such as a sudden change in loads or power generations or fault occurrences [238].

One of the proposed solutions to solve these problems is integrating energy storage systems with RERs. ESSs can store the energy at off-peak periods and supply the required load at peak periods, so they achieve the power balance between the supply and demand. Furthermore, they can be included in a system for emulating the conventional synchronous generator to compensate for the lack of rotating inertia to address the transient changes. This methodology is known as a virtual synchronous generator [235, 239]. These ESSs help to provide virtual inertia to improve the system stability against different disturbances. Furthermore, the continuous research and developments in ESSs technologies improved the cost effectiveness of ESSs as viable solutions for power system applications. The authors of [240, 241] described how they can be used for power balancing, smoothing power flow, fluctuation suppression, black start, and voltage and frequency control.

One of the popular types of ESSs is the battery energy storage system. Battery systems have been used for a long time in power system applications. They are used in storage energy applications. Batteries have many advantages such as high energy density, high efficiency, long life, and low self-discharge. Then, BESSs can be used in power system applications such as power quality enhancement, energy management, and smoothing the long-term power fluctuations in microgrids. The authors of [23] described the usage of batteries in power system applications in detail.

On the contrary, batteries have some disadvantages that make them unable to achieve all the system requirements. Due to the chemical kinetic involvement, batteries have a low response time, a limited voltage and current rating, and so low power capacity. Hence, BESSs can't respond rapidly to the different transients in power systems. Furthermore, they have a poor life cycle, so the number of lifetime charging and discharging cycles is limited. Moreover, the deep frequent charging and discharg-

ing processes shorten the battery lifetime, since the heat produced from the chemical reaction in these operations reduces their lifetime. Also, some environmental hazards may be caused by batteries during their charge and discharge processes and disposal of their hazard materials.

To address the limitations of the batteries and improve the operational performance of the power system, a hybrid energy storage system is proposed. The authors of [24, 242] described the different types of ESSs, their contributions to HESS, and their effect on improving power system operation. HESS can be implemented to provide high energy and power capabilities and rapid response time. Hence, they can address the different transient disturbances, smooth the power flow, and improve the system's stability and operation. Then, the HESS reduces battery cycling and the stresses due to large charging and discharging currents at different transient periods. So the battery lifetime is being improved.

There are various types of ESSs that can be integrated with the batteries to form HESS. The most common energy storage types are pumped storage hydroelectric systems, flywheels, supercapacitors, and superconducting magnetic energy storage (SMES). The authors of [242] summarized these ESSs and their usage in microgrids in detail.

In [243, 244], the authors recommend using the supercapacitors in conjunction with the batteries as a HESS because of their advantages. Supercapacitors have a high-power density, long lifetime, fewer energy losses, high-speed responding time, and high efficiency. On the contrary, supercapacitors have many disadvantages. A supercapacitor is a series of multiple capacitor cells with a voltage range limited to 2.5 - 3 Volt. This series connection is inevitable to obtain the required voltage, but it reduces the total capacitance. Moreover, a protection circuit should be integrated with the system to protect the cells from overvoltage and non-uniform cell problems. Furthermore, step-up and step-down converters are required to match supercapacitor

voltage with the power system voltage. The converters should have a complicated design since the terminal voltage changes with the stored energy variations which change with the charging and discharging processes. On the other hand, the SMES can overcome the supercapacitors' drawbacks and support the power system operation. Moreover, it has the same supercapacitors' advantages such as the high-power density capabilities, long lifetime, fewer energy losses, high-speed responding time, and high efficiency. So it can address the short-term transient power [26]. Then, in this chapter, SMES will be used in conjunction with the battery system to form a HESS for improving the operation of the system.

In this chapter, the importance of the SMES system and its advantages are described. In addition, modeling and control of the dc-dc SMES converter are presented. Moreover, the simulation of the proposed control methodologies is carried out using an electromagnetic transients simulation program.

The rest of this chapter is arranged as follows. Section 7.2 describes the system layout. In Sections 7.3 and 7.4, the energy storage systems and the converter controllers are described. Hereafter, a comparison between different ESSs is described in Section 7.5. Simulation of the proposed system is introduced in Section 7.6. Verification of the proposed model by a comparison between VSG and conventional SG is described in Section 7.8. Finally, in Section 7.9, some relevant conclusions are drawn.

7.2 System layout

The proposed system layout is shown in Fig. 7.1. In this system, a VSG-based controller is exploited to control the PV system which is connected with a HESS. The main source of electrical energy in this system is the PV array. It generates electrical power at a low voltage and is stepped up using a dc-dc boost converter to match the dc-link voltage. Furthermore, it maximizes the energy extracted from the

PV array by using a maximum power point tracking scheme. A detailed description of the PV array and its boost converted are described in [205, 245, 246].

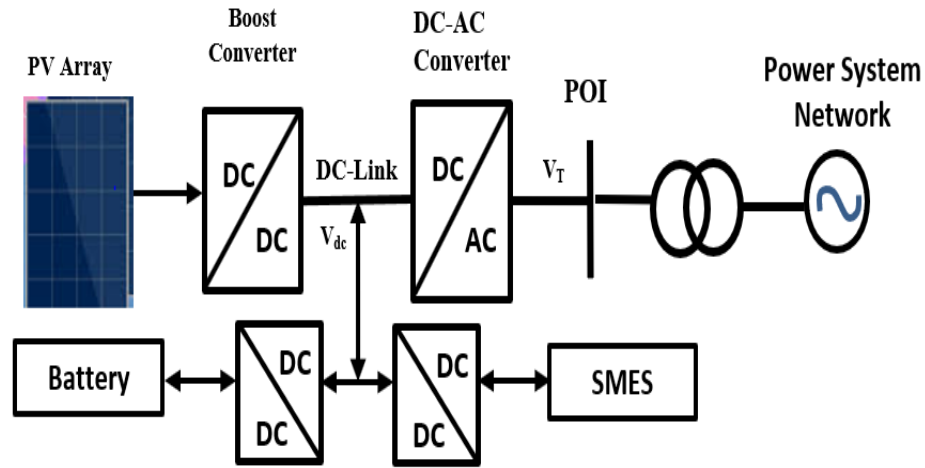


Figure 7.1: General layout of the proposed system with a HESS

The dc-ac converter and the HESS are controlled to emulate the conventional synchronous generator inertial features. The operation of the converter depends on the dc-link configuration where the power fluctuation due to the different disturbances is compensated from the dc-link and then from the storage systems. HESS is composed of SMES and battery, and they are connected to a common dc-link.

DC-AC converter delivers power from the dc-link to the grid which is simulated by a voltage source. The model and the control system of the converter are implemented in dq reference frame. It is described in detail in [228, 247].

7.3 Energy Storage Systems

The energy storage systems consists of a SMES and a Battery system. The SMES responds to high rate of change of power fluctuations and short-time disturbances, it can support the system with high current and high power in a short time. It interacts with the variations of the dc-link voltage magnitude. In case of disturbance that causes the system output power to exceed the PV generated power, the dc-

link voltage decreases, and the SMES discharges to keep the dc-link voltage constant. Contrarily, if the disturbance causes the dc-link voltage to increase, the SMES charges to return the dc-link voltage back to the nominal range values.

On the other hand, the battery addresses the low-frequency fluctuation. If the generated power doesn't match the demand power, the battery compensates for the difference to stabilize the system. The battery can handle cases that require high energy capacities. Hence, the HESS can support the system at different disturbances, improve the system's stability and operation, and provide both high power and energy capabilities.

7.3.1 Battery energy Storage System

Batteries are widely exploited in power system applications because of their ability to supply high energy. Moreover, they are the most cost-effective energy storage system. The battery system consists of several parallel and series combinations of battery modules to produce the desired electrical requirements. It is considered the low-cost storage option in power system applications. The development and research in battery technology led to the advent of batteries that have better features, performance characteristics, and cost.

Controlling the state of charge (SoC) within certain limits is important to increase the battery lifetime. Battery SoC increases with charging and decreases with the discharging process as per energy conservation law. The controller limits the SoC to be within 20-90 %. Battery SoC can be determined as [248]:

$$SoC = SOC_o + \frac{1}{Q} \int_0^T i(t) dt \quad (7.1)$$

where SOC_o is the starting state of charge value, Q is the battery's capacity (Ah) and i is the battery current (A) that is charging or discharging the battery for a time (T).

Since the battery has a high energy density, it handles the low power fluctuations, charges, and discharge slowly, and lasts a long time to respond to the system. Then, it meets the steady demand of the system which increases the battery lifetime.

The battery system and its converters are described in Section 3.4, and 4.1.2, and the SMES system will be described in the next subsection.

7.3.2 SMES System and Controller

Superconductivity was discovered in 1911, but the research and development of its application in power systems started in the 1970s. SMES stores the electric energy in a magnetic field generated by the current flowing through superconducting wires configured in coils. SMES has many advantages that make it viable in power system applications. It has a high power density, low-self discharge rate, large number of charge and discharge cycles, high efficiency, and ease of controllability. Moreover, it can handle a high peak current and power, so it is a viable solution to handle the short-term power oscillations and improve power system operations. SMES system can be used for controlling both the active and reactive power and so the voltage and the frequency of the system. Fig. 7.2 shows the schematic diagram of the SMES system. It consists of three main parts; superconducting coil, cryostat refrigeration system, and power conditioning unit (PCU). The superconducting coil is made of superconducting material which may be a low-temperature superconducting material (LTS) that works at ~ 5 k or high-temperature superconducting material (HTS) that works at ~ 70 k. The coil is immersed in a dewar consisting of a vacuum vessel and liquid vessel with a coolant liquid such as Helium or Nitrogen to maintain the coil temperature below the superconducting critical temperature.

The cryostat or refrigeration system reduces the temperature of the coil to keep it in its superconducting state during SMES operations. The power conditioning unit

addresses power transfer between the coil and the power system. The VSC-based SMES system is used in this work. It consists of a dc-dc chopper and dc-ac converter. It controls the dc-link voltage by controlling the power transfer between the coil and the dc-link. Fig. 7.3 shows the dc-dc chopper that connects the SMES coil to the dc-link. The energy stored in the SMES coil and the available power are proportional to the current flowing it and can be expressed as:

$$E_{stored} = \frac{1}{2}LI_{coil}^2 \quad (7.2)$$

$$P_{SMES} = \frac{dE}{dt} = V_{dc} I_{coil} \quad (7.3)$$

where L is the coil inductance, I_{coil} is the SMES coil current, and V_{dc} is the dc-link voltage.

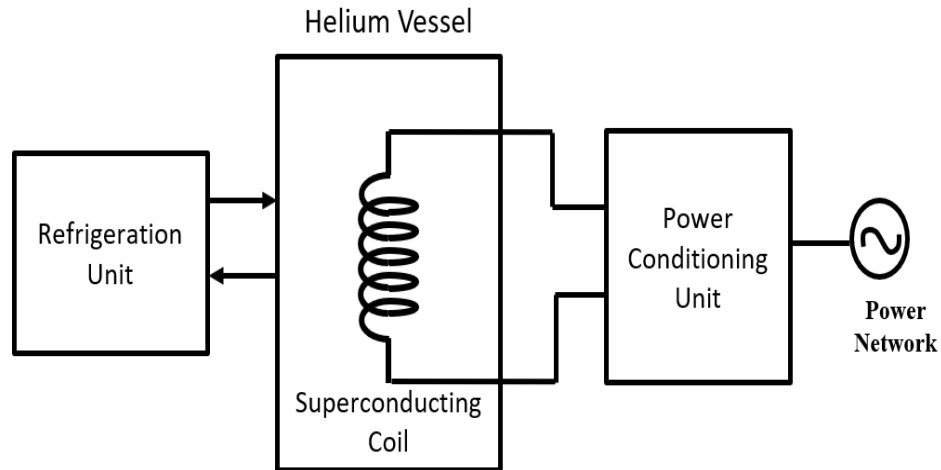


Figure 7.2: Schematic diagram of a SMES system

The power flow is controlled to keep the dc-link voltage magnitude within the normal operating range. In the charging process, both the switches S_1 and S_2 are turned on, and the coil current increases. On the contrary, when both switches are turned off, the SMES turns to the discharge state, and it delivers the power to the dc-link. When switch S_1 is turned off and the switch S_2 is turned on, the SMES coil is no

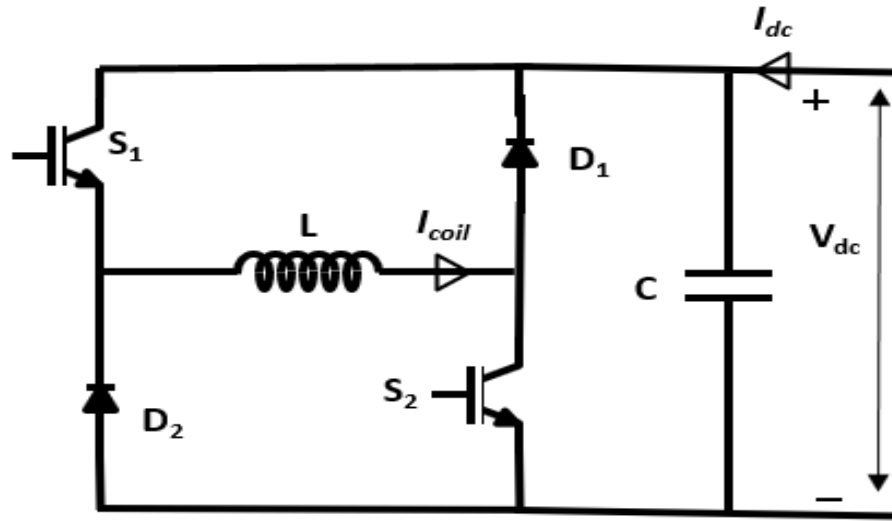


Figure 7.3: DC-DC chopper of the SMES coil

longer charged nor discharged, and this is the standby mode. The dc-chopper circuit allows the SMES coil to control the dc-link voltage variation within milliseconds such that it may change from charge to discharge states at this time. This high-speed response allows the SMES system to provide a spinning reserve to enhance the system's operation and stability. Although the SMES system is a competitive ESS in power system application to improve stability, it has some disadvantages such as high cost and coil sensitivity to temperature variations. However the SMES system has a high cost today, the continuous research and developments in the SMES systems is projected to finally drive its cost down.

7.4 DC-AC Converter Controller

The dc-ac converter emulates the SG features, damping and inertia constants. The control structure consists of two main outer and inner loops. The outer loops are representing the inertia emulation and ac terminal voltage magnitude control. VI emulation produces the virtual rotor angular position of the VSG. Furthermore, the

voltage controller produces the VSG voltage signals and this will be applied to the inner loops. From the reference voltage signals, the controller calculates and produces the reference currents to the inner control loops. The dc-ac is described in detail in Section 6.3.

7.5 Comparison between Different ESSs

The energy and power required to emulate the VSG can be provided from different ESSs. They have different applications, energy density, power density, cost and lifetime [249, 250]. Table 7.1 describes the different characteristics for some of the most ESSs in power industry. It is shown that li-ion battery has the highest energy density and the lowest capital cost per unit energy. On the other hand, it has the highest cost per unit power, and its power density is lower than SMES and supercapacitor.

Table 7.1: Comparison between different energy storage systems [249, 250]

Characteristics of ESS	SMES	Li-ion	Lead-acid	Supercapacitor
Energy density (Wh/Kg)	1-10	70 - 200	30 - 50	0.5 - 5
Power density (W/Kg)	500-2000	150-500	75-300	1000-10000
Capital cost(\$/kWh)	1000-10000	600-2500	200-400	500-15000
Capital cost(\$/kW)	200-500	1200-4000	300-600	100-400
Life (cycles)	100000+	1000-10000	500-1000	-
Discharge time	m sec - hrs	mins-hrs	secs-hrs	m sec-60 min

Also, it can be shown that the SMES has a low energy density and its cost per unit energy is still high; however, it has a high power density. One of the main advantages of the SMES system is its rapid charge and discharge rate that makes the SMES the best ESS to counteract the high rate of change of the generated or load power.

Since the RERs depends on the natural sources such as wind and solar irradiation, their output changes continuously. So the ESSs connected to these resources have a high number of charge and discharge cycles that affects their lifetime. Table 7.1 describes that the battery has a limited number of cycles; however, SMES can fit

well the applications that have a continuous power oscillations. Moreover, SMES can charge and discharge so fast that makes it competitive over a long time with respect to other energy storage system such as batteries.

One of the important features on the ESSs is their range of SoC variation. The SoC of the ESS is fixed at 50 % to let the ESS system operates at both charging and discharging modes based on the disturbance types. However, the battery SoC is set to vary between 20 - 90 % to protect the battery from deep discharge or overcharging in different scenarios.

On the contrary, SoC of the SMES can vary between 0 and 100 % without a dramatic effect on its lifetime or efficiency. But the lifetime of other ESSs such as batteries can go down due to the higher depth of discharge (DOD) as shown in Fig. 7.4 and Fig. 7.5.

SMES system can be charged and discharged fast with a high different rates. However, forcing current into other ESSs such as the batteries during the charging and discharging processes cause serious capacity loss and internal resistance growth as described in Fig. 7.6 and Fig. 7.7. On the contrary, the SMES system can't be diminished due to the charging or discharging processes; however, the current has to be controlled to avoid over current or over heating.

The cost of the SMES still challenging; however, the research in the high-temperature superconducting material reduces the cost of the SMES down. Moreover, the cost of SMES may be a comparable for the battery system in some applications. Since the lifetime of the battery system may be affected dramatically by the DOD and the number of charge and discharge cycles, the SMES can has a long lifetime that may be equivalent to tens of battery systems for the same operating scenarios. For example, if 1 kW, 1 kWh ESS need to be designed, and from Table 7.1 the average cost of the SMES is considered to be 350 \$/kW and 5500 \$/kWh. The average cost of li-ion battery is 2600 \$/kW and 1550 \$/kWh and the cost of lead-acid battery is 450 \$/kW

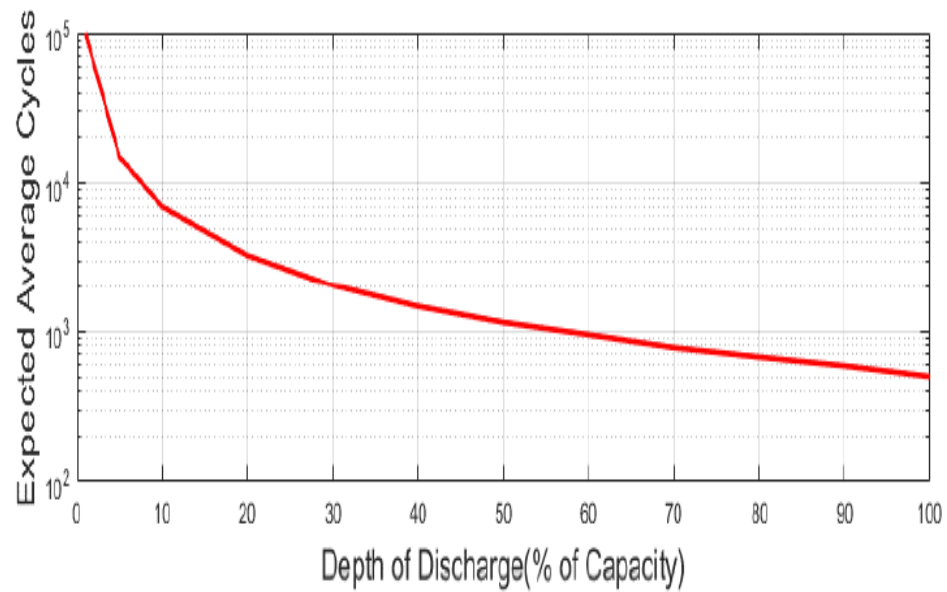


Figure 7.4: Cycle life versus DOD curve for a lead-acid battery[251]

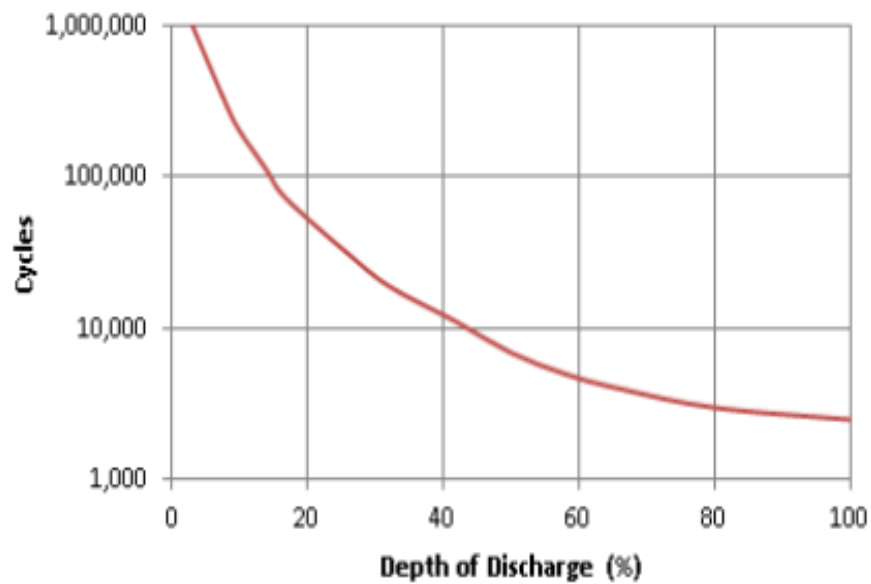


Figure 7.5: Cycle life versus DOD curve for a li-ion battery [252]

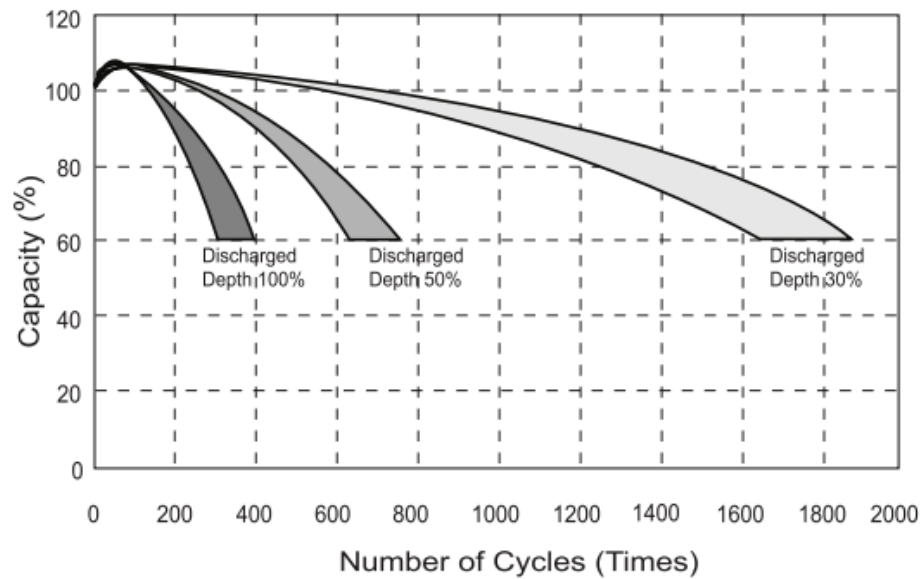


Figure 7.6: Battery capacity versus number of cycles for lead-acid battery [253]

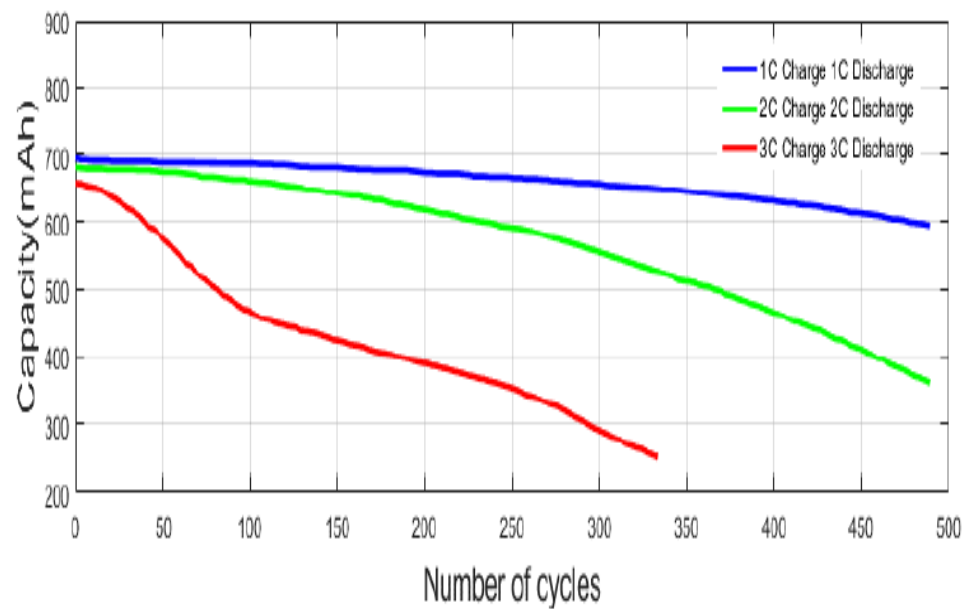


Figure 7.7: Battery capacity versus number of cycles under different rates for Li-ion battery [251]

and 300 \$/kWh. So 1 kW, 1 kWh SMES system is:

$$Total\ cost = 350 * P + 5500 * E = 350 * 1 + 5500 * 1 = \$ 5850 \quad (7.4)$$

The cost of the li-ion battery system is:

$$Total\ cost = 2600 * P + 1550 * E = 2600 * 1 + 1550 * 1 = \$ 4150 \quad (7.5)$$

The cost of the lead-acid battery system is:

$$Total\ cost = 450 * P + 300 * E = 450 * 1 + 300 * 1 = \$ 750 \quad (7.6)$$

From this simple example, it can be seen that the SMES can be more effective than 2 sets of li-ion batteries. Moreover, its cost may equivalent to 7 sets of lead-acid batteries. However, if the battery operates for the same operating conditions including rapid charge and discharge and deep DOD like SMES, the SMES would be more effective and cheaper than the batteries , since it can be equivalent to tens of the batteries from the lifetime point of view.

7.6 Simulation Results

To verify the proposed control structure, the system that is shown in Fig. 7.1 is implemented and modeled in an electromagnetic transients program. The simulation is carried out at different scenarios for different conditions to clarify the operation of the HESS controller and how the converter emulates the SG inertial features. Moreover, it describes how the inertia and damping constants affect the operation of the system and the rating of both the converter and the HESS power and energy. The first scenario describes the VSG operation at grid frequency change and how it emulates the inertial features of the SG when the grid frequency changes. The

simulation is done at different values of damping and inertia time constants. Fig. 7.8 describes the drop in frequency from 60 Hz to 59.4 Hz, due to an event on the external microgrid, at different damping constants while the inertia time constant is kept at a constant value ($T_a=5$).

The converter output power changes in response to the grid frequency change as shown in Fig. 7.9. The power profile depends on the damping constant value, such that when the damping constant increases the output power has less magnitude and oscillations and reaches its steady state sooner. The power and the energy generated in response to the frequency change are supplied from the SMES system. The SMES is charged at 2.35 MJ at the start of the simulation. As shown in Fig. 7.10 and Fig. 7.11, when the damping constant increases, the peak power and energy required from the SMES system is decreased. Moreover, the SMES can supply 0.5 pu in a very short time; less than 0.2 sec which is faster than the battery response and protect the battery from this high discharge or charge rate.

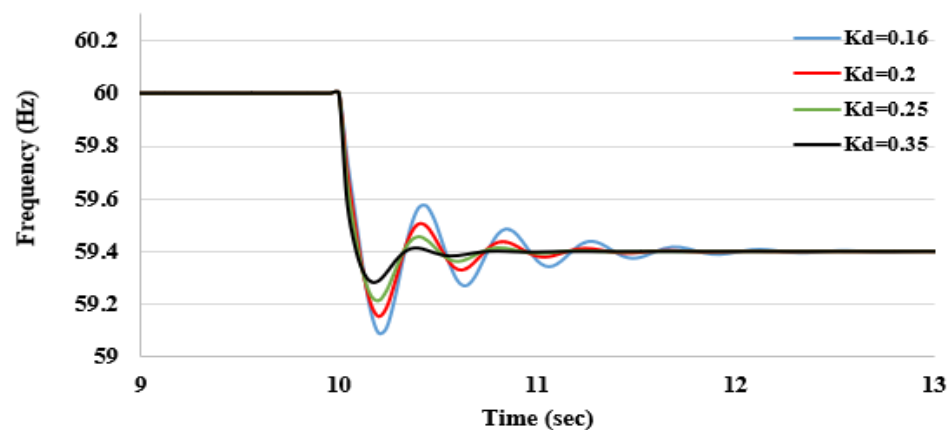


Figure 7.8: Response to a microgrid frequency drop at different damping constants

It is shown that the damping constant affects the design and rating of both the converter and the SMES system. Fig. 7.12 describes the change in the maximum converter output power values with respect to the damping constant and how the

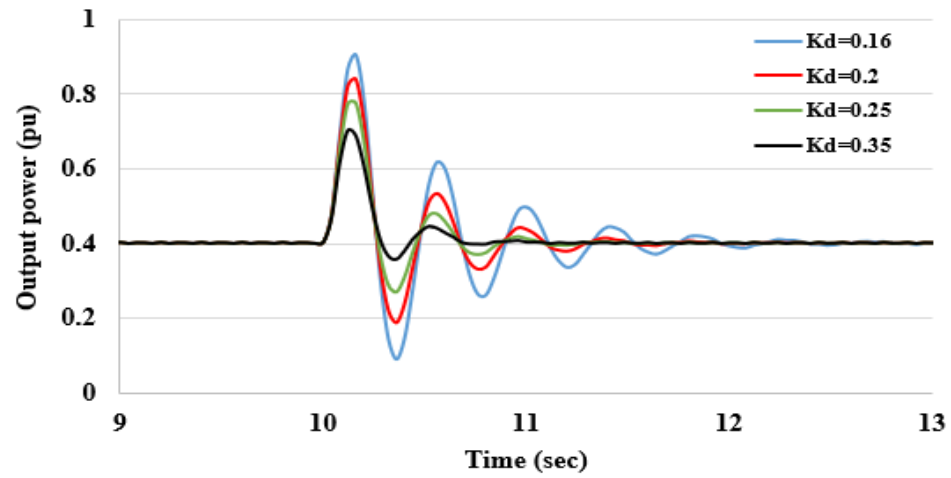


Figure 7.9: Converter output power at different damping constants in response to a microgrid frequency drop

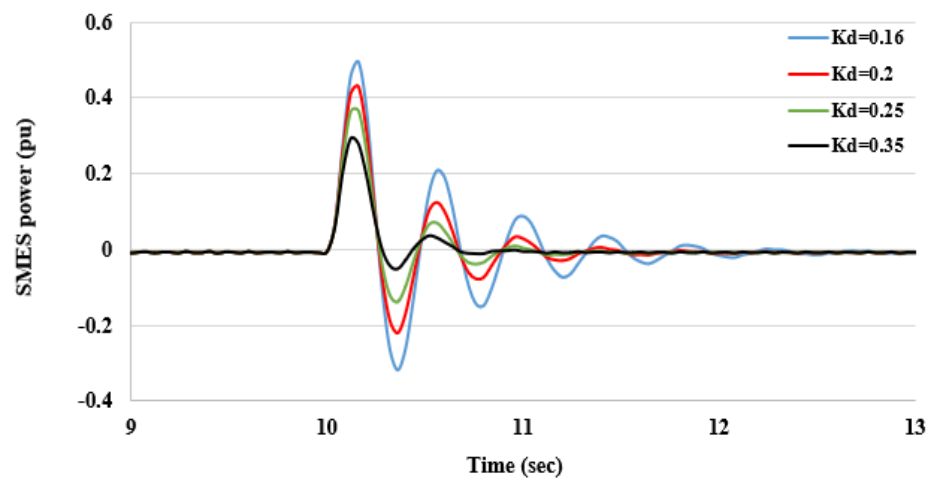


Figure 7.10: SMES instantaneous power in response to a microgrid frequency drop

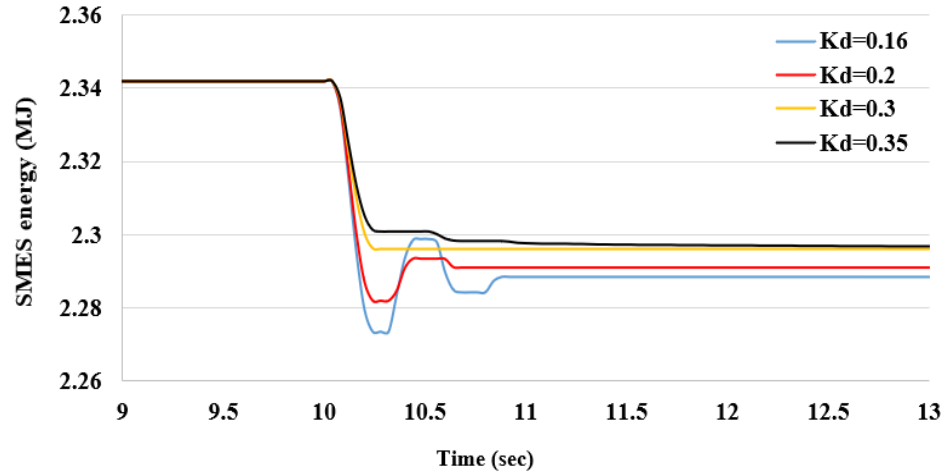


Figure 7.11: SMES energy at different damping constant in response to a microgrid frequency drop

converter power is affected by the damping constant. It can be seen that the converter power is reduced when the damping constant increases. Fig. 7.13 and Fig. 7.14 describe the supplied SMES power and energy with respect to the damping constant, and how the size of the SMES system is reduced with increasing the damping constant. Then the SMES energy and power design and rating should be based on the emulated damping constants. The simulation results show that when the damping constant increases, the maximum converter output power decreases, and hence, the power required from the HESS decreases.

The previous simulation case is repeated at different inertia time constants, while the damping constant is fixed ($K_d=0.16$). This case describes how the inertia time constant change affects the converter output power and the SMES system performances. Fig 7.15 describes the converter output power. It is seen that when the inertia time constant increases, the converter supplies more instantaneous power. This power is supplied by the SMES system. Fig. 7.16 and Fig. 7.17 describe the SMES power and energy that are required to emulate the inertia time constants for the given values. It can be shown that by increasing the inertia time constant, the SMES power and energy increase.

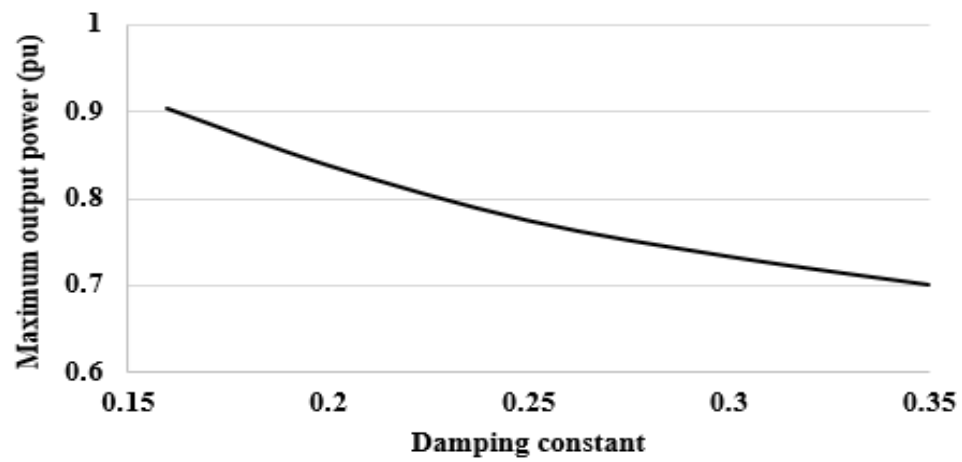


Figure 7.12: Maximum converter output power versus damping constant in response to a microgrid frequency drop

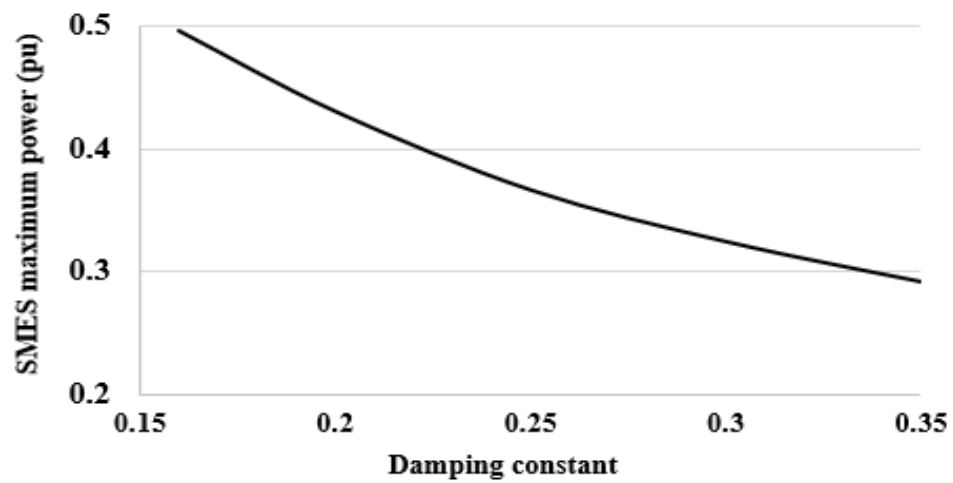


Figure 7.13: SMES maximum power versus damping constant in response to a microgrid frequency drop

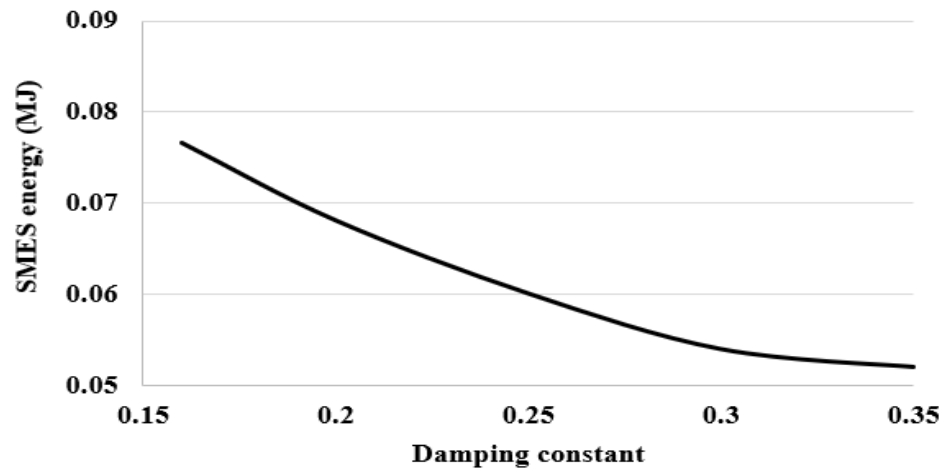


Figure 7.14: SMES energy versus damping constant in response to a microgrid frequency drop

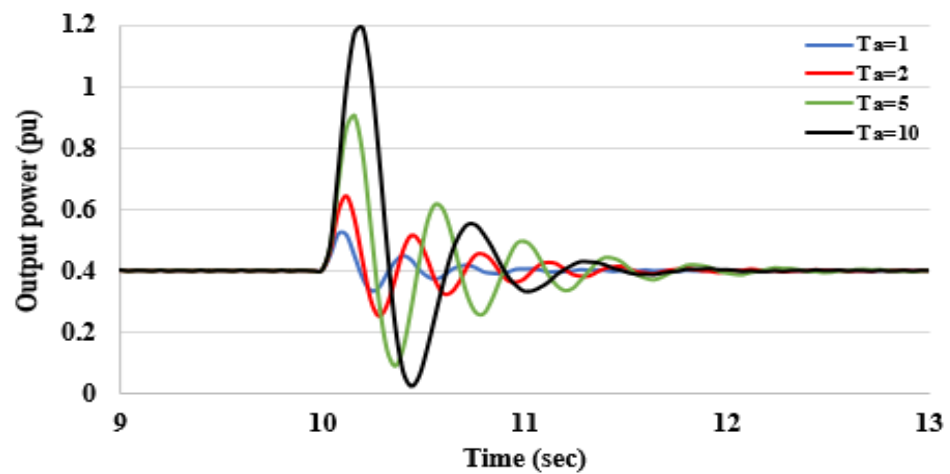


Figure 7.15: Converter output power at different inertia constants in response to a microgrid frequency drop

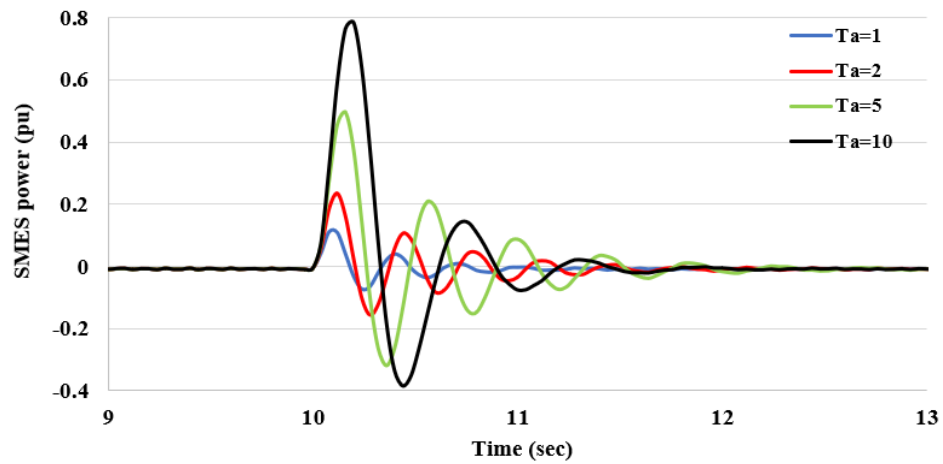


Figure 7.16: SMES power at different inertia constants in response to a microgrid frequency drop

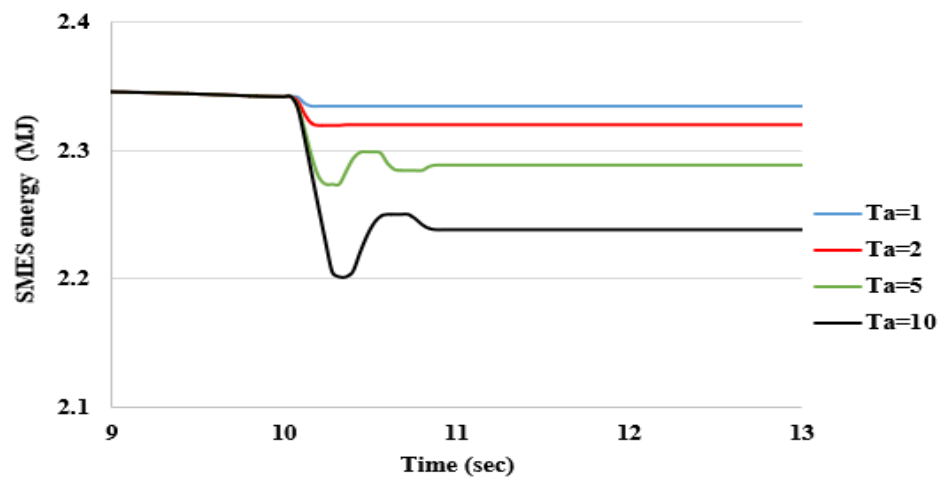


Figure 7.17: SMES energy at different inertia constants in response to a microgrid frequency drop

To easily describe the effect of the inertia time constant on the converter power rating, the maximum converter output power values at each inertia time constant are traced with respect to the inertia time constants in Fig. 7.18. It is seen that the converter power increases when the inertia time constant increases. Moreover, the maximum SMES power and the supplied energy are shown in Fig. 7.19 and Fig. 7.20. It is shown that the SMES needs to supply more power and energy when the inertia time constant increases.

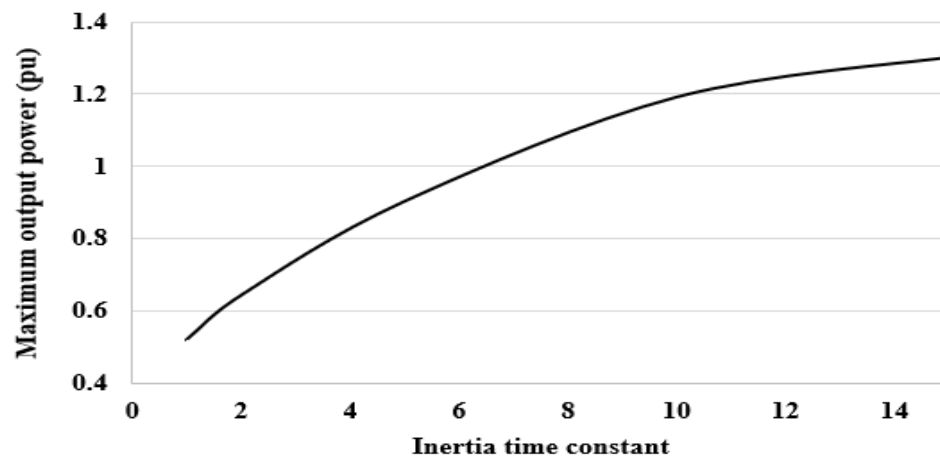


Figure 7.18: Maximum output power versus inertia constants in response to a micro-grid frequency drop

The next set of simulations describes the VSG operation when the reference power is changed. The reference power increased from 0.4 pu to 0.7 pu, and the system is simulated at different damping and inertia time constants. This change may be activated by the local controller or from a hierarchical control system in response to a load or generating power change.

Fig. 7.21 describes the change in the reference power at different damping constants, while the inertia time constant is kept constant ($T_a=6$). It is shown that the converter output power follows the reference values; however, the response depends on the damping constant. When the damping constant increases, the converter maximum output power decreases and it reaches the steady state sooner. The PV

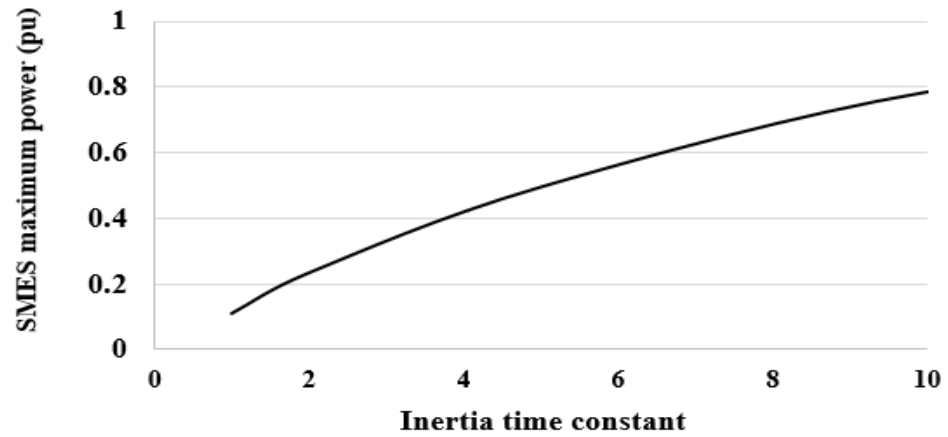


Figure 7.19: SMES maximum power versus inertia constants in response to a microgrid frequency drop

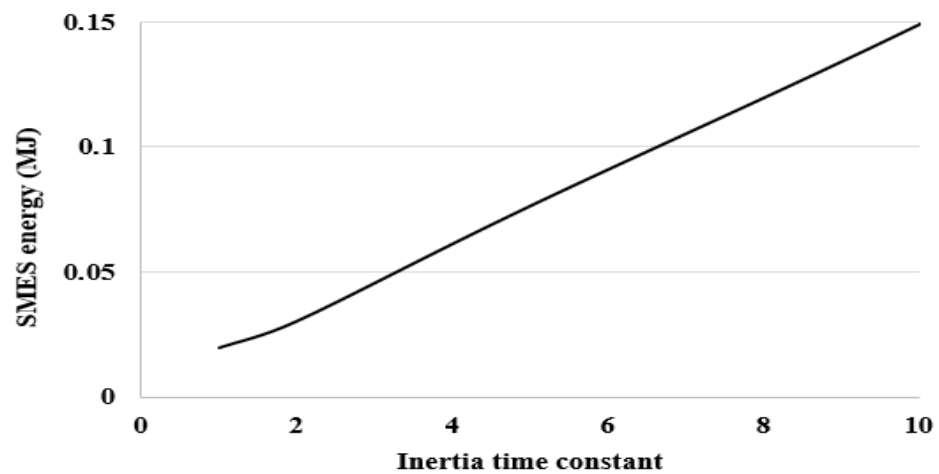


Figure 7.20: SMES energy versus inertia constants in response to a microgrid frequency drop

array generates 0.4 pu, and the converter output power increased from 0.4 pu to 0.7 pu. The difference is compensated by the HESS. The SMES has a fast response and handles the transient power oscillation. The SMES compensates for the oscillation of the converter output power due to its fast response. Then, it helps to reduce the stress on the battery and extends to increase its lifetime. The battery supplies the steady state power (0.3 pu). Fig. 7.22 describes the SMES supplied power and it shows that the SMES power increased when the damping constant decreased and it takes more time to reach its steady-state value. Fig. 7.23 describes how the virtual mechanical frequency changes. It is shown that when the damping constant increases, the frequency has a higher frequency nadir and the system is more stable against the system disturbance. Fig. 7.24 describes the battery discharge to compensate the steady state difference between the PV and load power, it supplies 0.3 pu.

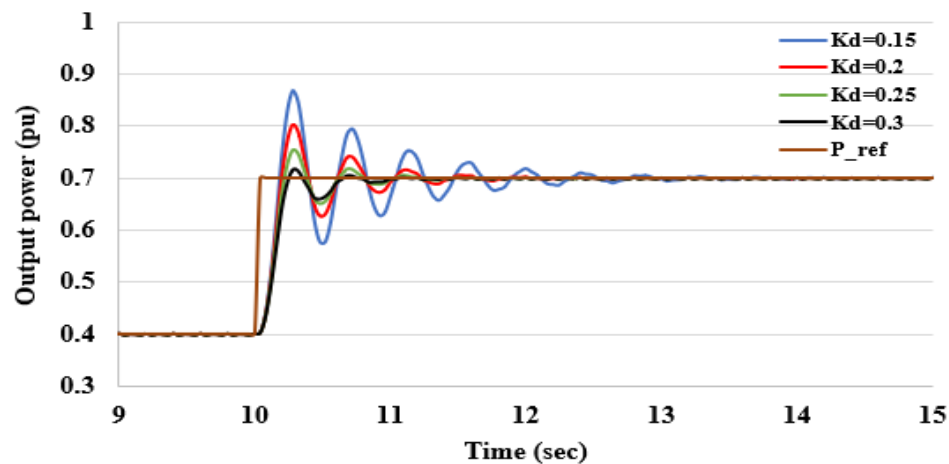


Figure 7.21: Converter power at different damping constants in response to step power setpoint increase

This test is repeated, the reference input power to the converter is increased at different inertia time constants, while the damping constant is kept constant ($K_d=0.16$). The converter output power profile is shown in Fig. 7.25, it is shown that the converter output power follows the reference power with a profile depending on the inertia time constant. At a smaller inertia time constant, the VSG supplies less power, and

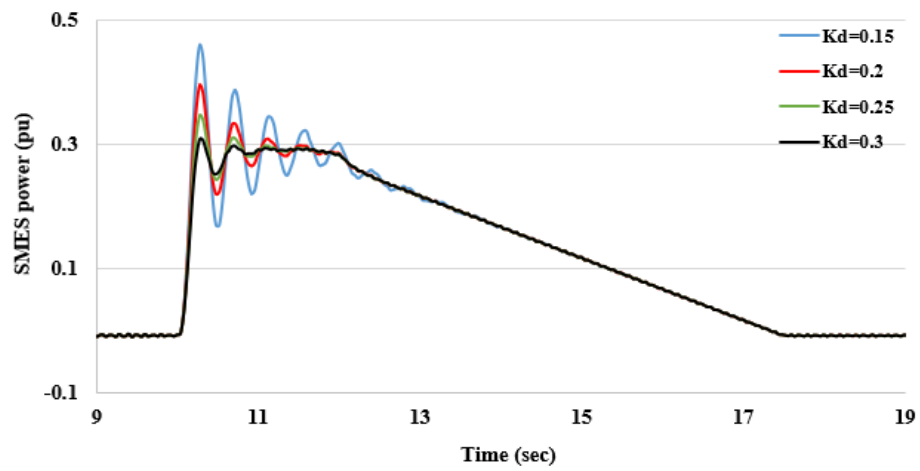


Figure 7.22: SMES power at different damping constant in response to step power setpoint increase

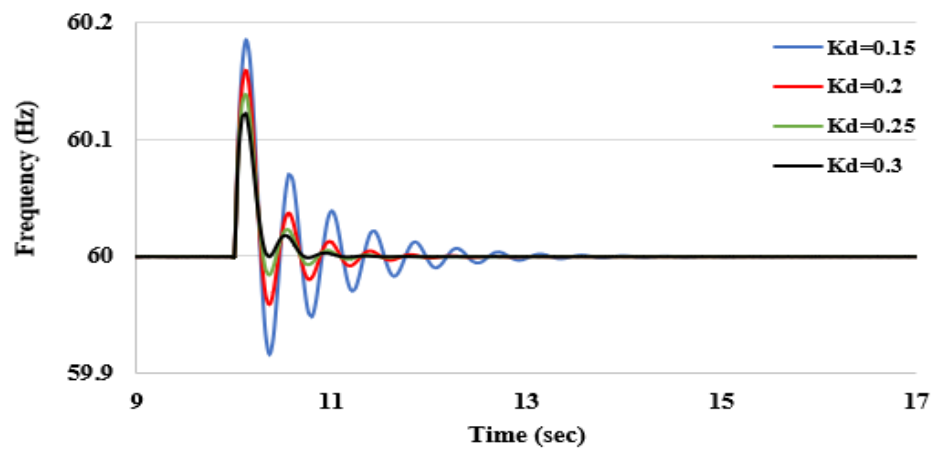


Figure 7.23: Frequency change at different damping constants in response to step power setpoint increase

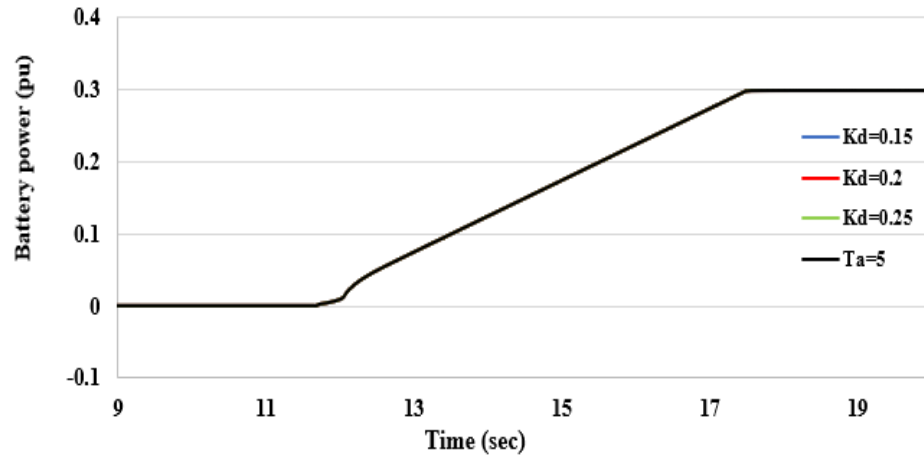


Figure 7.24: Battery power profile

it has a larger number of oscillations until it reaches its steady-state value.

The PV array generates 0.4 pu and the difference between the PV array power and the converter output power is compensated by the ESS. The SMES supplies the transient power and the battery supplies the steady state power. The SMES power is shown in Fig. 7.26. It is shown that at a smaller inertia time constant the SMES needs to supply less power. Then the rating power of the converter and the SMES system should be based on the emulated inertia time constants. Increasing the inertia helps the system to be more stable at different disturbances. As shown in Fig. 7.27, when the inertia time constant increases, the frequency has a smaller rate of change of the frequency (RoCoF) and a larger value of frequency nadir. Fig. 7.28 describes the battery discharge power, it supplies 0.3 pu.

To show the effect of both the inertia and damping constants on the system performance and the SMES power and energy rating, the system is simulated at different values of inertia and damping constants. Fig. 7.29 describes the converter maximum output power oscillation with respect to inertia time constant at different damping constants when the frequency change from 60 Hz to 59.5 Hz. It can be shown that the maximum value increases with increasing the inertia time constant

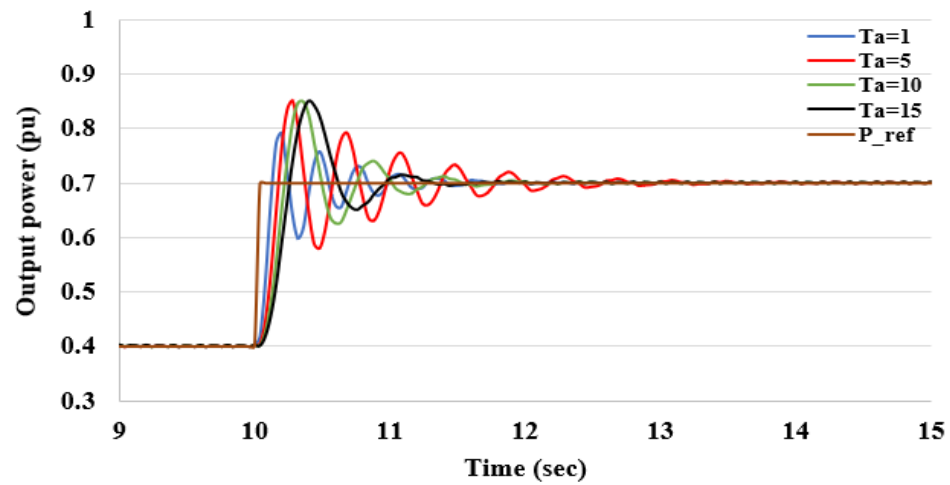


Figure 7.25: Converter power at different inertia constants in response to step power setpoint increase

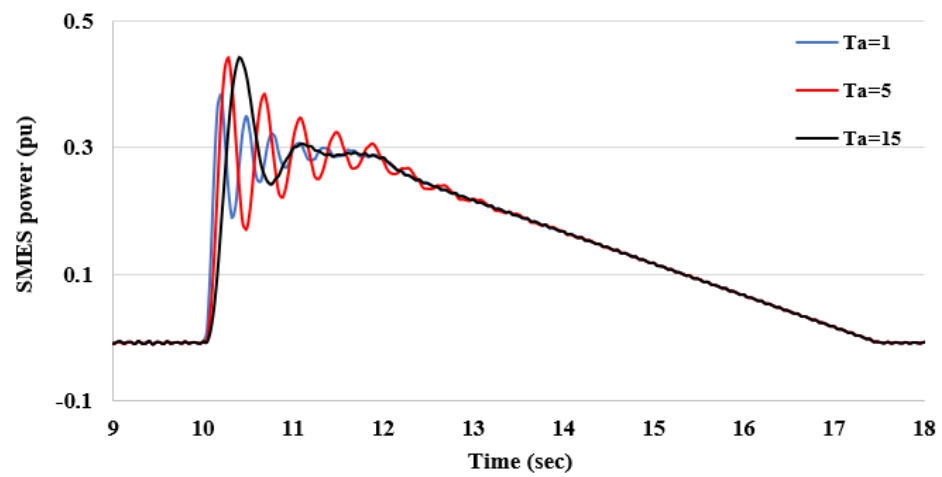


Figure 7.26: SMES power at different inertia constants in response to step power setpoint increase

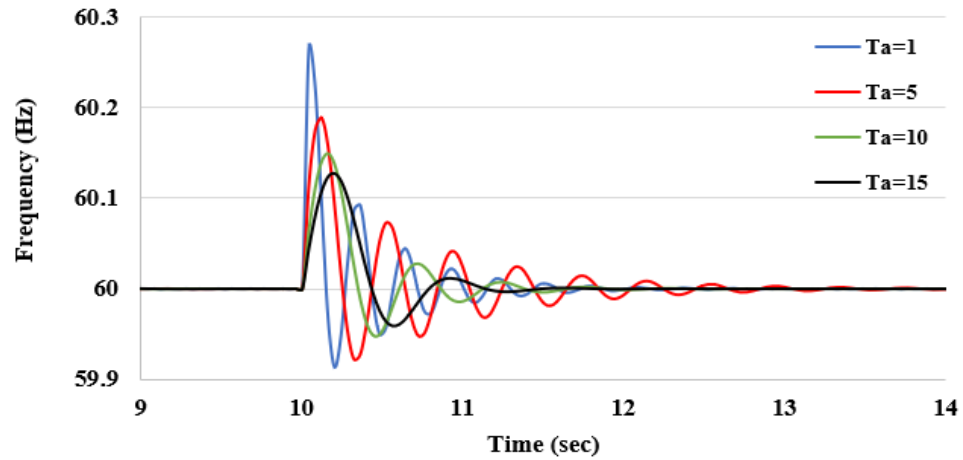


Figure 7.27: Frequency change at different inertia constants in response to step power setpoint increase

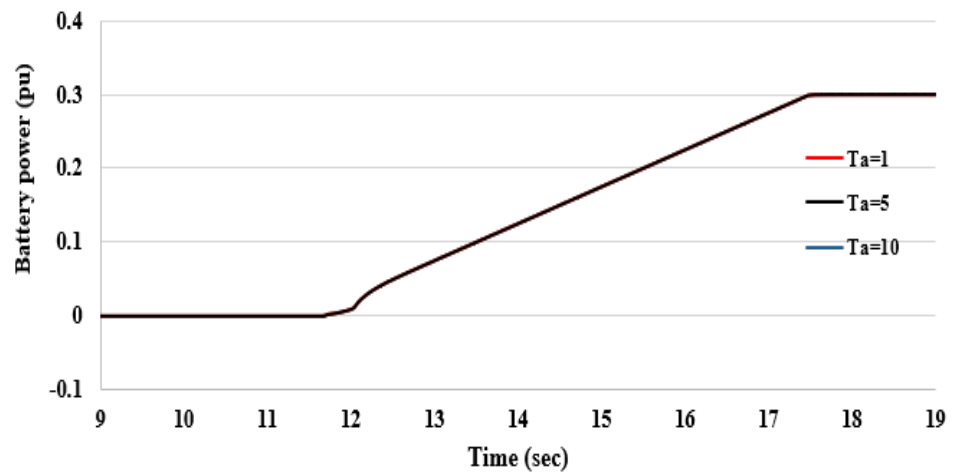


Figure 7.28: Battery power profile

and reduction in the damping constant.

Fig. 7.30 and Fig. 7.31 describe the SMES power and energy at different values of both inertia and damping constants. The SMES power and energy decrease with damping constant increase. Also, SMES power and energy are increased when the emulated inertia time constant increases. It can be shown from the simulation results that the inertia time constant and the damping constant affects the system performance and sizing of both the converter and the SMES power and energy. Moreover, using the SMES, the converter can emulate the inertial feature of a proposed SG by adjusting the inertia and damping constants.

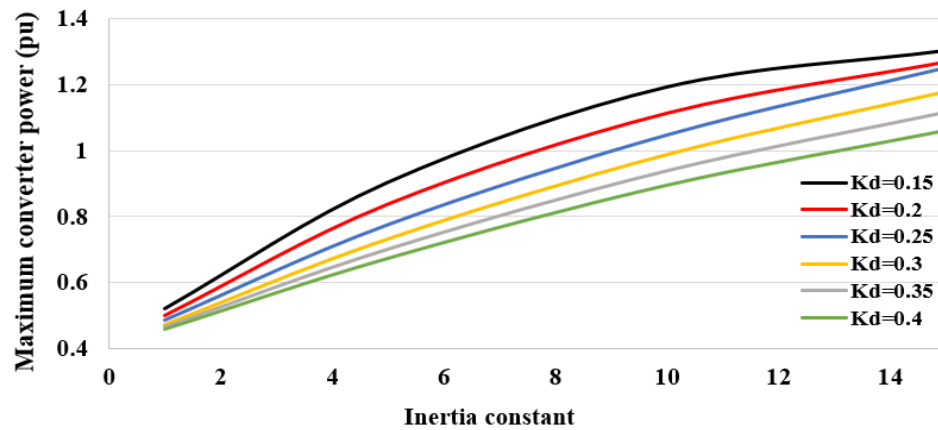


Figure 7.29: Converter output power at different inertia and damping constants

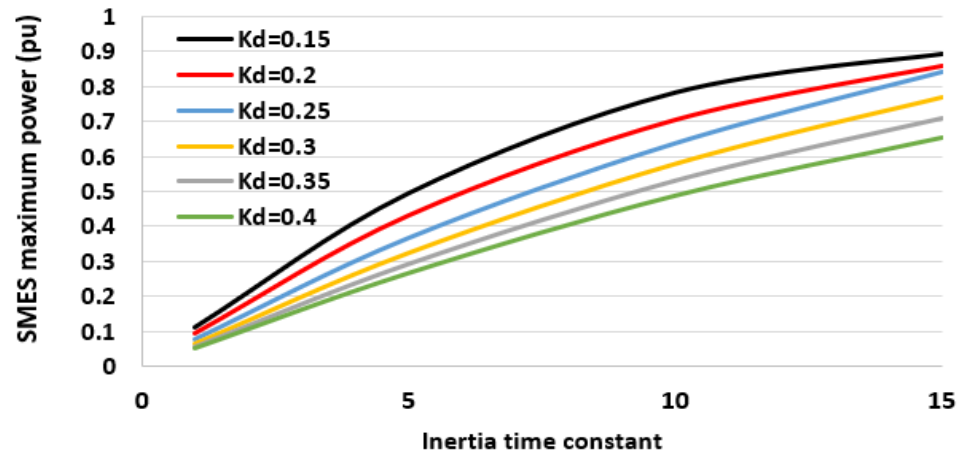


Figure 7.30: SMES maximum power at different inertia and damping constants

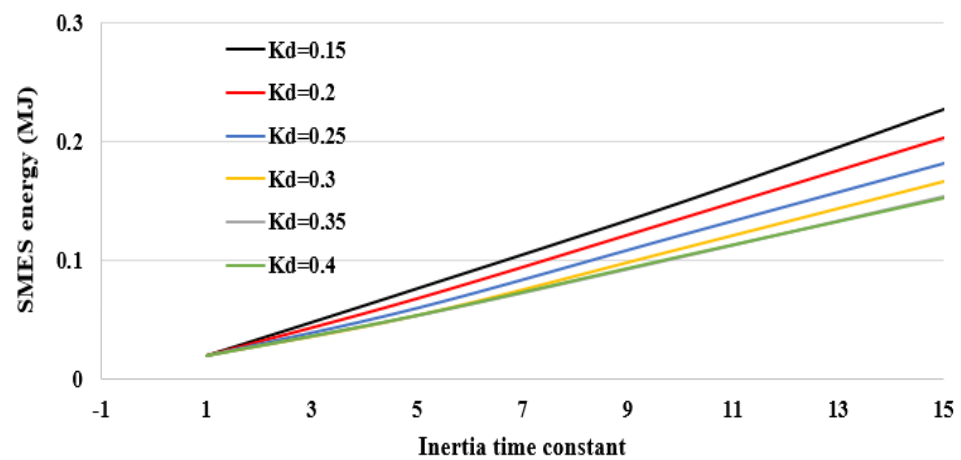


Figure 7.31: SMES energy at different inertia and damping constants

As shown in Fig. 7.9 and Fig. 7.21, increasing the damping constant stabilizes the VSG against frequency oscillations. On the other hand, increasing the damping constant reduces the required converter output power. In some cases, the power required increases with the damping constant increase. One of the methods available to do this is to set the damping constant to act as a frequency droop constant. In that case, the frequency, ω_g , in (6.8) is set a constant value (ω_{ref}). In this case, the phase locked loop (PLL) is not required to track the grid frequency which simplifies the controller design.

In this case the damping constant works as a frequency droop gain in the frequency droop control loop as described in [254]. However, increasing the damping constant reduces frequency oscillation in the VSG response but increases the required converter output power, and the steady state active power deviates from its reference value when the system is subject to a frequency drop contingency.

Fig. 7.32 shows the results when the frequency in the microgrid drops from 60 Hz to 59.7 Hz at $t=5$ sec at different damping constants, while the inertia time constant is fixed at constant value ($T_a=6$).

Fig. 7.33 shows the converter output power variation in response to the frequency drop and how the damping constant affects the output power profile. The plot shows that the system can work stably without a PLL. Also, the transient active output power increases when the damping constant increases. Furthermore, the steady state active power value deviated from its reference value due to the droop term. This deviation depends on the frequency variation and the damping constant value [254].

Fig. 7.34 shows the ESS power in response to the same case. It is shown that increasing the damping constant increases the ESS power output, unlike performance described earlier in Fig. 7.10, so the design of the ESS is dependant on how the emulated damping constant values are applied in the control strategy.

In this scheme, the frequency drop value also affects the total steady state con-

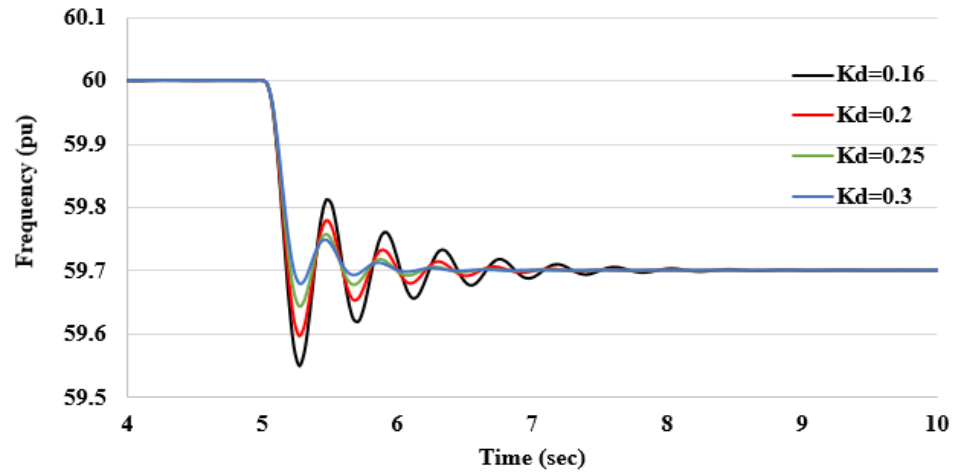


Figure 7.32: VSG frequency response to a microgrid frequency drop with different damping constants applied in the frequency droop function

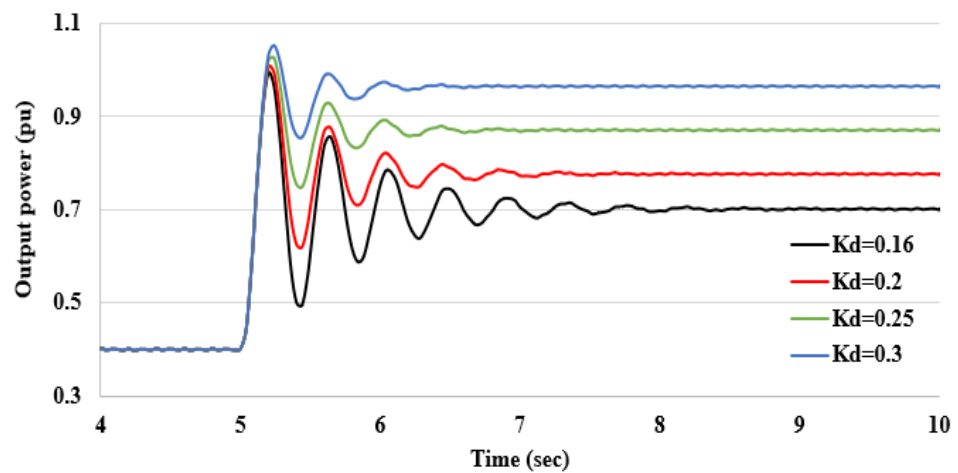


Figure 7.33: Converter output power at different damping constants in the frequency droop function in response to microgrid frequency drop

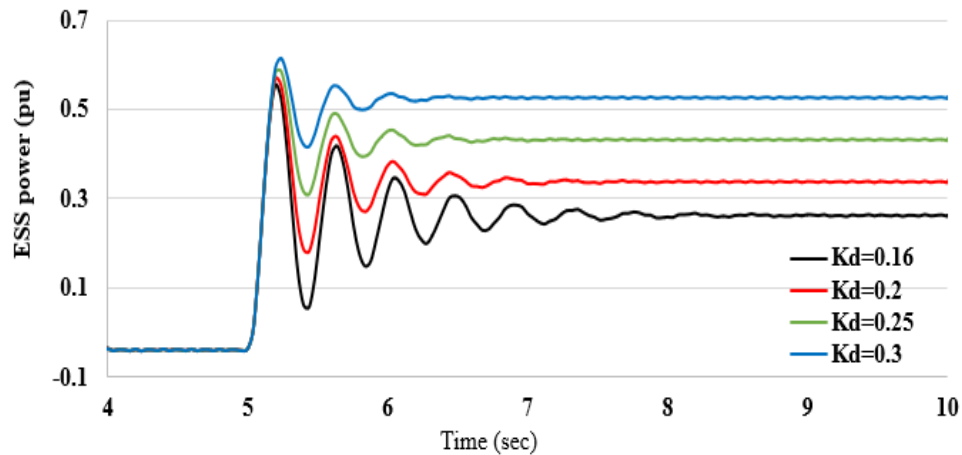


Figure 7.34: ESS power output at different damping constants in the frequency droop control in response to microgrid frequency drop

verter output power. Fig. 7.35 shows the converter output power when the microgrid frequency drops by different amounts for constant damping and inertia time constants in the frequency droop function ($K_d=0.2$ and $T_a=6$). The results show that the converter output power increases when the frequency drop value increases as expected for a frequency droop scheme. Also, this power is supplied from the ESS since the RER can't do that, and the ESS power demand increases when the frequency drop value increases as shown in Fig. 7.36.

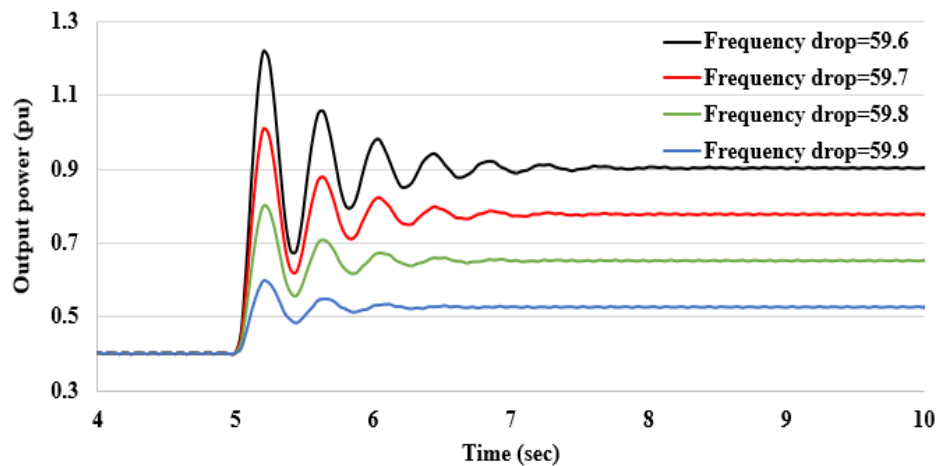


Figure 7.35: Converter output power in response to microgrid different frequency drop values with $T_a=6$ and $K_d=0.2$

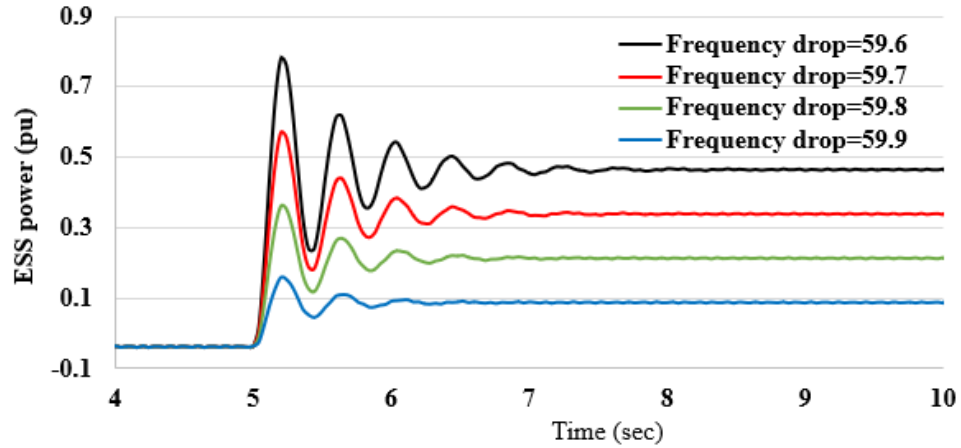


Figure 7.36: ESS power supplied in response to a microgrid different frequency drop with $T_a=6$ and $K_d=0.2$

Although increasing the transient output power is sometimes required with increasing damping constant. Supplying steady state power and dispatchable generation or load decrease is needed for long term response.

To eliminate the steady state deviation, the grid frequency is measure using PLL. However the PLL design may affect the system performance and operation. The design of the PLL may be used to control the converter output power at both the transient and steady state periods. In this work the direct measured frequency is used in the controller to avoid having the response of PLL affected the performance of the system. To control the converter active power to follow a reference in steady state and responds to transient disturbances a phase compensation method is used. The phase compensation method is described in the next subsection.

7.7 Phase Compensation Method

The phase compensation method adds a lead-lag compensator, $H(S)$, that is cascaded with the measured microgrid frequency to reshape the frequency characteristics as shown in Fig. 7.37.

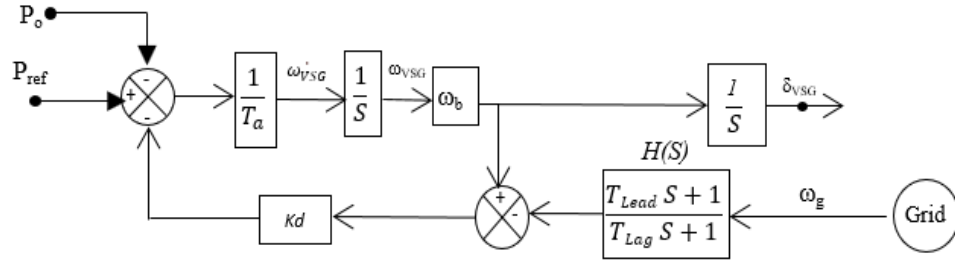


Figure 7.37: Lead-lag compensator cascaded with the measured microgrid frequency

The lead-lag compensator can be described as:

$$H(s) = \frac{T_{Lead} + 1}{T_{Lag} + 1} \quad (7.7)$$

From the equation (7.7), the maximum phase lag can be calculated by:

$$\phi_{Lag-max} = \arctan \frac{T_{Lag} - T_{Lead}}{2\sqrt{T_{Lag}T_{Lead}}} \quad (7.8)$$

The frequency that can occur at this phase lag can be obtained by:

$$F_{Lag-max} = \frac{\omega_{Lag-max}}{2\pi} = \frac{1}{2\pi\sqrt{T_{Lag}T_{Lead}}} \quad (7.9)$$

Using equations (7.7) to (7.9), the design for the compensator can be done. $F_{Lag-max}$ can be chosen approximately equal to the lowest frequency of oscillation that is expected to occur in the microgrid. The desired phase lag $\phi_{Lag-max}$ is assumed. The value of $F_{Lag-max}$ is chosen to be 0.6 Hz and phase lag $\phi_{Lag-max}$ is chosen to be 20° and 50° in two different cases in this work. Then T_{Lead} and T_{Lag} can be calculated by solving (7.8) and (7.9) with the chosen $F_{Lag-max}$ and $\phi_{Lag-max}$.

Fig. 7.38 describes the converter output power for several cases. At this case the PV generates 0.4 pu, and the converter supplies this power before the disturbance. The frequency drops from 60 Hz to 59.5 at 5 sec at different cases of compensator parameter values. Case 1 describes the operation of the system when $H(s)=1$. At

case 2, $T_{Lead} = 0.2$ sec, $T_{Lag} = 0.4$ sec and $\phi_{Lag-max} = 20^\circ$. At case 3, $T_{Lead} = 0.1$ sec, $T_{Lag} = 0.8$ sec and $\phi_{Lag-max} = 50^\circ$. The results show that the required converter output power depends on the parameters of the phase compensator.

The ESS supplies the difference between the PV generated power and the converter output power as shown in Fig. 7.39.

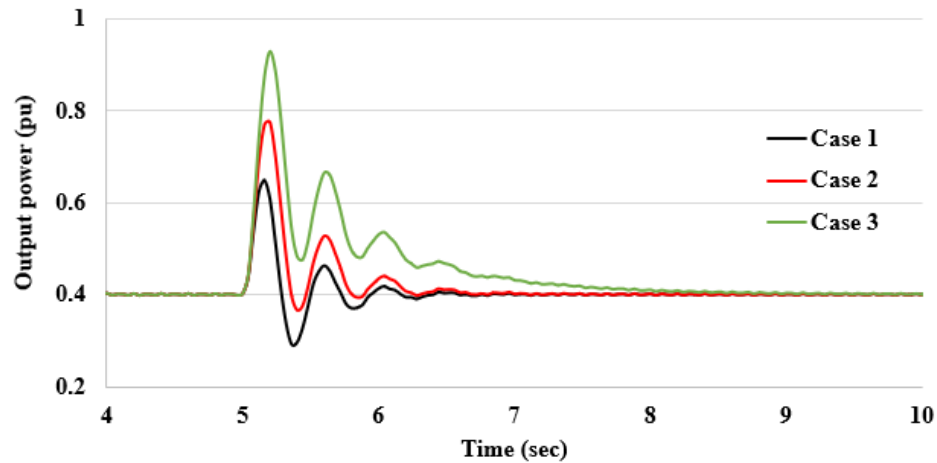


Figure 7.38: Converter output power at different cases; at case 1 $H(s)=1$, at case 2 $T_{Lead} = 0.2$ sec, $T_{Lag} = 0.4$ sec and at case 3, $T_{Lead} = 0.1$ sec, $T_{Lag} = 0.8$ sec

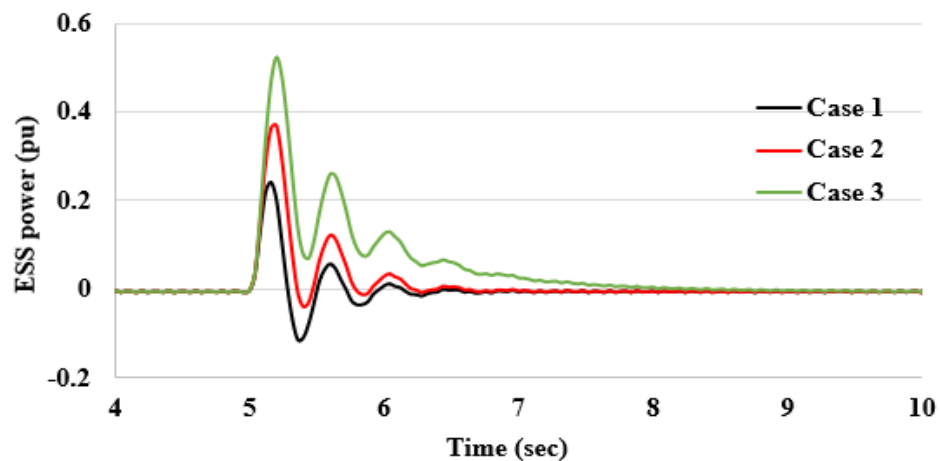


Figure 7.39: ESS power at different cases; at case 1 $H(s)=1$, at case 2 $T_{Lead} = 0.2$ sec, $T_{Lag} = 0.4$ sec and at case 3, $T_{Lead} = 0.1$ sec, $T_{Lag} = 0.8$ sec

Case 2 is chosen to study the effect of damping constant on the converter output power. Fig. 7.40 describes the converter output power at different damping constant

values when the microgrid frequency drops from 60 Hz to 59.5 Hz. The results show that increasing the damping constant increases the transient converter output power, however, unlike the results in Fig. 7.33 the steady state power is not changed.

The difference between the converter output power and the PV generated power is supplied from the ESS as shown in Fig. 7.41. It can be shown that the rating of the ESS depends on the emulated damping constants such that, increasing the damping constant increases the peak ESS power rating in this simulation case.

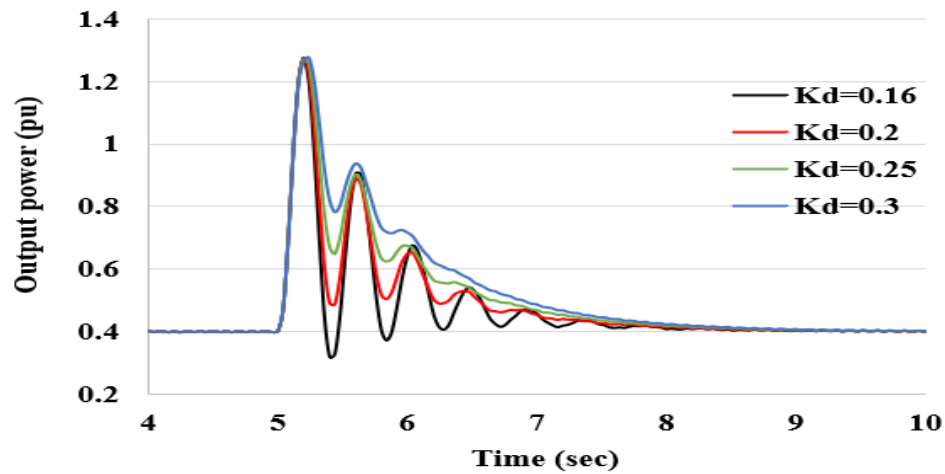


Figure 7.40: Converter output power at different damping constants for the parameters at case 2, ($T_{Lead} = 0.2$ sec, $T_{Lag} = 0.4$ sec, and $P_{PV} = 0.4$ pu)

7.8 Verification of Virtual Synchronous Generator Compared to Conventional Synchronous Generator

7.8.1 Introduction

Since the dependency on VSG-based controllers has been increased, the performance of VSG with respect to the SG should be compared to check if they have the same performance at both the steady-state and transient response. In this section, VSG controller based converter is incorporated into a system consisting of a solar photo-

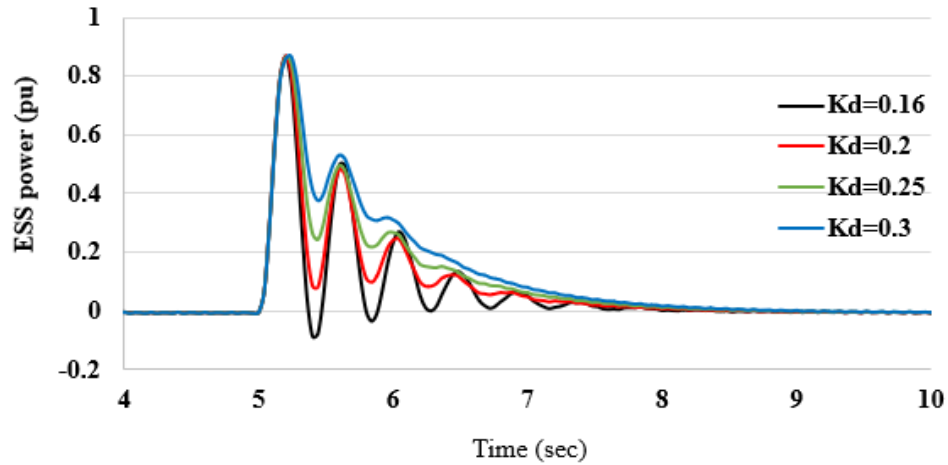


Figure 7.41: ESS power at different different damping constants for the parameters at case 2, ($T_{Lead}=0.2$ sec, $T_{Lag}=0.4$ sec and $P_{PV}=0.4$ pu)

voltaic and a hybrid energy storage system. The layout of the VSG and SG systems is shown in Fig. 7.42.

The modeling of the different parts in fig. 7.42 are well-reviewed in [204, 205, 228]. This section is concentrating only on the comparison between the inertial features of VSG and conventional SG. The aim of this section is to review the fundamental concepts of both VSG and SG to compare their response in case of changing the reference set points. The dynamic behavior of SG can be emulated by the VSG controller by modeling the fundamental swing equation. Moreover, different operating conditions can be attained by controlling the parameters of the VSG controller, unlike the SG that has fixed parameters and characteristics.

7.8.2 Conventional Synchronous Generator

The conventional synchronous generator was previously well researched in much literature. However, the SG and its associated controls will be briefly reviewed in order to compare its operation with the VSG. Synchronous generators can be considered as voltage sources forming the grid. They provide regulation for the amplitude and

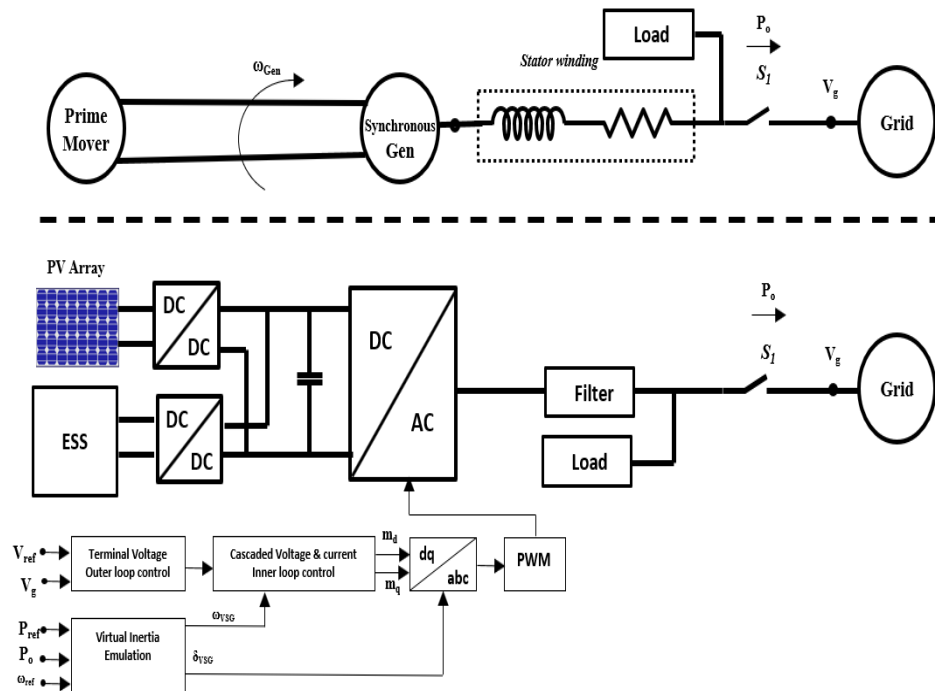


Figure 7.42: General layout of VSG and conventional SG systems

frequency of the system voltage. The voltage magnitude is regulated by an automatic voltage regulator (AVR). It stabilizes the terminal voltage of the generator by adjusting the electromotive force in the machine. The frequency regulation is carried out by the prime mover governor. The governor acts on the fuel rack position of the prime mover to maintain a constant rotor speed by providing a balance between the generation and the demand.

Since controlling the system frequency is essential in the power system, the main purpose of the VSG is to improve the system's frequency and stability at different disturbances. So the inertial features of the SG will be mimicked by VSG that can be described by the swing equation that represents the dynamic power balance between the electric and mechanical power. The authors of [255, 256] described the model of SG and its associated controls in detail.

7.8.3 Simulation Results

The VSG model and its controller are validated by comparison with a SG, and an electromagnetic transients program is used for this comparison. In this simulation case, the reference power is changed as shown in Fig. 7.43 and 7.44. This step-change may be activated by the local controller or from a hierarchical control system due to a sudden change in the generation or the electric demand. The simulation is carried out for two different values for inertia time constant ($T_{a1} = 1$ and $T_{a2} = 5$). The simulation results describe that the converter output power tracks its reference values and its profile depends on the emulated inertia settings. Also, it can be shown that both the VSG and conventional SG have comparable performance.

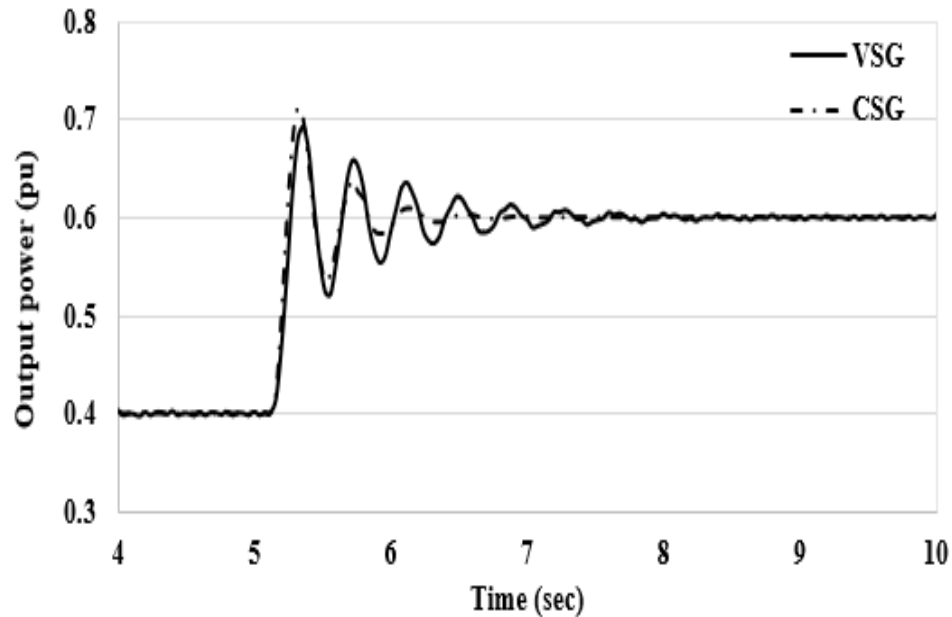


Figure 7.43: VSG and SG active power step change at inertia time constant = 1

Since the irradiation level and the PV output power is considered constant at this simulation, the output converter power has to be compensated from the energy storage system. Fig. 7.45 shows the power compensated by the ESS. At a higher inertia time constant, the power supplied from the ESS is larger than its value when

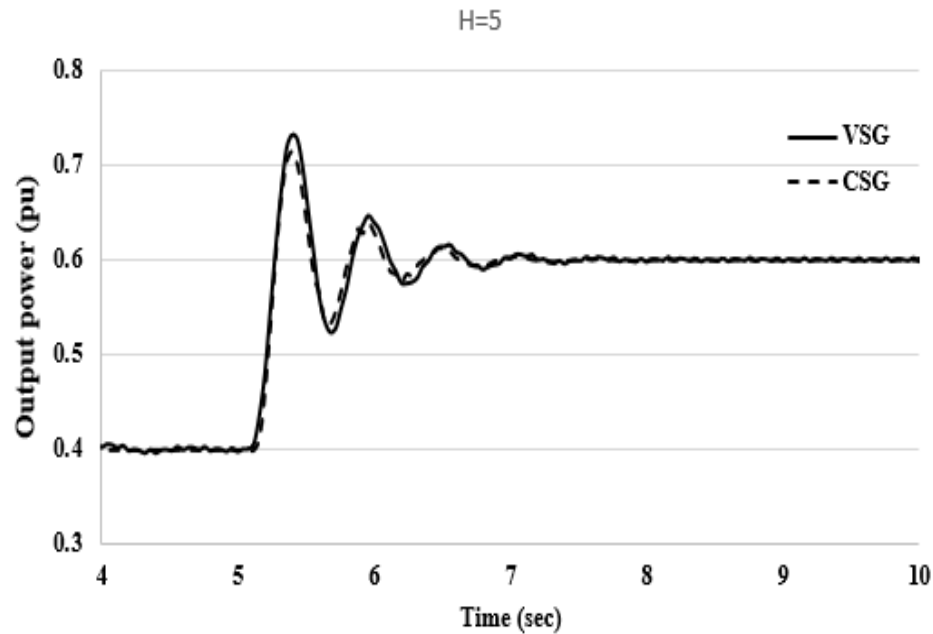


Figure 7.44: VSG and SG active power step change at inertia time constant = 5

the inertia time constant has a smaller value.

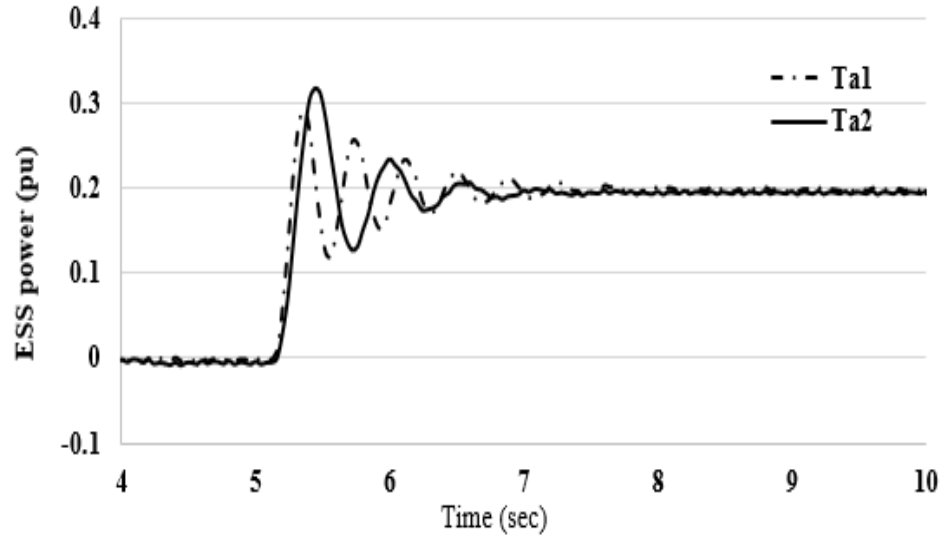


Figure 7.45: ESS power at different inertia time constants

The change in the frequency is described in Fig. 7.46 and Fig. 7.47. It is shown that the VSG performance closely matches the SG performance. Furthermore, at a lower inertia time constant value, the frequency variation is more pronounced and

has a high rate of change. On the other hand, when inertia time constant increases, it helps the system to counteract the frequency change.

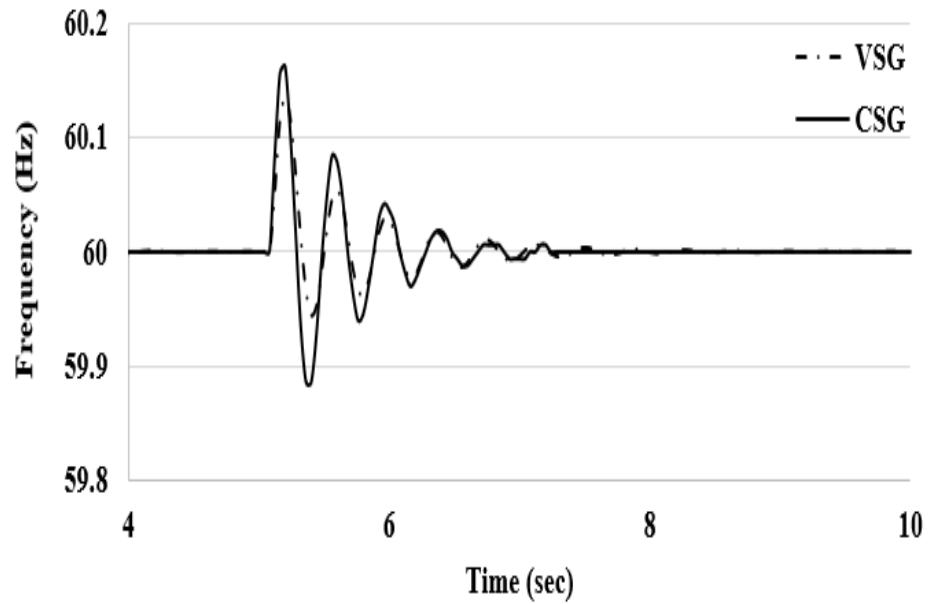


Figure 7.46: Frequency profile at inertia time constant = 2

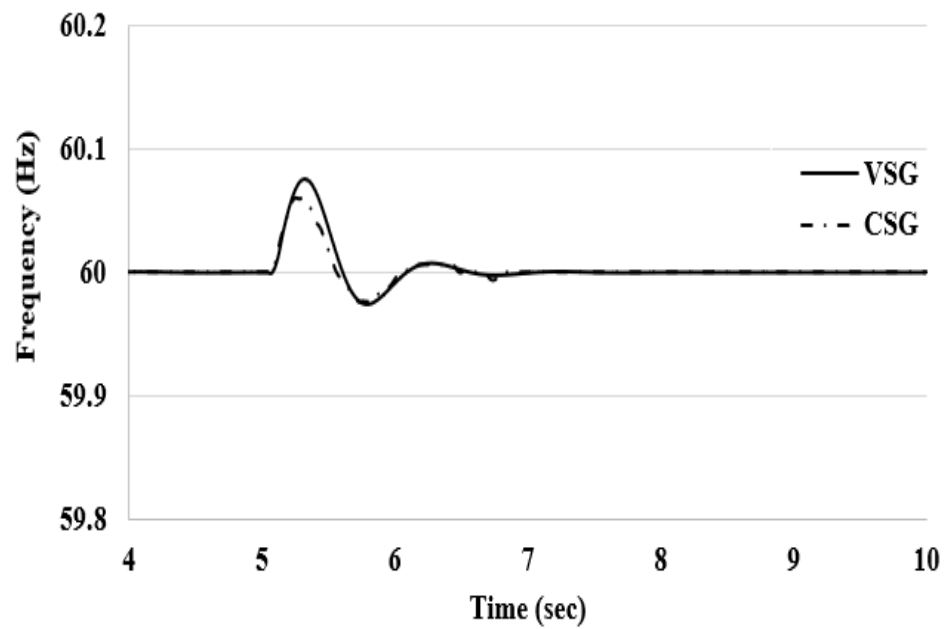


Figure 7.47: Frequency profile at inertia time constant = 8

7.9 Conclusion

The sudden changes in the load and generated power from RERs may cause fluctuations in the system and deteriorate the power quality. To counteract these changes, ESSs are used to emulate the conventional synchronous generator inertia and damping constants, hence improving the system stability and operation against different disturbances. In this chapter, a hybrid energy storage system consists of a SMES system and a battery system is described. The system is implemented using an electromagnetic transients program. The system is simulated at different values of inertia time and damping constants. The impact of different values of constants affect the ratings of the converter and the SMES was described.

The converter output power and the SMES power and energy increases when the inertia time constant increases or the damping constant decreases. Also, VSG converter can emulate many SG inertial features through changing the inertia and damping constants. Furthermore, VSG can enhance the system stability such as reducing the RoCoF or increasing the frequency nadir through emulating the SG inertial features. Supplementing the battery with the SMES reduces the number of charging and discharging cycles of the battery. Hence, this reduces the stress on the battery system and increases its lifetime.

However the SMES is more expensive than the battery, it may be more effective and cheaper in some applications such as in fast charge and discharge, and deep DOD ones. The SMES lifetime may be equivalent to tens of battery systems. VSG controllers combined with ESSs play a vital role to stabilize power system specially the small size systems such as microgrids and reshape the architecture of power networks. Also, this increases the ability of the system to support increasing penetration of RERs which helps to optimize using the available energy resources and minimize conventional fuel consumption and greenhouse gas emissions.

Chapter 8: Summary, Conclusions and Future Work

8.1 Summary

Increasing installation of inverter based RERs and the desire to improve the resilience of the power system led researchers to explore microgrid concepts. Microgrids can potentially enhance the utilization of electric resources and provide reliable, efficient, and secure operation for the power system. Use of microgrids reduces the dependence on the transmission system for some classes of loads. This dissertation described the operation, power management, and some possible control systems for microgrids. Different control strategies based on hierarchical control levels were reviewed. Such control systems depend on communication systems for monitoring and control of operation for microgrids. This dissertation described the most discussed communication media and protocols for use in microgrids.

There are different types of RERs that can be used in microgrids. Wind energy generation are seeing significant adoption in transmission system and to an external in microgrids. Modeling for the WECS system was described in this dissertation. The modeling of the wind turbine, the RSC, the GSC, pitch angle controller, and dc-link chopper protection circuit were described. Simulation for the system at different wind speeds was presented to verify the proposed control system operation. Also, a battery energy storage system was modeled and connected with the WECS to compensate the difference between the available wind power and the load demand. Furthermore, the system was used for supporting the terminal voltage through controlling reactive power.

PV systems have seen a rapid increase in installation since they have many advantages, especially as costs have gone down. This dissertation describes equivalent modeling of the whole PV system. The work involved the modeling of the PV array and dc-ac converter. In addition, a battery energy storage system was added to the

system. Modeling and controls for the battery system were described. The system simulation was carried out at different irradiation levels and different load levels to verify the proposed control systems.

Because of expansion of variable output of RERs and loads in power system, voltage level in microgrids can experience rapid variation. This voltage variation has to be mitigated in the modeled microgrid to achieve decent power system performance and operation. In this dissertation the voltage variation was mitigated by absorbing or supplying the reactive power using the PV converter. Consequently, the voltage level was controlled through a volt/var strategy to keep the microgrid within a safe operating margin. Moreover, the inverter prioritizes the active and reactive power based on the voltage level and controls both independently.

Large changes in load or in generated power from RERs cause the frequency of the system to fluctuate. The amplitude, frequency, and damping of this oscillation fluctuation depend on the rotor inertia and damping coefficient of synchronous machines connected to the power network. Since RERs such as wind systems have a reduced inertia and PV systems have no kinetic inertia if controlled in grid following mode, the system may be vulnerable to stability problem in case of disturbances. In this dissertation a VSG concept was adopted for controlling the system stability. An explanation of VSG was presented with the aim of emulating a conventional SG and enhancing response. Then modeling of VSG control structure in synchronously rotating dq reference frame was described. The power converter that emulates the SG is connected to the PV array and a battery system. The battery system was integrated with the dc bus of the PV system to provide the power needed to enable the system to emulate a SG response. The simulation cases and scenarios include the effect of varying the inertia time constants and the damping constants on the system performance.

Since a battery bank can't provide all the required response features, a HESS

consisting of a SMES system and a battery system was used. The system was modeled using an electromagnetic transients program and simulated at different values of inertia time constants and damping constants. The simulation results show how these constants affect the power and energy rating for the ESS and the power ratings of the converter. Moreover, the constants affects the maximum output power of the combined HESS plus PV system.

The validation of VSG is important to describe the ability of VSG to emulate the SG features. This comparison was done by comparing the VSG to a SG. The comparison was made when a step changing is applied at both VSG and SG.

The system was integrated, implemented, and simulated using PSCAD/EMTDC to show that the VSG can add virtual inertia to increase the effective system inertia. Moreover, it can emulate many SG features and its parameters can be regulated to change the dynamic performance of the converter to get better performance.

8.2 Conclusions

The microgrid concept has power to be a promising methodology for integrating the distributed renewable resources and sensitive loads for achieving the power system resilience.

Since the RERs with commonly used control schemes reduce the system inertia, the VSG methodology is a convenient method for improving system stability and achieving resilient system operation. The VSG-based controlled inverter combined with BESS can emulate the behavior of SG to regulate and support the frequency of the power system following a disturbance and improve system performance. Furthermore, VSG parameters can be set according to the best performance without being limited by the characteristics of a physical SG, and can be set to change the dynamic performance of the converter to get better performance. Moreover, these constants affect the real power of the converter and the ESS peak power and stored energy ratings. Moreover, a VSG scheme can support the system voltage even in the case of grid voltage fluctuations.

At a larger inertia time constant, the system experience a larger amplitude power oscillations, but fewer oscillations, and increased ability to counteract a frequency change. On the contrary, at a lower inertia time constant value the amplitude of the power oscillation is reduced, the frequency variation is more pronounced, and the system reaches steady-state after more oscillations.

The damping constant selection affects the system performance such that at a larger damping constant, the system has a lower amplitude power oscillations and it takes smaller time to reach the new steady-state value.

Using a VSG controller can enhance the system stability by reducing the RoCoF or increasing the frequency nadir. Using a hybrid energy storage system can support the system at different operating conditions and scenarios. A combined SMES and

battery system is a promising solution. The SMES can support the rapid and high rate of change of power fluctuation, on the other hand, the battery can support the slower and steady state power fluctuation. The HESS reduces the number of fast charging and discharging cycles of the battery. Hence, this reduces the stress on the battery system and increases its lifetime. Although the SMES is more expensive than the battery, it may be more effective and cheaper in some applications resulting fast charge and discharge, and deep depth of discharge. The SMES lifetime may be equivalent to that of tens of battery systems.

VSG concepts expand the ability to support RERs in the power system and VSGs can support system frequency and stability to improve resilience. Furthermore, VSG controllers combined with ESSs play a vital role to enable the spread microgrid concepts and reshape the architecture of power networks. Supporting increased penetration of RERs helps to optimize using the available energy resources, and minimize conventional fuel consumption and greenhouse gas emissions.

8.3 Future Work

The following research topics can be studied based on the results in this dissertation.

- The VSG implemented in this dissertation is based on a HESS consisting of a SMES and battery. Other ESS can be used in conjunction with this HESS such as mechanical energy storage system (flywheel, pumped hydro-storage, a compressed air energy storage), chemical energy storage (fuel cell or flow battery), thermal energy storage or electrical energy storage (supercapacitors). Future work should study these options. Also, alternative coordination between different ESSs can be put into consideration based on the different features for each ESS type. How each ESS type affects the system stability during different disturbances and contingency scenarios should be studied. Also, the effect of different disturbances on the VSG system size and operation should be investigated. An economic analysis should also be performed.
- The model of the different system components may be enhanced by including more realistic models of weather variation to study the performance of the system at different changing wind, temperature and irradiation conditions. The impact of weather conditions on RER output and the ESS behavior on VSG response should be studied.
- This research implemented a VSG-based solar PV system under constant PV conditions. Future research may explore the VSG operation when it is working in conjunction with RERs with fast changing output as well as other sources such as WECS, biomass generators, or micro-hydropower systems. Moreover, a comparison between system performance with a large central ESS-based VSG versus distributed ESSs is a point to study. The coordination between distributed VSGs needs to be studied. Furthermore, the effect of each configura-

tion on the system performance versus total cost may be a considerable research point.

- The configuration implemented in this dissertation has the components of the HESS connected to the dc-link through separate dc-dc converter. A future study may compare between this configuration versus having each ESS connected the ac bus through its own inverter.
- This dissertation implements a single VSG system connected to a stiff power grid. Future research has to be conducted determining how to manage the operation and coordination of multi-VSGs in a system. Determining the damping and inertia time constants for each virtual generator to achieve the best system performance may be a point to be explored in the future. VSGs may be owned by many entities, but connected to a microgrid or distribution owned by one organization. Determination of who provides grid services in case of emergency disturbance events to stabilize the system.
- The work was done in this dissertation doesn't make cost estimation for the system. Future work could perform cost analysis for each part of the system. Moreover, use calculations for the impact of selection damping and inertia time constants on the cost of the system would be a valuable for industry especially how this affects the tariff for each unit and setting a rate of return of investment should be described in future work.
- The switching action of the power electronic switches in VSG converters produce a high frequency and non-linear harmonics. Research on the impact of VSG control versus grid following control on harmonic performance should be explored.
- Future work should be done to study the performance of the VSG controller

based grid forming converter when islanding from a more realistic power grid. Also, system performance and frequency profile should be studied when the energy storage system run out of reserve such that its performance should be controlled to match the control and protection system requirements.

- The standards and indices related to the overall performance and operation of the microgrids should be developed. Part of the development should include VSGs. Moreover, most researchers have evaluated VSG based on a comparison between VSG and SG. An independent evaluation and understanding of what VSGs can do beyond conventional SGs should be performed, and interface standards should be developed for integrating VSGs from different vendors with different controls.

Bibliography

- [1] Chao Long and Luis F Ochoa. “Voltage control of PV-rich LV networks: OLTC-fitted transformer and capacitor banks”. In: *IEEE Transactions on Power Systems* 31.5 (2015), pp. 4016–4025.
- [2] Ibtihal Abdelmotteleb, Tomás Gómez, and Jose Pablo Chaves-Avila. “Benefits of PV inverter volt-var control on distribution network operation”. In: *2017 IEEE Manchester PowerTech*. IEEE. 2017, pp. 1–6.
- [3] Rajiv K Varma et al. “Grid Support Benefits of Solar PV Systems as STATCOM (PV-STATCOM) Through Converter Control: Grid Integration Challenges of Solar PV Power Systems”. In: *IEEE Electrification Magazine* 9.2 (2021), pp. 50–61.
- [4] Foad H Gandoman et al. “Distributed FACTS stabilization scheme for efficient utilization of distributed wind energy systems”. In: *International Transactions on Electrical Energy Systems* 27.11 (2017), E2391.
- [5] Hyeon-Jin Moon et al. “Decentralised active power control strategy for real-time power balance in an isolated microgrid with an energy storage system and diesel generators”. In: *Energies* 12.3 (2019), p. 511.
- [6] Marito Ferreira et al. “Normal Operation Characteristics of 30 kW Scale CVCF Inverter-Based Micro-grid System”. In: *Journal of the Korea Academia-Industrial cooperation Society* 21.6 (2020), pp. 662–671.
- [7] Yuko Hirase et al. “Analysis of resonance in microgrids and effects of system frequency stabilization using a virtual synchronous generator”. In: *IEEE Journal of Emerging and Selected Topics in Power Electronics* 4.4 (2016), pp. 1287–1298.

- [8] Yousef Khayat et al. “On the secondary control architectures of AC microgrids: An overview”. In: *IEEE Transactions on Power Electronics* 35.6 (2019), pp. 6482–6500. ISSN: 0885-8993.
- [9] Ebrahim Rokrok, Miadreza Shafie-Khah, and João PS Catalão. “Review of primary voltage and frequency control methods for inverter-based islanded microgrids with distributed generation”. In: *Renewable and Sustainable Energy Reviews* 82 (2018), pp. 3225–3235.
- [10] Sayli E Mhankale and AR Thorat. “Droop Control Strategies of DC Microgrid: A Review”. In: *2018 International Conference on Current Trends towards Converging Technologies (ICCTCT)*. IEEE, pp. 372–376. ISBN: 1538637022.
- [11] Amira Mohammed et al. “Ac microgrid control and management strategies: Evaluation and review”. In: *IEEE Power Electronics Magazine* 6.2 (2019), pp. 18–31. ISSN: 2329-9207.
- [12] Josep M Guerrero et al. “Hierarchical control of droop-controlled AC and DC microgrids. A general approach toward standardization”. In: *IEEE Transactions on industrial electronics* 58.1 (2010), pp. 158–172. ISSN: 0278-0046.
- [13] Hans-Peter Beck and Ralf Hesse. “Virtual synchronous machine”. In: *2007 9th International Conference on Electrical Power Quality and Utilisation*. IEEE. 2007, pp. 1–6.
- [14] Salvatore D’Arco and Jon Are Suul. “Virtual synchronous machines Classification of implementations and analysis of equivalence to droop controllers for microgrids”. In: *2013 IEEE Grenoble Conference*. IEEE. 2013, pp. 1–7.
- [15] Toshinobu Shintai, Yuushi Miura, and Toshifumi Ise. “Reactive power control for load sharing with virtual synchronous generator control”. In: *Proceedings*

- of *The 7th International Power Electronics and Motion Control Conference*. Vol. 2. IEEE. 2012, pp. 846–853.
- [16] Qing-Chang Zhong and George Weiss. “Synchronverters: Inverters that mimic synchronous generators”. In: *IEEE transactions on industrial electronics* 58.4 (2010), pp. 1259–1267.
- [17] Kah Yung Yap, Charles R Sarimuthu, and Joanne Mun-Yee Lim. “Virtual inertia-based inverters for mitigating frequency instability in grid-connected renewable energy system: A review”. In: *Applied Sciences* 9.24 (2019), p. 5300.
- [18] Yuko Hirase et al. “A grid-connected inverter with virtual synchronous generator model of algebraic type”. In: *Electrical Engineering in Japan* 184.4 (2013), pp. 10–21.
- [19] K Sakimoto, Y Miura, and T Ise. “Stabilization of a power system with a distributed generator by a virtual synchronous generator function”. In: *8th International Conference on Power Electronics-ECCE Asia*. IEEE. 2011, pp. 1498–1505.
- [20] Hassan Bevrani, Toshifumi Ise, and Yushi Miura. “Virtual synchronous generators: A survey and new perspectives”. In: *International Journal of Electrical Power & Energy Systems* 54 (2014), pp. 244–254.
- [21] Khalid Mehmood Cheema. “A comprehensive review of virtual synchronous generator”. In: *International Journal of Electrical Power & Energy Systems* 120 (2020), p. 106006.
- [22] Deeksha Singh and K Seethalekshmi. “A review on various virtual inertia techniques for distributed generation”. In: *2020 International Conference on Electrical and Electronics Engineering (ICE3)*. IEEE. 2020, pp. 631–638.

- [23] KC Divya and Jacob Østergaard. “Battery energy storage technology for power systems: An overview”. In: *Electric power systems research* 79.4 (2009), pp. 511–520.
- [24] Salman Hajiaghahi, Ahmad Salemnia, and Mohsen Hamzeh. “Hybrid energy storage system for microgrids applications: A review”. In: *Journal of Energy Storage* 21 (2019), pp. 543–570.
- [25] Aitor Etxeberria et al. “Hybrid energy storage systems for renewable energy sources integration in microgrids: A review”. In: *2010 Conference Proceedings IPEC*. IEEE, pp. 532–537. ISBN: 1424473985.
- [26] Thongchart Kerdphol et al. “Applying virtual inertia control topology to SMES system for frequency stability improvement of low-inertia microgrids driven by high renewables”. In: *Energies* 12.20 (2019), p. 3902.
- [27] Jackson John Justo et al. “AC-microgrids versus DC-microgrids with distributed energy resources: A review”. In: *Renewable and sustainable energy reviews* 24 (2013), pp. 387–405. ISSN: 1364-0321.
- [28] GAO Fei et al. “Primary and secondary control in DC microgrids: a review”. In: *Journal of Modern Power Systems and Clean Energy* 7.2 (2019), pp. 227–242. ISSN: 2196-5625.
- [29] Christoph Kammer and Alireza Karimi. “Decentralized and distributed transient control for microgrids”. In: *IEEE Transactions on Control Systems Technology* 27.1 (2017), pp. 311–322. ISSN: 1063-6536.
- [30] M Fadaeenejad et al. “Assessment of hybrid renewable power sources for rural electrification in Malaysia”. In: *Renewable and Sustainable Energy Reviews* 30 (2014), pp. 299–305. ISSN: 1364-0321.

- [31] Douglas F Barnes. “Effective solutions for rural electrification in developing countries: Lessons from successful programs”. In: *Current Opinion in Environmental Sustainability* 3.4 (2011), pp. 260–264. ISSN: 1877-3435.
- [32] Nikos Hatziargyriou et al. “Microgrids”. In: *IEEE power and energy magazine* 5.4 (2007), pp. 78–94. ISSN: 1540-7977.
- [33] Ritu Raj Shrivastwa et al. “Understanding microgrids and their future trends”. In: *2019 IEEE International Conference on Industrial Technology (ICIT)*. IEEE. 2019, pp. 1723–1728.
- [34] Lubna Mariam, Malabika Basu, and Michael F Conlon. “A review of existing microgrid architectures”. In: *Journal of engineering* 2013 (2013). ISSN: 2314-4904.
- [35] Makbul AM Ramli et al. “A review on maximum power point tracking for photovoltaic systems with and without shading conditions”. In: *Renewable and Sustainable Energy Reviews* 67 (2017), pp. 144–159. ISSN: 1364-0321.
- [36] Deepak Verma et al. “Maximum power point tracking (MPPT) techniques: Recapitulation in solar photovoltaic systems”. In: *Renewable and Sustainable Energy Reviews* 54 (2016), pp. 1018–1034. ISSN: 1364-0321.
- [37] Nabil Karami, Nazih Moubayed, and Rachid Outbib. “General review and classification of different MPPT Techniques”. In: *Renewable and Sustainable Energy Reviews* 68 (2017), pp. 1–18. ISSN: 1364-0321.
- [38] Adel Mellit et al. “Artificial intelligence techniques for sizing photovoltaic systems: A review”. In: *Renewable and Sustainable Energy Reviews* 13.2 (2009), pp. 406–419. ISSN: 1364-0321.

- [39] Hongxing Yang, Lin Lu, and Wei Zhou. “A novel optimization sizing model for hybrid solar-wind power generation system”. In: *Solar energy* 81.1 (2007), pp. 76–84. ISSN: 0038-092X.
- [40] Inaki Arrambide, Itziar Zubia, and Ander Madariaga. “Critical review of offshore wind turbine energy production and site potential assessment”. In: *Electric Power Systems Research* 167 (2019), pp. 39–47. ISSN: 0378-7796.
- [41] Mahmoud M Badreldien et al. “Modeling, Analysis and Control of Doubly Fed Induction Generators for Wind Turbines”. In: *The International Conference on Electrical Engineering*. Vol. 9. Military Technical College, pp. 1–17. ISBN: 2636-4433.
- [42] Muhd Khudri Johari, Muhammad Azim A Jalil, and Mohammad Faizal Mohd Shariff. “Comparison of horizontal axis wind turbine (HAWT) and vertical axis wind turbine (VAWT)”. In: *International Journal of Engineering and Technology* 7.4.13 (2018), pp. 74–80.
- [43] Ion Paraschivoiu, Sami Ammar, and Farooq Saeed. “VAWT versus HAWT: a comparative performance study of 2–6 MW rated capacity turbines”. In: *Transactions of the Canadian Society for Mechanical Engineering* 42.4 (2018), pp. 393–403. ISSN: 0315-8977.
- [44] Hale Cetinay, Fernando A Kuipers, and A Nezih Guven. “Optimal siting and sizing of wind farms”. In: *Renewable Energy* 101 (2017), pp. 51–58. ISSN: 0960-1481.
- [45] Ali M Abdelsalam and MA El-Shorbagy. “Optimization of wind turbines siting in a wind farm using genetic algorithm based local search”. In: *Renewable Energy* 123 (2018), pp. 748–755. ISSN: 0960-1481.

- [46] Alireza Emami and Pirooz Noghreh. “New approach on optimization in placement of wind turbines within wind farm by genetic algorithms”. In: *Renewable Energy* 35.7 (2010), pp. 1559–1564. ISSN: 0960-1481.
- [47] Sajid Hussain Qazi and Mohd Wazir Mustafa. “Review on active filters and its performance with grid connected fixed and variable speed wind turbine generator”. In: *Renewable and Sustainable Energy Reviews* 57 (2016), pp. 420–438. ISSN: 1364-0321.
- [48] Darya Khan Bhutto et al. “Wind energy conversion systems (WECS) generators: A review”. In: *2019 2nd International Conference on Computing, Mathematics and Engineering Technologies (iCoMET)*. IEEE, pp. 1–6. ISBN: 153869509X.
- [49] Dipesh Kumar and Kalyan Chatterjee. “A review of conventional and advanced MPPT algorithms for wind energy systems”. In: *Renewable and sustainable energy reviews* 55 (2016), pp. 957–970. ISSN: 1364-0321.
- [50] Shilpa Mishra, Sandeep Shukla, and Nitin Verma. “Comprehensive review on maximum power point tracking techniques: wind energy”. In: *2015 Communication, Control and Intelligent Systems (CCIS)*. IEEE, pp. 464–469. ISBN: 1467375411.
- [51] LJR Nunes, TP Causer, and D Ciolkosz. “Biomass for energy: A review on supply chain management models”. In: *Renewable and Sustainable Energy Reviews* 120 (2020), p. 109658. ISSN: 1364-0321.
- [52] Maninder Kaur et al. “Techno-economic analysis of photovoltaic-biomass-based microgrid system for reliable rural electrification”. In: *International Transactions on Electrical Energy Systems* 30.5 (2020), e12347. ISSN: 2050-7038.

- [53] Marte Lotveit et al. “A study of biomass in a hybrid stand-alone microgrid for the rural village of Wawashang, Nicaragua”. In: *2014 Ninth International Conference on Ecological Vehicles and Renewable Energies (EVER)*. IEEE, pp. 1–7. ISBN: 1479937878.
- [54] M Marsadek and V Kumaran. “Feasibility study for grid-connected biomass and biogas”. In: *2015 IEEE 15th International Conference on Environment and Electrical Engineering (EEEIC)*. IEEE, pp. 1806–1810. ISBN: 1479979937.
- [55] Raul Banos et al. “Optimization methods applied to renewable and sustainable energy: A review”. In: *Renewable and sustainable energy reviews* 15.4 (2011), pp. 1753–1766. ISSN: 1364-0321.
- [56] Jirasak Ji et al. “Biomass power generation supply chain planning”. In: *2017 IEEE International Conference on Smart Grid and Smart Cities (ICSGSC)*. IEEE, pp. 115–119. ISBN: 153860504X.
- [57] Changquan Xiong et al. “Expansion Planning of Wind-Biomass Co-Generation System in the Micro-Grid”. In: *2011 Asia-Pacific Power and Energy Engineering Conference*. IEEE, pp. 1–4. ISBN: 142446255X.
- [58] Ferdous Ahmed et al. “Alternative energy resources in Bangladesh and future prospect”. In: *Renewable and sustainable energy reviews* 25 (2013), pp. 698–707. ISSN: 1364-0321.
- [59] Ibrahim Yuksel, Hasan Arman, and Ibrahim Halil Demirel. “As a clean, sustainable and renewable energy-hydropower in Turkey”. In: *MATEC Web of Conferences*. Vol. 120. EDP Sciences, p. 08004. ISBN: 2261-236X.
- [60] Pablo Carpejani et al. “Affordable and Clean Energy: A Study on the Advantages and Disadvantages of the Main Modalities”. In: *International Business, Trade and Institutional Sustainability*. Springer, 2020, pp. 615–627.

- [61] M Boninella, L Solheim, and M Molinas. “Hybrid micro grid feasibility study for the wawashang complex in Nicaragua”. In: *2013 4th International Youth Conference on Energy (IYCE)*. IEEE, pp. 1–8. ISBN: 1467355569.
- [62] R Sebastian and J Quesada. “Modeling and simulation of an isolated wind Hydro Power System”. In: *IECON 2016-42nd Annual Conference of the IEEE Industrial Electronics Society*. IEEE, pp. 4169–4174. ISBN: 1509034749.
- [63] Seema Kewat, Bhim Singh, and Ikhlaq Hussain. “Power management in PV-battery-hydro based standalone microgrid”. In: *IET Renewable Power Generation* 12.4 (2017), pp. 391–398. ISSN: 1752-1424.
- [64] I Tamrakar et al. “Voltage and frequency control of parallel operated synchronous generator and induction generator with STATCOM in micro hydro scheme”. In: *IET Generation, Transmission & Distribution* 1.5 (2007), pp. 743–750. ISSN: 1751-8695.
- [65] Umesh C Rathore and Sanjeev Singh. “Power quality control of SEIG based isolated pico hydro power plant feeding non-linear load”. In: *2014 IEEE 6th India International Conference on Power Electronics (IICPE)*. IEEE, pp. 1–5. ISBN: 1479960462.
- [66] CF Nicy and R Punitharaji. “Isolated wind-hydro hybrid system using permanent magnet synchronous generator and battery storage with fuzzy logic controller”. In: *2014 International Conference on Green Computing Communication and Electrical Engineering (ICGCCCE)*. IEEE, pp. 1–6. ISBN: 1479949825.
- [67] Duclair Tiomo and Rene Wamkeue. “Dynamic Modeling and Analysis of a Micro-Hydro Power Plant for Microgrid Applications”. In: *2019 IEEE Canadian Conference of Electrical and Computer Engineering (CCECE)*. IEEE, pp. 1–6. ISBN: 1728103193.

- [68] Veselin Skendzic and Gary W Scheer. “Performance of Redundant Ethernet Networks for Electric Substation Instrumentation and Control”. In: *SEL Journal of Reliable Power* 3 (August 2012).
- [69] A Mallikarjuna et al. “Optimal sizing of Wind/Solar/Hydro in an isolated power system using SMFFT based Cuckoo Search Algorithm”. In: *2016 IEEE 6th International Conference on Power Systems (ICPS)*. IEEE, pp. 1–6. ISBN: 150900128X.
- [70] Huiting Xu et al. “Optimal sizing of small hydro power plants in consideration of voltage control”. In: *2015 International Symposium on Smart Electric Distribution Systems and Technologies (EDST)*. IEEE, pp. 165–172. ISBN: 1479977365.
- [71] Indrajit Das and Claudio A Canizares. “Renewable Energy Integration in Diesel-Based Microgrids at the Canadian Arctic”. In: *Proceedings of the IEEE* 107.9 (2019), pp. 1838–1856. ISSN: 0018-9219.
- [72] B Blackstone et al. “Development of an Outdoor Diesel Generator-PV Microgrid for Education and Research”. In: *2018 IEEE Power and Energy Society General Meeting (PESGM)*. IEEE, pp. 1–5. ISBN: 1538677032.
- [73] Mahsa Zarrini Farahmand, Mohammad Esmail Nazari, and Sadegh Shamlou. “Optimal sizing of an autonomous hybrid PV-wind system considering battery and diesel generator”. In: *2017 Iranian Conference on Electrical Engineering (ICEE)*. IEEE, pp. 1048–1053. ISBN: 1509059636.
- [74] Wenxia Pan, Wenzhong Gao, and Eduard Muljadi. “The dynamic performance and effect of hybrid renewable power system with diesel/wind/PV/battery”. In: *2009 International Conference on Sustainable Power Generation and Supply*. IEEE, pp. 1–5. ISBN: 1424449340.

- [75] Chem Nayar, Markson Tang, and Wuthipong Suponthana. “Wind/PV/diesel micro grid system implemented in remote islands in the Republic of Maldives”. In: *2008 IEEE international conference on sustainable energy technologies*. IEEE, pp. 1076–1080. ISBN: 1424418879.
- [76] AA Khodadoost Arani, GB Gharehpetian, and M Abedi. “Review on energy storage systems control methods in microgrids”. In: *International journal of electrical power & energy systems* 107 (2019), pp. 745–757. ISSN: 0142-0615.
- [77] Ahmet Cansiz et al. “Integration of a SMES–battery-based hybrid energy storage system into microgrids”. In: *Journal of Superconductivity and Novel Magnetism* 31.5 (2018), pp. 1449–1457. ISSN: 1557-1939.
- [78] Mohammad Faisal et al. “Review of energy storage system technologies in microgrid applications: Issues and challenges”. In: *IEEE Access* 6 (2018), pp. 35143–35164. ISSN: 2169-3536.
- [79] A Hina Fathima and K Palanisamy. “Optimization in microgrids with hybrid energy systems: A review”. In: *Renewable and Sustainable Energy Reviews* 45 (2015), pp. 431–446. ISSN: 1364-0321.
- [80] Ahmed A Kamel et al. “Energy management of a DC microgrid composed of photovoltaic/fuel cell/battery/supercapacitor systems”. In: *Batteries* 5.3 (2019), p. 63.
- [81] Hengzhao Yang. “A review of supercapacitor-based energy storage systems for microgrid applications”. In: *2018 IEEE Power & Energy Society General Meeting (PESGM)*. IEEE, pp. 1–5. ISBN: 1538677032.
- [82] Mohammed Yekini Suberu, Mohd Wazir Mustafa, and Nouruddeen Bashir. “Energy storage systems for renewable energy power sector integration and

- mitigation of intermittency”. In: *Renewable and Sustainable Energy Reviews* 35 (2014), pp. 499–514. ISSN: 1364-0321.
- [83] Konstantinos Oikonomou, Vijay Satyal, and Masood Parvania. “Energy storage in the western interconnection: Current adoption, trends and modeling challenges”. In: *2017 IEEE Power & Energy Society General Meeting*. IEEE, pp. 1–5. ISBN: 1538622122.
- [84] Xingguo Tan, Qingmin Li, and Hui Wang. “Advances and trends of energy storage technology in microgrid”. In: *International Journal of Electrical Power & Energy Systems* 44.1 (2013), pp. 179–191. ISSN: 0142-0615.
- [85] Francisco Diaz-Gonzalez et al. “A review of energy storage technologies for wind power applications”. In: *Renewable and sustainable energy reviews* 16.4 (2012), pp. 2154–2171. ISSN: 1364-0321.
- [86] Furquan Nadeem et al. “Review of Smart and Innovative Energy Storage Systems”. In: *2019 International Conference on Vision Towards Emerging Trends in Communication and Networking (ViTECoN)*. IEEE, pp. 1–6. ISBN: 1538693534.
- [87] Heri Suyanto and Rina Irawati. “Study trends and challenges of the development of microgrids”. In: *2017 6th IEEE International Conference on Advanced Logistics and Transport (ICALT)*. IEEE, pp. 160–164. ISBN: 1538616238.
- [88] Matthieu Dubarry et al. “Battery energy storage system modeling: A combined comprehensive approach”. In: *Journal of Energy Storage* 21 (2019), pp. 172–185. ISSN: 2352-152X.
- [89] Chao Zhang et al. “Energy storage system: Current studies on batteries and power condition system”. In: *Renewable and Sustainable Energy Reviews* 82 (2018), pp. 3091–3106. ISSN: 1364-0321.

- [90] Jaephil Cho, Sookyung Jeong, and Youngsik Kim. “Commercial and research battery technologies for electrical energy storage applications”. In: *Progress in Energy and Combustion Science* 48 (2015), pp. 84–101. ISSN: 0360-1285.
- [91] Chun Sing Lai et al. “A comprehensive review on large-scale photovoltaic system with applications of electrical energy storage”. In: *Renewable and Sustainable Energy Reviews* 78 (2017), pp. 439–451. ISSN: 1364-0321.
- [92] Amjad Anvari-Moghaddam et al. “Optimal Design and Operation Management of Battery-Based Energy Storage Systems (BESS) in Microgrids”. In: *Advancements in Energy Storage Technol.* IntechOpen, 2018, pp. 145–165.
- [93] Muhammad Sufyan et al. “Sizing and applications of battery energy storage technologies in smart grid system: A review”. In: *Journal of Renewable and Sustainable Energy* 11.1 (2019), p. 014105. ISSN: 1941-7012.
- [94] F Perez et al. “The use of Supercapacitors in Microgrids as Hybrid Energy Storage Systems-a review”. In: *2019 IEEE PES Innovative Smart Grid Technologies Conference-Latin America (ISGT Latin America)*. IEEE, pp. 1–6. ISBN: 1538695677.
- [95] Roja Peri, D Venkatramanan, and Vinod John. “Optimal Design of Energy Storage System using Ultracapacitors for Contingency Power Applications”. In: *2020 IEEE International Conference on Power Electronics, Smart Grid and Renewable Energy (PESGRE2020)*. IEEE, pp. 1–6. ISBN: 1728142512.
- [96] Dilini Jayananda, Nihal Kularatna, and D Alistair Steyn-Ross. “Design approach for Supercapacitor Assisted LED lighting (SCALED) technique for DC-microgrids”. In: *2018 IEEE International Conference on Industrial Electronics for Sustainable Energy Systems (IESES)*. IEEE, pp. 27–31. ISBN: 1509049746.

- [97] Jayathu Fernando and Nihal Kularatna. “Supercapacitors for distributed energy storage in DC microgrids and loads”. In: *2015 IEEE First International Conference on DC Microgrids (ICDCM)*. IEEE, pp. 339–342. ISBN: 147999880X.
- [98] Wu Bingbing, Yin Zhongdong, and Xiao Xiangning. “Super-capacitors energy storage system applied in the microgrid”. In: *2010 5th IEEE Conference on Industrial Electronics and Applications*. IEEE, pp. 1002–1005. ISBN: 1424450454.
- [99] Prashant Kumar Soori, Subhas Chandra Shetty, and Sibi Chacko. “Application of super capacitor energy storage in microgrid system”. In: *2011 IEEE GCC Conference and Exhibition (GCC)*. IEEE, pp. 581–584. ISBN: 1612841198.
- [100] Anupama Singh, PB Karandikar, and NR Kulkarni. “Feasibility of energy storage systems in different applications for sustainable energy”. In: *2016 International Conference on Emerging Technological Trends (ICETT)*. IEEE, pp. 1–6. ISBN: 1509037519.
- [101] Sohrab Mirsaeidi, Xinzhou Dong, and Dalila Mat Said. “Towards hybrid AC/DC microgrids: critical analysis and classification of protection strategies”. In: *Renewable and Sustainable Energy Reviews* 90 (2018), pp. 97–103. ISSN: 1364-0321.
- [102] Hossein Lotfi and Amin Khodaei. “AC versus DC microgrid planning”. In: *IEEE Transactions on Smart Grid* 8.1 (2015), pp. 296–304. ISSN: 1949-3053.
- [103] Estefania Planas et al. “AC and DC technology in microgrids: A review”. In: *Renewable and Sustainable Energy Reviews* 43 (2015), pp. 726–749. ISSN: 1364-0321.
- [104] Jian-ping Zhu, Jian-ping Zhou, and Hao Zhang. “Research progress of AC, DC and their hybrid micro-grids”. In: *2014 IEEE International Conference on System Science and Engineering (ICSSE)*. IEEE, pp. 158–161. ISBN: 1479943673.

- [105] Eklas Hossain et al. “Microgrid testbeds around the world: State of art”. In: *Energy Conversion and Management* 86 (2014), pp. 132–153. ISSN: 0196-8904.
- [106] Siavash Beheshtaein et al. “Protection of AC and DC microgrids: challenges, solutions and future trends”. In: *IECON 2015-41st Annual Conference of the IEEE Electronics Society*. IEEE, pp. 005253–005260. ISBN: 1479917621.
- [107] Lie Xu and Dong Chen. “Control and operation of a DC microgrid with variable generation and energy storage”. In: *IEEE transactions on power delivery* 26.4 (2011), pp. 2513–2522. ISSN: 0885-8977.
- [108] Luis Eduardo Zubieta. “Are microgrids the future of energy?: DC microgrids from concept to demonstration to deployment”. In: *IEEE Electrification Magazine* 4.2 (2016), pp. 37–44. ISSN: 2325-5897.
- [109] Farzam Nejabatkhah and Yun Wei Li. “Overview of power management strategies of hybrid AC/DC microgrid”. In: *IEEE Transactions on Power Electronics* 30.12 (2014), pp. 7072–7089. ISSN: 0885-8993.
- [110] Mousa Marzband et al. “A real-time evaluation of energy management systems for smart hybrid home Microgrids”. In: *Electric Power Systems Research* 143 (2017), pp. 624–633. ISSN: 0378-7796.
- [111] Ajay Gupta, Suryanarayana Doolla, and Kishore Chatterjee. “Hybrid AC–DC microgrid: systematic evaluation of control strategies”. In: *IEEE Transactions on Smart Grid* 9.4 (2018), pp. 3830–3843. ISSN: 1949-3053.
- [112] Yanghong Xia et al. “Power management for a hybrid AC/DC microgrid with multiple subgrids”. In: *IEEE Transactions on Power Electronics* 33.4 (2017), pp. 3520–3533. ISSN: 0885-8993.

- [113] Pratiksha Gupta and MA Ansari. “Analysis and Control of AC and Hybrid AC-DC Microgrid: A Review”. In: *2019 2nd International Conference on Power Energy, Environment and Intelligent Control (PEEIC)*. IEEE, pp. 281–286. ISBN: 1728117933.
- [114] Ali Bidram and Ali Davoudi. “Hierarchical structure of microgrids control system”. In: *IEEE Transactions on Smart Grid* 3.4 (2012), pp. 1963–1976. ISSN: 1949-3053.
- [115] Shiwei Xia et al. “A fully distributed hierarchical control framework for coordinated operation of DERs in active distribution power networks”. In: *IEEE Transactions on Power Systems* 34.6 (2018), pp. 5184–5197. ISSN: 0885-8950.
- [116] Zhikang Shuai et al. “Hierarchical structure and bus voltage control of DC microgrid”. In: *Renewable and Sustainable Energy Reviews* 82 (2018), pp. 3670–3682. ISSN: 1364-0321.
- [117] Zheyuan Cheng, Jie Duan, and Mo-Yuen Chow. “To centralize or to distribute: That is the question: A comparison of advanced microgrid management systems”. In: *IEEE Industrial Electronics Magazine* 12.1 (2018), pp. 6–24. ISSN: 1932-4529.
- [118] Ebrahim Rokrok, Miadreza Shafie-Khah, and Joao PS Catalao. “Review of primary voltage and frequency control methods for inverter-based islanded microgrids with distributed generation”. In: *Renewable and Sustainable Energy Reviews* 82 (2018), pp. 3225–3235. ISSN: 1364-0321.
- [119] Ibrahim Alsaleh and Lingling Fan. “DQ-axis current-based droop controller”. In: *2017 North American Power Symposium (NAPS)*. IEEE, pp. 1–6. ISBN: 1538626993.

- [120] VM Najda and Surya Susan Alex. “Performance Analysis of Synchronous Reference Frame Based Controller for Grid Interconnected Microgrid”. In: *2014 Fourth International Conference on Advances in Computing and Communications*. IEEE, pp. 255–259. ISBN: 1479943630.
- [121] RJ Lee, P Pillay, and RG Harley. “D, Q reference frames for the simulation of induction motors”. In: *Electric power systems research* 8.1 (1984), pp. 15–26. ISSN: 0378-7796.
- [122] Qing-Chang Zhong and George Weiss. “Synchronverters: Inverters That Mimic Synchronous Generators”. In: *IEEE Transaction on industrial electronics* VOL. 58.NO. 4, April 2011 (2011).
- [123] S Monesha, S Ganesh Kumar, and M Rivera. “Microgrid energy management and control: Technical review”. In: *2016 IEEE International Conference on Automatica (ICA-ACCA)*. IEEE, pp. 1–7. ISBN: 1509011471.
- [124] Mohammad Jafar Hadidian Moghaddam, Mehdi Bigdeli, and Mohammad Reza Miveh. “A Review of the Primary-Control Techniques for the Islanded Microgrids”. In: *Elektrotehniski Vestnik* 82.4 (2015), p. 169. ISSN: 0013-5852.
- [125] N Sharmila, KR Nataraj, and KR Rekha. “An Overview on Design and Control Schemes of Microgrid”. In: *2019 Global Conference for Advancement in Technology (GCAT)*. IEEE, pp. 1–4. ISBN: 1728136946.
- [126] D Semenov et al. “Recent development in AC microgrid control: A survey”. In: *2017 Australasian Universities Power Engineering Conference (AUPEC)*. IEEE, pp. 1–6. ISBN: 1538626470.
- [127] Tong Qian et al. “Event-triggered updating method in centralized and distributed secondary controls for islanded microgrid restoration”. In: *IEEE Transactions on Smart Grid* 11.2 (2019), pp. 1387–1395. ISSN: 1949-3053.

- [128] Guannan Lou et al. “Distributed MPC-based secondary voltage control scheme for autonomous droop-controlled microgrids”. In: *IEEE transactions on sustainable energy* 8.2 (2016), pp. 792–804. ISSN: 1949-3029.
- [129] Fen Tang et al. “Distributed active synchronization strategy for microgrid seamless reconnection to the grid under unbalance and harmonic distortion”. In: *IEEE Transactions on Smart Grid* 6.6 (2015), pp. 2757–2769. ISSN: 1949-3053.
- [130] Alshammari Fahad and El-Refaie Ayman. “Functions of Microgrid Hierarchical Control Structure”. In: *2019 IEEE 7th International Conference on Smart Energy Grid Engineering (SEGE)*. IEEE, pp. 17–25. ISBN: 1728124409.
- [131] Quan Zhou et al. “Two-stage load shedding for secondary control in hierarchical operation of islanded microgrids”. In: *IEEE Transactions on Smart Grid* 10.3 (2018), pp. 3103–3111. ISSN: 1949-3053.
- [132] Sertac Bayhan. “Predictive load shedding method for islanded AC microgrid with limited generation sources”. In: *2018 IEEE 12th International Conference on Compatibility, Power Electronics and Power Engineering (CPE-POWERENG 2018)*. IEEE, pp. 1–5. ISBN: 1538625083.
- [133] Zhenyu Tan et al. “Microgrid black-start after natural disaster with load restoration using spanning tree search”. In: *2016 IEEE Power and Energy Society General Meeting (PESGM)*. IEEE, pp. 1–5. ISBN: 1509041680.
- [134] Dianbiao Dong et al. “Investigation of a microgrid with vanadium redox flow battery storages as a black start source for power system restoration”. In: *2014 9th IEEE Conference on Industrial Electronics and Applications*. IEEE, pp. 140–145. ISBN: 1479943150.

- [135] Edoardo De Din et al. “An Emergency Energy Management System for Microgrid Restoration After Blackout”. In: *2018 International Conference on Smart Energy Systems and Technologies (SEST)*. IEEE, pp. 1–6. ISBN: 1538653265.
- [136] Agustin Aguera-Perez et al. “Weather forecasts for microgrid energy management: Review, discussion and recommendations”. In: *Applied Energy* 228 (2018), pp. 265–278. ISSN: 0306-2619.
- [137] Shreya Dutta et al. “Load and renewable energy forecasting for a microgrid using persistence technique”. In: *Energy Procedia* 143 (2017), pp. 617–622. ISSN: 1876-6102.
- [138] Asma Alfergani et al. “Control strategies in AC microgrid: A brief review”. In: *2018 9th International Renewable Energy Congress (IREC)*. IEEE, pp. 1–6. ISBN: 1538609983.
- [139] Daniel E Olivares et al. “Trends in microgrid control”. In: *IEEE Transactions on smart grid* 5.4 (2014), pp. 1905–1919. ISSN: 1949-3053.
- [140] Yong Zhang and Wei Wei. “Decentralised coordination control strategy of the PV generator, storage battery and hydrogen production unit in islanded AC microgrid”. In: *IET Renewable Power Generation* 14.6 (2020), pp. 1053–1062. ISSN: 1752-1424.
- [141] Mahmuda Begum, Li Li, and Jianguo Zhu. “Distributed control techniques for autonomous AC microgrid-A brief review”. In: *2017 IEEE Region 10 Technology Conference (R10-HTC)*. IEEE, pp. 357–362. ISBN: 1538621754.
- [142] Kyriaki E Antoniadou-Plytaria et al. “Distributed and decentralized voltage control of smart distribution networks: Models, methods, and future research”. In: *IEEE Transactions on smart grid* 8.6 (2017), pp. 2999–3008. ISSN: 1949-3053.

- [143] ML Di Silvestre et al. “Robust multi-objective optimal dispatch of distributed energy resources in micro-grids”. In: *2011 IEEE Trondheim PowerTech*. IEEE, pp. 1–5. ISBN: 1424484189.
- [144] Jacqueline Llanos Proano et al. “Economic dispatch for optimal management of isolated microgrids”. In: *2016 IEEE 36th Central American and Panama Convention (CONCAPAN XXXVI)*. IEEE, pp. 1–6. ISBN: 1467395781.
- [145] Jing Wang et al. “Design of a generalized control algorithm for parallel inverters for smooth microgrid transition operation”. In: *IEEE Transactions on Industrial Electronics* 62.8 (2015), pp. 4900–4914. ISSN: 0278-0046.
- [146] Payam Teimourzadeh Baboli et al. “Energy management and operation modelling of hybrid AC-DC microgrid”. In: *IET Generation, Transmission & Distribution* 8.10 (2014), pp. 1700–1711. ISSN: 1751-8695.
- [147] Karel De Brabandere et al. “Control of microgrids”. In: *2007 IEEE Power Engineering Society General Meeting*. IEEE, pp. 1–7. ISBN: 142441296X.
- [148] Lexuan Meng et al. “Agent-based distributed unbalance compensation for optimal power quality in islanded microgrids”. In: *2014 IEEE 23rd International Symposium on Industrial Electronics (ISIE)*. IEEE, pp. 2535–2540. ISBN: 1479923990.
- [149] Aleksandra Krkoleva Mateska et al. “Controllable load operation in microgrids using control scheme based on gossip algorithm”. In: *Applied Energy* 210 (2018), pp. 1336–1346. ISSN: 0306-2619.
- [150] Eneko Unamuno and Jon Andoni Barrena. “Hybrid ac/dc microgrids—Part II: Review and classification of control strategies”. In: *Renewable and Sustainable Energy Reviews* 52 (2015), pp. 1123–1134. ISSN: 1364-0321.

- [151] Palak P Parikh, Mitalkumar G Kanabar, and Tarlochan S Sidhu. “Opportunities and challenges of wireless communication technologies for smart grid applications”. In: *IEEE PES General Meeting*. IEEE, pp. 1–7. ISBN: 1424465516.
- [152] PD Chavan and Rajan J Devi. “Survey of communication system for DG’s and microgrid in electrical power grid”. In: *Int. Res. J. Eng. Technol* 3.7 (2016), pp. 1155–1164.
- [153] Ioan Serban et al. “Communication Requirements in Microgrids: A Practical Survey”. In: *IEEE Access* 8 (2020), pp. 47694–47712. ISSN: 2169-3536.
- [154] Ian F Akyildiz and Xudong Wang. “A survey on wireless mesh networks”. In: *IEEE Communications magazine* 43.9 (2005), S23–S30. ISSN: 0163-6804.
- [155] Hak-Man Kim and Yujin Lim. “A communication framework in multiagent system for islanded microgrid”. In: *International Journal of Distributed Sensor Networks* 8.3 (2012), p. 382316. ISSN: 1550-1477.
- [156] Mohamed Riduan Abid et al. “A wireless mesh architecture for the advanced metering infrastructure in residential smart grids”. In: *2013 IEEE Green Technologies Conference (GreenTech)*. IEEE, pp. 338–344. ISBN: 0769549667.
- [157] Ahmad Almadhor. “Intelligent Control Mechanism in Smart Microgrid with Mesh Networks and Virtual Power Plant Model”. In: *2019 16th IEEE Annual Consumer Communications & Networking Conference (CCNC)*. IEEE, pp. 1–6. ISBN: 1538655535.
- [158] Richard Peter Lewis, Petar Igić, and Zhongfu Zhou. “Assessment of communication methods for smart electricity metering in the UK”. In: *2009 IEEE PES/IAS Conference on Sustainable Alternative Energy (SAE)*. IEEE, pp. 1–4. ISBN: 1424444306.

- [159] Jingcheng Gao et al. “A survey of communication/networking in smart grids”. In: *Future generation computer systems* 28.2 (2012), pp. 391–404. ISSN: 0167-739X.
- [160] N Shaukat et al. “A survey on consumers empowerment, communication technologies, and renewable generation penetration within Smart Grid”. In: *Renewable and Sustainable Energy Reviews* 81 (2018), pp. 1453–1475. ISSN: 1364-0321.
- [161] Mini S Thomas and John Douglas McDonald. *Power system SCADA and smart grids*. CRC press, 2017. ISBN: 1482226758.
- [162] Donald Chang, Joe Lee, and Tzer-Hso Lin. “Smart satellites in smart grids”. In: *2014 IEEE International Conference on Smart Grid Communications (Smart-GridComm)*. IEEE. 2014, pp. 487–492.
- [163] Vehbi C Gungor and Frank C Lambert. “A survey on communication networks for electric system automation”. In: *Computer Networks* 50.7 (2006), pp. 877–897. ISSN: 1389-1286.
- [164] Yurong Hu and Victor OK Li. “Satellite-based internet: a tutorial”. In: *IEEE Communications Magazine* 39.3 (2001), pp. 154–162. ISSN: 0163-6804.
- [165] Xi Fang et al. “Smart grid-The new and improved power grid: A survey”. In: *IEEE communications surveys & tutorials* 14.4 (2011), pp. 944–980. ISSN: 1553-877X.
- [166] Salman Safdar et al. “A survey on communication infrastructure for micro-grids”. In: *2013 9th international wireless communications and mobile computing conference (IWCMC)*. IEEE, pp. 545–550. ISBN: 1467324809.

- [167] LK Siow et al. “Wi-Fi based server in microgrid energy management system”. In: *TENCON 2009-2009 IEEE Region 10 Conference*. IEEE, pp. 1–5. ISBN: 1424445469.
- [168] Ming-Yue Zhai. “Transmission characteristics of low-voltage distribution networks in China under the smart grids environment”. In: *IEEE Transactions on Power Delivery* 26.1 (2010), pp. 173–180. ISSN: 0885-8977.
- [169] Niovi Pavlidou et al. “Power line communications: state of the art and future trends”. In: *IEEE Communications magazine* 41.4 (2003), pp. 34–40. ISSN: 0163-6804.
- [170] M McGranaghan and F Goodman. “Technical and system requirements for advanced distribution automation”. In: *18th International Conference and Exhibition on Electricity Distribution*. Vol. 5. IET, p. 93.
- [171] Ken-ichi Kitayama and Nikolaos-Pantaleimon Diamantopoulos. “Few-mode optical fibers: Original motivation and recent progress”. In: *IEEE Communications Magazine* 55.8 (2017), pp. 163–169. ISSN: 0163-6804.
- [172] Niv Goldenberg and Avishai Wool. “Accurate modeling of Modbus/TCP for intrusion detection in SCADA systems”. In: *International Journal of Critical Infrastructure Protection* 6.2 (2013), pp. 63–75. ISSN: 1874-5482.
- [173] Abedalsalam Bani-Ahmed et al. “Microgrid communications: State of the art and future trends”. In: *2014 International Conference on Renewable Energy Research and Application (ICRERA)*. IEEE, pp. 780–785. ISBN: 1479937959.
- [174] Silvia Marzal et al. “Current challenges and future trends in the field of communication architectures for microgrids”. In: *Renewable and Sustainable Energy Reviews* 82 (2018), pp. 3610–3622. ISSN: 1364-0321.

- [175] Mojtaba Moghimi et al. “Communication architecture and data acquisition for experimental Microgrid installations”. In: *2015 IEEE PES Asia-Pacific Power and Energy Engineering Conference (APPEEC)*. IEEE, pp. 1–5. ISBN: 1467381322.
- [176] George Thomas. “Introduction to modbus serial and modbus TCP”. In: *Contemporary Control Systems 9.4* (2008).
- [177] George Thomas. “Introduction to the modbus protocol”. In: *The extension a technical supplement to control network* (2008), p. 9.
- [178] Albert Ruiz-Alvarez et al. “Operation of a utility connected microgrid using an IEC 61850-based multi-level management system”. In: *IEEE Transactions on Smart Grid 3.2* (2012), pp. 858–865. ISSN: 1949-3053.
- [179] Fanny Clavel et al. “Integration of a new standard: A network simulator of IEC 61850 architectures for electrical substations”. In: *IEEE Industry Applications Magazine 21.1* (2014), pp. 41–48. ISSN: 1077-2618.
- [180] Raimarius Delgado, Byoung Wook Choi, and Hwachang Song. “Application of EtherCAT in Microgrid Communication Network: A Case Study”. In: *2018 International Conference on Platform Technology and Service (PlatCon)*. IEEE, pp. 1–6. ISBN: 1538647109.
- [181] Valeriy Vyatkin et al. “Towards intelligent smart grid devices with IEC 61850 interoperability and IEC 61499 open control architecture”. In: *IEEE PES T&D 2010*. IEEE, pp. 1–8. ISBN: 1424465486.
- [182] Vinicius de o Villalta et al. “Benchmarking of Performance Requirements between IEC 61850 and DNP3 in Real-Time Monitoring Context”. In: *2018 IEEE International Conference on Environment and Electrical Engineering and 2018*

- IEEE Industrial and Commercial Power Systems Europe (IEEEIC/I&CPS Europe)*. IEEE, pp. 1–4. ISBN: 1538651866.
- [183] Babak Tavassoli, Alireza Fereidunian, and Savaghebi Mehdi. “Communication system effects on the secondary control performance in microgrids”. In: *IET Renewable Power Generation* (2020). ISSN: 1752-1424.
- [184] Raphael Amoah, Seyit Camtepe, and Ernest Foo. “Securing DNP3 broadcast communications in SCADA systems”. In: *IEEE Transactions on Industrial Informatics* 12.4 (2016), pp. 1474–1485. ISSN: 1551-3203.
- [185] Raphael Amoah, Seyit Camtepe, and Ernest Foo. “Formal modelling and analysis of DNP3 secure authentication”. In: *Journal of Network and Computer Applications* 59 (2016), pp. 345–360. ISSN: 1084-8045.
- [186] Dong-joo Kang and Rosslin John Robles. “Compartmentalization of protocols in SCADA communication”. In: *International Journal of Advanced Science and Technology* 8 (2009), pp. 27–36.
- [187] Samer Jaloudi et al. “Communication strategy for grid control and monitoring of distributed generators in Smart Grids using IEC and IEEE standards”. In: *2011 2nd IEEE PES International Conference and Exhibition on Innovative Smart Grid Technologies*. IEEE, pp. 1–6. ISBN: 1457714213.
- [188] S Jaloudi et al. “General communication strategy for control of distributed energy resources in smart grids via international standards”. In: *2011 16th International Conference on Intelligent System Applications to Power Systems*. IEEE, pp. 1–6. ISBN: 1457708094.
- [189] Vladan Skoko, Branislav Atlagic, and Nemanja Isakov. “Comparative realization of IEC 60870-5 industrial protocol standards”. In: *2014 22nd Telecommunications Forum Telfor (TELFOR)*. IEEE, pp. 987–990. ISBN: 1479961914.

- [190] Mitalkumar G Kanabar, Ilia Voloh, and David McGinn. “Reviewing smart grid standards for protection, control, and monitoring applications”. In: *2012 IEEE PES Innovative Smart Grid Technologies (ISGT)*. IEEE, pp. 1–8. ISBN: 1457721597.
- [191] Yi Yang et al. “Intrusion detection system for IEC 60870-5-104 based SCADA networks”. In: *2013 IEEE power & energy society general meeting*. IEEE, pp. 1–5. ISBN: 1479913030.
- [192] Set Muller, M Deicke, and Rik W De Doncker. “Doubly fed induction generator systems for wind turbines”. In: *IEEE Industry applications magazine* 8.3 (2002), pp. 26–33.
- [193] Farzaneh Mirzapour et al. “A new prediction model of battery and wind-solar output in hybrid power system”. In: *Journal of Ambient Intelligence and Humanized Computing* 10.1 (2019), pp. 77–87.
- [194] Ghulam Sarwar Kaloi, Jie Wang, and Mazhar Hussain Baloch. “Dynamic modeling and control of DFIG for wind energy conversion system using feedback linearization”. In: *Journal of Electrical Engineering and Technology* 11.5 (2016), pp. 1137–1146.
- [195] Hicham Lhachimi, Youssef El Kouari, and Yassine Sayouti. “Control strategy of DFIG for wind energy system in the grid connected mode”. In: *2016 International Renewable and Sustainable Energy Conference (IRSEC)*. IEEE. 2016, pp. 515–520.
- [196] Wei Qiao. “Dynamic modeling and control of doubly fed induction generators driven by wind turbines”. In: *2009 IEEE/PES Power Systems Conference and Exposition*. IEEE. 2009, pp. 1–8.

- [197] Vijay Chand Ganti et al. “DFIG-based wind power conversion with grid power leveling for reduced gusts”. In: *IEEE Transactions on Sustainable Energy* 3.1 (2011), pp. 12–20.
- [198] T Lei, M Ozakturk, and M Barnes. “Modelling and analysis of DFIG wind turbine system in PSCAD/EMTDC”. In: *6th IET International Conference on Power Electronics, Machines and Drives (PEMD 2012)*. IET. 2012, pp. 1–6.
- [199] Choroq Zadelkhair El Archi et al. “Real Power Control: MPPT and Pitch Control in a DFIG Based Wind Turbine”. In: *2020 3rd International Conference on Advanced Communication Technologies and Networking (CommNet)*. IEEE. 2020, pp. 1–6.
- [200] Peng Guo. “Research of a new MPPT strategy based on gray wind speed prediction”. In: *2009 Second International Symposium on Knowledge Acquisition and Modeling*. Vol. 3. IEEE. 2009, pp. 120–123.
- [201] Ahmed G Abo-Khalil and Dong-Choon Lee. “MPPT control of wind generation systems based on estimated wind speed using SVR”. In: *IEEE transactions on Industrial Electronics* 55.3 (2008), pp. 1489–1490.
- [202] Seyed Behzad Naderi, Michael Negnevitsky, and Kashem M Muttaqi. “A modified DC chopper for limiting the fault current and controlling the DC-link voltage to enhance fault ride-through capability of doubly-fed induction-generator-based wind turbine”. In: *IEEE Transactions on Industry Applications* 55.2 (2018), pp. 2021–2032.
- [203] Olivier Tremblay, Louis-A Dessaint, and Abdel Dekkiche. “A generic battery model for the dynamic simulation of hybrid electric vehicles”. In: *2007 IEEE Vehicle Power and Propulsion Conference*. Ieee. 2007, pp. 284–289.

- [204] Mohamed Abuagreb, Hussain Beleed, and Brian K Johnson. “Energy Management of a Battery Combined with PV Generation”. In: *2019 North American Power Symposium (NAPS)*. IEEE. 2019, pp. 1–6.
- [205] Mohamed Abuagreb, Mohammed Allehyani, and Brian K Johnson. “Design and test of a combined PV and battery system under multiple load and irradiation conditions”. In: *2019 IEEE Power & Energy Society Innovative Smart Grid Technologies Conference (ISGT)*. IEEE. 2019, pp. 1–5.
- [206] Mohamed M Abuagreb. “Allowing Distributed Generation to Improve Power System Stability by Applying Virtual Synchronous Machine Approach”. PhD thesis. University of Idaho, 2020.
- [207] Amirnaser Yazdani and Reza Iravani. *Voltage-sourced converters in power systems: modeling, control, and applications*. John Wiley & Sons, 2010. ISBN: 0470551569.
- [208] Rahul Rawat, SC Kaushik, and Ravita Lamba. “A review on modeling, design methodology and size optimization of photovoltaic based water pumping, standalone and grid connected system”. In: *Renewable and Sustainable Energy Reviews* 57 (2016), pp. 1506–1519.
- [209] Souleman Njoya Motapon et al. “A generic electrothermal li-ion battery model for rapid evaluation of cell temperature temporal evolution”. In: *IEEE transactions on industrial electronics* 64.2 (2016), pp. 998–1008.
- [210] Davinder Singh and Harjinder Singh. “Technical Survey and review on MPPT techniques to attain Maximum Power of Photovoltaic system”. In: *2019 5th International Conference on Signal Processing, Computing and Control (IS-PCC)*. IEEE. 2019, pp. 265–268.

- [211] Ashraf Khalil, Khalid Ateea Alfaitori, and Ali Asheibi. “Modeling and control of PV/Wind Microgrid”. In: *2016 7th international renewable energy congress (IREC)*. IEEE, pp. 1–6. ISBN: 1467397687.
- [212] Muamer M Shebani, Tariq Iqbal, and John E Quaicoe. “Comparing bisection numerical algorithm with fractional short circuit current and open circuit voltage methods for MPPT photovoltaic systems”. In: *2016 IEEE Electrical Power and Energy Conference (EPEC)*. IEEE. 2016, pp. 1–5.
- [213] S Sumathi, L Ashok Kumar, and P Surekha. *Solar PV and wind energy conversion systems: an introduction to theory, modeling with MATLAB/SIMULINK, and the role of soft computing techniques*. Vol. 1. Springer, 2015.
- [214] Elsayed Saad, Yasser Elkotesy, and Usama AbouZayed. “Modelling and analysis of grid-connected solar-PV system through current-mode controlled VSC”. In: *E3S Web of Conferences*. Vol. 167. EDP Sciences. 2020, p. 05005.
- [215] Ramdan BA Koad, Ahmed Faheem Zobaa, and Adel El-Shahat. “A novel MPPT algorithm based on particle swarm optimization for photovoltaic systems”. In: *IEEE Transactions on Sustainable Energy* 8.2 (2016), pp. 468–476.
- [216] Reza Iskharisma Yuwanda, Eka Prasetyono, and Rachma Prilian Eviningsih. “Constant Power Generation Using Modified MPPT P & O to Overcome Overvoltage on Solar Power Plants”. In: *2020 International Seminar on Intelligent Technology and Its Applications (ISITIA)*. IEEE. 2020, pp. 392–397.
- [217] Siddhartha A Singh et al. “Modeling, design, control, and implementation of a modified Z-source integrated PV/grid/EV DC charger/inverter”. In: *IEEE Transactions on Industrial Electronics* 65.6 (2017), pp. 5213–5220.

- [218] Pedram Jahangiri and Dionysios C Aliprantis. “Distributed Volt/VAr control by PV inverters”. In: *IEEE Transactions on Power Systems* 28.3 (2013), pp. 3429–3439.
- [219] Ankit Singhal et al. “Real-time local volt/var control under external disturbances with high PV penetration”. In: *IEEE Transactions on Smart Grid* 10.4 (2018), pp. 3849–3859.
- [220] Monsef Tahir et al. “A review of Volt/Var control techniques in passive and active power distribution networks”. In: *2016 IEEE Smart Energy Grid Engineering (SEGE)*. IEEE. 2016, pp. 57–63.
- [221] Amit Kumer Podder, Naruttam Kumar Roy, and Hemanshu Roy Pota. “MPPT methods for solar PV systems: a critical review based on tracking nature”. In: *IET Renewable Power Generation* 13.10 (2019), pp. 1615–1632.
- [222] Pawan Kumar Pathak, Anil Kumar Yadav, and PA Alvi. “Advanced solar MPPT techniques under uniform and non-uniform irradiance: A comprehensive review”. In: *Journal of Solar Energy Engineering* 142.4 (2020).
- [223] Tawfik Radjai et al. “Implementation of a modified incremental conductance MPPT algorithm with direct control based on a fuzzy duty cycle change estimator using dSPACE”. In: *Solar Energy* 110 (2014), pp. 325–337.
- [224] R Palanisamy et al. “Simulation of various DC-DC converters for photovoltaic system”. In: *International Journal of Electrical and Computer Engineering* 9.2 (2019), p. 917.
- [225] Mohamadsaleh Jafari, Temitayo O Olowu, and Arif I Sarwat. “Optimal smart inverters volt-var curve selection with a multi-objective volt-var optimization using evolutionary algorithm approach”. In: *2018 North American Power Symposium (NAPS)*. IEEE. 2018, pp. 1–6.

- [226] Joan Rocabert et al. “Control of power converters in AC microgrids”. In: *IEEE transactions on power electronics* 27.11 (2012), pp. 4734–4749.
- [227] Mohamed Abuagreb, Mohammed F Allehyani, and Brian K Johnson. “Overview of Virtual Synchronous Generators: Existing Projects, Challenges, and Future Trends”. In: *Electronics* 11.18 (2022), p. 2843.
- [228] Mahmoud M Badreldien et al. “Modeling and Control of Solar PV System Combined with Battery Energy Storage System”. In: *2021 IEEE Electrical Power and Energy Conference (EPEC)*. IEEE. 2021, pp. 373–377.
- [229] Elsayed Saad et al. “Implementation of a Modified MPPT Strategy for Solar-PV Arrays Connected to Harmonic-Polluted Grids Under Partial Shading Conditions”. In: *2021 International Telecommunications Conference (ITC-Egypt)*. IEEE. 2021, pp. 1–4.
- [230] Omar Beltran et al. “Inertia estimation of wind power plants based on the swing equation and phasor measurement units”. In: *Applied Sciences* 8.12 (2018), p. 2413.
- [231] BL Agrawal et al. “Damping representation for power system stability studies”. In: *IEEE Transactions on Power Systems* 14.1 (1999), pp. 151–157.
- [232] Mohammad Dreidy, H Mokhlis, and Saad Mekhilef. “Inertia response and frequency control techniques for renewable energy sources: A review”. In: *Renewable and sustainable energy reviews* 69 (2017), pp. 144–155.
- [233] Yong Chen et al. “Improving the grid power quality using virtual synchronous machines”. In: *2011 international conference on power engineering, energy and electrical drives*. IEEE. 2011, pp. 1–6.

- [234] Jia Liu, Yushi Miura, and Toshifumi Ise. “Comparison of dynamic characteristics between virtual synchronous generator and droop control in inverter-based distributed generators”. In: *IEEE Transactions on Power Electronics* 31.5 (2015), pp. 3600–3611.
- [235] Mohamed Abuagreb, Babatunde Ajao, and Brian K Johnson. “Implementation of Emulated Inertia using PV Generation with Energy Storage to Improve Integrated Grid Response”. In: *2020 IEEE Texas Power and Energy Conference (TPEC)*. IEEE. 2020, pp. 1–6.
- [236] Mohamed Abuagreb, Ahmed Abuhussein, et al. “Sizing of Energy Storage System for Virtual Inertia Emulation”. In: *2022 IEEE 31st International Symposium on Industrial Electronics (ISIE)*. IEEE. 2022, pp. 374–379.
- [237] Mohamed Abuagreb, Mohammed Allehyani, and Brian K Johnson. “Design and test of a combined pv and battery system under multiple load and irradiation conditions”. In: *2019 IEEE Power & Energy Society Innovative Smart Grid Technologies Conference (ISGT)*. IEEE. 2019, pp. 1–5.
- [238] MS Haritha and Divya S Nair. “Review on virtual synchronous generator (VSG) for enhancing performance of microgrid”. In: *2018 International Conference on Power, Signals, Control and Computation (EPSCICON)*. IEEE. 2018, pp. 1–5.
- [239] Mohd Hanif Othman et al. “Progress in control and coordination of energy storage system-based VSG: A review”. In: *IET Renewable Power Generation* 14.2 (2020), pp. 177–187.
- [240] Jianwei Li et al. “Design and test of a new droop control algorithm for a SMES/battery hybrid energy storage system”. In: *Energy* 118 (2017), pp. 1110–1122.

- [241] Mohammad Faisal et al. “Review of energy storage system technologies in microgrid applications: Issues and challenges”. In: *IEEE Access* 6 (2018), pp. 35143–35164.
- [242] Aitor Etxeberria et al. “Hybrid energy storage systems for renewable energy sources integration in microgrids: A review”. In: *2010 Conference Proceedings IPEC*. IEEE. 2010, pp. 532–537.
- [243] Mahmoud M Mohamed et al. “Optimal virtual synchronous generator control of battery/supercapacitor hybrid energy storage system for frequency response enhancement of photovoltaic/diesel microgrid”. In: *Journal of Energy Storage* 51 (2022), p. 104317.
- [244] MS Haritha and Divya S Nair. “Review on virtual synchronous generator (VSG) for enhancing performance of microgrid”. In: *2018 International Conference on Power, Signals, Control and Computation (EPSCICON)*. IEEE. 2018, pp. 1–5.
- [245] Elsayed Saad et al. “Implementation of a Modified MPPT Strategy for Solar-PV Arrays Connected to Harmonic-Polluted Grids Under Partial Shading Conditions”. In: *2021 International Telecommunications Conference (ITC-Egypt)*. IEEE. 2021, pp. 1–4.
- [246] Elsayed Saad, Yasser Elkoteshy, and Usama AbouZayed. “Modelling and analysis of grid-connected solar-PV system through current-mode controlled VSC”. In: *E3S Web of Conferences*. Vol. 167. EDP Sciences. 2020, p. 05005.
- [247] Mahmoud M Badreldien and Brian K Johnson. “Virtual Synchronous Generator Controller for Solar Photovoltaic System”. In: *2021 IEEE Electrical Power and Energy Conference (EPEC)*. IEEE. 2021, pp. 480–485.

- [248] Sabine Piller, Marion Perrin, and Andreas Jossen. “Methods for state-of-charge determination and their applications”. In: *Journal of power sources* 96.1 (2001), pp. 113–120.
- [249] Mustafa Farhadi and Osama Mohammed. “Energy storage technologies for high-power applications”. In: *IEEE Transactions on Industry Applications* 52.3 (2015), pp. 1953–1961.
- [250] Attapong Mamen and Uthane Supatti. “A survey of hybrid energy storage systems applied for intermittent renewable energy systems”. In: *2017 14th International Conference on Electrical Engineering/Electronics, Computer, Telecommunications and Information Technology (ECTI-CON)*. IEEE. 2017, pp. 729–732.
- [251] Peng Zhang, Jun Liang, and Feng Zhang. “An overview of different approaches for battery lifetime prediction”. In: *IOP Conference Series: Materials Science and Engineering*. Vol. 199. 1. IOP Publishing. 2017, p. 012134.
- [252] PE Will Ayers. “Comparative Payback of Lithium-Ion Batteries for Pacific NW Ferries”. In: *Elliott Bay Design Group* (2016).
- [253] Witold Marańda. “Capacity degradation of lead-acid batteries under variable-depth cycling operation in photovoltaic system”. In: *2015 22nd International Conference Mixed Design of Integrated Circuits & Systems (MIXDES)*. IEEE. 2015, pp. 552–555.
- [254] Salvatore D’Arco and Jon Are Suul. “Equivalence of virtual synchronous machines and frequency-droops for converter-based microgrids”. In: *IEEE Transactions on Smart Grid* 5.1 (2013), pp. 394–395.
- [255] Chang-Hua Zhang et al. “An improved synchronverter model and its dynamic behaviour comparison with synchronous generator”. In: (2013).

- [256] Junru Chen, Muyang Liu, and Terence O'Donnell. "Replacement of synchronous generator by virtual synchronous generator in the conventional power system". In: *2019 IEEE Power & Energy Society General Meeting (PESGM)*. IEEE, 2019, pp. 1–5.

Appendix A: IEEE Formal Reuse License

As list in the dissertation, some of the content of these chapters are currently copyrighted by the Institute of Electrical and Electronics Engineers Inc. (IEEE). Permission for reproduction of the complete article for use in this dissertation was given by (IEEE). Figures A.1, A.2, A.3, and A.4 are proofs of this permission. Some of the content of these reproduced articles was changed to suit the format of dissertation. Also, in the dissertation chapters, there may be some figures and paragraphs not present in the publications. This is due to work performed after paper submission and publication, and also not included due to conference proceeding length limitations.



Requesting
permission
to reuse
content from
an IEEE
publication

Modeling and Control of Wind Energy Conversion System with Battery Energy Storage System

Conference Proceedings: 2021 North American Power Symposium (NAPS)
 Author: [::Mahmoud::] [::M::], [::Badreldien::]; Yacine Chakhchoukh; Brian K Johnson
 Publisher: IEEE
 Date: 14-16 Nov. 2021

Copyright © 2021, IEEE

Thesis / Dissertation Reuse

The IEEE does not require individuals working on a thesis to obtain a formal reuse license, however, you may print out this statement to be used as a permission grant:

Requirements to be followed when using any portion (e.g., figure, graph, table, or textual material) of an IEEE copyrighted paper in a thesis:

- 1) In the case of textual material (e.g., using short quotes or referring to the work within these papers) users must give full credit to the original source (author, paper, publication) followed by the IEEE copyright line © 2011 IEEE.
- 2) In the case of illustrations or tabular material, we require that the copyright line © [Year of original publication] IEEE appear prominently with each reprinted figure and/or table.
- 3) If a substantial portion of the original paper is to be used, and if you are not the senior author, also obtain the senior author's approval.

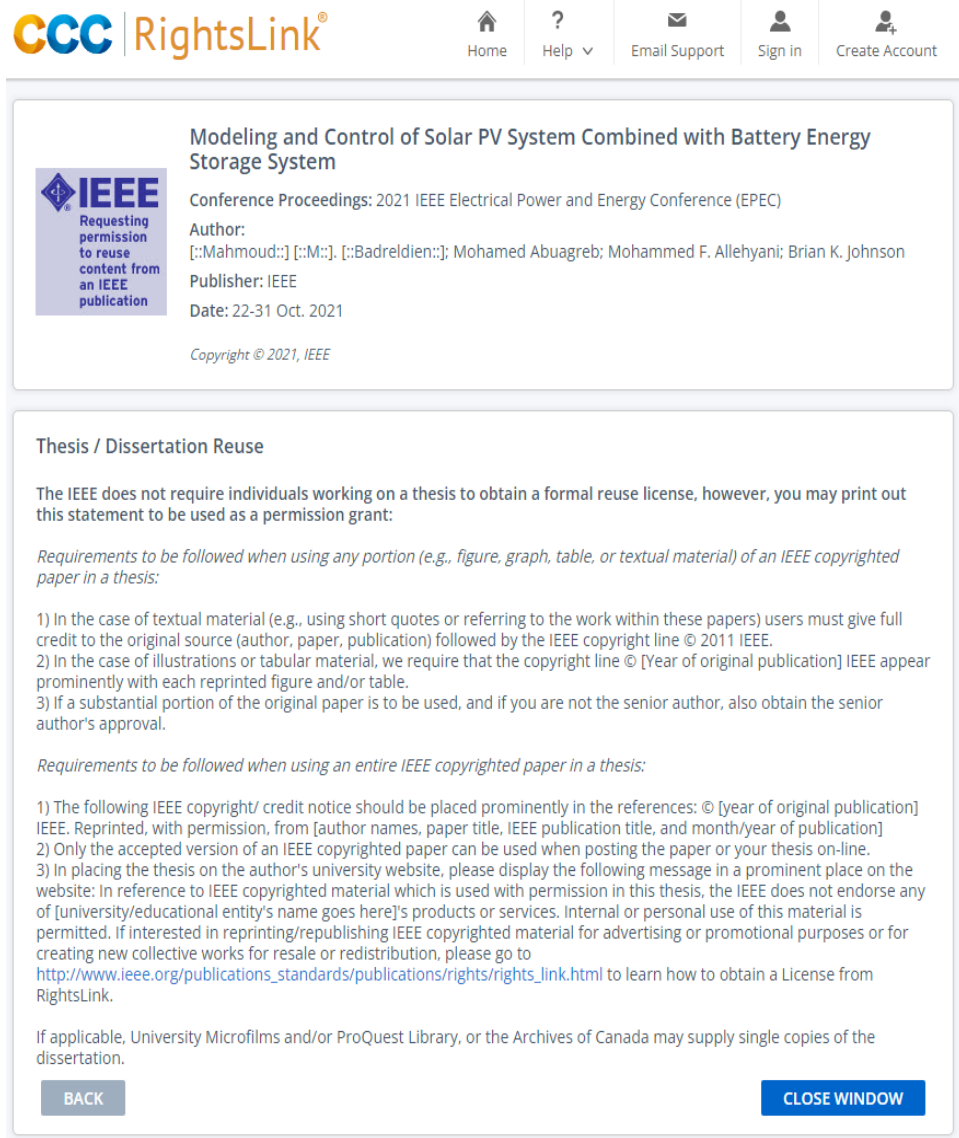
Requirements to be followed when using an entire IEEE copyrighted paper in a thesis:

- 1) The following IEEE copyright/ credit notice should be placed prominently in the references: © [year of original publication] IEEE. Reprinted, with permission, from [author names, paper title, IEEE publication title, and month/year of publication]
- 2) Only the accepted version of an IEEE copyrighted paper can be used when posting the paper or your thesis on-line.
- 3) In placing the thesis on the author's university website, please display the following message in a prominent place on the website: In reference to IEEE copyrighted material which is used with permission in this thesis, the IEEE does not endorse any of [university/educational entity's name goes here]'s products or services. Internal or personal use of this material is permitted. If interested in reprinting/republishing IEEE copyrighted material for advertising or promotional purposes or for creating new collective works for resale or redistribution, please go to http://www.ieee.org/publications_standards/publications/rights/rights_link.html to learn how to obtain a License from RightsLink.

If applicable, University Microfilms and/or ProQuest Library, or the Archives of Canada may supply single copies of the dissertation.

BACK
CLOSE WINDOW

Figure A.1: Permission from IEEE to reuse an article as Chapter 3 of this dissertation



The screenshot shows the IEEE RightsLink interface. At the top, there is a navigation bar with the IEEE RightsLink logo and icons for Home, Help, Email Support, Sign in, and Create Account. The main content area is divided into two sections. The first section, titled "Modeling and Control of Solar PV System Combined with Battery Energy Storage System", provides details about the publication: Conference Proceedings: 2021 IEEE Electrical Power and Energy Conference (EPEC), Author: [::Mahmoud::] [::M::], [::Badreldien::]; Mohamed Abuagreb; Mohammed F. Allehyani; Brian K. Johnson, Publisher: IEEE, and Date: 22-31 Oct. 2021. A "Requesting permission to reuse content from an IEEE publication" icon is visible. The second section, titled "Thesis / Dissertation Reuse", contains a statement from IEEE regarding reuse permissions, followed by requirements for using portions or entire papers in a thesis. At the bottom, there are "BACK" and "CLOSE WINDOW" buttons.

IEEE
Requesting permission to reuse content from an IEEE publication

Modeling and Control of Solar PV System Combined with Battery Energy Storage System
Conference Proceedings: 2021 IEEE Electrical Power and Energy Conference (EPEC)
Author: [::Mahmoud::] [::M::], [::Badreldien::]; Mohamed Abuagreb; Mohammed F. Allehyani; Brian K. Johnson
Publisher: IEEE
Date: 22-31 Oct. 2021
Copyright © 2021, IEEE

Thesis / Dissertation Reuse

The IEEE does not require individuals working on a thesis to obtain a formal reuse license, however, you may print out this statement to be used as a permission grant:

Requirements to be followed when using any portion (e.g., figure, graph, table, or textual material) of an IEEE copyrighted paper in a thesis:

- 1) In the case of textual material (e.g., using short quotes or referring to the work within these papers) users must give full credit to the original source (author, paper, publication) followed by the IEEE copyright line © 2011 IEEE.
- 2) In the case of illustrations or tabular material, we require that the copyright line © [Year of original publication] IEEE appear prominently with each reprinted figure and/or table.
- 3) If a substantial portion of the original paper is to be used, and if you are not the senior author, also obtain the senior author's approval.

Requirements to be followed when using an entire IEEE copyrighted paper in a thesis:

- 1) The following IEEE copyright/ credit notice should be placed prominently in the references: © [year of original publication] IEEE. Reprinted, with permission, from [author names, paper title, IEEE publication title, and month/year of publication]
- 2) Only the accepted version of an IEEE copyrighted paper can be used when posting the paper or your thesis on-line.
- 3) In placing the thesis on the author's university website, please display the following message in a prominent place on the website: In reference to IEEE copyrighted material which is used with permission in this thesis, the IEEE does not endorse any of [university/educational entity's name goes here]'s products or services. Internal or personal use of this material is permitted. If interested in reprinting/republishing IEEE copyrighted material for advertising or promotional purposes or for creating new collective works for resale or redistribution, please go to http://www.ieee.org/publications_standards/publications/rights/rights_link.html to learn how to obtain a License from RightsLink.

If applicable, University Microfilms and/or ProQuest Library, or the Archives of Canada may supply single copies of the dissertation.

BACK **CLOSE WINDOW**

Figure A.2: Permission from IEEE to reuse an article as Chapter 4 of this dissertation

CCC | RightsLink®

Home ? Help v Email Support Sign in Create Account

Volt/Var Control of Solar Photovoltaic System

Conference Proceedings: 2021 North American Power Symposium (NAPS)

Author: [::Mahmoud::] [::M::], [::Badreldien::]; Brian K Johnson

Publisher: IEEE

Date: 14-16 Nov. 2021

Copyright © 2021, IEEE

Thesis / Dissertation Reuse

The IEEE does not require individuals working on a thesis to obtain a formal reuse license, however, you may print out this statement to be used as a permission grant:

Requirements to be followed when using any portion (e.g., figure, graph, table, or textual material) of an IEEE copyrighted paper in a thesis:

- 1) In the case of textual material (e.g., using short quotes or referring to the work within these papers) users must give full credit to the original source (author, paper, publication) followed by the IEEE copyright line © 2011 IEEE.
- 2) In the case of illustrations or tabular material, we require that the copyright line © [Year of original publication] IEEE appear prominently with each reprinted figure and/or table.
- 3) If a substantial portion of the original paper is to be used, and if you are not the senior author, also obtain the senior author's approval.

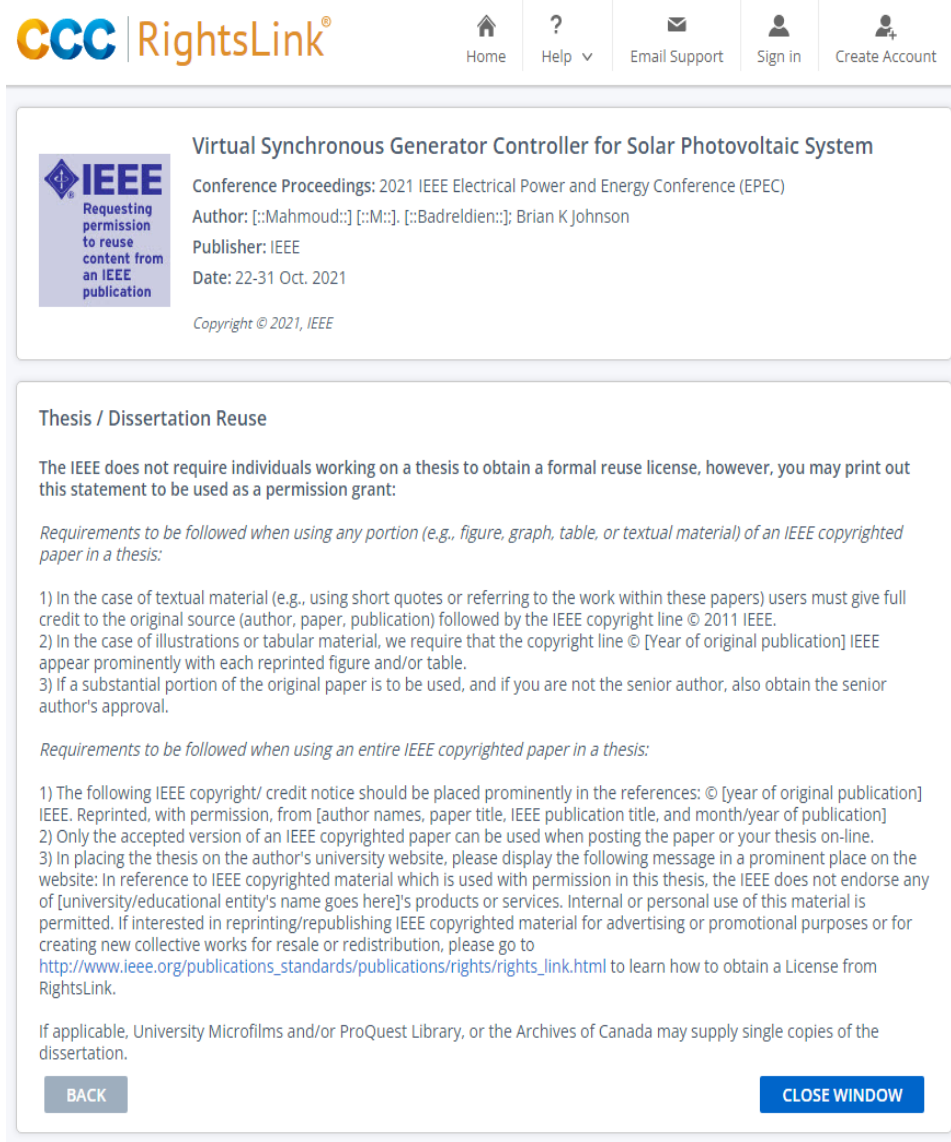
Requirements to be followed when using an entire IEEE copyrighted paper in a thesis:

- 1) The following IEEE copyright/ credit notice should be placed prominently in the references: © [year of original publication] IEEE. Reprinted, with permission, from [author names, paper title, IEEE publication title, and month/year of publication]
- 2) Only the accepted version of an IEEE copyrighted paper can be used when posting the paper or your thesis on-line.
- 3) In placing the thesis on the author's university website, please display the following message in a prominent place on the website: In reference to IEEE copyrighted material which is used with permission in this thesis, the IEEE does not endorse any of [university/educational entity's name goes here]'s products or services. Internal or personal use of this material is permitted. If interested in reprinting/republishing IEEE copyrighted material for advertising or promotional purposes or for creating new collective works for resale or redistribution, please go to http://www.ieee.org/publications_standards/publications/rights/rights_link.html to learn how to obtain a License from RightsLink.

If applicable, University Microfilms and/or ProQuest Library, or the Archives of Canada may supply single copies of the dissertation.

BACK CLOSE WINDOW

Figure A.3: Permission from IEEE to reuse an article as Chapter 4 of this dissertation



The screenshot shows the IEEE RightsLink interface. At the top, there is a navigation bar with the IEEE logo and 'RightsLink' text, and icons for Home, Help, Email Support, Sign in, and Create Account. Below this, a card displays the title 'Virtual Synchronous Generator Controller for Solar Photovoltaic System' and its details: 'Conference Proceedings: 2021 IEEE Electrical Power and Energy Conference (EPEC)', 'Author: [::Mahmoud::] [::M::], [::Badreldien::]; Brian K Johnson', 'Publisher: IEEE', and 'Date: 22-31 Oct. 2021'. A copyright notice 'Copyright © 2021, IEEE' is also present. Below the card, a section titled 'Thesis / Dissertation Reuse' provides instructions. It states that the IEEE does not require a formal reuse license but offers a permission grant. It lists requirements for using portions of the paper (e.g., figure, graph, table, or textual material) and for using the entire paper in a thesis. The requirements for using a portion include giving full credit to the original source, using the IEEE copyright line, and obtaining the senior author's approval. The requirements for using the entire paper include placing a copyright/credit notice in the references, using only the accepted version, and displaying a message on the author's university website. A 'CLOSE WINDOW' button is visible at the bottom right of the interface.

Virtual Synchronous Generator Controller for Solar Photovoltaic System

Conference Proceedings: 2021 IEEE Electrical Power and Energy Conference (EPEC)

Author: [::Mahmoud::] [::M::], [::Badreldien::]; Brian K Johnson

Publisher: IEEE

Date: 22-31 Oct. 2021

Copyright © 2021, IEEE

Thesis / Dissertation Reuse

The IEEE does not require individuals working on a thesis to obtain a formal reuse license, however, you may print out this statement to be used as a permission grant:

Requirements to be followed when using any portion (e.g., figure, graph, table, or textual material) of an IEEE copyrighted paper in a thesis:

- 1) In the case of textual material (e.g., using short quotes or referring to the work within these papers) users must give full credit to the original source (author, paper, publication) followed by the IEEE copyright line © 2011 IEEE.
- 2) In the case of illustrations or tabular material, we require that the copyright line © [Year of original publication] IEEE appear prominently with each reprinted figure and/or table.
- 3) If a substantial portion of the original paper is to be used, and if you are not the senior author, also obtain the senior author's approval.

Requirements to be followed when using an entire IEEE copyrighted paper in a thesis:

- 1) The following IEEE copyright/ credit notice should be placed prominently in the references: © [year of original publication] IEEE. Reprinted, with permission, from [author names, paper title, IEEE publication title, and month/year of publication]
- 2) Only the accepted version of an IEEE copyrighted paper can be used when posting the paper or your thesis on-line.
- 3) In placing the thesis on the author's university website, please display the following message in a prominent place on the website: In reference to IEEE copyrighted material which is used with permission in this thesis, the IEEE does not endorse any of [university/educational entity's name goes here]'s products or services. Internal or personal use of this material is permitted. If interested in reprinting/republishing IEEE copyrighted material for advertising or promotional purposes or for creating new collective works for resale or redistribution, please go to http://www.ieee.org/publications_standards/publications/rights/rights_link.html to learn how to obtain a License from RightsLink.

If applicable, University Microfilms and/or ProQuest Library, or the Archives of Canada may supply single copies of the dissertation.

BACK CLOSE WINDOW

Figure A.4: Permission from IEEE to reuse an article as Chapter 5 of this dissertation